Identifying the molecular mechanisms of the anticonvulsant drugs cannabidiol, cannabidivarin and cannabidiolic acid using the model organism Dictyostelium discoideum

Christopher Perry

Research thesis submitted for the degree of Doctor of Philosophy at the Royal Holloway University of London in September 2018

Declaration of Authorship

I, Christopher Perry, hereby declare that the work presented in this thesis is my own unless otherwise stated, and that all published work has been acknowledged. Furthermore, I affirm that I have neither fabricated nor falsified the results reported herein.

Signed:

Date:

Abstract

Cannabis has been used for the treatment of seizures for many centuries. Recent medical interest has focused upon the non-psychotropic compounds found in cannabis plants, such as cannabidiol (CBD), cannabidivarin (CBDV) and cannabidiolic acid (CBDA). CBD has been demonstrated to provide effective control of seizures in recent phase III clinical trials as a treatment (Epidolex®) for specific refractory epilepsies such as Dravet syndrome. However, the molecular mechanism(s) in which CDB and other cannabinoids exert their therapeutic effects remain unknown. This study aimed to identify the molecular mechanism(s) of CBD, CBDV and CBDA using *D. discoideum* as a model system, translating any findings across to mammalian epilepsy models. Screening of a mutant library with each of these cannabinoids identified 4 genes of interest that show cannabinoid resistance when disrupted. Of these genes *gcvH1* (DDB_G0287773) was investigated further due to its role in the metabolism of the neurotransmitter glycine and its close association with the one carbon cycle. The resistance to CBD seen in the mutant screen was recapitulated by independently ablating *gcvH1* from wild-type cells (Ax3). When either *gcvH1* or the human orthologue *gcsH* was replaced back into the *gcvH1* null cell by use of an RFP tagged extra chromosomal vector, sensitivity to CBD was reinstated. Furthermore, we show that the *D. discoideum* and the *H. sapiens* RFP-fusion proteins both localize to the mitochondria. Using both GC-MS and NMR analysis we show that CBD treatment in *D. discoideum* significantly lowered cellular methionine levels, a key component of the one carbon cycle, whereas no change was detected in the *gcvH1* null. These findings were translated across to rat primary hippocampal neurons treated with PTZ to induce seizure like activity. It was found that following PTZ treatment, cellular methionine levels were significantly elevated compared to untreated cells. However, if an intervention group *was* pre-treated with CBD prior to PTZ treatment, methionine levels remained stable. We further show the effects of CBD within an *in vivo* epilepsy model, where heterozygous mice for the Dravet syndrome linked *Scn1a* gene are prone to convulsive episodes. We show that brain methionine levels within this model are significantly elevated following an oral treatment regime with CBD. Thus, our research strongly suggests that CBD may exert its anticonvulsant properties by altering cellular methionine levels, by targeting the one carbon cycle through the mitochondrial protein GCVH1.

Table of Contents

List of Tables and Figures

Abbreviations

AARS	Alanyl-tRNA Synthetase
ADRA2 B	Alpha-2B-adrenergic Receptor
APS	Ammonium persulphate
ARHGEF9	RHO Guanine nucleotide Exchange Factor 9
ATP	Adenosine Trisphosphate
BHMT	Betaine Homocysteine Methyltransferase
BSA	Bovine Serum Albumin
BsR	Blasticidin Resistance
CACNA1A	Calcium Channel, voltage-dependent, T type, Alpha-1H subunit
cAMP	Cyclic Adenosine Monophosphate
CBD	Cannabidiol
CBDA	Cannabidiolic acid
CBDV	Cannabidivarin
CBS	Cystathione β-Synthase
cDNA	Complementary Deoxyribonucleic Acid
CHRNA2	Cholinergic Receptor, Neuronal nicotinic, Alpha polypeptide 2
CLCN2a	Chloride Channel 2
CNTN2	Contactin 2
COX2	Cyclooxygenase 2
CSE	Cystathione γ-lyase
DLAT	Dihydrolipoyllysine-residue Acetyltransferase
DLST	Dihydrolipoamide Succinyltransferase
DMSO	Dimethyl Sulfoxide
DNA	Deoxyribonucleic Acid
DNMT	DNA Methyltransferase
DMEM	Dulbeccos Modified Eagles Medium
dNTP	Deoxynucleotide Triphosphatases
EDTA	Ethylenediaminetetraacetic Acid
EEF1A2	Eukaryotic translation Elongation Factor 1

EEG	Electroencephalogram
EFHC1	EF-Hand domain (C-terminal)-containing protein 1
ELISA	Enzyme-Linked Immunosorbent Assay
ETB	Embedded Trace Buffer
FDA	Food and Drug Administration
FFT	Fast Fourier Transform
FID	Free Induction Decay
GABRA1	Gamma-Aminobutyric acid Receptor, Alpha-1
GCL	Glutamate Cysteine Ligase
GC-MS	Gas Chromatography–Mass Spectrometry
GCS	Glycine Cleavage System
GFP	Green Fluorescent Protein
GOSR2	Golgi snap Receptor complex member 2
GRIN2A	Glutamate Receptor Ionotropic N-methyl-D-aspartate, subunit 2A
GSS	Glutathione Synthetase
HBSS	Hanks Balanced Salt Solution
HCN1	Hyperpolarization-activated Cyclic Nucleotide-gated potassium channel 1
iPCR	Inverse Polymerase Chain Reaction
KCNA2	Potassium Channel voltage-gated, shaker-related subfamily, member 2
LC-MS	Liquid Chromatography- Mass Spectrometry
LIMR	Lipocalin-Interacting Membrane Receptor
Li-Pilo	Lithium-Pilocarpine
Lmbd2b	LMBR1 domain-containing protein 2 homolog B
LMNB2	Lamin B2
mES	Maximal Electric Shock
MS	Methionine Synthase
MTRR	Methionine Synthase Reductase
NAD	Nicotinamide Adenine Dinucleotide
NADP	Nicotinamide Adenine Dinucleotide Phosphate
NICE	National Institute for Clinical Excellence
NMDA	N-Methyl-D-Aspartate

NMR	Nuclear Magnetic Resonance
PBS	Phosphate Buffered Saline
PBST	Phosphate Buffered Saline with TWEEN 20
PCR	Polymerase Chain Reaction
PDB	Protein Database
PLD	Poly D-lysine
POR	Cytochrome P450 Reductase
PTZ	Pentylenetetrazole
PVDF	Polyvinylidene Difluoride
qPCR	Quantitative Polymerase Chain Reaction
RedA	Reductase A
RFP	Red Fluorescent Protein
rRNA	Ribosomal Ribonucleic Acid
RNA	Ribonucleic Acid
ROS	Reactive Oxygen Species
RT-PCR	Reverse Transcriptase- Polymerase Chain Reaction
SAH	S-Adenosylhomocysteine
SAM	S-Adenosyl Methionine
SCN1A	Sodium Channel Neuronal type I Alpha subunit
SibB	Similar to Integrin B
SIM	Selected Ion Monitoring
SDS	Sodium Dodecyl Sulfate
SLC1A2	Solute Carrier family 1 (glial high affinity glutamate transporter), member 2
TEMED	Tris, N,N,N,N-tertamethylethylene-1,2-diamine
TBE	Tris/Borate/EDTA
TRPM8	Transient Receptor Potential of Melastatin type 8
TIC	Total Ion Current
UV	Ultra violet
VPA	Valproic Acid

Acknowledgements

Firstly I would like to thank my supervisor Professor Robin Williams for all the support and guidance he has given me over these last four years. I would also like to thank my advisors Professor Peter Bramley and Professor Phillip Beasley for all the advice and help they have given. I am also appreciative of the support and friendship from all members of the Williams lab, both past and present, who have made my time at Royal Holloway an enjoyable one. A big thank you also needs to be given to all the technicians and support staff within the School of Biosciences, especially to Paul Finch for his patience and willingness to help me with GC-MS.

This project would not have been possible without the funding from GW pharmaceuticals. I would also like to extend a big thank you to all my collaborators who have helped me along the way: To Professor Adrian Harwood and Dr Amy Baldwin (Cardiff University) and Professor Chris Thompson and Dr Balint Stewart (UCL) for their help with the mutant libraries. To Professor Rob Harvey (UCL) for his help and expertise in whole genome sequencing. To Dr Annette Müller-Taubenberger (LMU Biomedical centre, Munich) for her help with microscopy. To Dr Sandrine Claus and Joanna Boberska (Reading University) for helping to validate our findings using NMR. To Dr Fabiana Piscitelli (Consiglio Nazionale delle Ricerche, Italy) for her help in the quantification of cellular cannabinoid levels. To Professor Ben Whalley, Dr Alister McNeish, Pabitra Patra and Sarah Glyn (Reading University) for their help with the translational studies in mammalian seizure models.

I would also like to thank my family and friends for their support over these last few years, without which I would have struggled. I especially want to thank my wife Debbie without whom I would never have gotten this far, her support and encouragement has seen me through the worst of times. Thanks babe.

Thank you to everyone.

Chapter 1

Introduction

1.1 Introduction

1.1.1 Epilepsy

Epilepsy is a chronic neurological condition characterized by spontaneous recurrent seizures that vary in their type and severity, depending upon where in the brain they originate. At present approximately one in every 100 people live with epilepsy in the UK (Epilepsy action). Seizure onset arises through the abnormal or excessive neuronal activity within the brain (Reddy, 2014), with many people experiencing up to 100 plus episodes a day. There are several different types of seizures, which can be categorized as either focal or generalized. Focal seizures are localized to just one hemisphere of the brain and can involve the individual either retaining or losing full awareness during the seizure. The symptoms experienced during a focal seizure vary depending upon where in the brain seizure onset occurs. If seizure onset occurs within a region responsible for visual processing, the individual may experience visual distortions, etc. Focal seizures can develop further into more generalized seizures. Generalized seizures occur when seizure activity spreads across both hemispheres of the brain, and can be classed into a further six groups, these being: absence, tonic-clonic, tonic, clonic, myoclonic and atonic seizures. Absence seizures are a mild form of seizure that does not involve the individual experiencing convulsions, however the individual has no memory of the seizure. Tonic-clonic seizures are involve the individual loosing consciousness and dropping to the floor as a result of muscle contraction (tonic phase). The individual will then experience rhythmical jerking in their extremities such as arms and legs (clonic phase). Typically this type of seizure will last for a few minutes. During tonic seizure individuals extremities such as arms and legs will undergo extension through muscle contraction, with the person losing consciousness. Tonic seizures are uncommon but do manifest in individuals with Lennox-Gastaut syndrome, discussed below. A clonic seizure typically involves the loss of bodily control, with the individual experiencing jerking across regions of the body. Myoclonic seizures involve abrupt muscle jerks within the body. These can be focused upon just one area such as an arm or a leg resulting in the individual flinging or kicking out, etc, or they can be generalised across the entire body. During a myoclonic seizure the individual typically retains consciousness. Atonic seizures (drop seizures) are very uncommon and involve the individual losing consciousness and falling to the floor, commonly seen in Lennox-Gastaus syndrome. Atonic seizures can be specifically dangerous due to the secondary injury that could result from a drop seizure.

Seizure occurrence can be triggered by a number of neurological and physiological causes including trauma (Englander *et al,* 2014), tumours within the brain (Maschio, 2012), infection of the central nervous system (Singhi. 2011), stroke (Myint, 2005) and alcohol or drug abuse (Leach *et al*, 2012). Epileptogenesis and the resulting seizures can also arise through dysfunctional metabolic processes such as mitochondrial disorders (Finsterer and Mahjoub, 2012). Other studies have suggested that the dysfunction of the blood brain barrier may cause epilepsy through the intake of the blood protein albumin (Ivens et al, 2007). It has long been recognized that individuals can also have a genetic predisposition to epilepsy, caused by mutations within certain genes linked to seizure onset (Meisler and Kearney, 2005). The sheer number of genes now linked to epilepsy is too great to list here in their entirety, however table 1.1 gives an example of the broad spectrum of genes linked to epilepsy. With new advancements in genetic screening more and more genes are being linked to epilepsy (Poduri, 2017), thereby providing a better understanding to seizure development while also facilitating the development of personalized medicine.

Dravet syndrome is a severe form of epilepsy that occurs in approximately 1 in every 500 cases. Seizures manifest in the first year and are typically febrile seizures which are associated with elevated body temperature. These febrile seizures can last for as long as 30 minutes or longer and typically involve tonic-clonic seizures (stiffness and jerking) or clonic seizures (jerking). During the second year of life seizure episodes become more frequent and myoclonic seizures (muscle jerking) become more common. Individuals quite often become photosensitive in their second year and experience seizures brought on by flashing lights.

Lennox-Gastaut syndrome is a severe form of epilepsy that occurs in 1-5 individuals out of every 100 cases. Seizures typically manifest between the ages of 3-5 years and can include a wide range of different seizure types including tonic-clonic seizures (stiffness and jerking). The most common form of seizures in Lennox-Gastaust syndrome however are atonic seizures (drop seizures) which result in the individual falling to the ground. Another form of seizure common in Lennox-Gastaut syndrome is the atypical absence seizure whereby an individual will appear vacant, and not in tune with the local surroundings. Pretty much all children with Lennox-Gastaut syndrome develop severe learning difficulties.

Gene	Encoded protein function
SCN1A (sodium channel, neuronal type I, alpha subunit)	Sodium channel
KCNA2 (potassium channel, voltage-gated, shaker-related subfamily, member 2)	Pottasium channel
HCN1 (hyperpolarization-activated cyclic nucleotide-gated potassium channel 1)	HCN channel
CACNA1A (calcium channel, voltage-dependent, T type, alpha-1H subunit)	Calcium channel
CLCN2α (chloride channel 2)	Chloride channel
GABRA1 (gamma-aminobutyric acid receptor, alpha-1)	GABA-A receptor
GRIN2A (glutamate receptor, ionotropic, N-methyl-D-aspartate, subunit 2A)	NMDA receptor
CHRNA2 (cholinergic receptor, neuronal nicotinic, alpha polypeptide 2)	Acetylcholine receptor
AARS (alanyl-tRNA synthetase)	Enzyme
ARHGEF9 (RHO guanine nucleotide exchange factor 9)	Enzyme modulator
SLC1A2 (solute carrier family 1 (glial high affinity glutamate transporter), member 2)	Transporter
ADRA2 B (alpha-2B-adrenergic receptor)	Receptor
CNTN2 (contactin 2)	Cell adhesion molecule
EFHC1 (EF-hand domain (C-terminal)-containing protein 1)	Signal transduction
GOSR2 (golgi snap receptor complex member 2)	Membrane trafficking
LMNB2 (lamin B2)	Cytoskeletal protein
EEF1A2 (eukaryotic translation elongation factor 1)	Nucleic acid binding

Table 1.1 Genes responsible for epilepsy, and their biological function. Table gives examples of genes linked to epilepsy and their biological functional role. Information was adatpted from Wang *et al*, 2017.

The risks associated with epilepsy can be severe, and include direct trauma through loss of unconsciousness, neuronal damage, depression and the onset of sudden unexpected death (Tellex-Zentenoa *et al*, 2005). Epilepsy can also decrease the quality of life in patients, with some individuals experiencing many seizures per day. Great emphasis has therefore been placed on identifying new treatments and therapies to combat seizure onset. Examples include those that

target dysfunctional metabolic processes such as the ketogenic diet (Vining *et al,* 1998), and a range of anticonvulsants such as Valproic acid (Mattson *et al,* 1978). See table 1.2 for a comprehensive list of current anticonvulsants and the range of seizure types ther are prescribed for. While most individuals can control seizure onset through just one anticonvulsant, others require multiple medications. Unfortunately 30% of patients suffer with intractable epilepsy and are unable to benefit from a suitable and effective treatment (Kwan and Brodie, 2000). Since the 1990's new anticonvulsants have not reduced the number of refractory epilepsy patients, (Kwan and Brodie, 2000). One possible explanation for this lack of enhanced therapeutic efficacy is that new anticonvulsants act via the same target as previous anticonvulsants. For individuals in which current medications have no effect in controlling seizures the option of resective surgery exists. This physical removal of the brain tissue from which the seizure focus originates can have positive effects (Jobst and Cascino, 2015), however this is a very intrusive procedure. Clearly, new and unique treatments are needed to help manage the intractable epilepsy found within this 30% of epileptic individuals.

1.1.2 Cannabinoids

1.1.2.1 The anticonvulsant and analgesic effects of cannabidiol (CBD), cannabidiolic acid (CBDA) and cannabidivarin (CBDV)

One particular source of interest for new anticonvulsant drug discoveries are the cannabis plants; *Cannabis sativa*, *Cannabis indica* and *Cannabis ruderalis* (Devinsky *et al*, 2014). The use of cannabis for treating seizure activity has been around for many centuries and is still used today (Devinsky *et al*, 2014). Unfortunately the psychoactive properties and the social abuse of cannabis have hindered acceptance of cannabis as a viable therapy in treating epilepsy. Over the last few years this stigma has significantly changed with cannabinoids becoming approved for wide spread use in treating different conditions. The multiple sclerosis (MS) medication 'Sativex' developed by GW pharma, was the first therapy to be approved by the National Institute for Clinical Excellence (NICE). Sativex relieves neuropathic pain and spasticity in patients with multiple sclerosis and contains cannabidiol (CBD) and the psychoactive compound delta-9 tetrahydrocannabinol (THC). In June 2018, following months of phase III clinical trials, the US Food and Drug Administration (FDA) approved CBD for the treatment of epilepsy under the pharmaceutical name 'Epidolex'.

Anticonvulsant	Drug class	Seizure type	Mechanism of action
Acetazolamide	Thiadiazole sulfonamides	Tonic-clonic, absence, myoclonic, atonic	Carbonic anhydrase inhibitor
Brivaracetam	Alpha amino acids and derivatives	Partial onset seizures	Binds to the Synaptic vesicle glycoprotein 2A
Carbamazepine	Dibenzazepines	Generalised tonic–clonic, Focal	Inhibits sustained repetitive firing by blocking use-dependent sodium channels
Clobazam	1,5-benzodiazepine	Generalised tonic–clonic, Focal, Absence	Binds to GABAreceptor, increases time that chloride ionopre is open
Clonazepam	Benzodiazepine	Myoclonic, Absence	Potentiate the effects of GABA
Eslicarbazepine acetate	Dibenzazepines	Focal	Unknown. Believed to inhibit voltage gate sodium channels.
Ethosuximide	Pyrrolidine-2-ones	Absence	Binds to voltage sensitive calcium channels
Gabapentin	Gabapentinoid	Focal	Increases the synaptic concentration of GABA
Lacosamide	Amino acid	Focal	Inhibits voltage gated sodium channels
Lamotrigine	Phenyltriazine	Generalised tonic–clonic, Focal, Absence	Inhibits voltage sensitive sodium channels.
Levetiracetam	Alpha amino acids and derivatives	Generalised tonic–clonic, Myoclonic, Focal	Mechanism unknown
Oxcarbazepine	Dibenzazepines	Generalised tonic–clonic, Focal	Inhibits sustained repetitive firing by blocking use-dependent sodium channels
Perampanel	Bipyridines and Oligopyridines	Focal	A non-competitive AMPA receptor antagonist
Phenobarbital	Barbituric acid derivatives	Convulsive status epilepticus in hospital	Acts on GABA receptors increasing synaptic inhibition
Phenytoin	Phenylhydantoins	Convulsive status epilepticus in hospital	Acts on sodium channels, promoting sodium efflux from neurons
Piracetam	Alpha amino acids and derivatives	Myoclonic	Mechanism unknown
Pregabalin	Gabapentinoid	Focal	Binds to presynaptic voltage gated calcium channels.
Primidone	Hydropyrimidines	Tonic-clonic, focal	A GABA receptor agonist
Rufinamide	Triazole derivative	Tonic or Atonic	Mechanism unknown
Sodium valproate	Fatty acid	Generalised tonic–clonic, Tonic or Atonic, Focal, Absence, Myoclonic	Believed to increase levels of GABA by inhibiting GABA transaminase
Stiripentol	Benzodioxoles	Tonic-clonic, myoclonic	Enhances GABAergic inhibition
Tiagabine	Piperidinecarboxylic acids	Focal	Believed to be a selective GABA reuptake inhibitor
Topiramate	Dioxolopyrans	Generalised tonic–clonic, Tonic or Atonic, Absence, Myoclonic	Mechanism unknown
Valproic acid	Methyl-branched fatty acids	Generalised tonic–clonic, Tonic or Atonic,	Not well understood. May act by increasing GABA levels

		Focal, Absence, Myoclonic	
Vigabatrin	Analogue of GABA	Focal	Increases GABA levels by inhibiting 4-aminobutyrate transaminase
Zonisamide	Sulfonamide	Absence, Myoclonic, Focal	Suppresses neuronal depolarization by binding to sodium channels and voltage sensitive calcium channels

Table 1.2 Anticonvulsant pharmaceuticals available by seizure type. The table lists the anticonvulsants available and the varying seizure types that they are prescribed for. The drug class for each anticonvulsant is shown and each drug's prpoposed mechanism of action. Information was sourced from the National Institute for Health and Care Excellence (https://bnfc.nice.org.uk) and the drug bank (https://www.drugbank.ca/drugs).

Of the ~100 phytocannabinoids found within the three cannabis species CBD (Fig 1.1a) has received the most interest as a therapeutic treatment of epilepsy. CBD is the most abundant of the non-psychoactive cannabinoids present in its precursor form as CBDA, and has been shown to counter act the psychoactive influence of THC (Morgan and Curran, 2008). CBD has been shown to display antiepileptiform and anticonvulsant properties within both *in vitro* and *in vivo* rat epilepsy models (Jones et al, 2009, 2012). Epileptiform can be defined as the effects of epilepsy or its manifestations, and can be present independent of seizure occurrence, e.g. epileptiform discharges involving electroencephalogram (EEG) waveform abnormalities. In an Mg^{2+} free epilepsy model using rat hippocampal brain slices, CBD has been shown to reduce burst amplitude and duration of epileptiform local field potentials at concentrations ranging from 0.01-100 µM (Jones et al, 2009). Within the same study CBD also decreased burst amplitude, duration and frequency within a rat based 4-aminopyridine model at similar concentrations (Jones et al, 2009). Similarly, within a pentylenetrazole rat model CBD was shown to have clear anticonvulsant effects at 100 mg/kg, and reduced mortality from 47% in control subjects to 7% in CBD treated subjects (Jones et al, 2009). In other mammalian studies CBD significantly reduced the number of pilocarpine rat models experiencing the most severe seizures at just 1 mg/kg (Jones et al, 2012). Similarly, in rat seizure models induced with penicillin it was found that CBD significantly decreased the mortality rate from seizures at concentrations >10 mg/kg (Jones et al, 2012). Following on from these mammalian seizure model studies, a number of multicentre phase III clinical trials were performed into the efficacy of CBD in treating seizures within rare forms of epilepsy. In these studies it was found that the

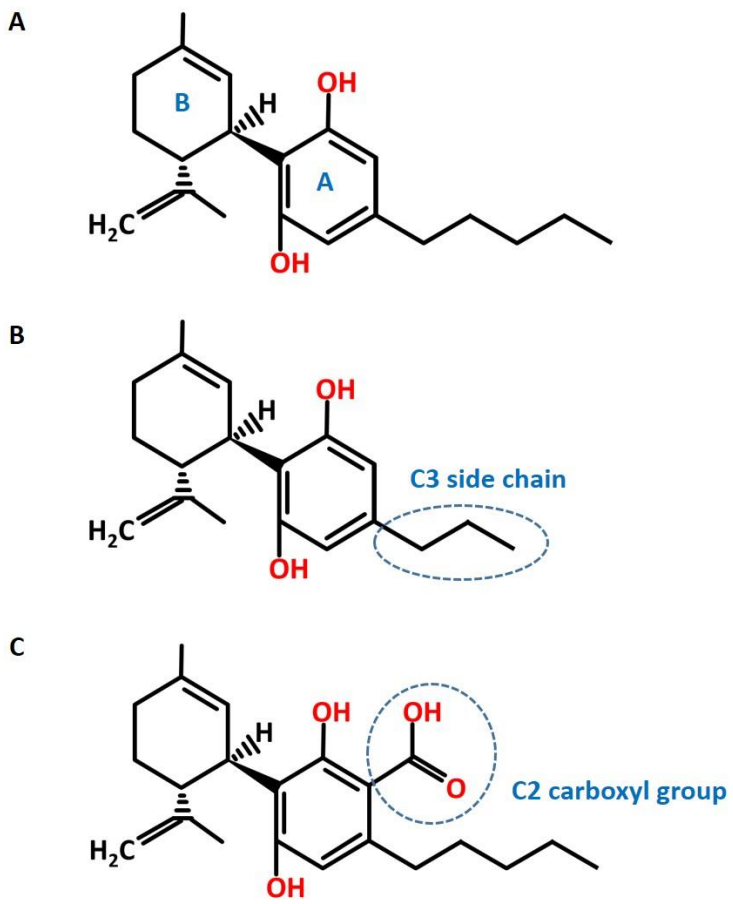

Figure 1.1 Cannabinoid structure. The cannabinoids (A) cannabidiol (CBD), (B) c cannabidivarin (CBDV) and (C) cannabidiolic acid (CBDA) all possess the same basic structure consisting of an aromatic ring (Blue A), a cyclohexene ring (Blue B) and a side chain at the C3 position. CBD, CBDA and CBDV differ only in the length of the C3 side chain and the presence of a carboxyl group at the C2 position on CBDA.

concomitant treatment of CBD with the individuals' normal treatment regimen significantly lowered the number of seizures experienced in individuals with Dravet syndrome (Devinsky *et al,* 2017) and Lennox-Gastaut syndrome (Devinsky *et al*, 2018., Thiele *et al,* 2018). Dravet Syndrome and Lennox-Gastaut syndrome are associated with drug-resistant seizures, whereby no real treatment is available. Cannabis oil on the other hand that is high in CBD content was widely known to have an effect in treating these severe disorders. Dravet Syndrome and Lennox-Gastaut syndrome were therefore considered suitable for clinical treatment with CBD. The results of these clinical trials were instrumental to FDA approval of 'Epidolex', a treatment for Dravet syndrome and Lennox-Gastaut syndrome whos active component is CBD.

Seizure control has also been demonstrated with other cannabinoids structurally similar to CBD. The cannabinoid Cannabidivarin (CBDV) (Fig 1.1b) is the propyl derivative of CBD and has been shown to display both antiepileptiform and anticonvulsant properties both *in vitro* and *in vivo*. In both Mg^{2+} free and 4-aminopyridine rat models CBDV reduced local field potentials significantly at concentrations >10 µM (Hill *et al*, 2012). In maximal electric shock (mES) studies using mice, CBDV displayed significant anticonvulsant effects when administered at 50 mg/kg. Similarly, in a mouse audiogenic seizure model it was shown that CBDV reduced the number of seizures when administered at 50 mg/kg (Hill *et al*, 2012). In the pentylenetrazole rat model CBDV treatment was also shown to significantly reduce seizure severity at 100 mg/kg (Hill *et al*, 2012).

As well as the therapeutic effects of cannabis in preventing seizure onset, cannabis is also considered to have analgesic effects (Elikottil *et al*, 2009), believed to be from the presence of CBDA. CBDA is the precursor to CBD, and differs only by the addition of a carboxyl group at the C2 position (Fig 1.1c). Studies have shown that CBDA directly inhibits cyclooxygenase 2 (COX2) activity with an IC_{50} of 2 µM (Takeda *et al*, 2008). Salicylic acid containing anti-inflammatories such as aspirin are known to exert their analgesic effects by also suppressing COX2 activity (Lucido *et al,* 2016). Therefore, it is most likely that the analgesic effects of CBDA also originate from the direct inhibition of COX2.

1.1.2.2 Potential targets of the cannabinoids in treating epilepsy

How cannabinoids exert their antiepileptiform and anticonvulsant properties within both humans and epilepsy models is still uncertain. A number of studies have attempted to elucidate these molecular targets by looking at those accepted as having a role in seizure onset. These targets include the cannabinoid receptors (Devinsky et al, 2014), channel proteins (De Petrocellis et al, 2011), mitochondrial targets involved in regulating intracellular Ca2+ levels (Ryan et al,

2009), the cytochrome P450 family of enzymes (Yamaori *et al*, 2011; Jiang *et al*, 2013) and the endocannabinoid system (Devinsky et al, 2014). One hypothesis for the anti-epileptic effects of cannabinoids is through the targeting of receptors involved in the endocannabinoid system (Devinsky *et al*, 2014). The endocannabinoid system is endogenous in mammals and involves the regulation of synaptic activity. The endocannabinoid ligands anandamide and 2-arachidonoylglycerol bind to the cannabinoid receptors CB_1 and CB_2, on presynaptic neurons and modulate the release of neurotransmitters. The psychoactive component of cannabis, tetrahydrocannabinol (THC) has been shown to act as an agonist of CB_1 and CB_2 while CBD has been shown to act as an antagonist of CB_1 and CB_2 (Pertwee, 2008), however this was shown *in vitro* and in supraphysiological concentrations. CBD has also been shown to interact with other targets such as the equilibrative nucleoside transporters involved in adenosine transport (Carrier *et al*, 2006), and the transient receptor potential of melastatin type 8 protein (TRPM8) (De Petrocellis *et al*, 2008). The number of potential targets identified for CBD is diverse (Bih *et al*, 2015), however the exact mechanism by which CBD infers its anticonvulsant effect is still unknown. The identification of the molecular targets responsible for a pharmaceuticals seizure control is extremely difficult in higher organisms. One alternative approach is to use a simple biomedical model such as *D. discoideum* and then translate into mammalian models to validate.

1.1.3 *D.discoideum* as a biomedical model

D.discoideum is a member of the amoebozoa group and found within the top soil of temperate zones around the globe. They are unicellular, eukaryotic organisms and are more evolutionary related to animals and fungi than to plants and bacteria. *D.discoideum* predate bacteria through the detection of bacterially secreted folic acid (Segota *et al,* 2013). During times of nutrient abundance *D.discoideum* remain unicellular, however, cells will take on a social role when put under environmental stress, particularly when their bacterial food source is in low supply. At times of low nutrient availability the cell population enters the developmental stage of their life cycle (Fig 1.2). Development is initiated by the mass movement of cells towards a central region where they form an aggregate. This is facilitated by the release of the extracellular chemoattractant cAMP into the local environment, thereby forming a gradient to which cells chemotax (Brzostowski *et al*, 2013). Upon aggregation the cell population forms a pseudoplasmodium which allow the entire cell population to move together away from the

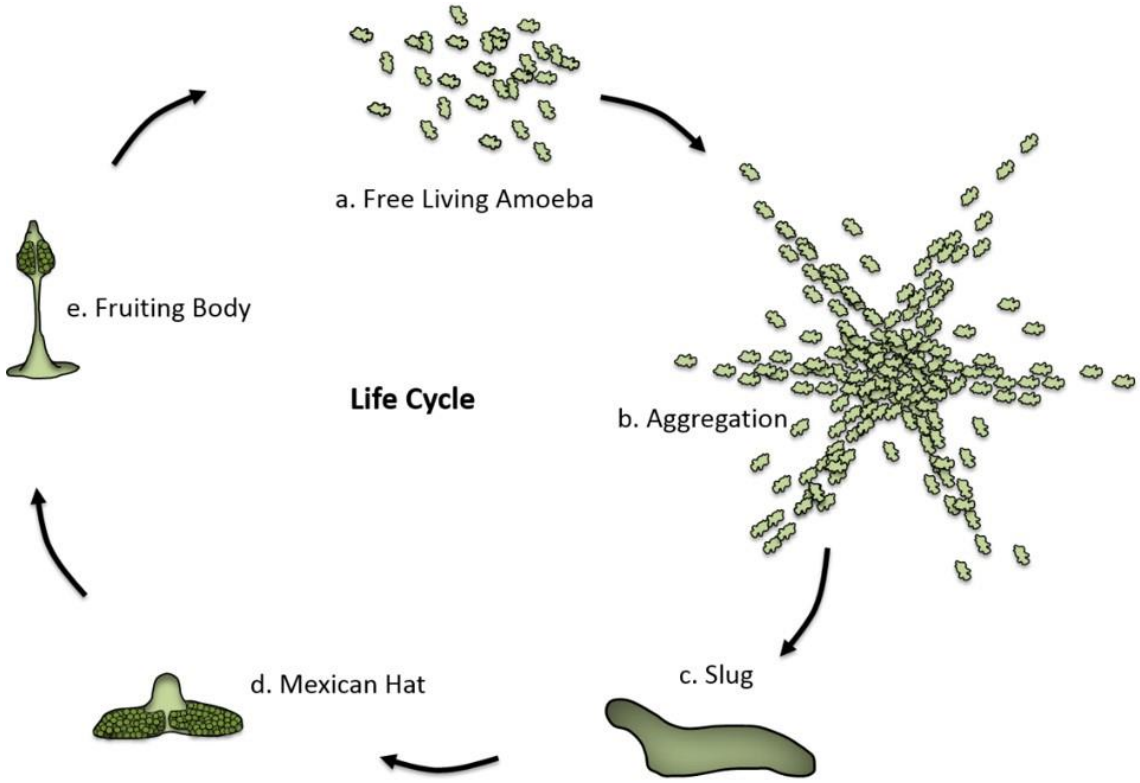

Figure 1.2 The Life cycle of the amoeba *D. discoideum*. (A) During the normal growth phase cells are unicellular and live as free living amoeba. (B) At times of nutrient depletion *D.discoideum* cells enter the developmental stage. Cells chemotax towards a central region facilitated by cAMP gradients and aggregate into a multicellular body. (C) This multicellular pseudoplasmodium is motile and able to locate to areas with more favourable conditions, influenced by factors such as light, heat and humidity. (D) Cells undergo differentiation forming either pre-spore or pre-stalk cells. (E) Development culminates with the formation of a mature fruiting body containing spore cells elevated to a maximum height for dispersion.

nutrient depleted environment. Pseudoplasmodium movement is influenced by attractants such as light, heat and humidity (Vasiev and Weijer, 2003), thereby directing the pseudoplasmodium to a more suitable environment. When in a more suitable environment cells differentiate into either pre-stalk or pre-spore cells during the development of a fruiting body. The pre-stalk cells altruistically die and form the stalk of the fruiting body, thereby elevating the pre-spore cells to maximum height ready for dispersion (Uchinomiya and Iwasa, 2013).

D.discoideum has been used in many areas of research, advancing our understanding of processes such as cell proliferation, chemotaxis, cytokinesis, cell-motility, phagocytosis and signal transduction (Bozzaro, 2013). Research using *D.discoideum* has also increased our understanding of many diseases within humans, including Parkinson's disease (Gilsbach *et al,*

2012). The use of *D.discoideum* as a biomedical model has helped us to better understand cell proliferation in tumorigenesis (Hikuchi *et al*, 2006). Similarly, studies into cell motility have answered fundamental questions into the mobility of metastatic cancerous cells (Nelson *et al*, 2012). Investigation of the molecular mechanisms and pathways involved in the response to certain chemotherapeutic therapies have been facilitated by use of *D. discoideum* (Alexander and Alexander, 2011). *D.discoideum* has also been used to determine the normal function of genes commonly linked to diseases such as the neurodegenerative Alzheimer's disease (Myre, 2012). The use of *D. discoideum* has been utilized in many areas of human health and disease, and as such is one of the few simple biomedical model organisms recognized by the American Institute of Health.

D.discoideums usefulness as a biomedical model is due to its many convenient genomic attributes. The genome of *D.discoideum* is 34 Mb in size and spread across six chromosomes (Eichenger *et al*, 2005) with a further 100 copies of an 88 kb palindrome that carries the genes for rRNA (Sucgang, 2003). It has approximately 12,500 genes, roughly the same size as the *Drosophila melanogaster* genome and one half of the *H.sapiens* genome. Many of the proteins found within the *D. discoideum* proteome are homologous to those found within *H.sapiens* and are not found in other simple models such as *S.cerevisiae*. The sequencing of the *D.discoideum* genome was achieved in 2004 (Eichenger *et al,* 2005) and has allowed the functional analysis of many of its genes. In particular, having the genome sequenced has allowed its utilization as a convenient model for carrying out pharmacogenetic analysis (Williams et al, 1999; Williams et al, 2002). This involves the screening of a mutant library for a pharmaceuticals recognizable trait in order to identify the molecular mechanism in which it acts. By using such a method previous studies have established the mechanism of action for a range of compounds and pharmaceuticals (Williams et al., 2002, Williams et al., 1999., Robery et al, 2011., Robery et al, 2013., Waheed et al, 2014., Cocorocchio et al, 2015., Otto et al, 2016., Cocorocchio et al, 2018). Such an experimental approach could not be carried out upon mammalian models due to the sheer number of genes that would require independednt ablation. Similarly, the production of a mammalian cell library would be a slow and laborious process. *D. discoideum* as a model organism provides a compromise between relevance and its ease of use. *D.discoideum* is therefore a convenient model for which to use in elucidating the molecular targets of CBD, CBDA and CBDV and then characterizing the mechanisms involved. These findings can then be translated across to mammalian seizure models and their efficacy in reducing seizure severity validated.

1.1.4 The one carbon cycle, Glycine cleavage system and the Transsulfuration pathway

One particular hypothesis that attempts to explain epileptogenesis and the onset of seizures within individuals is the methylation hypothesis (Kobow et al, 2013). Here it has been suggested that seizure occurrence negatively affects cellular methylation, which then positively feeds back to promote further seizures. The methylation of DNA and other molecules within the cell requires the presence of the one carbon cycle. The one carbon cycle (Fig 1.3) is a series of reactions that centres upon the transfer of a single carbon from either 5-methyl-tetrahydrofolate or betaine to homocysteine, concomitantly producing methionine and tetrahydrofolate or di-methyl glycine respectively (Ducker and Rabinowitz, 2017). Methionine is fundamentally important in many biological pathways due to its conversion to s-adenosyl-methionine (SAM), by receiving an adenosine group from ATP (Eustáquio et al, 2008). SAM is responsible for the transfer of its methyl group to a number of acceptor molecules, such as neurotransmitters and DNA methyltransferases for DNA methylation (Ulrey, 2005). Following the donation of its methyl group, SAM is further hydrolysed to form adenosine and homocysteine which can re-enter the cycle and again be converted into methionine (Ducker and Rabinowitz, 2017). Adenosine is an endogenous anticonvulsant within the brain (Young and Dragunow, 1994), while elevated levels of homocysteine have been linked to seizure occurrence (Baldelli *et al*, 2010). Homocysteine can also enter the transsulfuration pathway and be converted into cysteine. Here cysteine is coupled with both glycine and glutamate to form glutathione, the cells principal anti-oxidant (Mosharov *et al*, 2000).

Also linked to the one carbon cycle through tetrahydrofolate usage is the glycine cleavage system, responsible for the metabolism of cellular glycine levels, one of the central nervous systems key neurotransmitters (Dutertre *et al*, 2012). The glycine cleavage system is localized at the inner mitochondrial membrane, and contains four proteins; H-protein (GcsH), T-protein (GcvT), L-protein (GcvL) and the P-protein (GcvP), that form a complex. The glycine cleavage system is known to function in both directions, being involved in both the catabolic (Kikuchi *et al*, 1992) and anabolic (Okamura-Ikeda *et al*, 1987) regulation of glycine (Fig 1.4).

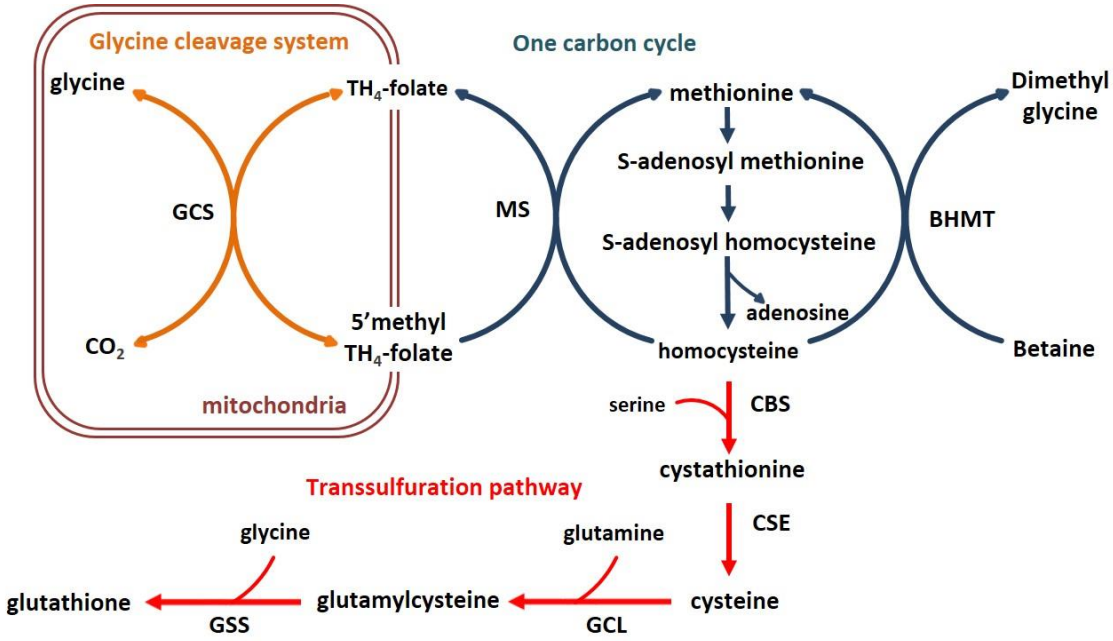

Figure 1.3 The One Carbon Cycle, Glycine cleavage system and Transsulfuration pathway. The one carbon cycle (Blue) is responsible for the production of methionine via two distinct enzymatic pathways. The first is catalysed by Methionine synthase (MS) and involves the transfer of a methyl group from 5' methyl tetrahydrofolate to homocysteine concomitantly producing methionine and tetrahydrofolate. The second is catalysed by Betaine homocysteine methyltransferase (BHMT) and involves the transfer of a methyl group from betaine to homocysteine concomitantly producing methionine and dimethylglycine. Methionine is then converted to s-adenosyl methionine (SAM) the cells principal methyl donor, which is then converted to s-adenosyl homocysteine following donation of the methyl group, and back to homocysteine with the disassociation of adenosine. The glycine cleavage system (GCS) (Yellow) is linked to the one carbon cycle via its use of tetrahydrofolate and is involved in glycine metabolism within the mitochondria. The transsulfuration pathway (Red) is responsible for the production of glutathione, the cells principal anti-oxidant which is formed from glycine, cysteine and glutamine involving the enzymes glutamate cysteine ligase (GCL) and glutathione synthetase (GSS). The main source of cysteine for glutathione production comes from the one carbon cycle via the conversion of homocysteine. Cysteine is formed from homocysteine in a multi-step process involving the enzymes Cystathione β-synthase (CBS) and cystathione γ-lyase (CSE).

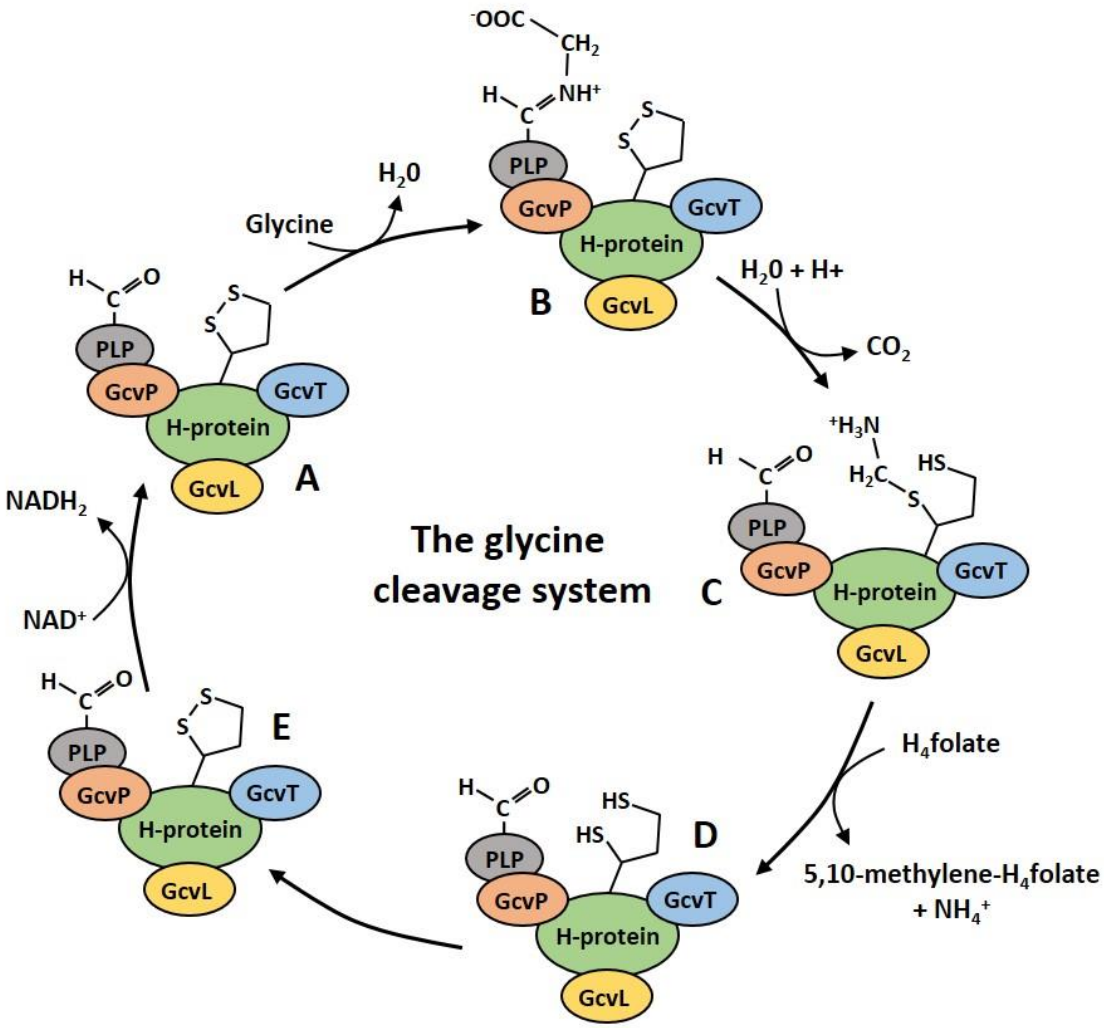

Figure 1.4 The Glycine Cleavage System. For the Glycine cleavage system to function, lipoic acid is required as an essential co-factor for the H-protein. During the decarboxylation of glycine (A) the P-protein first binds to the alpha-amino group of glycine via its pyridoxal phosphate co-factor. (B) Glycine subsequently undergoes decarboxylation with the release of CO_2 and the transfer of the glycine intermediate methylamine to the lipoamide co-factor of the H-protein. (C) The H-protein then forms a complex with the T-protein which requires tetrahydrofolate as a co-factor. The amino methyltransferase activity of the T-protein then facilitates the completion of glycine degradation, yielding both ammonia and 5,10-methylenetetrahydrofolate. (D) Following reaction completion the lipoate co-factor of the H-protein is left in a reduced state with two reduced thiol groups which need to be re-oxidized to allow the reaction to proceed again. (E) This is facilitated through the interaction with the L-protein, which has dihydrolipoyl dehydrogenase activity and oxidizes the thiol groups to regenerate the disulfide bond, while reducing NAD+ to $NADH_2$ in the process.

Despite the reaction being reversible, it has been shown that the catabolic role does predominate within higher organisms (Kikuchi *et al*, 1992). For the glycine cleavage system to function, lipoic acid is required as an essential co-factor for the H-protein (Fig 1.4). During the decarboxylation of glycine (forward reaction), the P-protein first binds to the alpha-amino group of glycine via its pyridoxal phosphate co-factor (Fig 1.4a). Glycine subsequently undergoes decarboxylation with the release of CO_2 and the transfer of the glycine intermediate methylamine to the lipoamide co-factor of the H-protein (Fig 1.4b). The H-protein then forms a complex with the T-protein which requires tetrahydrofolate as a co-factor (Fig 1.4c). The amino methyltransferase activity of the T-protein then facilitates the completion of glycine degradation, yielding both ammonia and 5,10-methylenetetrahydrofolate (Fig 1.4d). Following reaction completion the lipoate co-factor of the H-protein is left in a reduced state with two reduced thiol groups which need to be re-oxidized to allow the reaction to proceed again. This is facilitated through the interaction with the L-protein, which has dihydrolipoyl dehydrogenase activity and oxidizes the thiol groups to regenerate the disulphide bond, while reducing NAD^+ to $NADH_2$ in the process (Fig 1.4e).

1.1.5 Aims

The aims of this study were:

1. To characterise the role that the cannabinoids CBD, CBDA and CBDV have upon *D. discoideum* growth and development.

2. To use *D. discoideum* in a pharmacogenetic approach to identify mutants resistant to cannabinoids.

3. To characterise mechanisms leading to cannabinoid resistance in these mutants, to better understand the cellular mechanism of cannabinoids.

4. To translate the molecular mechanisms identified in *D. discoiduem* to *in vitro* and *in vivo* seizure models, to investigate if these roles were relevant to seizure control.

Chapter 2

Methods and Materials

2.1 Materials

2.1.1 Reagents purchased from Sigma-Aldrich (Poole, Dorset, England)

2-propanol (#I9516), ammonium persulphate (APS) (#A3678), bacteriological agar (#A5306), beta-mercaptoethanol (#M6250), Complete protease cocktail inhibitors (#11697498001), ethylenediaminetetraacetic acid (EDTA) (#E5134), boric acid (#B6768), ddH_2O (#W4502), glycine (#G8898), DL-4-chlorophenylalanine (#C6506), Dulbeccos modified eagles medium (#D5796), horse serum (#H0146), Luria-Burtani (LB) broth tablets (#L7025), magnesium chloride (#63069), nonidet p-40 (NP40) (#74385), pentylenetetrazole (PTZ) (#P6500), poly-D-lysine (#A003), potassium acetate (#P1190), potassium chloride (#P9333), RIPA buffer (#R0278), sodium dodecyl sulfate, (SDS) (#L3771), sodium hydroxide (#71687), sodium acetate (#S2889), sodium chloride (#S7653), sucrose (#S7903), trichloroacetic acid (#T6399), Tris, N,N,N,N-tertamethylethylene-1,2-diamine (TEMED) (#T9281), trisma base (#T1503) TWEEN20 (#8.22184), valproic acid (#PHR1061), x-gal (#B4252)

2.1.2 Reagents purchased from other suppliers

1-propanol (#1.00996.2500), 2,2,4-Trimethylpentane (# 83630.320), acrylamide (#K548-5X1ML), bromophenol blue (#34307.237), Butyl acetate (#22081.326), Chloroform (#22711.260), di-methyl sulfoxide (DMSO) (#0231-4L), di-pottasium hydrogen phosphate (K_2HPO_4) (#ACRO204851000), ethanol (#20821.330DP), Isopropyl β-D-1-thiogalactopyranoside (IPTG) (#R036), glucose (#0188-500G), glycerol (#24388.238), hydrochloric acid (#20252.244), methanol (#0323-4L), phenol:chloroform:isoamyl alcohol (25:24:1) (#K169-400ML), nitric acid (#20425.242), phosphate buffer saline (PBS) (#437117K), potassium di-hydrogen phosphate (KH_2PO_4) (#0781-500G), propyl chloroformate (#ACRO245290250), pyridine (#1.07462.1000), tris-borate-EDTA (TBE) buffer (#0658-1LP), tris(3-hydroxypropyl)phosphine (THP) (#598250-1) (VWR international, England)

5x loading dye (#R0611) (Fermentas)

Ethidium bromide (#1610433) (Bio-Rad laboratories, England)

HL5 media (#HLB0102), SM media (#SMB0102), minimal media (#FMM0101) (Formedium, England)

5x loading buffer (#BIO-37045), deoxynucleotide triphosphatases (dNTPs) (#BIO-39029), molecular grade agarose (#BIO-41025), (Bioline)

B27 supplement (#17504044), bovine serum albumin (BSA) (#AM2616), glutamax (#35050061), hanks balanced salt solution (HBSS), neurobasal medium (##21103049), TrypLA™ express enzyme 1x (#12604021) (Thermo Fisher Scientific)

Fluoromount-G™, with DAPI (#00-4959-52) (Invitrogen)

Absorbent pads, nitrocellulose filters (Millipore, Cork)

x10 phosphate buffer pH 7 (#258590010) (Fisher BioReagents)

N-octyl-beta-glucopyranoside (Apollo Scientific)

2.1.3 Cannabinoids

Cannabidiol (CBD), cannabidivarin (CBDV) and cannabidiolic acid (CBDA) were provided by GW pharmaceuticals, England.

2.1.4 Antibiotics

Ampicillin (#A1593) (Sigma-Aldrich, Poole, England)

Blasticidin (#10166793), penicillin/streptomycin (Penstrep) (#11548876), G418 (#11558616) (PAA laboratories, England)

2.1.5 Molecular weight standards

Page ruler™ prestained protein ladder (#26616), (Thermo Scientific)

1 kb hyperladder (#BIO-33053) (Bioline)

2.1.6 Restriction enzymes

SpeI (#ER1251), PstI (#ER0611), KpnI (#ER0521), BamHI (#ER0052), RSAI (#ER1122), EcoRI (#ER0271), SacI (#ER0271), XbaI (#ER0681), BglII (#ER0081), NcoI (#ER0572). All restriction enzymes were obtained from Thermo Scientific.

2.1.7 Other enzymes

Taq polymerase (#BIO-21040) (BIOTAQ DNA polymerase)

Q5® High fidelity DNA polymerase (#M0491S) (New England Biolab)

T4 DNA ligase (#15224041) (Fermentas)

Proteinase K (#EO0491) (Fermentas)

RNase A (#R6148-25ML) (Sigma Aldrich, Poole, England)

2.1.8 Antibodies

mouse anti-porin (#70-100-1) (Developmental studies hybridoma bank)

mouse anti-calnexin (#270-390-2) (Developmental studies hybridoma bank)

conjugated anti-streptavidin (#S32358) (Streptavidin Alexa Fluor™ 680 conjugate, Invitrogen)

rat anti-RFP (#5F8-20) (5F8 anti-red rat mAb, Chromatek)

rat anti-GFP (#3h9-20) (3H9 anti-GFP rat mAb, Chromatek)

mouse anti-RFP (#6G6-100) (6G6 anti-red mouse mAb, Chromatek)

goat anti-mouse (#ab175473) (Alexa fluor® 568 goat anti-mouse IgG, Life Technologies)

rabbit anti-rat (#ab169346) (Alexa fluor® 488 rabbit anti-rat IgG, Life Technologies)

anti-mouse (anti-mouse IR Dye™, Li-Cor)

anti-rat (anti-rat IR Dye™, Li-Cor)

2.1.9 Commercial kits

Bovine serum albumin Protein Assay Kit (#23225) (Thermo Scientific)

Q5® site directed mutagenesis kit (#E0554) (New England Biolabs inc)

TOP10F' chemically competent cells (#C404006) (Invitrogen)

RNeasy mini-kit (#74104) (Qiagen)

First strand cDNA synthesis kit (#K1612) (Thermo Scientific)

DNA-free kit (#AM1906) (Ambion).

GeneJet® plasmid mini-prep kit (#K0502) (Thermo Scientific)

QIAquick® Gel Extraction kit (#28704) (Qiagen)

QIAquick® PCR purification kit (#28104) (Qiagen)

pCR 4-Topo® vector (#K457502) (Invitrogen)

ELISA kit specific for Vitamin B12 (#B12-E01) (Immunolab Vitamin B12 ELISA, Immunolab GmbH)

DNeasy® Blood and tissue kit (#69506) (Qiagen)

2.1.10 Primers

All primers were obtained from Sigma Aldrich (Poole, Dorset, England)

2.1.11 Equipment

colourimetric plate reader

HP5890 Series II chromatograph interfaced to an HP5972 MSD mass spectrometer

Olympus IX71 stage microscope

Peqlab electrophoresis tank

Gene flash UV visualization machine

Shaker x2

Heat block

Borosilicate tubes and caps (VWR)

2.1.12 Cell lines and plasmids

All cell lines and plasmids not included within commercially available kits were obtained from the dicty stock center (https://www.dictybase.org/StockCenter)

2.2 Methods

2.2.1 *D. discoideum* methods

2.2.1.1 Storage of Cell Lines

D. discoideum stock cell lines obtained from the dicty stock center were stored within freezing media (Horse serum, 7% DMSO) at $^{-}$196°C in liquid nitrogen, and a $^{-}$80°C freezer. Cells were taken from stock every month and grown up on SM plates containing *R. planticola*. After one weeks growth on bacteria *D. discoideum* cells were taken from an isogenic colony and transferred into HL5 liquid media containing glucose. HL5 medium also contained 100 µg/ml penicillin and 100 µg/ml streptomycin. Cells were maintained at 22°C within the exponential phase at a density of 2-4 x10^6 cells/ml and washed every two days to remove dead cells

2.2.1.2 Growth assays

Cells were grown to confluency in a 10 cm tissue culture dish suspended in liquid media (HL5 medium). Cells (5x10^3 in 495 µl of fresh media) were added to each well of a 24 well plate and allowed to adhere for 20 minutes. CBD, CBDA or CBDV suspended in 5 µl DMSO was added to each well to achieve final concentrations of 0 to 20 µM (1% final DMSO concentration). These concentrations were used as they are physiologically relevant in mammalian models (Jones *et al,* 2009), and they provide a range in which cell proliferation is not effected to that which does inhibit cell proliferation. Negative controls contained DMSO only. Cells were maintained at 22°C, counted at 72 hours, and then every 24 hours. Each concentration was carried out in triplicate and experiments were repeated.

2.2.1.3 Development assays

D. discoideum cells were grown in HL5 shaking culture for two days prior to the development assay. Cells were washed twice in KK2 buffer (16.2 mM KH_2PO_4, 4 mM K_2HPO_4. pH 6.8) by centrifuging at 437 g and the supernatant removed. 1x10^7 cells were re-suspended in 1 ml of KK2 and placed onto nitrocellulose filters (Millipore, Cork). Absorbent pads (Millipore, Cork), divided into quarters, were placed in 2 ml culture dishes and soaked with 0.5 ml KK2 containing cannabinoids at a range of concentrations. 1 mM Valproic acid in 1% DMSO was used as a positive control, while KK2 containing 1% DMSO was used as a solvent only control. Nitrocellulose filters containing cells were quartered and place upon the absorbent pads

containing the drug and maintained in a humid environment at 22°C for 24 h. Fruiting body morphology was recorded using a dissection microscope and camera.

2.2.1.4 Transfection of *D. discoideum* cells by electroporation

D. discoideum cells ($5x10^6$) within the exponential phase of growth (2 - $4x10^6$ cells per ml) were pelleted by centrifugation at 500 g, media removed and washed in 10 ml of ice cold KK2 buffer (16.2 mM KH_2PO_4, 4 mM K_2HPO_4. pH 6.8). Cells were again centrifuged at 500 g, KK2 removed and washed twice in ice cold H-50 buffer (20 mM HEPES, 50 mM KCl, 10 mM NaCl, 1 mM $MgSO_4$, 5 mM $NaHCO_3$, 1 mM NaH_2PO_6, pH 7.0) before being pelleted. The cell pellet was re-suspended in 100 µl of H-50 buffer and 1-5 µg of DNA added. Re-suspended cells were transferred to a cold 0.1 cm electroporation cuvette, allowed to rest on ice for 5 minutes and then electroporated at 0.85 KV and 25 µF. Following electroporation the cuvette was placed on ice for 5 minutes. For the transformation of over expression plasmids the cells were removed from the cuvette and placed into a 10 cm dish containing 10 ml HL5 media. Antibiotic selection was added to the media 24 hours later. For the creation of knock out cell lines the cells were placed into a 10 cm dish containing 10 ml of HL5 media and immediately transferred into a 96 well plate with 100 µl placed into each well. 100 µl of antibiotic (x2 concentration) in 100 µl of HL5 media was added to each well of the 96 well plate 24 hours later.

2.2.2 Molecular Biology methods

2.2.2.1 Restriction digests

A large number of digests were done within the experiments using varying restriction enzymes each with their own reaction conditions. An average digest involved adding 16 µl nuclease-free water, 2 µl 10X Buffer (specific to each enzyme), (0.5-1 µg/µL) 1 µL DNA and 0.5-2 µL restriction enzyme. All restriction digests were done in accordance with the manufaturers instructions. Where two restriction enzymes were required in a reaction mixture (double digest), the appropriate buffer and reaction conditions were identified using the Thermo Fisher double digest calculator (https://www.thermofisher.com)

2.2.2.2 Polymerase chain reaction (PCR) amplification

Amplification of DNA was carried out using either a standard polymerase (BIOTAQ DNA polymerase) or a proof reading polymerase (Q5® High fidelity DNA polymerase, New England Biolab). For multiple standard PCR reactions a master mix was created with each individual reaction containing: 0.5 µg DNA, 0.2 µM 5' primer, 0.2 µM 3' primer, 2 µl 2.5 mM dNTPs, 0.8 µl 50 mM $MgCl_2$, 2 µl 10x NH_4 reaction buffer, 0.2 µl BIOTAQ DNA polymerase (5 U/µl), made up to 20 µl with molecular grade ddH_2O. For reactions requiring a proof reading polymerase each reaction contained: 0.5 µg DNA, 0.2 µM 5' primer, 0.2 µM 3' primer, 2 µl 2.5 mM dNTPs, 5 µl 5x Q5 buffer, 0.25 µl Q5® DNA polymerase (2 U/µl), made up to 20 µl with molecular grade ddH_2O. Reactions underwent amplification in a PCR machine under the following conditions: An initial denaturation step for 1 minute at 95^0C, followed by 30 cycles at 95^0C for 30 s (denaturation), 50-65^0C for 30 s (annealing) and 72^0C for 1 minute per kb (extension). A final extension of 10 minutes was also carried out at 72^0C prior to storing at 4^0C.

2.2.2.3 Agarose gel electrophoresis

Electrophoresis was used to separate and visualize DNA. Molecular grade agarose (Bioline) and 1x TBE buffer was used to make 1% gels containing ethidium bromide. 5x loading buffer (Bioline) was added to DNA samples and 20 µl was placed into each well of the agarose gel. 5 µl of the 1 kb hyperladder (Bioline) was used as a molecular marker. Samples were run at 110 V for 35-40 minutes in a Peqlab electrophoresis tank while submerged in 1x TBE buffer. DNA bands were visualized under UV on a Gene flash visualization machine.

2.2.2.4 Extraction of genomic DNA

Cells were grown to confluency in HL5 medium (100 µg/ml penicillin and 100 µg/ml streptomycin) within a 10 cm tissue culture dish. Cells were re-suspended and pelleted by centrifuging at 437 g for 3 min. KK2 buffer (16.2 mM KH_2PO_4, 4 mM K_2HPO_4. pH 6.8) was used to re-suspend and wash the cells prior to a second centrifugation step. KK2 was removed and the DNA extracted from the cell pellet using either a DNeasy® Blood and tissue kit (Qiagen) as per manufacturer's instructions or by phenol chloroform extraction. For phenol chloroform extraction the cell pellet was re-suspended in 1 ml of NP40 lysis buffer, pH 8.0, vortexed briefly and then incubated for 10 min at room temperature. Samples were microfuged at 1500 g for 8 min at 4^0C. NP40 lysis buffer was removed and discarded and the cell pellet re-suspended in

200 µl TE buffer (Qiagen). 4 µl of RNaseA (100 mg/ml) and 7 µl 10% SDS was added and incubated at room temperature for 2 min. 15 µl of proteinase K (600 U/ml) was added and the sample incubated at 55^0C for 1 hour. All subsequent procedures were carried out on ice as much as possible to avoid DNA degradation. One volume of phenol:chloroform:isoamyl alcohol (25:24:1) was added, inverted for 20 sec to mix and then microfuged at 16,000 g for 5 min at 4^0C. The upper aqueous layer was transferred to a fresh 1.5 ml tube ensuring that no interphase protein was carried over. A further one volume of phenol: chloroform: isoamyl alcohol was added to the upper aqueous phase that was transferred to a fresh tube and microfuged at 16,000 g for 5 min at 4^0C. The upper aqueous layer was removed, placed into a fresh tube and one volume of chloroform was added and inverted by hand for 20 sec. Samples were microfuged at 16,000 g for 5 min at 4^0C and the top layer transferred to a fresh tube. Samples were ethanol precipitated (see 2.2.2.5), re-suspended in 50 µl of Sigma water, nano-dropped to establish concentration and yield and run on a 1 % gel to check for any DNA degradation.

2.2.2.5 Ethanol precipitation

DNA samples were treated with 1 µl Glycogen (20 µg/µl), 3 M sodium acetate (0.1x volume of sample) and 100 % ice cold ethanol (2x sample volume). Samples were placed at -20^0C for 30 min to precipitate the DNA. Following DNA precipitation samples were microfuged at 16,000 g for 15 min at 4^0C and the supernatant was discarded. 150 µl of 70 % ethanol was added and samples microfuged at 16,000 g for 2 min at 4^0C. DNA was air dried and then re-suspended in 50 µl sigma water.

2.2.2.6 RNA extraction and gene expression analysis via RT-PCR

Cells ($1x10^7$) were grown in a 10 cm dish in liquid media, harvested once confluent and then washed twice with KK2 buffer (16.2 mM KH_2PO_4, 4 mM K_2HPO_4. pH 6.8). Total RNA was extracted using an RNeasy mini-kit (Qiagen) and DNAse treated with a DNA-free kit (Ambion). cDNA was created using a First Strand cDNA Synthesis Kit (Thermo scientific), as per manufacturer's instructions using 2 µg total RNA. cDNA created from each cell line was amplified in a subsequent PCR reaction with primers designed complementary to the 3' region of the gene of interest (See Table 2.1 for primer sequences) then visualised by gel electrophoresis.

2.2.2.7 Bacterial transformation

Top10 (ampicillin selection) or TOP10F' (blue/white selection) chemically competent cells (Invitrogen) were thawed on ice and 2 µl of plasmid reaction placed directly into the cells as per manufatureres protocol. Contents were mixed by gently stirring with a pipette tip. Samples were incubated on ice for 30 minutes and then heat shocked for 1 minute at 42°C. Samples were immediately transferred to ice and left for 3 minutes. 250 µl LB containing no selection was added to each vial and then shaken at 37°C for 1 hour at 225 rpm in a shaking incubator. For ampicillin selection 200 µl of each transformation was spread upon LB agar plates containing 100 µg/ml ampicillin. For blue white selection 200 µl of each transformation was spread upon LB agar plates containing 100 µg/ml ampicillin along with X-gal and IPTG. Plates were allowed to dry briefly in the hood and then incubated for 16 hours at 37°C.

2.2.2.8 Plasmid Extraction from Bacterial Cells

Bacterial cells were grown in 5 ml liquid broth overnight at 37^0C on a shaker at 220 rpm. Samples were vortexed and 2 ml transferred to a fresh 2 ml Eppendorf tube. Bacteria cells were pelleted by centrifuging at 17,000 g for 2 min at room temp and the supernatant discarded. Plasmids were extracted from the cell pellet by using either a GeneJet® plasmid mini-prep kit (Thermo Scientific) or by using a non-commercial method. For the non-commercial method 200 µl of P1 solution (10 ml 0.5 M EDTA, 90 g glucose, 6.25 ml 2 M Tris. pH 8.0, made up to 500 ml) was added to the pelleted cells and vortexed. 200 µl of P2 solution (50 ml 10% SDS, 20 ml NaOH, made up to 500 ml) was added to each sample, mixed by inverting and incubated for 5 min at room temp. 200 µl of P3 solution (147 g potassium acetate, 57.5 ml glacial acetate acid, made up to 500 ml) was added to each sample, mixed by inverting and centrifuged at 17,000 g for 15 min at room temperature. Supernatant was removed and placed into a fresh Eppendorf tube containing 420 µl of Isopropanol, then vortexed. Samples were centrifuged at 17,000 g for 15 min at room temp and the supernatant discarded. 500 µl of 80% ethanol was added and mixed by vortexing. Samples were centrifuged at 17,000 g for 5 min at room temp and the supernatant discarded. Tubes were placed in a dry heat block for 10 min at 50^0C to dry DNA. DNA was re-suspended in 30µl Sigma water and mixed by vortexing.

2.2.2.9 Disrupted gene identification using iPCR

Isogenic mutant cell lines were grown in HL5 media within a 10 cm plate to confluency. Genomic DNA was extracted using phenol: chloroform extraction (see 2.2.2.4). Genomic DNA was digested with the RsaI restriction enzyme for one hour at 37°C and purified by ethanol precipitation (see 2.2.2.5). Digested fragments were then ligated (circularized) by treating with T4 DNAse ligase as per manufaturers instructions overnight at 16°C. The resultant circularized genomic DNA fragments underwent PCR using primers (11 and 12, fig2.1) complementary to the blasticidin resistance gene initially inserted into the disrupted gene. Using this method the blasticidin resistance gene and a small sequence of the disrupted gene was amplified. The amplified PCR product was cloned into the pCR 4-Topo® vector (Invitrogen) and transformed into chemically competent *E. coli* cells (see 2.2.2.7). Transformants were selected for using x-gal blue/white selection. *E. coli* colonies possessing the transformed vector were grown overnight at 37°C in shaking LB broth containing ampicillin 10 µg/ml. A mini-prep was carried out to isolate the topo vector (see 2.2.2.8) and an EcoRI digestion performed to confirm the presence of the amplified PCR product. Mini-prep samples were sequenced and the disrupted gene sequence identified by aligning against the *D. discoideum* genome using a BLAST search (https://blast.ncbi.nlm.nih.gov).

2.2.2.10 Quantitative polymerase chain reaction (qPCR)

Total RNA was extracted from cell lines using an RNeasy mini-kit (Qiagen). cDNA was created from 2 µg total RNA using a first strand cDNA synthesis kit (Thermo scientific) and treated with DNase (Life technologies). Primers were designed complementary to the 3' region of the gene and expression levels quantified by qPCR using SYBR® Green Jump Start™ Taq Ready Mix, as per manufactures instructions. Amplification was carried out on a ThermoFisher thermal cycler. Because of Ig7 is constitutively expressed it was deemed suitable for use to normalize gene expression. Ig7 produces the mitochondrial large subunit rRNA. Gel electrophoresis was also used to confirm primer specificity.

2.2.2.11 Construction of knock out vectors

Fragments of approximately 500 bp in size were amplified by PCR from both the 5' and 3' regions of the gene being ablated using wild type (AX3) gDNA. Primers contained restriction sites to allow the consecutive cloning of the fragments into the pLPBLP knock out vector (See table 2.1

for primer sequences and restriction sites used). Following amplification the fragments were purified by use of a QIAquick® PCR purification kit (Qiagen). Both the purified PCR fragments and pLPBLP were cut using complementary restriction enzymes (see table 2.1) and then heat inactivated as per manufacturers recommendations. The 5' or 3' fragment was then ligated into the linearized pLPBLP vector using T4 DNA ligase (Fermentas) as per manufacturer's instructions, with an insert: vector molar ratio of 3:1. Ligation reactions were incubated for 2 hours at 22°C then overnight at 16°C. Reactions were terminated by heat inactivating at 70°C for 10 minutes before being transformed into chemically competent *E. coli* cells (see 2.2.2.7). Transfected *E. coli* cells were plated onto SM agar plates containing 20 µg/ml ampicillin and incubated for 16 hours at 37°C. Resistant colonies were selected for and grown in liquid broth containing ampicillin 10 µg/ml for 16 hours at 37°C. The pLPBLP plasmid was extracted from each bacterial colony (see 2.2.2.8) and the presence of the cloned pLPBLP vector confirmed by restriction digest. Following the successful integration of one fragment into pLPBLP, the second fragment was then also cloned in and confirmed. pLPBLP containing both the 5' and 3' fragments was then digested using the two outermost restriction sites (Fig 2.1 and table 2.1), then ethanol precipitated (see 2.2.2.5) and transformed into wild type (AX3) cells via electroporation.

2.2.2.12 Screening for knockout cell lines

AX3 cells were transfected with the linearized pLPBLP knockout construct by electroporation and grown under 10 µg/ml blasticidin selection in a 96 well plate. Once a well upon the plate became confluent the resistant cells were detached and spun down in a PCR tube. The media was removed and 48 µl of lyse B buffer (10 mM TRIS-HCL pH 8.3, 50 mM KCL, 2.5 mM $MgCl_2$, 0.45% TWEEN, 0.45% NP40) and 2 µl Proteinase K (600 U/ml) was added. Cells were incubated at room temperature for 5 minutes and then incubated at 95°C to denature the proteinase K. The resulting cell lysate was subsequently used in PCR analysis to identify the homologous integration of the respective knockout construct at both the 5' and 3' regions of the gene (Adley et al, 2006). Primers were designed for each gene that would produce six diagnostic fragments unique to the homologous transformants (See fig 2.1 and table 2.1). PCR primer combinations were designed that would identify homologous integrants. Three primer combinations targeted both the 5' and 3' regions of the knockout construct. Of the three primer combinations used; one pair (genomic control) consisted of a primer located in the gDNA outside of the target genes knockout construct sequence coupled with a primer located within the genes knockout

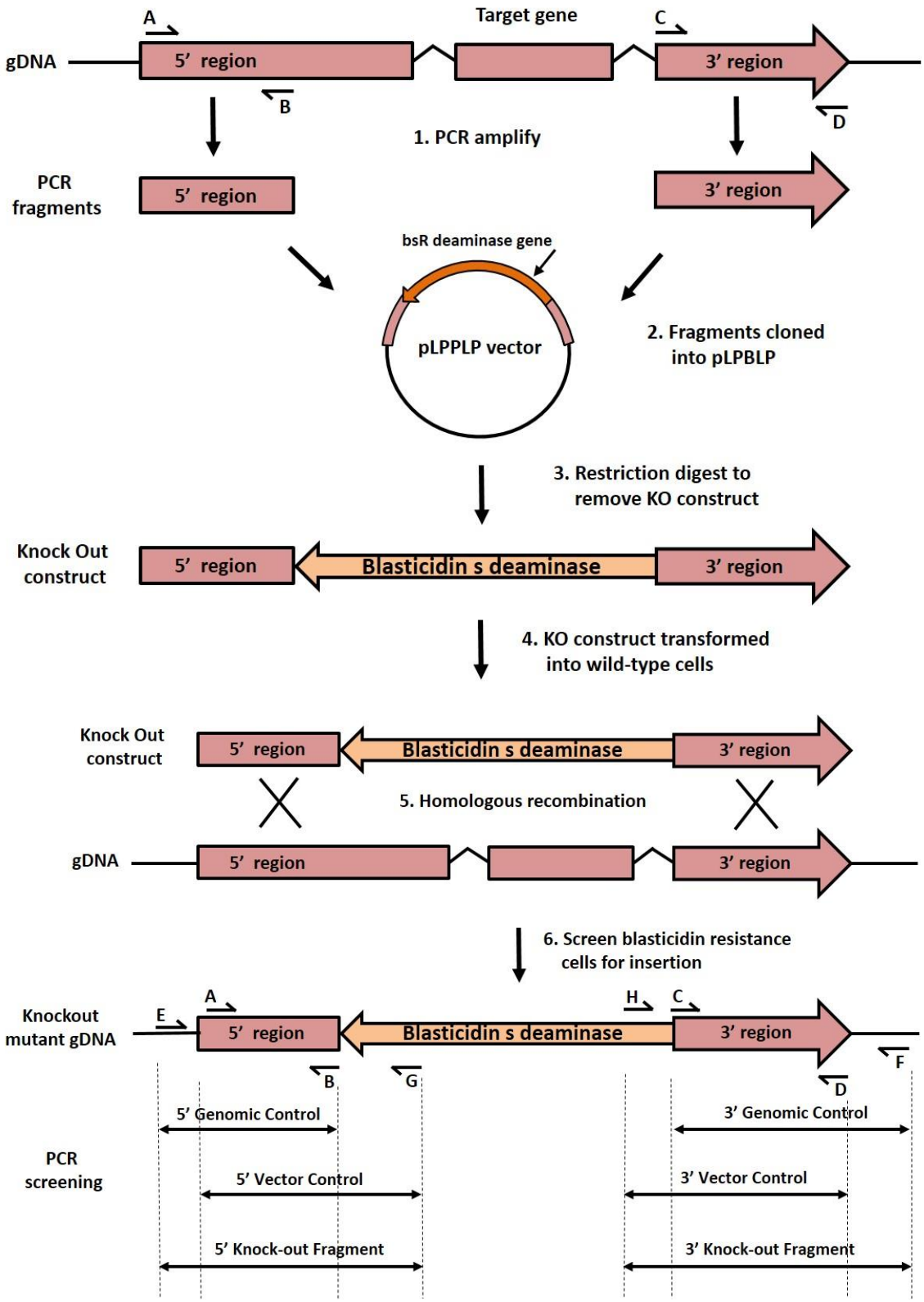

Figure 2.1 Schematic showing an overview of the gene ablation and screening method adopted for creating gene knock out cell lines. (1) Two fragments of approximately 500 base pairs from the 5' and 3' regions of a target gene were amplified by PCR. (2) These PCR fragments were then cloned into the pLPBLP vector at multiple cloning sites immediately flanking the *blasticidin s*

deaminase gene. Both PCR fragments were cloned into pLPBLP with their reading frames in the opposite orientation to the *blasticidin s deaminase* gene. (3) Both the *blasticidin s deaminase* gene and flanking fragments (KO construct) were restriction digested from the pLPBLP vector and (4) transformed into *D. discoideum* AX3 cells (5) to allow homologous recombination. (6) Cells were selected for blasticidin resistance and screened. Resistant cells were PCR screened using primers that would produce a diagnostic knock out band in homologous integrants. Further primers were used as controls, producing both genomic control bands and vector control bands. The primers are coded A-H so that they can be linked with the primer sequences in table 2.1.

construct sequence. The second pair (vector control) consisted of a primer found within the target genes knockout sequence coupled with a primer located within the BsR gene sequence. The third pair (knockout fragment) consisted of a primer found within the gDNA outside of the target genes knockout construct sequence coupled with a primer located within the BsR gene sequence. Homologous integration of the BsR gene into the genomic target gene was achieved if the genomic control, vector control and knockout fragment bands were detected in both the 5’ and 3’ regions of a screened cell line. Only the two genomic bands would be detected in untransformed AX3 wildtype cells. Transformants producing all six PCR fragments were spread onto SM agar plates containing *R. planticola* and allowed to form plaques. Individual isogenic colonies were picked and grown within HL5 media containing 10 µg/ml blasticidin. PCR analysis was carried out a second time to confirm homologous integration, followed by RT-PCR to confirm loss of gene expression.

2.2.2.13 Re-introduction of an ablated gene by use of an extra chromosomal plasmid for the creation of an N-terminal or C-terminal tagged fusion protein.

Primers complementary to the extremities of the 5' and 3' region of each gene were used to amplify the entire gene coding sequence from cDNA of AX3 wildtype cells. In the case of C-terminal tagged genes the stop codon within the 3’ primer sequence was omitted. Primer sequences possessed restriction cut sites immediately outside the gene sequence for ligation into the empty vector. The codon ATA was also incorporated into the primer sequence flanking the restriction site to aid restriction digest (For restriction sites and primer sequences see table 2.1). The extra chromosomal plasmid pTX-GFP-MCS was used for N-terminal tagging, while pDXA-MCS-RFP was used for C-terminal tagging. PCR amplification was carried out using a proof reading polymerase (Q5 high fidelity DNA polymerase, NEB, M0491S). The PCR products and empty vectors were cut using the appropriate restriction enzymes and separated by gel

electrophoresis. The PCR products were gel extracted (QIAquick® Gel Extraction kit, Qiagen) and then ligated into the expression vectors. The gene was sequenced to confirm that no mutations were introduced. Following successful sequencing the plasmid was transformed into the null cell line and selected for using G418 10 µg/ml. Gene expression within transformants was confirmed by RT-PCR.

2.2.3 Restriction enzyme mediated integration (REMI) mutant library screen

REMI library cells were received as a gift from Professor Harwood, Cardiff University and Professor Thomson, Manchester University. The REMI library was created as detailed in Kuspa, 2006, whereby AX2 cells were transfected with the DpnII restriction enzyme, and linearized DNA containing the blasticidin resistance gene. Because the transfected DNA was linearized with BamHI the presence of DpnII allows the incorporation of the DNA into the genome at compatible cohesive sites created by DpnII. The amount of DpnII restriction enzyme transfected into cells typically results in a single copy insertion event occurring with only one gene being disrupted. Where the insertional sequence disrupts depends upon the location of the DpnII restriction site. Any insertional mutants identified within the REMI screen could be a result of independent targeting of the same gene, but only if the gene has more than one DpnII restriction sites. However, it is more likely that multiple hits for the same gene during the screening process are a result of multiple clonal lines from the same original targeting event. REMI library cells were grown in shaking HL5 medium for two days prior to screening. Cells ($2.5x10^4$ in 2 ml of media) were added to each well of a 6 well plate and allowed to adhere for 20 minutes. The media from each well was replaced with media containing either 4.88 µM CBDA, 9.47 µM CBD or 11.79 µM CBDV. These concentrations were used as dose response curves plotted for cell proliferation over a one week period showed that these concentrations greatly impeded cell proliferation, but not quite inhibit cell proliferation. Cells were screened in triplicate for resistance over a three week period, maintained at 22°C with the media replaced every two days. Resistant mutant colonies were isolated and transferred to SM plates containing *R. planticola*. Isogenic mutant cell lines were established from individual colonies on the bacterial plates and grown to confluency in a 10 cm culture in HL5 media. Cells ($1.0x10^4$ in 495 µl of media) were added to each well of a 24 well plate and re-tested for sensitivity to the cannabinoids at 4.88 µM CBDA, 9.47 µM CBD or 11.79 µM CBDV.

2.2.4 Bioinformatics analysis

In order to identify homologous proteins across species the Protein BLAST function of the Basic Local Alignment Search Tool (BLAST) was used from the National Centre for Biotechnology Information (NCBI) (https://blast.ncbi.nlm.nih.gov). Primary protein sequences were obtained from uniprot.org and cross referenced against the non-redundant protein sequences (nr) database of BLAST using the blastp (protein-protein BLAST) program selection. The following parameters were also used to carry out the search: matrix=blosum62, threshold=0.01.

Molecular Evolutionary Genetic Analysis version 6.06 (MEGA6) was used to carry out phylogenetic analysis of each protein studied. To produce phylogenetic trees the neighbour-joining statistical method was performed with the bootstrap method test of phylogeny with 500 replications.

2.2.5 Preparation of *D. discoideum* cells for Vitamin B12 analysis by ELISA

Cells were grown to a density of ~2.0×10^6 cells per ml in shaking culture (HL5 medium). Cells were washed twice with sterile KK2 (16.2 mM KH_2PO_4, 4 mM K_2HPO_4. pH 6.8) then re-suspended in minimal media (Formedium). During the wash stage cells were pelleted by centrifugation at 500 g for 3 minutes. Re-suspended cells were split into a number of 100 ml or 500 ml flasks, each flask containing 10 ml or 50 ml minimal media respectively with cells at a final density of 2.0×10^6 cells per ml. Flasks were treated with either CBD to a final concentration of 1.89 µM (IC_{50} for *D. discoideum* wildtype cell proliferation) or vehicle alone. This concentration was used as it was previously shown (Fig 3.2a) to have a negative effect, inhibiting cell proliferation by 50%. Flasks were shaken for 12 hours at 120 rpm on an Innova 4330 refrigerated shaker, maintained at 22°C. Following the 12 hour incubation, cells was removed and washed twice in KK2. Cells were pelleted, snap frozen, and stored at -80°C. Immediately prior to B12 analysis the pelleted cells were re-suspended in 200 µl of sterile KK2 buffer containing added protease inhibitors. Samples underwent five freeze thaw cycles from -80°C on dry ice to 30°C on a heat block. Samples were centrifuged at 5000 g for 5 minutes and the cell lysate removed. The cell lysate was further centrifuged at 21,000 g for 10 minutes and the lysate collected for ELISA analysis. A commercial ELISA kit specific for Vitamin B12 was used (Immunolab Vitamin B12 ELISA, Immunolab GmbH).

2.2.6 Ultra cold Methanol Fixation and Immunofluorescence

The fixation method used was adapted from that described by Hagedorn *et al*, 2006. Glass coverslips were prepared by submersion in 50% nitric acid for 2 hours at room temperature in a fume hood. Coverslips were routinely swirled and splashing avoided. The nitric acid was decanted and the coverslips washed 10 times in 100% ethanol and stored in a beaker with a lid containing 100% ethanol until use. Coverslips were placed into the base of a 12 well plate and cells in liquid media added and allowed to adhere overnight. A 100 ml glass beaker containing 50 ml of methanol was cooled in a $^{-}$80°C freezer for 2 hours immediately prior to cell fixation. To fix the cells, the cooled beaker of 100% methanol was placed onto the lid of a petri dish and this then placed onto dry ice. Coverslips containing adhered cells were briefly dabbed on tissue to remove excess media then plunged into the methanol at an angle of 15 degrees from the vertical with the cells facing upwards. Fixed coverslips were then placed into a rack at the base of the ultra-cold methanol beaker for 30 minutes. If more than one coverslip was being fixed at any one time forceps were rinsed between coverslips with ddH_20 to prevent unwanted removal of cells. Following an incubation of 30 minutes, coverslips were removed and plunged 4 times into a beaker of room temperature 1x PBS, pH 7.2 (VWR) at an angle of 15 degrees from the vertical with the cells facing upwards. Cells were then blocked for 30 minutes by inverting each coverslip onto a 50 µl drop of 1x PBS containing 5% BSA on a piece of para-film. Excess blocking agent was removed by dabbing on tissue paper and the coverslip then inverted onto a second 50 µl drop of 1x PBS containing 5% BSA and primary antibodies. Primary antibodies used

2 µg of mouse anti-porin (70-100-1, Developmental studies hybridoma bank) and a 1:1,000 dilution of rat anti-RFP (6G6 anti-red rat mAb, Chromatek). After incubating with primary antibodies for 1 hour, the coverslips were washed twice by placing coverslips in the well of a 12 well plate containing 3 ml of 1x PBS and soaked for 5 minutes each time. Coverslips were not swirled to avoid loss of fixed cells. Coverslips were then inverted onto a 50 µl drop of 1x PBS containing 5% BSA and secondary antibodies. Secondary antibodies used were a 1:1,000 dilution of goat ant-mouse (Alexa fluor® 568 goat anti-mouse IgG, Life technologies) and a 1:1,000 dilution of rabbit anti-rat (Alexa fluor® 488 rabbit anti-rat IgG, Life technologies). For the blocking and antibody incubations the para-film containing coverslips were placed on top of wet tissue in a sealed container. Coverslips were washed twice in 1x PBS as before, plus a final wash in ddH_2O to remove excess salt. All coverslips were mounted onto glass slides using Fluoromount-G™, with DAPI (Invitrogen) and allowed to adhere overnight in the dark. Fluorescent images were obtained using an Olympus IX71 stage microscope with fluorescent capabilities.

2.2.7 Western Blot

Electrophoresis gels for western blot were cast, consisting of a 12.5% resolving gel (2.125 ml acrylamide, 0.95 ml Tris 8.8, 1.825 ml dH_20, 100 µl 10% SDS, 50 µl 10% APS, 5 µl TEMED) and stacking gel (212.5 µl acrylamide, 78.75 µl Tris 6.8, 0.938 µl dH_20, 12.5 µl 10% SDS, 12.5 µl 10% APS, 3.75 µl TEMED). Cell samples ($2x10^6$ in 100 µl KK2, pH 6.8) were prepared by incubating with 20 µl loading buffer (0.8 ml 2 M Tris pH 6.8, 3 ml 80% glycerol, 5 ml 10% SDS, 1.25 ml β-mercaptoethanol, 0.001 g bromophenol blue) at 95^0C for 10 minutes. 10 µl of cell lysate samples and 3 µl of marker (Page ruler™ prestained protein ladder, Thermo Scientific) were loaded into the stacking gel and run at 70 V in running buffer (3 g Tris base, 14.5 g glycine, 10 ml 10% SDS, made up to 1L) for 30 minutes then 100 V for a further 40-60 minutes. The electrophoresis gel was removed and the protein transferred to a PVDF membrane by running at 400 mA within ETB buffer (3 g Tris base, 14.4 g glycine, 1 ml 10% SDS, made up to 1 L) for 1 hour. The PVDF membrane was removed and blocked with 5% BSA in PBST (0.1% Tween20 in 1 L 1x PBS), pH 7.4 for 1 hour. After blocking, the PVDF membrane was incubated overnight at 4^0C with either an anti-RFP primary antibody (6G6 anti-red mouse mAb, Chromatek) at a 1:1,000 dilution or an anti-GFP primary antibody (3H9 anti-GFP rat mAb, Chromatek) at a 1:1,000 dilution. Loading control primary antibodies used included a mouse anti-calnexin (270-390-2, Developmental studies hybridoma bank) at a 1:500 dilution or the conjugated (primary and secondary) streptavidin antibody (Streptavidin Alexa Fluor™ 680 conjugate, Invitrogen) at a 1:10,000 dilution. The membrane was rinsed twice in 1x PBS and then underwent three 10 minute washes in PBST on a bench top shaker. After the wash steps either an anti-mouse secondary antibody (goat anti-mouse IR Dye™, Li-Cor) or an anti-rat secondary antibody (anti-rat IR Dye™, Li-Cor) was added to 5 ml of 5% BSA in PBST at a dilution of 1:10,000 and the membrane submersed for 1 hour at room temperature. The PVDF membrane was rinsed twice in 1x PBS and then underwent three 10 minute washes in PBST (1x PBS, 0.05% TWEEN 20. pH 7.4) on a bench top shaker. Protein bands were visualised upon a LI-COR Odyssey CLx machine using odyssey software.

2.2.8 Predicted protein structural analysis

The primary protein sequences for both *D.discoideum* and *H. sapiens* proteins were obtained from uniprot.org. Protein tertiary structure was predicted using Phyre2 (Protein Homology and Analogy Recognition Engine V2.0) in the intensive modelling mode (Kelley *et al*, 2015). Phyre2 uses homology modelling to predict a proteins tertiary structure based upon the proteins

primary sequence and an experimentally gotten three dimensional structure of a homologous protein. By utilising the 100,000 experimentally determined protein structures stored in the protein data bank, Phyre2 compares the sequence of interest with these known structures to predict the sequences tertiary structure (http://www.sbg.bio.ic.ac.uk/phyre2).

2.2.9 Protein quantification for normalization

Cell lysate protein levels were quantified by comparing against a bovine serum albumin (BSA) known standard using a commercial kit (Pierce™ BCA Protein Assay Kit, Thermo Scientific). The procedure was carried out as per the manufacturer's directions, using the microplate method of the protocol throughout. Absorbance was measured at 560 nm using a colorimetric plate reader.

2.2.10 GC-MS and NMR analysis methods

2.2.10.1 Preparation of Ax3 parental and *gcvh1* null cells for gas chromatography mass spectrometry (GC-MS) analysis following CBD treatment

Both the parental and *gcvH1* null cell lines were grown to a density of ~2.0×10^6 cells per ml in shaking culture (HL5 medium). Cells were washed twice with sterile KK2 (16.2 mM KH_2PO_4, 4 mM K_2HPO_4. pH 6.8) then re-suspended in minimal media (Formedium). During the wash stage cells were pelleted by centrifugation at 500 g for 3 minutes. Re-suspended cells were split into a number of 100 ml flasks, each flask containing 10 ml minimal media with cells at a final density of 2.0×10^6 cells per ml. Flasks were treated with either CBD to a final concentration of 1.89 µM or vehicle alone. This concentration was used as it is known to inhibit *D. discoideum* cell proliferation by 50%. Flasks were shaken for 12 hours at 120 rpm on an Innova 4330 refrigerated shaker, maintained at 22°C. Following the 12 hour incubation, 9 ml of cells were removed and washed twice in KK2. Cells were pelleted, snap frozen, and stored at -80°C. Immediately prior to GC-MS analysis the pelleted cells were re-suspended in 200 µl of sterile KK2 buffer containing added protease inhibitors. Samples underwent five freeze thaw cycles from -80°C on dry ice to 30°C on a heat block. Samples were centrifuged at 5000 g for 5 minutes and the cell lysate removed. The cell lysate was further centrifuged at 21,000 g for 10 minutes and the lysate collected for GC-MS analysis.

2.2.10.2 Extraction of plasma from *Rattus norvegicus* for amino acid analysis using gas chromatography mass spectrometry (GC-MS)

Venous blood samples from untreated animals were collected into heparin containing vials and cooled immediately on ice (performed by Dr Ursu). Plasma was separated from blood by centrifugation at 2000 g for 15 minutes. Plasma extraction was carried out within 30 minutes of collection. Samples were aliquoted and stored at -80°C for further processing.

2.2.10.3 GC-MS analysis of amino acid levels within either cell lysate or plasma samples

40 µl of sample (cell lysate or plasma) was spiked with 10 µl of DL-4-chlorophenylalanine (internal standard) followed by 10 µl of the reducing agent Tris (3-hydroxypropyl) phosphine 23 mM. Samples were gently mixed and left to stand for 1 minute before adding 40 µl trichloroacetic acid 0.6 M. Contents were vigorously vortexed for 15 s and allowed to stand for 3 minutes. Vortexing was briefly repeated and samples were centrifuged at 3000 g for 10 minutes at 4°C. Approximately 80 µl of supernatant was removed and transferred to a clean glass culture tube. After adding 40 µl of a 3:1 1-propanol:pyridine mixture, 130 µl of a reactive organic phase was added. The organic phase contained a 10:3:1 mixture of 2,2,4-Trimethylpentane, Butyl acetate and Propyl Chloroformate. Samples were vortexed vigorously for 30 s, centrifuged at 3000 g for 10 s and the upper organic phase was aspirated off and used in GC-MS analysis. All steps were carried out in borosilicate glass. GC-MS was carried out on an HP5890 Series II chromatograph interfaced to an HP5972 MSD mass spectrometer. 2 µL samples were injected in splitless mode (injector temp 250°C, purge delay 1.0 min) on a J&W DB5 column (30 m x 0.25 mm dia x 0.25 u film) using helium as the carrier gas at constant flow of 30 cm/s. The column oven was programmed from 90°C (2 min) to 330°C at 7.5 deg/min, the GC-MS interface temperature was 300°C. Retention times and mass spectra of derivatives of amino acids were determined in TIC mode and confirmed to be in agreement with library and literature data. Quantitative analysis was carried out in SIM mode using p-chlorophenylalanine as an internal standard. Data were manually processed to yield peak areas of amino acid derivatives relative to that from the internal standard. Sample amino acid values were normalized to the protein content of each sample using a Pierce® BCA protein assay kit (Thermo Scientific).

2.2.10.4 NMR sample preparation

The samples were provided in methanol suspension. A two phase extract was generated using a mixture of methanol, chloroform and water in the volume ratio of 4:4:2.85. The aqueous phase containing water soluble low-molecular-weight endogenous metabolites was transferred to microtubes and solvents were removed using a vacuum concentrator Eppendorf AG (Eppendorf, Hamburg, Germany), 8 h at 60°C. Samples were then reconstituted in 70 µL of NMR phosphate buffer (pH 7.4) 0.2 M (80% of D_2O, 20% of H_2O, 3-(Tri-methylsilyl)propionic-2,2,3,3- d_4 acid (TSP) (Sigma-Aldrich) 1 mM, serving as NMR reference, vortexed for 10 s and centrifuged at 10 000 rpm at 4°C for 10 min. 60 µL of resulting supernatant was pipetted into a 1.7 mm capillary tube (Bruker, UK) for NMR analysis (Preparation of NMR samples was carried out by Joanna Boberska).

2.2.10.5 NMR analysis

The NMR experiment was carried out in the Chemical Analysis Facility (CAF, University of Reading) using a Bruker AV700 NMR instrument equipped with a 5 mm inverse cryoprobe. A standard 1 dimensional nuclear Overhauser effect spectroscopy (NOESY) experiment was performed on each sample, using a standard pre-set pulse sequence (noesypr1d, 90°C pulse length at 9.25 µs, total acquisition time of 2 s and water pre-saturation during relaxation delay of 5 s). All samples were analysed at 297ºK and free induction decay (FID) was acquired on 19607 data points (spectral width 9803.9 Hz) using 512 scans (8 dummy scans). FID was then zero filled to 64k points and line broadening of 0.6 Hz was applied prior to fast Fourier transform (FFT). Phase and baseline corrections were performed manually using MestreNova software (version 10.0m MestreLab Research). NMR spectra were referenced to TSP peak at 0 ppm. The processed spectra were digitalised and imported in Matlab (version R2017a) for statistical analysis. The residual water signal was removed (δ 4.58–5.009), as well as signals produced by residual methanol (δ 3.35–3.37) and ethanol (δ 1.17–1.205 and δ 3.64–3.68). Relative spectra were mean centred and scaled to unit variance. Principal component analysis (PCA) was used to display the largest source of variation among samples. Orthogonal Projection to Latent Structure (OPLS) analysis was then performed (no orthogonal components used). NMR spectra were used as a matrix of variables X, and CBD treatment was used as a predictor Y (1=treatment, 0=no treatment). This analysis was used to construct a model identifying metabolites differentiating between the two groups. The predictive ability of the model was evaluated by the goodness of fit (R^2Y), showing what percentage of variation is explained by the model, and goodness of

prediction (Q^2Y), constituting the percentage of Y predicted after 7-fold cross-validation (NMR analysis was carried out by Joanna Boberska, Reading University (method provided by Joanna Boberska)).

2.2.11 Primary neuron methods

2.2.11.1 Primary neuron extraction and cell culture (Performed by Dr Simona Ursu)

Prior to neuron extraction, 6 well plates were UV treated for 20 minutes then each well coated with 0.5 ml of Poly-D-lysine (PLD, Sigma P7886). PLD was used at a final concentration of 100 µg/ml in sterile borate buffer (1.24 g boric acid, 1.9 g borax, made up to 400 ml with pH 8.5 water). Plates were left to incubate for either 5 hours at 37^0C or overnight at 4^0C. Following incubation with PLD, plates were washed three times with sterile dH_20 and left to dry in a 37^0C incubator. The extraction of primary hippocampal neurons was carried out in accordance with the Home office regulations in appliance with the Animals Scientific Act 1986. Female Sprague Dawley rats were housed individually and mated at the age of 4-5 months. At day 18 of gestation rats were culled by concussion and the embryos immediately removed and placed into ice cold hanks balanced salt solution (HBSS, Thermo Fisher Scientific). The hippocampi were manually removed from all the embryos and temporarily placed into ice cold HBSS. Once all embryos had been processed the HBSS solution was removed and replaced with filter sterilised dissociation media (4.5 ml Dulbeccos modified eagles medium containing 500 µg DNase, 0.5 ml TrypLA™ express enzyme (1x), 2 ml penstrep (100 units/ml penicillin final concentration; 100 µg/ml streptomycin final concentration), 2 ml glutamax, made up to 5 ml) pre-warmed to 37^0C. Cells were gently triturated to produce a homogenous solution then pelleted by centrifugation at 1500 g for 3 minutes. Cells were re-suspended in DMEM pre-warmed to 37^0C, then plated onto 6 well plates at a density of $5x10^6$ cells per well, and left overnight at 37^0C and 5% CO_2. The DMEM was replaced with 2 ml of filter sterilised modified neurobasal medium pre-warmed to 37^0C, containing a B27 supplement (1 ml/50 ml), penstrep (100 units/ml penicillin, 100 µg/ml streptomycin) and glutamax. Neurons were stored at 37^0C and 5% CO_2 and allowed to mature for 21 days with modified neurobasal media being monitored and topped up when necessary.

2.2.11.2 The primary hippocampal neurons acute treatment model

Primary hippocampal neurons from the embryos of female Sprague-Drawley rats were treated with both CBD and PTZ to determine whether CBD had any effect in negating any effects induced

by PTZ. Previous studies have shown that treatment of primary cultured neurons with 5 mM pentylenetetrazole (PTZ) induces bursting activity in a manner similar to hippocampal slices (Sugaya et al., 1989). This method has therefore been used as a simple procedure in which to induce seizure like activity within primary neurons *in vitro* (Chang et al, 2013). The neurobasal media of the intervention groups were treated with CBD at a final concentration of 1.89 µM taken from a 100 mM stock of CBD in DMSO. This concentration was used as it falls within the physiologically range in which epileptiform local field potentials are reduced (Jones *et al*, 200). Neurons were placed in an incubator for 1 hour at 37°C and 5% CO_2. Following the 1 hour incubation, 5 mM PTZ was added to the neurobasal media and plates returned to the 37°C incubator for a further 20 minutes at 5% CO_2. This concentration was used as previous studies have shown PTZ to be effective within neuronal cells at this concentration (Chang *et al*, 2013). The media was aspirated and cells washed three times in ice cold 1x PBS, pH 7.2. Cells were lysed for 10 minutes using 200 µl RIPA buffer, pH 8.0 (Sigma) with added 0.1% n-octyl-beta-glucopyranoside (Apollo Scientific), and protease inhibitors (Sigma). The lysate was then collected using a cell scraper. Samples were immediately frozen at $^{-}$80°C and used in subsequent GC-MS and protein analysis.

2.2.12 Lithium-pilocarpine treated rat models with CBD

Male Wistar rats 3-4 weeks old (45-80 g) were housed at a constant temperature of 21°C and humidity of 50±10 %, with ad libitum access to both food and water. On day one animals were treated with lithium chloride (127 mg/kg), administered via subcutaneous injection. Twenty four hours later animals were treated with α-methyl scopolamine (1 mg/kg) subcutaneously, followed by pilocarpine (25 mg/kg) 30 minutes later. Intervention groups were also treated with CBD (200 mg/kg) orally, prior to receiving lithium chloride. Our collaborators used this concentration of CBD as previous studies by them have shown this concentration to be effective in this animal model. Animals were then sacrificed by cervical dislocation and blood collected in heparinized tubes (Fisher Scientific, UK). Plasma was obtained by centrifuging blood for 15 minutes at 2,000 g in a refrigerated centrifuge. GC-MS was then used to analyse the plasma samples for amino acid content. All animal handling and their treatment was carried out by our collaborators at Reading University. Sample preparation and GC-MS analysis was carried out by ourselves. All animal experiments were conducted under licence, following UK Home Office regulations (Animals (Scientific Procedures) Act, 1986).

2.2.13 Creation of a homozygous *Scn1a* mouse model, treatment with CBD and analysis of its plasma with GC-MS

A homozygous *Scn1a* knock-out mouse model was developed by breeding from 129S-Scn1a$^{tm1Kea/Mmjax}$ heterozygote (+/-) mice (Jackson Laboratory, USA). A loxP-flanked neomycin resistance cassette replaced the first coding exon of *Scn1a*. The *Scn1a*$^{-/-}$ mice were confirmed to be epileptic and displayed the characteristics of Dravet syndrome. Mice homozygous for the null *Scn1a* allele exhibited tremors, ataxia and seizures, however death occured by postnatal day 16. Epileptic animals (*Scn1a*$^{-/-}$) were treated with either CBD (100 mg/kg) twice daily via subcutaneous injections or with vehicle alone (ethanol: kolliphor®: 0.9% saline at a 2:1:17 ratio). This concentration of CBD was used as previous studies have shown positive results in epileptic animal models using this concenntration (Devinsky *et al*, 2014). Healthy wildtype animals also underwent a treatment of vehicle alone. All animals were treated from day 8 postnatal to day 25, or until death, whichever came sooner. Animals were housed at a constant temperature of 21°C and humidity of 50±10 %, with ad libitum access to both food and water. At day 25 animals were sacrificed by cervical dislocation and blood collected in heparinized tubes (Fisher Scientific, UK). Animals killed by seizures during the treatment period were not used for analysis. Plasma was obtained by centrifuging blood for 15 minutes at 2,000 g in a refrigerated centrifuge and then used in GC-MS analysis. The creation of homozygous *Scn1a* animals and their treatment was carried out by our collaborators at Reading University. Sample preparation and GC-MS analysis was carried out by ourselves. All animal experiments were conducted under licence, following UK Home Office regulations (Animals (Scientific Procedures) Act, 1986).

2.2.14 Creation of a heterozygous *Scn1a* mouse model, treatment with CBD and the analysis of its plasma and whole brain samples with GC-MS

A heterozygous *Scn1a* mouse model was developed by breeding 129S-Scn1a$^{tm1Kea/Mmjax}$ heterozygote (+/-) male mice (Jackson Laboratory, USA), with female C57BL/6 mice (Charles River, UK). The 129S-Scn1a$^{tm1Kea/Mmjax}$ mice contained a loxP-flanked neomycin resistance cassette replacing the first coding exon of *Scn1a.* The *Scn1a*$^{+/-}$ mice were confirmed to be epileptic and displayed the characteristics of Dravet syndrome. The *Scn1a*$^{+/-}$ mice exhibited tremors, ataxia and seizures, but differed in phenotype to the homozygous strain in that they only experienced a 50% lethality by one month of age. Epileptic animals (*Scn1a*$^{+/-}$) were treated with either CBD (100 mg/kg) twice daily via subcutaneous injections or with vehicle alone (ethanol: kolliphor®: 0.9% saline at a 2:1:17 ratio). This concentration of CBD was used as

previous studies have shown positive results in epileptic animal models using this concentration (Devinsky *et al*, 2014). Healthy wildtype animals also underwent a treatment of vehicle alone. All animals were treated for 6 weeks from day 8 postnatal. Animals were housed at a constant temperature of 21°C and humidity of 50±10 %, with ad libitum access to both food and water. Immediately following treatment animals were sacrificed by cervical dislocation and blood collected in heparinized tubes (Fisher Scientific, UK). Plasma was obtained by centrifuging blood for 15 minutes at 2,000 g in a refrigerated centrifuge. Whole brain samples were also removed and flash frozen in liquid nitrogen, then stored at -80°C until used for GC-MS analysis. Immediately prior to GC-MS analysis the brain samples were re-suspended in 200 µl of artificial cerebral spinal fluid (in mM: NaCl 119, KCl 2.5, $MgSO_4$ 1.3, $CaCl_2$ 2.5, $NaH2PO_4$ 1, $NaHCO_3$ 26.2 and glucose 16.6) containing added protease inhibitors. Re-suspended brain samples were homogenized in a cold room for 2 minutes on a Qiagen tissue lyzer II machine using 3 mm tungsten beads. Homogenized samples then underwent five freeze thaw cycles from -80°C on dry ice to 30°C on a heat block. Samples were centrifuged at 5000 g for 5 minutes and the lysate removed. The lysate was further centrifuged at 21,000 g for 10 minutes and the lysate collected for GC-MS analysis. The creation of *Scn1a*$^{+/-}$ animals and their treatment was carried out by our collaborators at Reading University. Sample preparation and GC-MS analysis was carried out by ourselves. All animal experiments were conducted under licence, following UK Home Office regulations (Animals (Scientific Procedures) Act, 1986).

No	Primer function	Primer sequence (5' to 3')	Cut site	Link to figure 2.1	Product size
1	gcsH 5' RT-PCR forward	ATAGAATTCATGGCTTTAAGAGTTG			(2) 537
2	gcsH 3' RT-PCR reverse	TATGGATCCTTCTTCAATTG			(1) 537
3	redA 5' OE forward	ATAAGATCTATGAAATCAGTAATTTTAAAACC	BglII		(4) 1887
4	redA 3' OE reverse	GTGTCTAGATTAAAACCAAACATCTTTTTG	XbaI		(3) 1887
5	redA 5' RT-PCR primers	CTTCTGCTCGTCCACCAATC			(6) 459
6	redA 3' RT-PCR primers	CTCTACACTGCTTTCTCTCGTG			(5) 459
7	Ig7 5' RT-PCR primers	GTACTGTGAAGGAAAGATGAAAA			(8) 559
8	Ig7 3' RT-PCR primers	GAGCGCTAAGGTCCATAGG			(7) 559
9	lmbd2b 5' OE forward	ATAGAGCTCATGTCAAGTAATACTACAAC	SacI		(10) 2390
10	lmbd2b 3' OE reverse	ATATCTAGATTACTTTTTATTTTTACGGCC	XbaI		(9) 2390
11	5' bsR primer sequence	AAAAAGATAAAGCTGACCCGAAAG		G	n/a
12	3' bsR primer sequence	TCAAATAATAATTAACCAACCCAAG		H	n/a
13	gcvh1 5' OE forward	ATAGAATTCATGTTAAAAACCTTAAGATTTGGAAC	EcoRI		(14) 422
14	gcvh1 3' OE reverse	ATAGGATCCATGTTCTTTAATATATTCATCATATTGG	BamHI		(13) 422
15	lmbd2b 5' RT-PCR primers	TATAAGCTTGGAATCATTACATTGTACTAG			(16) 460
16	lmbd2b 3' RT-PCR primers	TTAGGTACCCAATTTCTCATAGATTACCAT			(15) 460
17	mtrr 5' OE forward	ATAGAGCTCATGACAGAACCTGTTGCTG	SacI		(18) 1526
18	mtrr 3' OE reverse	ATATCTAGATTAAGACCAAACATCTAAGATATATC	XbaI		(17) 1526
19	mtrr 5' RT-PCR primers	GCACCAAGAGACTATGTATTAGTTC			(20) 686
20	mtrr 3' RT-PCR primers	CTAACACCAACAGCCATACC			(19) 686
21	gcvH1 5' RT-PCR primers	CTTAAGATTTGGAACAAGAGCATTC			(22) 422
22	gcvH1 3' RT-PCR primers	CTTTAATATATTCATCATATTGGGC			(21) 422
23	mtrr 5' genomic forward	GACAGAACCTGTTGCTGCAC		E	(25) 687/ (11) 786
24	mtrr 5' vector forward	ATAACTAGTGAGCAGCTGGTAGTAGTTCATCC	SpeI	A	(11) 742
25	mtrr 5' genomic reverse	ATAGGATCCCATATTCTTCTTTACCCTCAATTG	BamHI	B	(23) 687
26	mtrr 3' genomic forward	ATACCATGGCACCACTTTCAATGGAGAAAG	NcoI	C	(28) 658
27	mtrr 3' vector reverse	ATAGGTACCCTTGAACATATCCACATGTTGG	KpnI	D	(12) 730
28	mtrr 3' genomic reverse	CTAACACCAACAGCCATACC		F	(26) 658/ (12) 833
29	redA 5' genomic forward	ATGAAATCAGTAATTTTAAAACC		E	(31) 476/ (11) 575
30	redA 5' vector forward	ATAACTAGTATTAGGTGCTGGTGTAAC	SpeI	A	(11) 537
31	redA 5' genomic reverse	ATACTGCAGCTAAATTGAATATGTGAA	PstI	B	(29) 476
32	redA 3' genomic forward	ATACCATGGCACGTTACTATAGTATTG	NcoI	C	(34) 647
33	redA 3' vector reverse	ATAGGTACCGTAAAGCTTGAGCATC	KpnI	D	(12) 772
34	redA 3' genomic reverse	TTAAAACCAAACATCTTTTTG		F	(32) 647/ (12) 822

35	gcvH1 5' genomic forward	CTTAAGATTTGGAACAAGAGCATTC		E	(37) 324/ (11) 423
36	gcvH1 5' vector forward	ATAACTAGTGCCAAAAGAAACTTTTGTACTAGATAC	SpeI	A	(11) 380
37	gcvH1 5' genomic reverse	ATACTGCAGCTGATTCAACTACTGTTATTGGTTG	PstI	B	(35) 324
38	gcvH1 3' genomic forward	ATACCATGGCGATATCTATATTCCAATGGATGG	NcoI	C	(40) 381
39	gcvH1 3' vector reverse	ATAGGTACCCTTTGGAATTGATCAGTTTTGC	KpnI	D	(12) 518
40	gcvH1 3' genomic reverse	CTTTAATATATTCATCATATTGGGC		B	(38) 381/ (12) 556

Table 2.1 Primer sequences, their function and incorporated restriction sites. Table 2.1 shows the primer sequences and their function, as well as any restriction sites incorporated for cloning (underlined). The PCR product sizes are also shown with their respective partnered primer, given in brackets. No product size is shown next to the 5' and 3' bsr primers as these are paired with multiple primers and the size is given next to these. Primers used to create a knockout cell line have also been given a link (A-H) to figure 2.1 in order to show an overview of each primers function during the gene ablation process.

Chapter 3

Mutant Screen

3.1 Introduction

Understanding the molecular mechanisms by which newly developed pharmaceuticals operate is an important aspect of validation, but can be difficult to achieve. One important step in identifying the mechanism of drug action is the identification of genes involved in its resistance. These genes can be identified by performing genetic screens, in which mutants are screened for resistance or sensitivity to the drug in question. Obviously, such studies are difficult to perform within higher organisms due to the sheer number of genes that need to be mutated, however the use of simple biomedical models such as *D. discoideum* has already proved effective (Cocorocchio et al, 2015., Otto et al, 2016., Cocorocchio et al, 2018). *D. discoideum* possess a wide range of signalling pathways and proteins that are highly conserved and common to higher organisms such as mammals, of which many have been linked to human disease (Muller-Taubenberger et al., 2013, Williams et al., 2006).

The ability to identify genes involved in drug regulation within *D. discoideum* has been facilitated by the use of restriction enzyme mediated integration REMI libraries (Kuspa and Loomis, 1992). These involve the random insertion of a construct containing the blasticidin resistance gene into the *D. discoideum* genome thereby randomly disrupting the expression of individual genes. By screening these libraries it is possible to identify genes responsible for the regulatory effect of pharmaceuticals and other compounds (Robery et al, 2011., Robery et al, 2013., Waheed et al, 2014., Cocorocchio et al, 2015., Otto et al, 2016., Cocorocchio et al, 2018). A number of studies have used this method to elucidate the mechanism behind treatments for both psychiatric disorders (Williams et al., 2002, Williams et al., 1999) and epilepsy (Boeckeler et al, 2006., Xu et al, 2007., Shimshoni et al, 2007., Chang et al, 2012., Elphick et al, 2012., Cunliffe et al, 2015). Many of these studies have then directly translated their findings across to mammalian models and validated (Williams et al, 2002., Williams et al, 1999., Chang et al, 2014., Chang et al, 2015., Chang et al, 2013., Breen et al, 2004., Eickholt et al, 2005., Elphick et al, 2012., Waheed et al., 2014). Providing the cannabinoids have a recognizable trait within *D. discoideum* it should be possible to screen mutant libraries and identify genes that may potentially be involved in the cannabinoids mechanism of action.

In this chapter we investigate the effects that CBD, CBDA and CBDV have upon *D. discoideum* cell growth, and show that all three cannabinoids negatively affect growth in a dose dependant manner. We also investigate the affects that CBD, CBDA and CBDV have upon multicellular development under starvation conditions, and show that none of the cannabinoids effect development. Using the growth inhibitory effect we then screened a REMI library for insertional

mutants that displayed resistance to CBD, CBDA and CBDV. We show that the disruption of four independent genes of interest across 20 mutants infers resistance, with some inferring multiple cannabinoid resistance.

3.2 Results

3.2.1 The effects of cannabidiol (CBD), cannabidiolic acid (CBDA) and cannabidivarin (CBDV) treatment upon *D. discoideum* cell proliferation

In order for us to screen a mutant library and identify genes involved in cannabinoid resistance we first needed to identify a recognizable effect of cannabinoids within *D. discoideum*. Previous studies using mammalian cell lines have shown that cannabinoids can have a negative effect upon cell proliferation (McAllister *et al*, 2011, Solinas *et al,* 2013). As such, we first characterized the effects that CBD, CBDA and CBDV has upon wild type (AX3) cell proliferation within axenic media. Wild type (AX3) cells were treated with either CBD, CBDA or CBDV from 100 mM stocks in DMSO at a range of concentrations from 0 to 20 µM. Cell density was first measured after 72 hours, followed by every 24 hours. It was found that CBD (Fig 3.1a), CBDA (Fig 3.1b) and CBDV (Fig 3.1c) all affect wild type (AX3) cell proliferation in a dose dependent manner, with a total block at 20 µM. Dose response curves of normalised cell density against the Log (concentration) of CBD, CBDA and CBDV were then plotted using the rate of cell growth within the exponential phase (Fig 3.2). The dose response curves were then used to calculate the IC_{50} values and 95% confidence intervals for each cannabinoid. It was found that CBD has an IC_{50} value of 1.89 µM with a 95% confidence interval of 1.61 µM to 2.21 µM (Fig 3.2a). CBDA was found to have an IC_{50} value of 0.89 µM with a 95% confidence interval of 0.75 µM to 1.05 µM (Fig 3.2b), while CBDV was shown to have an IC_{50} value of 2.16 µM with a 95% confidence interval of 1.80 µM to 2.60 µM (Fig 3.2c). In terms of affecting wild type (AX3) cell proliferation, CBDA was found to be the most potent cannabinoid while CBDV was found to be the least potent (Fig 3.2d). These data show that all three cannabinoids have a recognizable effect within *D. discoideum* and may therefore form the basis of a mutant screen for resistance to CBD, CBDA and CBDV.

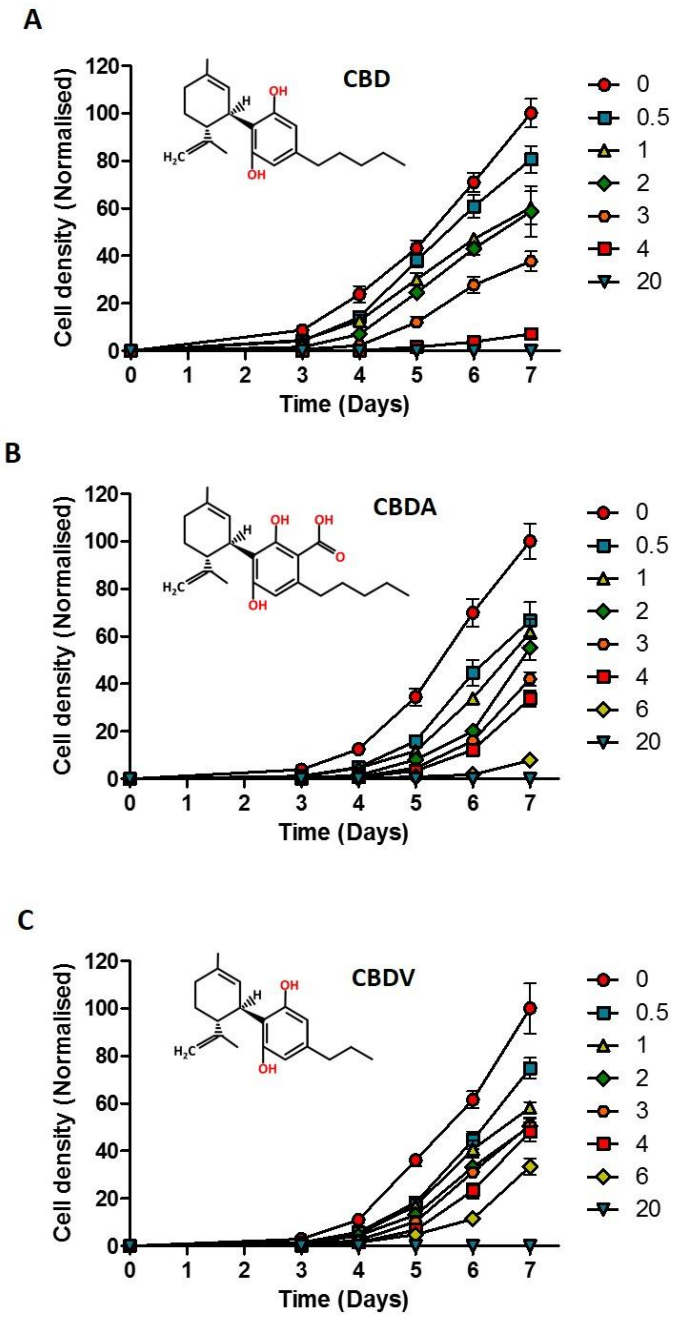

Figure 3.1. Cell proliferation effects of cannabidiol (CBD), cannabidiolic acid (CBDA) and cannabidivarin (CBDV) upon *D. discoideum* cells (Growth curves). Wild type (AX3) cells were treated with (A) CBD, (B) CBDA and (C) CBDV for seven days under a range of concentrations from 0 to 20 µM. Cell density was measured between days three and seven. Cell growth was shown to be blocked at 20 µM for all cannabinoids (n = 6-9, experiments were repeated).

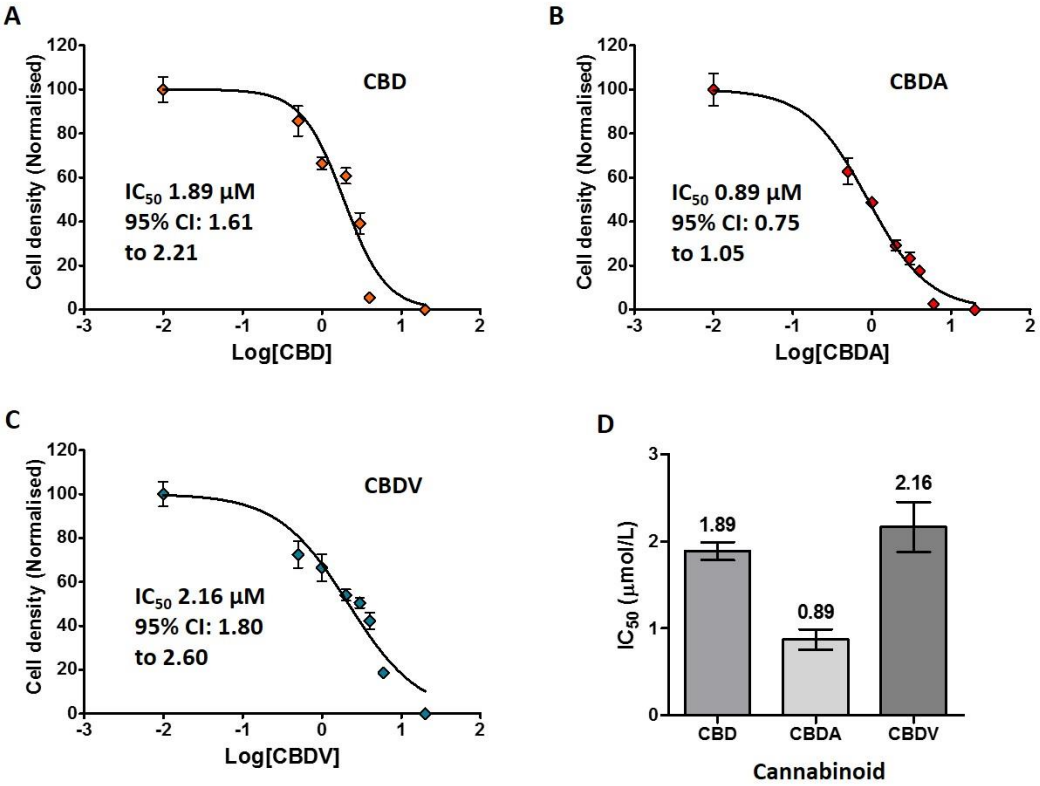

Figure 3.2. Cell proliferation effects of cannabidiol (CBD), cannabidiolic acid (CBDA) and cannabidivarin (CBDV) upon *D. discoideum* (Dose response curves). Dose response curves of normalised cell density against the Log (concentration) of CBD, CBDA and CBDV was used to calculate their IC_{50} values with 95% confidence intervals. (A) CBD was shown to have an IC_{50} value of 1.89 µM with a 95% confidence interval of 1.61 µM to 2.21 µM. (B) CBDA was shown to have an IC_{50} value of 0.89 µM with a 95% confidence interval of 0.75 µM to 1.05 µM. (C) CBDV was shown to have an IC_{50} value of 2.16 µM with a 95% confidence interval of 1.80 µM to 2.60 µM. (D) CBDA was found to be the most potent cannabinoid in inhibiting wild type (AX3) cell growth, while CBDV was the least potent. (n = 6-9).

3.2.2 Developmental and toxicity effects of cannabidiol (CBD), cannabidiolic acid (CBDA) and cannabidivarin (CBDV) upon *D. discoideum.*

As well as the growth inhibition effect of CBD, CBDA and CBDV we also investigated if these cannabinoids affected cellular development in *D. discoideum*. Other anti-convulsants such as valproic acid (VPA) have been shown to inhibit *D. discoideum* development at therapeutic concentrations, and arrests development at the mound stage (Terbach *et al,* 2011). We therefore placed wild type (AX3) cells upon nitrocellulose filters soaked in saline buffer containing either 20 µM CBD, CBDA or CBDV. Nitrocellulose filters were also soaked in DMSO

alone (positive control), or 1mM VPA (negative control). Cells were stored in a humid environment under starvation conditions to allow aggregation and the formation of fruiting bodies. After 24 hours the cells treated with CBD, CBDA and CBDV were confirmed to have undergone complete development forming mature fruiting bodies (Fig 3.3). The DMSO alone control was also confirmed to have undergone complete development (Fig 3.3) while the VPA treated cells were found to be arrested at the mound stage (Fig 3.3). These data suggest that CBD, CBDA and CBDV all regulate a molecular target involved in cell proliferation but not in cellular development. These data also suggest that within *D. discoideum* CBD, CBDA and CBDV act through a specific molecular effect, and not through a general toxic effect. To confirm that 20 µM CBD, CBDA or CBDV does not have a toxic effect upon AX3 wildtype cells, the media from the cell proliferation experiment (see 3.2.1) was replaced after day 7 with media lacking cannabinoids. Following removal of the cannabinoids cells underwent further proliferation (Fig 3.3b).

3.2.3 Mutant Screen

The growth inhibitory effect of CBD, CBDA and CBDV was used to screen a Restriction Enzyme Mediated Integration (REMI) mutant library for insertional mutants that displayed a resistance to cannabinoids. REMI library cells were treated with the cannabinoids at concentrations predicted to inhibit cell proliferation by 80% and screened for resistance over a three week period. In total 20 independent mutants were identified that exhibited resistance to one of the cannabinoids. These mutants were isolated from the rest of the library and isogenic colonies created. All 20 isogenic cell lines were then further tested for resistance and confirmed to be resistant to the appropriate cannabinoid. Due to the sheer number of cell lines being tested, resistance at this stage was confirmed by visual inspection rather than quantification.

The precise location of the REMI insert within the genome of each mutant was identified using either the inverse PCR technique (Keim *et al*, 2004) or whole genome sequencing. At first inverse PCR was used, and identified the insertion points for 13 insertional mutants. DNA from the remaining 7 unidentified mutants were sent to one of our collaborators at University College London (UCL) and the disrupted genes identified using whole genome sequencing. In total four genes were disrupted with the REMI insert across all 20 of the insertional mutants (Fig 3.4 and Table 3.1). One of these genes was *sibB* (Dicty base ID: DDB_G0288103), found disrupted within exon 3 of three insertional mutants and was found to be resistant to both CBD, CBDA and CBDV. Another of these genes was *reductaseA* (Dicty base ID: DDB_G0293904), found to be disrupted

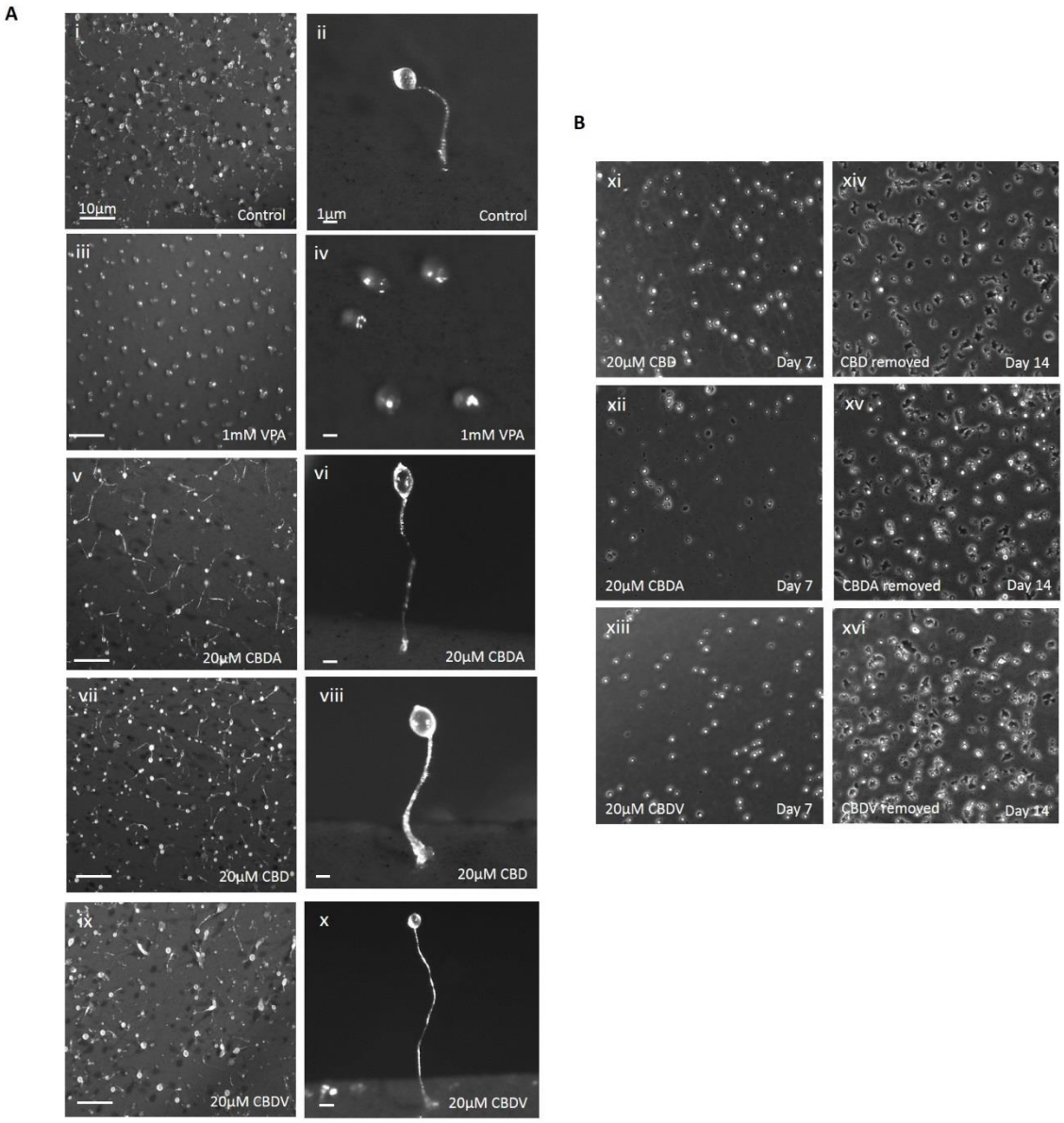

Figure 3.3. Developmental and toxicity effects of cannabidiol (CBD), cannabidiolic acid (CBDA) and cannabidivarin (CBDV) upon *D. discoideum*. (A) Wild type (AX3) cells were developed upon nitrocellulose filters under starvation conditions with either (I, ii) DMSO only control (iii, iv) 1 mM valproic acid, (v, vi) 20 µM CBDA, (vii, viii) 20 µM CBD, (ix, x) 20 µM CBDV. (B) Following 7 days treatment with (xi) 20 µM CBD, (xii) 20 µM CBDA, (xiii) 20 µM CBDV the media was replaced containing no cannabinoids (xiv, xv, xvi) to test whether cannabinoids had a toxic effect upon AX3 wildtype cells.

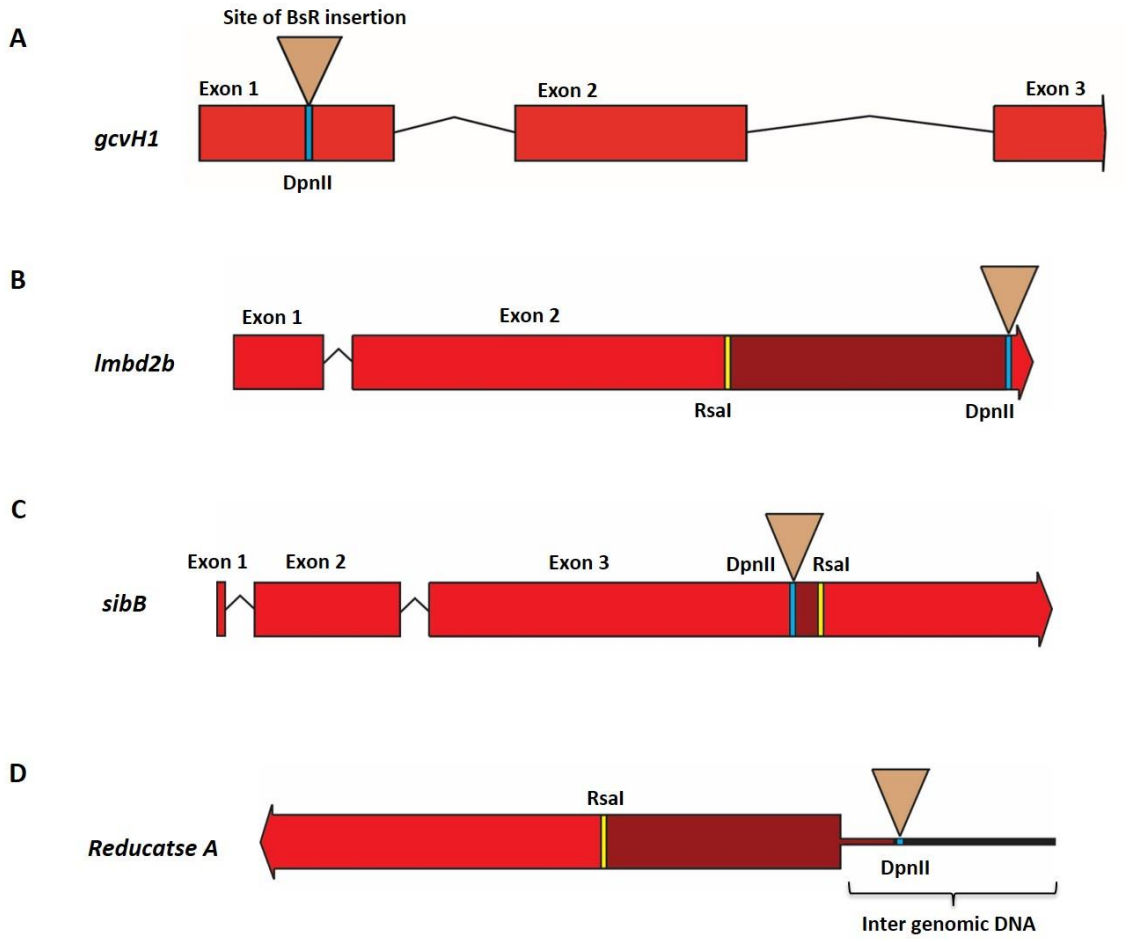

Figure 3.4. Disrupted genes identified in the mutant screen. A mutant screen identified (A) *gcvH1*, (B) *lmbd2b*, (C) *sibB* and (D) *redA* which when disrupted with the REMI insert inferred a resistance to CBD, CBDA or CBDV. The exact location in which each gene was disrupted is shown by the brown wedge and blue regions (DpnII restriction sites). Yellow regions indicate the RsaI restriction site used to identify the insertion site via inverse PCR.

185 base pairs upstream of the open reading frame within four insertional mutants, displaying resistance to CBD. The *lmbd2b* gene (Dicty base ID: DDB_G0281669) was found disrupted in 12 mutants within exon 2, and displayed resistance to both CBD and CBDA. Lastly, the gene *gcvH1* (Dicty base ID: DDB_G0287773), found to be disrupted within exon 1 of one insertional mutant, displaying resistance to CBD only. The multiple hits for each gene were found to be multiple clonal lines from the same original targeting event. These data show that the disruption of these four genes infers a resistance within *D. discoideum* to at least one cannabinoid, with some genes inferring a resistance to multiple cannabinoids.

Gene name	Gene size	Dictybase ID	Mutants identified	Location of disruption	Functional consequence
sibB	5,777 bp	DDB_G0288103	3	Exon 3	3,900 bp truncated protein
redA	1,896 bp	DDB_G0293904	4	Upstream Inter genomic DNA	6.25 fold reduced expression
lmbd2b	2,373 bp	DDB_G0281669	12	Exon 2	2,307 bp truncated protein
gcvH1	440 bp	DDB_G0287773	1	Exon 1	87 bp truncated protein

Table 3.1 Resistance screen of a Restriction enzyme mediated integration (REMI) library identified a number of genes, which when disrupted inferred a resistance to cannabinoids. Table shows the gene name and the corresponding Dicty base ID number for each disrupted gene. The number of mutants found with a particular gene disrupted and in which region of the gene is also shown.

3.3 Discussion

3.3.1 Integrin type proteins may play a role in cell cycle progression within *D. discoideum*

By testing the sensitivity of CBD, CBDA and CBDV treatment upon the proliferation and development of wild type (AX3) cells we have shown that these cannabinoids affect only cell proliferation and not development. This suggests that these cannabinoids do not have a general toxic effect but act through distinct molecular mechanisms. Similarly, the concentrations at which these cannabinoids affect cell proliferation is comparable to those that have been shown

to block seizure activity in mammalian models (Jones et al., 2012, Jones et al., 2010, Klein et al., 2017). By using this recognizable effect upon cell proliferation it was possible to screen a mutant library for insertional mutants that displayed resistance to these cannabinoids, and then identify genes which may shed light upon the mechanisms involved. By using this approach four genes of interest were identified.

Of the four genes identified *sibB* was not investigated any further. Previous studies have shown that SibB belongs to a family of five proteins within *D. discoideum* that have structural similarities to the mammalian Integrin family (Cornillon et al, 2006). It is widely accepted that Integrins are involved in the adhesion of cells to the extracellular environment, as well as being involved in cell proliferation and cell migration (Moreno-Layseca and Streuli, 2014). Studies into the Sib family of proteins within *D. discoideum* have shown the cytosolic component of Sib proteins to interact with the protein Talin (Cornillon *et al*, 2006), which itself has been shown to have a significant role in Integrin mediated adhesion (Calderwood, 2004). Similarly, the same study demonstrated the role that Sib proteins have in cellular adhesion, specifically through the regulation of phagocytosis (Cornillon *et al*, 2006).

Interestingly, studies have shown that cell cycle progression within mammalian cells is regulated by the adhesion of Integrins to the extracellular environment, and their cooperation with growth factors (Walker and Assoian, 2005). Specifically, Integrins are important for cell cycle progression to proceed from G1 to the S phase. The cooperation of Integrins with growth factors and the extracellular matrix promotes the accumulation of adaptor proteins such as Talin, Focal adhesion kinase, Paxillin and GTPases (Walker and Assoian, 2005). These adaptor proteins then initiate downstream signaling cascades that lead to the regulation of cyclins and the transcription of genes involved in cell proliferation (Schwartz and Assoian, 2001., Moreno-Layseca and Streuli). The resistance to CBD seen in the SibB mutant may therefore be a result of changes to adhesion or cell cycle regulation and progression, while the loss of SibB allows cells to proliferate quicker. However, previous studies have shown that complete loss of cell adhesion generally results in cell cycle arrest (Stoker et al, 1968). Unlike most mammalian cells however, *D. discoideum* do not require adhesion to an extracellular matrix to promote cell division, as exemplified by their ability to divide exponentially within shaking culture (Fey *et al,* 2007). It is possible that the role of SibB is not to facilitate adhesion to the extracellular matrix but instead to other cells, thereby identifying levels of cell density within a population. If SibB is involved in this role then SibB mutant cells may continue to proliferate beyond the confluent point at which normal cell proliferation would halt, thereby giving the impression of cell resistance.

Another possibility is that CBD interacts with SibB extracellularly. This interaction with CBD may prevent the SibB proteins from carrying out normal function of promoting cell proliferation, which maybe dose dependent. This interaction maybe the underlying cause of why we observe sensitivity in wild type (AX3) cells. The apparent resistance to CBD in the mutant SibB cell line maybe because the molecular target of CBD is no longer present, and cell cycle arrest is no longer occurring. Studies using mammalian cancer cell lines have shown that CBD inhibits both cell proliferation (McAllister *et al*, 2011, Solinas *et al,* 2013) and metastasis (Nabissi *et al*, 2016). The effects of CBD upon these cell lines may be a result of interaction with Integrins, thereby resulting in cell cycle arrest and inhibiting cell adhesion and consequently cell migration. With regards to treating cancer, CBD may play a significant role through the regulatory effects of Integrins and should be further investigated, however it is unlikely that the anticonvulsant effects of CBD operate through this pathway. As it was unlikely that CBD elicits its anticonvulsant effects through Integrins, and because the other genes seemed more relevent it was decided not to investigate SibB any further.

3.3.2 The RedA, Lmbd2b and GcvH1 proteins may all have links to the one carbon cycle

Interestingly, the other three genes identified in the mutant screen may possibly be linked to the same molecular pathway. As such further investigation was carried out into these, which will be expanded upon over the next three chapters. Briefly, the RedA protein which was disrupted in 4 mutants is an oxidoreductase enzyme responsible for catalysing the transfer of electrons from one molecule to another (Anzenbacher, P. and Anzenbacherová, 2001). It appears in *D. discoideum* that it is an ancestral protein of both the cytochrome P450 reductase and Methionine Synthase reductase enzymes, discussed in more detail within chapter 4. The P450 family of proteins are involved in xenobiotic removal (Anzenbacher, P. and Anzenbacherová, 2001), while Methionine Synthase is a key enzyme within the one carbon cycle, responsible for the production of methionine (Ducker and Rabinowitz, 2017). The LMBD2b protein which was disrupted within 12 mutants is a multi-pass transmembrane protein of which certain members of this family of proteins are responsible for the transport of cobalamin (Buers *et al*, 2016). Cobalamin is an essential co-factor for Methionine Synthase in order to allow the one carbon cycle to proceed. Lastly, GcvH1 which was found disrupted in one mutant is a mitochondrial protein, and is a key component of the glycine cleavage system. The glycine cleavage system is responsible for the metabolism of glycine within cells (Kikuchi *et al*, 2008, Okamura-Ikeda *et al*, 1987), and is linked to the one carbon cycle through its use of

tetrahydrofolate, which is concomitantly produced by Methionine Synthase with methionine. Because of the possible link between RedA, Lmbd2b and GcvH1 through the one carbon cycle we decided to investigate these further, of which each is investigated in more detail within chapters 4, 5 and 6 respectively.

In this chapter we have shown that CBD, CBDA and CBDV affect wild type (AX3) cell growth in a dose dependent manner, while having no effect upon multicellular development. This contrast suggests a non-toxic effect, and that the cannabinoids act through a distinct molecular mechanism. By using this growth inhibitory effect we screened an insertional mutant library for mutants that displayed a resistance to the cannabinoids. Using iPCR or whole genome sequencing we identified the disrupted gene in each mutant, and identified four genes of interest that infer cannabinoid resistance; these being *redA*, *lmbd2b*, *gcvH1* and *sibB*. Investigation into each gene resulted in *sibB* being ruled out for further investigation because of its likely involvement in cell cycle control. The remaining three genes however were all identified as possibly having an involvement in the regulation of the one carbon cycle. As such *redA, lmbd2b* and *gcvH1* were all investigated further and the findings from each are presented in the next three chapters.

Chapter 4

Reductase A

4.1 Introduction

By carrying out a genetic screen of a restriction enzyme mediated integration (REMI) mutant library a number of genes were identified that inferred resistance to the cannabinoids cannabidiol (CBD), cannabidiolic acid (CBDA) and cannabidivarin (CBDV) when disrupted. Four genes of interest were identified across 20 resistant mutants with one of these being the *redA* gene. The *redA* gene (DDB_G0293904) was identified in four independent mutants displaying resistance to CBD, and was found to be disrupted 185 base pairs upstream of the genes open reading frame.

The Reductase A (REDA) protein belongs to the oxidoreductase family of enzymes responsible for the transfer of electrons from NADPH to an acceptor molecule or protein. This then facilitates the reduction of further molecules such as cobalamin or xenobiotics (May and Padgett, 1983). The REDA protein has been shown to have about 50% similarity to the human NADPH-cytochrome P450 reductase enzyme (Gonzalez-Kristeller *et al,* 2008) involved in the reduction of cytochrome P450 (Pandey and Flück, 2013). The role of the Cytochrome P450 family of proteins is to facilitate the removal of xenobiotics (Anzenbacher and Anzenbacherová, 2001). This is achieved through the transfer of a reactive group to the xenobiotic thereby allowing subsequent conjugation and eventual removal (Zanger and Schwab, 2013). In order for Cytochrome P450 to transfer this reactive group it needs to remain in a reduced state, achieved through Cytochrome P450 reductase (POR) activity. We therefore initially hypothesized that REDA may have a role in xenobiotic removal, and that the disruption upstream of its open reading may increase *redA* expression and ultimately CBD degradation.

In this chapter we carry out phylogenetic analysis and show REDA to be an ancestral protein of both Cytochrome P450 reductase and Methionine Synthase reductase (MTRR). We further compare expression levels of *redA* within the REDA insertional mutant to wild type (AX3) cells and determine whether expression of *redA* is effected by the REMI insertion. We show that *redA* is expressed ~6.25 fold less in the mutant compared to wild type (AX3) cells. We also determine whether the ablation of REDA from wild type (AX3) cells produce a CBD resistant phenotype, comparable to the REMI mutant. We show that the ablation of REDA from wild type (AX3) cells increases sensitivity to CBD. We also investigate whether the resistance observed in the REMI mutant was a result of reduced MTRR activity, as REDA appears to be an ancestral protein of both POR and MTRR. We therefore ablated MTRR from wild type (AX3) cells and quantify CBD resistance. We show that the ablation of MTRR also increases sensitivity to CBD.

4.2 Results

4.2.1 Quantitative PCR (qPCR)

When identifying the regions disrupted in the REMI mutants resistant to cannabinoids (chapter 3), it was found that the insertion point for the REDA mutant was located 185 base pairs upstream of the open reading frame. Because of the potential role that REDA may have in xenobiotic degradation we set out to investigate the expression levels of *redA* within the REMI mutant. If REDA is involved in xenobiotic degradation then we would expect to find its expression levels elevated. To investigate this, both the REDA mutant and wildtype (AX3) cells were grown under the same conditions and their total RNA extracted and used for qPCR analysis. Primers for both *redA* and the mitochondrial large subunit rRNA gene (*Ig7*) were confirmed to be specific for their relevant genes by gel electrophoresis (Fig 4.1a). Quantitative PCR showed that expression levels of the *redA* gene within the REDA mutant were significantly ($P<0.01$) lower than those found in wildtype (AX3) cells (Fig 4.1b). These data suggest that the disruption of the mutant genome at this site infers a resistance to CBD by reducing *redA* expression. It is therefore unlikely that the resistance observed in the REMI mutants are a consequence of CBD degradation.

4.2.2 Ablation of *redA* from AX3 wildtype cells

We hypothesized that if resistance to CBD occurs through reduced REDA levels, then the ablation of REDA may infer a greater resistance. To investigate this we created an independent *redA*$^-$ mutant. This independent mutant was created by ablating a large portion of *redA* from the genome of wildtype (AX3) cells using homologous recombination. A knock out construct specific for *redA* was created by cloning the 5' and 3' terminal ends of *redA* into the pLPBLP knockout plasmid using the SpeI/PstI and NcoI/KpnI restriction sites (Fig 4.2a) (see 2.2.2.11 for method). The knock out construct was designed so that an 861 bp region of the gene would be removed, resulting in a non-functioning protein being produced. A series of double digests were performed on the knock out plasmid to insure that both the 5' and 3' fragments were correctly cloned into pLPBLP; these were visualized using gel electrophoresis (4.2b). A SpeI/PstI digest (438 bp) was used to confirm the correct cloning of the 5' fragment, while an NcoI/KpnI digest (597 bp) was used for the 3' fragment. A SpeI/KpnI double digest (2594 bp) was also carried out

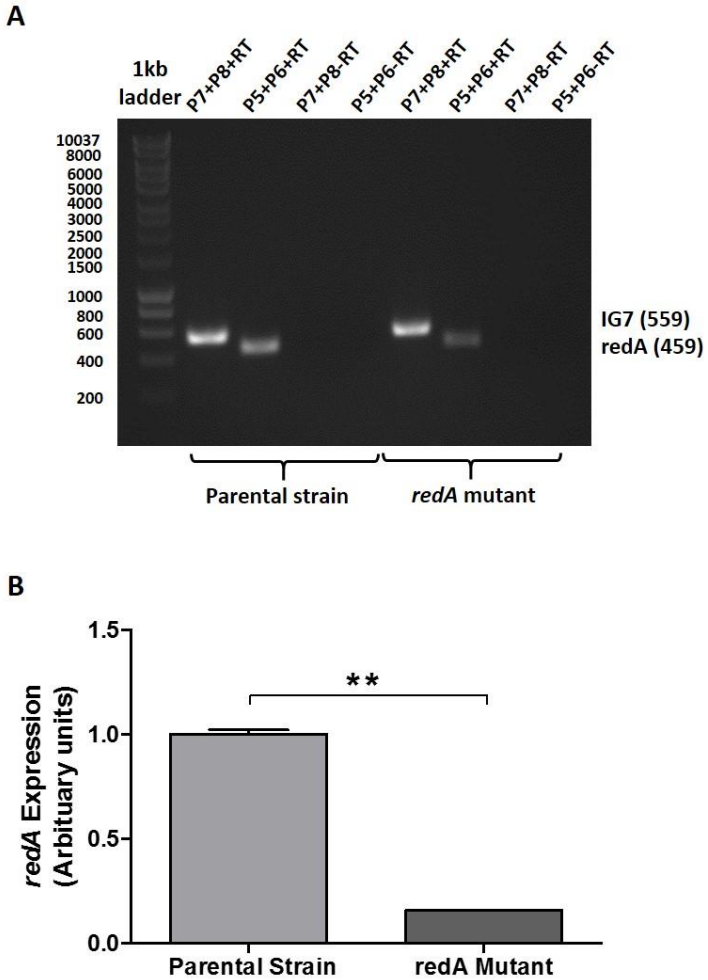

Figure 4.1 Expression levels of *redA* within the REMI mutant were compared to its parental strain. (A) PCR products were run on an agarose gel to confirm primer (P) specificity, with *redA* producing a 459 bp band and the house keeping gene *Ig7* producing a 559 bp band. The negative control lanes contained the same reaction composition less reverse transcriptase (RT) to confirm absence of contaminating DNA. (B) Quantitative PCR was carried out using cDNA from both the RedA REMI mutant and the parental strain. Expression levels were normalized using the *Ig7* house keeping gene. Disruption of the genome 185 bp upstream of *redA* resulted in a 6.25 fold decrease in expression levels. Data are mean +/- SEM ($P<0.01$, Students t test, n=6 per group, experiment was repeated).

to confirm the presence of a correctly constructed knock out construct. This was further validated by sequencing the knock out construct. The uniqueness of each restriction site used was confirmed by carrying out single digests upon the knockout plasmid (Fig 4.2b).

Wild type (AX3) cells were transfected with the purified knockout construct and selected for with blasticidin (20 mg/ml). Resistant cells were grown to confluency on a 96 well plate and PCR screened using six different primer combinations (Fig 4.3a) to identify homologous integrants (see 2.2.2.12 for method). The screening of 15 blasticidin resistant cell lines identified 6 homologous integrants, each with the 5' and 3' regions of the knock out construct integrated into the genome at the correct location (Fig 4.3b). Isogenic colonies of these homologous integrants were then created by sub-cloning onto bacteria and then underwent further screening. Following confirmation that cell lines were isogenic and that *redA* is ablated, reverse transcriptase PCR (RT-PCR) was then used to confirm the loss of *redA* expression (see 2.2.2.6 for method). Using primers complementary to the 3' region of the gene, *redA* expression was confirmed in wild type (AX3) cells by the presence of a 459 bp product, but absent in null cells (Fig 4.4a). The *Ig7* house keeping gene was used as a positive control, producing a 559 bp product in both null and wild type (AX3) cells (Fig 4.4a). Together, both the PCR screening procedure and RT-PCR confirmed that the *redA*- cell line contained an ablated *redA* gene.

4.2.3 Recapitulation of the Reductase A insertional mutant phenotype

Following the ablation of REDA we tested the sensitivity of *redA*- to CBD. Cells were treated with a range of CBD concentrations (0-20 µM) over a one week period and the growth-resistance to CBD assessed. The r*edA*$^-$ cell line displayed an increased sensitivity to CBD, with a total block in cell growth at 4 µM (Fig 4.4b). Using the rate of cell growth within the exponential phase a dose response curve was plotted of the normalised cell density against the Log of CBD concentration (Fig 4.4c). This secondary plot was used to calculate an IC_{50} value of 0.36 µM with a 95% confidence interval ranging between 0.26 µM and 0.49 µM. When compared to the IC_{50} value of wild type (AX3) cells, 1.89 µM, the *redA*$^-$ cell line showed a significant ($P<0.01$) increase in sensitivity to the effects of CBD (Fig 4.4d). These data suggest that the resistance displayed in the insertional mutant only arises through reduced expression of *redA* and not its entire removal.

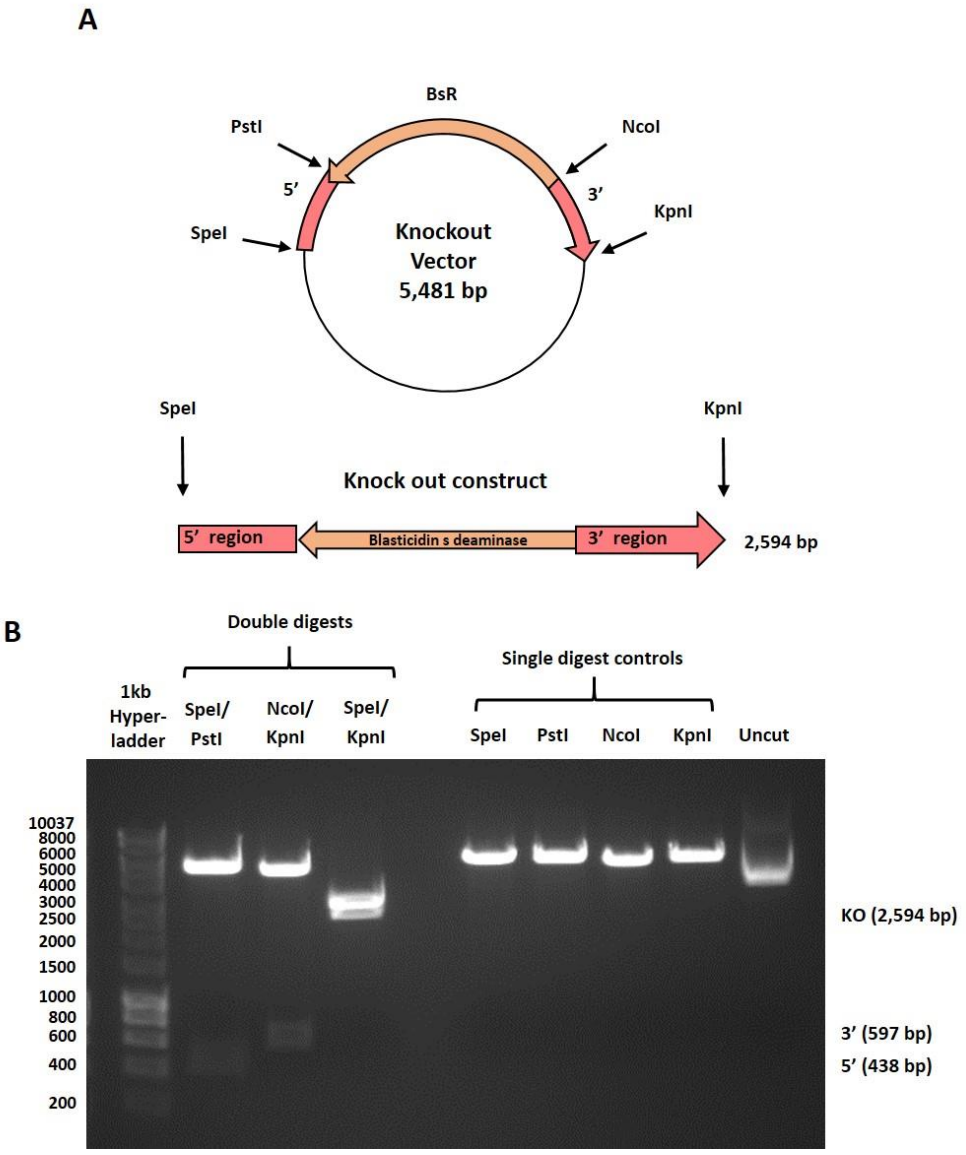

Figure 4.2 Creation of the redA knockout vector and confirmation by restriction digest. (A) Schematic showing how fragments from the 5' and 3' regions of the *redA* gene were amplified and ligated into the pLPBLP knock out vector flanking the blasticidin deaminase gene in the opposite orientation. The 5' fragment was ligated into the vector using the restriction enzymes SpeI and PstI, while the 3' fragment was ligated in using NcoI and KpnI. With the 5' and 3' *redA* fragments ligated into pLPBLP, the knock-out vector measures 5,481 bp. Prior to transformation the knockout vector was digested with SpeI and KpnI to produce the knockout construct which will undergo homologous recombination with redA in the genome. (B) Restriction digest analysis was used to confirm the presence of the fragments within the pLPBLP knockout vector. Double digests included SpeI/ PstI (438 bp) for the 5' fraqgment, NcoI/ KpnI (597 bp) for the 3' fragment, and Spei/ KpnI (2594 bp) for the knockout construct. Single digests and uncut vector were used as controls.

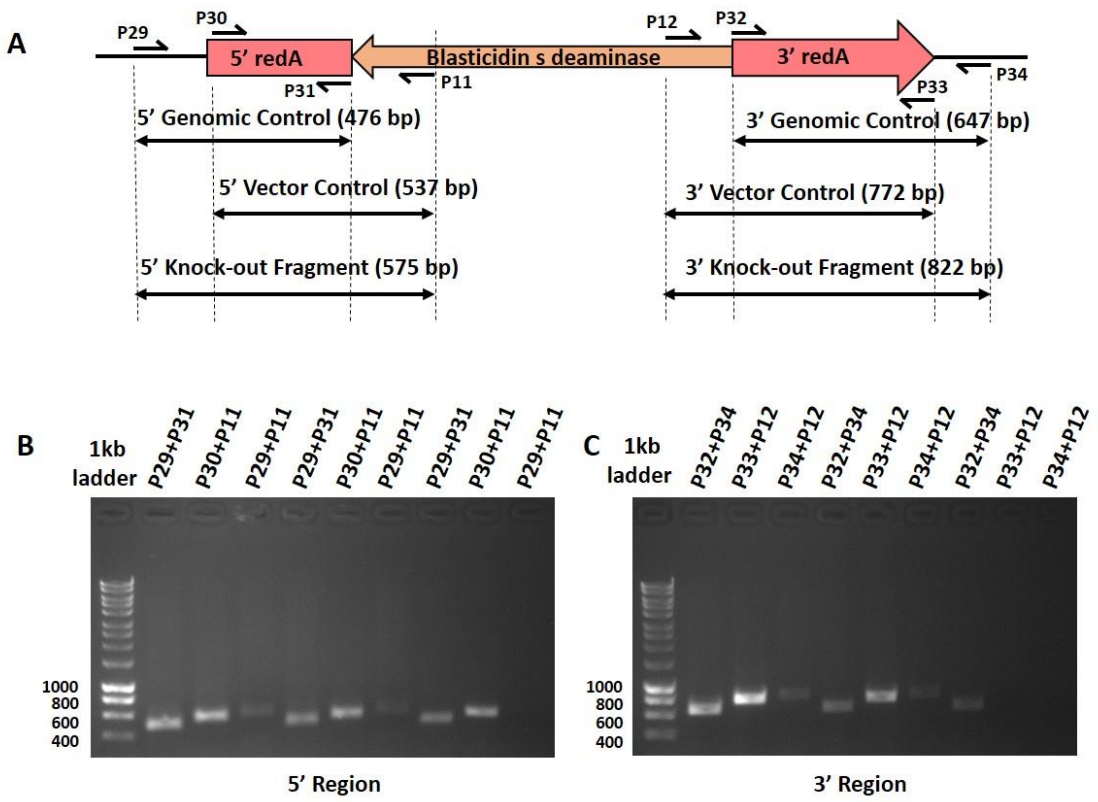

Figure 4.3 PCR screening to identify a *redA* null cell line. (A) A schematic showing the approach used to screen for a redA null cell line. Primer combinations (single sided arrows) were designed that would read from outside the *redA* gene (coloured red) into the blasticidin deaminase s gene (coloured orange). Only homologously integrated transformants would possess the unique knock-out fragment for both the 5' and 3' regions of the gene. Further primers labelled 'genomic control' and 'vector control' were designed for both the 5' and 3' regions to act as controls. (B & C) PCR analysis of all primer combinations (P) were used to identify homologously integrated transformants, which would possess the genomic control band, vector control band and knockout fragment band for both (B) 5' and (C) 3' regions. See figure 2.1 for primer sequences.

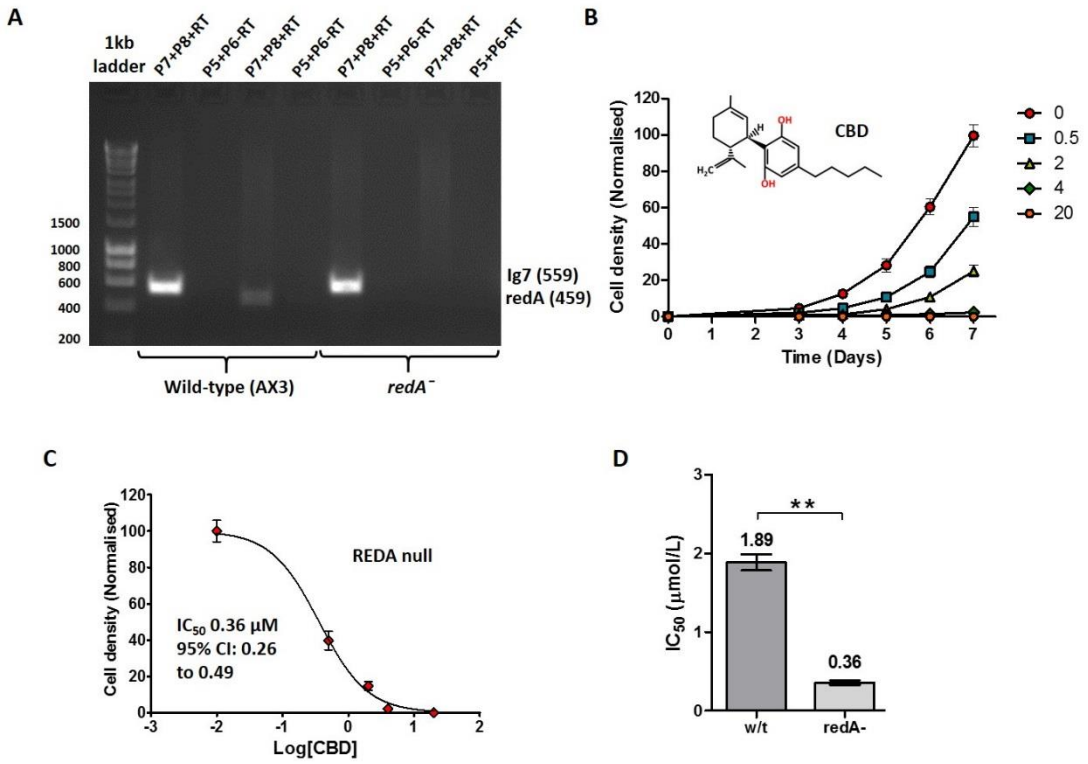

Figure 4.4 Ablation of *redA* creates a phenotype with a sensitivity to CBD greater than that found in AX3 wild type cells. (A) Creation of an isogenic redA null cell line was confirmed using RT-PCR. The mitochondrial large subunit rRNA gene, *Ig7* was used as a positive control. The negative control lanes contained the same reaction composition less reverse transcriptase (RT) to confirm absence of contaminating DNA. (B) *D. discoideum redA* null cells were treated with CBD for seven days under a range of concentrations. Cell growth was blocked at 4 µM. (C) A dose response curve of normalised *redA*- cell density against the Log (concentration) of CBD was used to calculate the IC_{50} value with a 95% confidence interval. (D) IC_{50} values of both AX3 wild-type and *redA* null cell lines. Data are mean +/- SEM (P<0.01, Students t test, n=6).

4.2.4 Phylogenetic analysis

In order to understand the potential role that REDA plays in *D. discoideum* we carried out Phylogenetic analysis of the proteins primary structure to identify homologous human proteins (Fig 4.5). While phylogenetic analysis yielded no direct human homologue, it appears that REDA is an ancestral protein of both the Cytochrome P450 reductase (POR) family of proteins and the Methionine synthase reductase (MTRR) family of proteins. Interestingly the *D. discoideum* proteome already has a number of oxidoreductase proteins with a greater homology to the human Cytochrome P450 reductase and MTRR enzymes. We therefore hypothesized that REDA may have a number of reductase roles within *D. discoideum*. The resistance seen in the insertional mutant maybe a consequence of just one of these mechanisms being disrupted. It is unlikely however that disrupting POR would infer a resistance to CBD as we would be removing the cells ability to remove CBD. We therefore hypothesised that REDA may also carry out the function of MTRR, and that the resistance observed is a result of decreased MTRR activity in the insertional mutant. MTRR is an integral component of the one carbon cycle, required for the reduction of cobalamin (Linden *et al,* 2006). Within the one carbon cycle homocysteine is converted to methionine by Methionine synthase using cobalamin as a co-factor, which is subsequently oxidized during each reaction (Ducker and Rabinowitz, 2017). For methionine synthase to correctly function the cobalamin co-factor needs to be maintained in a reduced state, which is achieved through MTRR activity (Linden *et al,* 2006). We therefore investigated the effects of ablating the *mtrr* gene from wild type (AX3) cells.

RNA sequence analysis data from the online gene expression depository Bgee (https://bgee.org) was also used to check the distribution and levels of *mtrr* expression within *H. sapiens*. Data used by Bgee is based exclusively on normal healthy expression data. It was found that the human *mtrr* gene is expressed within 223 varying tissue types throughout the body. Expression levels were found to be greatest within the corpus callosum region of the brain, a large nerve tract found beneath the cerebral cortex.

4.2.5 The effects of ablating Methionine synthase reductase (MTRR) from wild type (AX3) cells

The ablation of MTRR from wild type (AX3) cells was carried out by an undergraduate student, Awais Amir for his final year project, under my supervision. Following the creation of isogenic colonies RT-PCR was performed to validate the loss of *mtrr* expression within the null cell line.

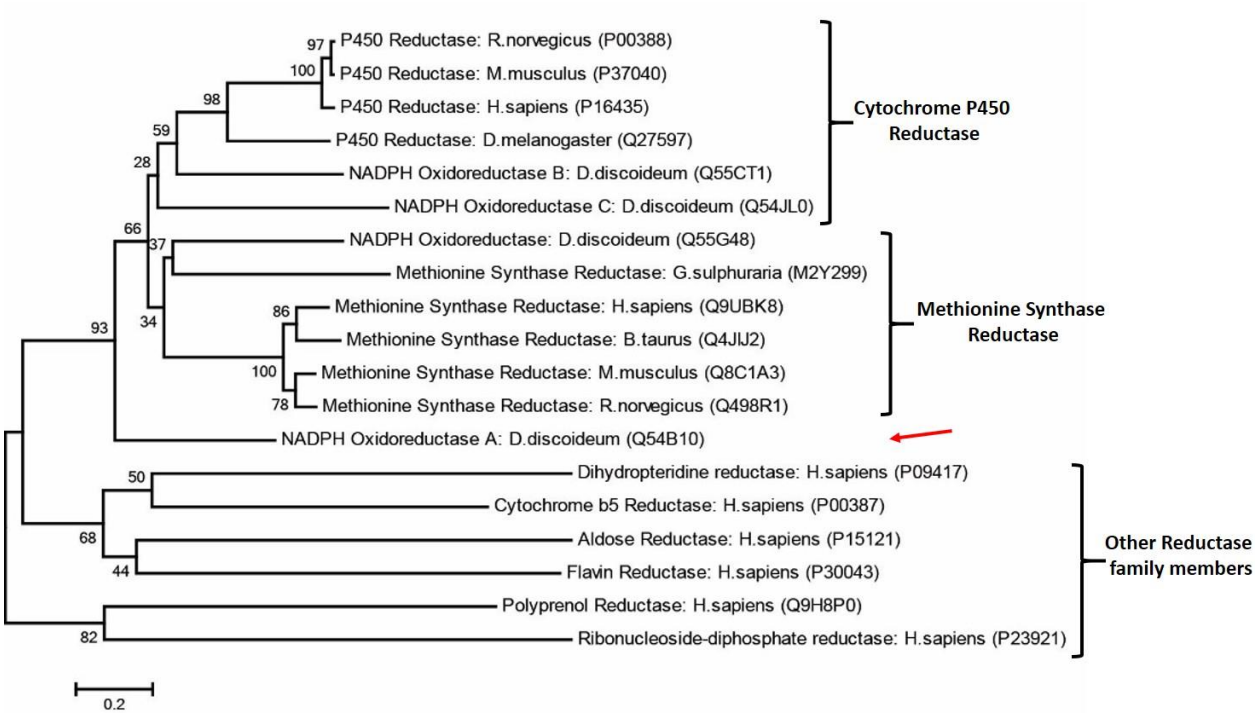

Figure 4.5 Phylogenetic analysis of Reductase A. Phylogenetic analysis of the *D. discoideum* Reductase A protein (Red arrow) shows it to have close homology with the *H. sapiens* Cytochrome P450 reductase and Methionine Synthase Reductase enzymes. The *D. discoideum* proteome is shown to already possess each of these conserved proteins, while Reductase A appears to be an ancestral protein of both.

Gel electrophoresis confirmed that *mtrr* expression was present in wild type (AX3) cells through the presence of a 686 bp band, but absent in the MTRR null cell line (Fig 4.6a). The *Ig7* house keeping gene was used as a positive control, confirmed through the presence of a 559 bp band (Fig 4.6a).

Following the ablation of *mtrr* we tested sensitivity to CBD. Cells were treated with a range of CBD concentrations (0-20 µM) over a one week period and the growth-resistance to CBD assessed. The *mtrr*- cell line displayed an increased sensitivity to CBD, with a total block in cell growth at 20 µM (Fig 4.6b). Using the rate of cell growth within the exponential phase a dose response curve was plotted of the normalised cell density against the Log of CBD concentration

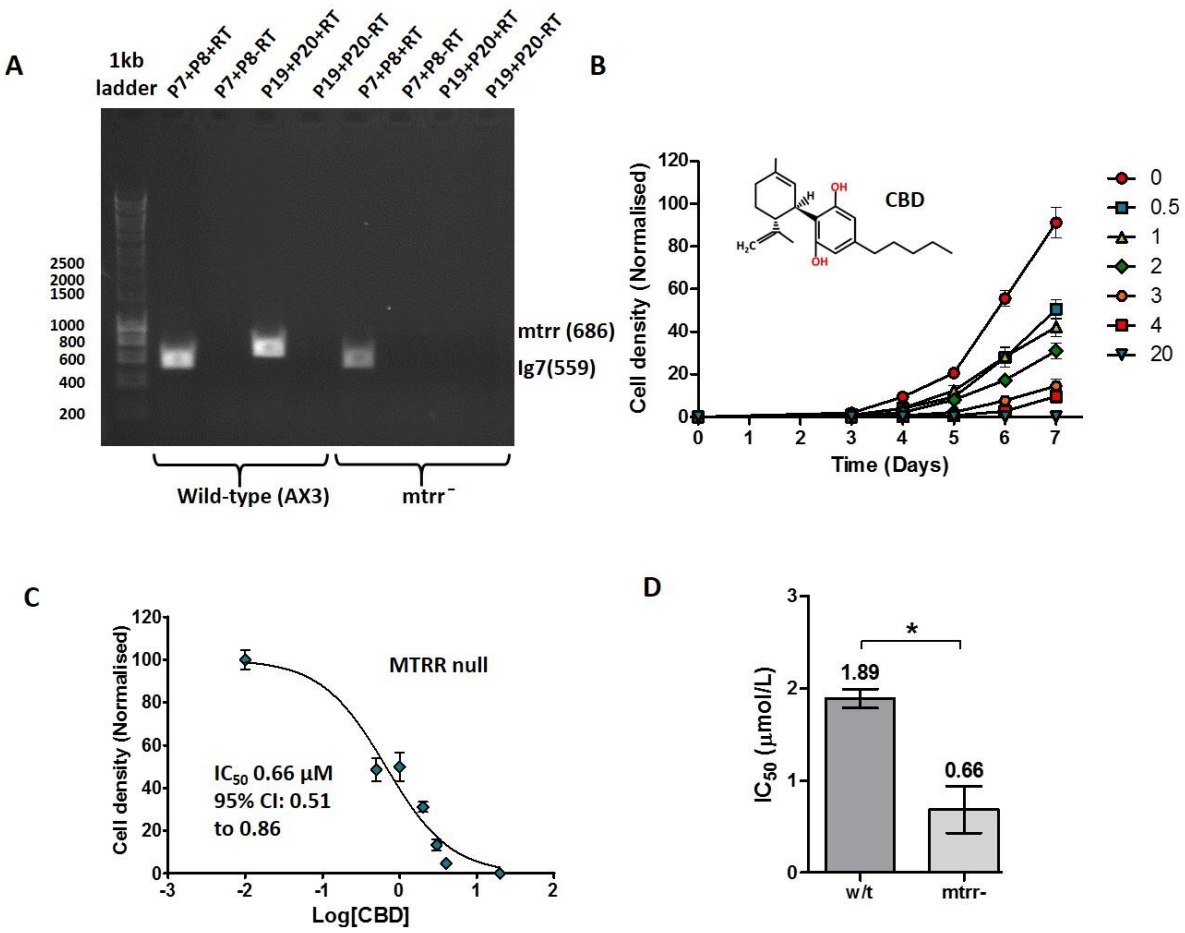

Figure 4.6 Ablation of *mtrr* creates a phenotype with a sensitivity to CBD greater than that found in AX3 wild type cells. (A) Creation of an isogenic *mtrr* null cell line was confirmed using RT-PCR. The mitochondrial large subunit rRNA gene, *Ig7* was used as a positive control. The negative control lanes contained the same reaction composition less reverse transcriptase (RT) to confirm absence of contaminating DNA. (B) *D. discoideum mtrr* null cells were treated with CBD for seven days under a range of concentrations. Cell growth was blocked at 20 µM. (C) A dose response curve of normalised *mtrr-* cell density against the Log (concentration) of CBD was used to calculate the IC_{50} value with a 95% confidence interval. (D) IC_{50} values of both AX3 wild-type and *mtrr* null cell lines. Data are mean +/- SEM ($P<0.05$, Students t test, n=6).

(Fig 4.6c). This secondary plot was used to calculate an IC_{50} value of 0.66 µM with a 95% confidence interval ranging between 0.51 µM and 0.86 µM. When compared to the IC_{50} value of wild type (AX3) cells, 1.89 µM, the *mtrr-* cell line showed a significant ($P<0.05$) increase in sensitivity to the effects of CBD (Fig 4.6d). These data suggest that the resistant phenotype observed in the REMI mutants is not from a disruption to MTRR activity.

4.3 Discussion

4.3.1 Ablation of Reductase A from wild type (AX3) cells does not recapitulate the resistant REMI mutant phenotype.

While it was understood that by ablating the *redA* gene we may not achieve the same level of resistance observed in the REMI mutant, we did anticipate some resistance. With total REDA activity removed it was hypothesized that resistance would be greater than that observed in wild type (AX3) cells under CBD treatment. However, our data shows that this is not so (Fig 4.4). Investigations into *redA* expression levels (Fig 4.1b) found that *redA* was expressed 6.25 fold less in the REMI mutant compared to wildtype (AX3) cells. It would seem that reduced *redA* expression levels may be responsible for the CBD resistant phenotype, while removal of the gene has a more negative impact.

To recapitulate the resistant phenotype found in the REMI mutant, we could mutate the genome of wild type (AX3) cells by inserting the REMI insert into the DpnII restriction site 185bp upstream of the *redA* open reading frame. This would directly mirror the mutation found in the REDA REMI mutants. However, while this method should recapitulate the resistance phenotype it would do nothing to confirm a role for REDA in this resistance. If the resistant phenotype is a result of reduced *redA* expression it may be possible to recapitulate the resistant phenotype by reducing expression levels to the same degree in wild type (AX3) cells. This could be achieved by knock down procedures using inhibitory RNA techniques (Friedrich *et al,* 2014), however it may be difficult to maintain the correct expression levels. Similarly, the exact role that REDA plays within *D. discoideum* is still unknown. While reducing *redA* expression levels by RNAi may possibly infer a resistance to CBD, we still have no idea as to the downstream mechanisms involved. It is also possible that the resistant phenotype observed in the REMI mutant may have nothing to do with *redA* expression levels at all. It is possible that reduced *redA* expression is just an effect of the nearby disruption, and not the actual cause of the resistant phenotype observed. While the REMI insertion site is close to the *redA* gene, this particular stretch of

sequence could play a regulatory role in the expression of another gene elsewhere by acting as an enhancer region. It is known that enhancer regions can affect the expression of specific genes on the same chromosome from 100 bp to Mb away, either upstream or downstream (Williamson *et al,* 2011). The resistant phenotype could therefore be the result of a different genes reduced expression, not identified in the mutant screen.

4.3.2 Possible roles of Reductase A

It was initially hypothesized that REDA may be involved in the removal of CBD. Previous studies have shown the REDA protein to have a 50% similarity to the human Cytochrome P450 reductase (POR) enzyme (Gonzalez-Kristeller *et al,* 2008). It is well known that NADPH-Cytochrome P450 is involved in the removal of foreign compounds such as pharmaceuticals that are taken up into cells (Anzenbacher and Anzenbacherová, 2001). It was initially thought that the REMI insertion may have increased expression levels of *redA* within the REMI mutant, thereby increasing the conversion of cannabinoids to their metabolites by increased activity of NADPH-Cytochrome P450. POR is responsible for the correct functioning of NADPH-Cytochrome P450 through the transfer of electrons from NADPH (Porter, 2012). Therefore, increased expression of POR should decrease cellular cannabinoid concentration through increased Cytochrome P450 activity. However, qPCR analysis showed that *redA* expression levels are actually 6.25 fold less in the REMI mutant than in the parental strain (Fig 4.1b). It is therefore unlikely that the REDA REMI mutant gains its resistant phenotype through the degradation of CBD, at least not through REDA activity.

Phenotypic analysis has shown that REDA has strong homology to two human proteins, these being the MTRR and POR proteins (Fig 4.5) involved in the reduction of B12 and cytochrome P450, respectively. Interestingly the *D. discoideum* proteome already possesses homologues of these two types of enzymes with greater similarity to the human MTRR and POR proteins. Phylogenetic analysis predicts REDA to be an evolutionary ancestral protein of the two oxidoreductase sub-classes (Fig 4.5). Based upon its similarity to MTRR and POR it was plausible that REDA may carry out the role of both MTRR and POR sub-classes. Despite showing the protein to have a 50% similarity to the human Cytochrome P450 reductase enzyme, the previous study investigating REDA linked the protein to multicellular development in *D. discoideum* (Gonzalez-Kristeller *et al,* 2008). In this study they showed that disruption of REDA (REMI mutant) arrested development at the mound stage, although they did not show this with a *redA* null cell line. Development within our *redA* null cell line wasn't disrupted. The methylation of

proteins, DNA and other molecular targets is essential for a number of cellular mechanisms and biological pathways within cells and may play a role in multicellular development. If REDA did have MTRR activity then this could be a plausible mechanism in which REDA ablation arrests development and may explain the underlying mechanism of the REMI mutant resistance. However, it was shown that the ablation of MTRR increased sensitivity to CBD within *D. discoideum* (Fig 4.6). This suggests that REDA does not carry out MTRR function but instead has a different, unknown role. Further to this, any role that REDA has is likely to be only required within *D. discoideum* and not humans, as no direct homologue has been identified. In light of the data obtained here it was questioned whether it was worthwhile pursuing our investigation into REDA. Further in depth investigation may have elucidated the role of REDA, but how this would translate across to human seizure onset may be questionable. As a number of genes were identified within the mutant screen it was decided that investigation into REDA be stopped and efforts concentrated upon the other genes identified.

In this chapter we have shown that REDA is an ancestral protein of both the Methionine synthase reductase (MTRR) and Cytochrome P450 reductase (POR) sub-classes of proteins. By adopting qPCR we show that the *redA* gene within the REMI mutant was expressed at significantly lower levels than what is found in wild type (AX3) cells. This suggests that REDA does not carry out the role of the POR sub-class of proteins, as a decrease in POR activity would sensitize cells to CBD, not make them more resistant. We also investigated whether REDA has MTRR function, and if the ablation of MTRR inferred resistance to CBD. Ablation of MTRR however, was found to sensitize wild type (AX3) cells to CBD even further. We therefore conclude that REDA most likely does not have POR or MTRR activity within *D. discoideum* and that the role of REDA is endogenous only to *D. discoideum* and not humans. We also ablated REDA from wild type (AX3) cells to investigate if this inferred a resistance to CBD. It was found that the ablation of REDA sensitized cells to CBD even further. This suggested that REDA either has multiple roles within *D. discoideum* or that the REMI insert has disrupted expression of a different gene, possibly through an enhancer region that is instead responsible for causing resistance to CBD. Because of the conflicting data and lack of a direct human homologue it was decided that our research should concentrate upon the other genes identified in the mutant screen.

Chapter 5

LMBR1 domain-containing protein 2 homolog B (Lmbd2b)

5.1 Introduction

Within chapter 3 we described the use of a genetic screen to identify insertional mutants showing resistance to the cannabinoids cannabidiol (CBD), cannabidiolic acid (CBDA) and cannabidivarin (CBDV). Four genes of interest were identified across 20 resistant mutants with 12 of these being the *lmbd2b* gene (DDB_G0281669). Whole genome sequencing and inverse PCR confirmed this disruption to be within exon 2 of the genes open reading frame.

The LMBD2b protein belongs to the lipocalin-interacting membrane receptor (LIMR) family of proteins, which are involved in the internalization of extracellular lipocalin proteins. The lipocalins are a wide spread family of proteins found within many species, and have diverse physiological roles (Ganfornina *et al*, 2000). Despite members of the lipocalin family having very little homology between themselves, they do form the same basic tertiary structure and have the common ability of binding lipophilic molecules such as lipids, sterols and drugs (Asimakopoulou and Weiskirchen, 2015). The first of the LIMR family to be identified was LIMR1 through its interaction with lipocalin Lcn-1 (Wojnar *et al*, 2001). This particular lipocalin has a broad ligand binding specificity (Redl, 2000), and is believed to be a scavenger of potentially harmful hydrophobic molecules (Redl, 2000). It is therefore possible that LMBD2b may have a role in cellular uptake, and that the resistance observed in the insertional mutants is a result of reduced cannabinoid uptake. Interestingly, studies have also linked a member of the LIMR family to the cbIF inborn error of vitamin B12 (cobalamin) metabolism (Rutsch *et al*, 2009). This particular member, LMBD1 appears to be responsible for the transport of cobalamin into the cell (Rutsch *et al*, 2009). It is interesting to find that the LIMR family of proteins are also involved in cobalamin transport, especially as cobalamin is required for the one carbon cycle (Ducker and Rabinowitz, 2017).

In this chapter we show that the LMBD2b protein is a member of the lipocalin-interacting membrane receptor (LIMR) family of proteins, within which are proteins involved in the transport of cobalamin. We also show that the ablation of LMBD2b from wild type (AX3) cells recapitulates the resistant phenotype found in the *lmbd2b*- insertional mutant. We further show that this resistance is not a result of changes in cellular CBD levels through altered uptake or expulsion. To ensure the resistance found in the LMBD2b null cell line is a direct result of LMBD2b ablation we reinstated the *lmbd2b* gene and show that sensitivity to CBD is also reinstated. We then investigate whether LMBD2b has a role in cobalamin transport by analysing cobalamin levels in wild type (AX3) cells using an enzyme-linked immunosorbent assay (ELISA).

5.2 Results

5.2.1 Phylogenetic analysis

In order to identify a possible role for the LMBD2 protein in *D. discoideum* phylogenetic analysis was carried out upon the proteins primary structure. Phylogenetic analysis showed that LMBD2b is a member of the lipocalin-interacting membrane receptor (LIMR) family of proteins (Fig 5.1). The LIMR family of proteins have a multi-pass transmembrane structure and are involved in the transport of small hydrophobic molecules such as steroids and lipids. In particular LMBD2b belongs to the LMBD2 sub-class of proteins, wherein two *D. discoideum* proteins are found, LMBD2a (uniprot: Q54Q92) and LMBD2b (uniprot: Q54TM2), with their genes found on chromosomes 4 and 3 respectively. The *D. discoideum* LMBD2b protein has a size of 790 amino acid residues, and is homologous to the human protein LMBD2 (Q68DH5). Comparison of the primary (amino acid) structure of the *D. discoideum* LMBD2b protein with the human LMBD2 protein indicates high conservation, with an E-value of 5e-60 across 66% of the *D. discoideum* protein sequence. A protein is commonly considered to be a homologue if it has an E-value of approximately 1e-40 or less (Eichinger *et al*, 2005). Other sub-classes of proteins found within the LIMR family are the lipocalin receptor proteins and interestingly the cobalamin transporter proteins. However, a further two *D. discoideum* LIMR proteins were found within each of these sub-classes with a greater homology to the human homologue of each.

5.2.2 Recapitulation of the *lmbd2b* insertional mutant phenotype

Because of the potential role that LMBD2b may have in detoxifying *D. discoideum* cells from the presence of CBD, we were initially reluctant to pursue investigation into LMBD2b further, despite a potential role in cobalamin transport. However, the group of Dr Daphne Blumberg (University of Maryland, USA) had previously created an *lmbd2b* null mutant which was available from the *D. discoideum* stock centre (North western university, Chicago). As such we obtained the *lmbd2b*$^-$ cell line to test whether the ablation of LMBD2b would recapitulate the resistance found in the REMI mutant screen, and if so does it have a role in cobalamin transport.

On receiving the cell line we initially confirmed ablation of LMBD2b by carrying out RT-PCR analysis upon the cell line. cDNA was created from both wild type (AX3) and *lmbd2b*$^-$ cells and used to check for gene expression. RT-PCR confirmed the presence of *lmbd2b* expression in vegetative wild type (AX3) cells by the presence of a 460 bp PCR product (Fig 5.2a). No such

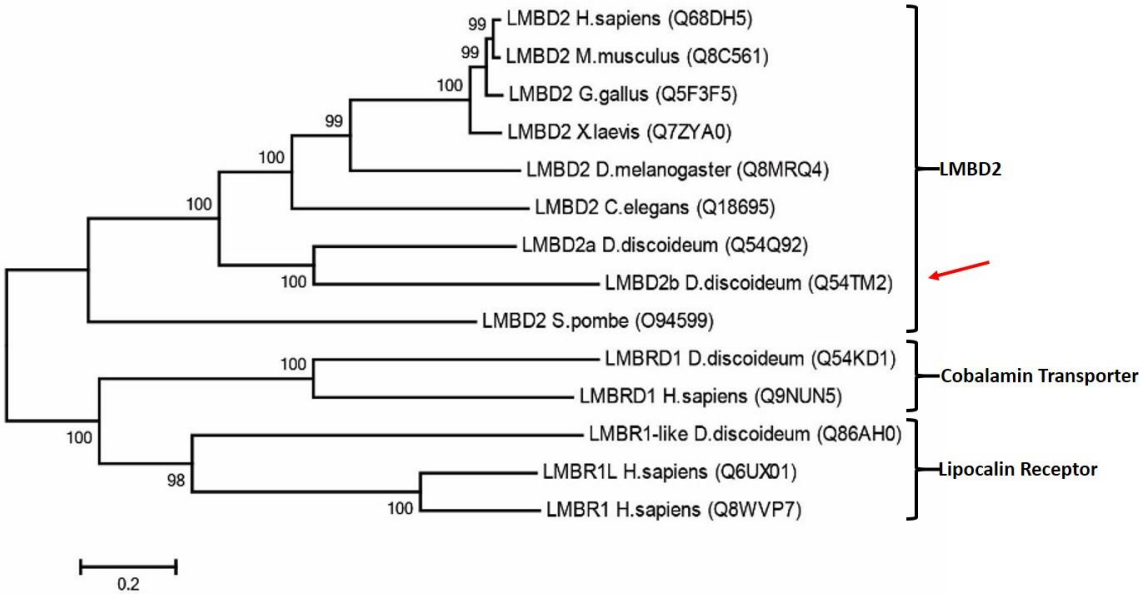

Figure 5.1 Phylogenetic analysis of LMBR1 domain-containing protein 2 homolog B (Lmbd2b). Phylogenetic analysis of the *D. discoideum* LMBD2b protein (Red arrow) shows it to have close homology with the *H. sapiens* LMBD2 protein. The *D. discoideum* proteome also possesses LMBD2a within the same sub-class of proteins. Within the larger family of LIMR proteins are found other sub-classes, one of which is involved in the transport of cobalamin.

band was found for the *lmbd2b*$^-$ cell line confirming the absence of *lmbd2b* expression. In both instances the mitochondrial large subunit rRNA gene (*lg7*) was used as a control producing a 559 bp PCR product in both wild type (AX3) and *lmbd2b*- cells (Fig 5.2a).

Following confirmation that *lmbd2b* was ablated from the null cell line, we carried out growth assays to determine the sensitivity of *lmbd2b*$^-$ to CBD. The *lmbd2b*$^-$ cell line was treated with a range of CBD concentrations (0-20 µM) over a one week period and the growth-resistance to CBD assessed. The *lmbd2b*- cell line displayed resistance to CBD, with cells still able to grow at 20 µM (Fig 5.2b). Using the rate of cell growth within the exponential phase a dose response curve was plotted of the normalised cell density against the Log of CBD concentration (Fig 5.2c). This secondary plot was used to calculate an IC_{50} value of 7.15 µM with a 95% confidence interval ranging between 4.99 µM and 10.25 µM. When compared to the IC_{50} value of wild type (AX3) cell, 1.89 µM, the *lmbd2b*-$^-$ cell line showed a significant ($P<0.01$) resistance to the effect of CBD (Fig 5.2d). These data suggest a role for LMBD2b in the regulation of CBD sensitivity, most likely by modulating cellular CBD levels through altered uptake or expulsion.

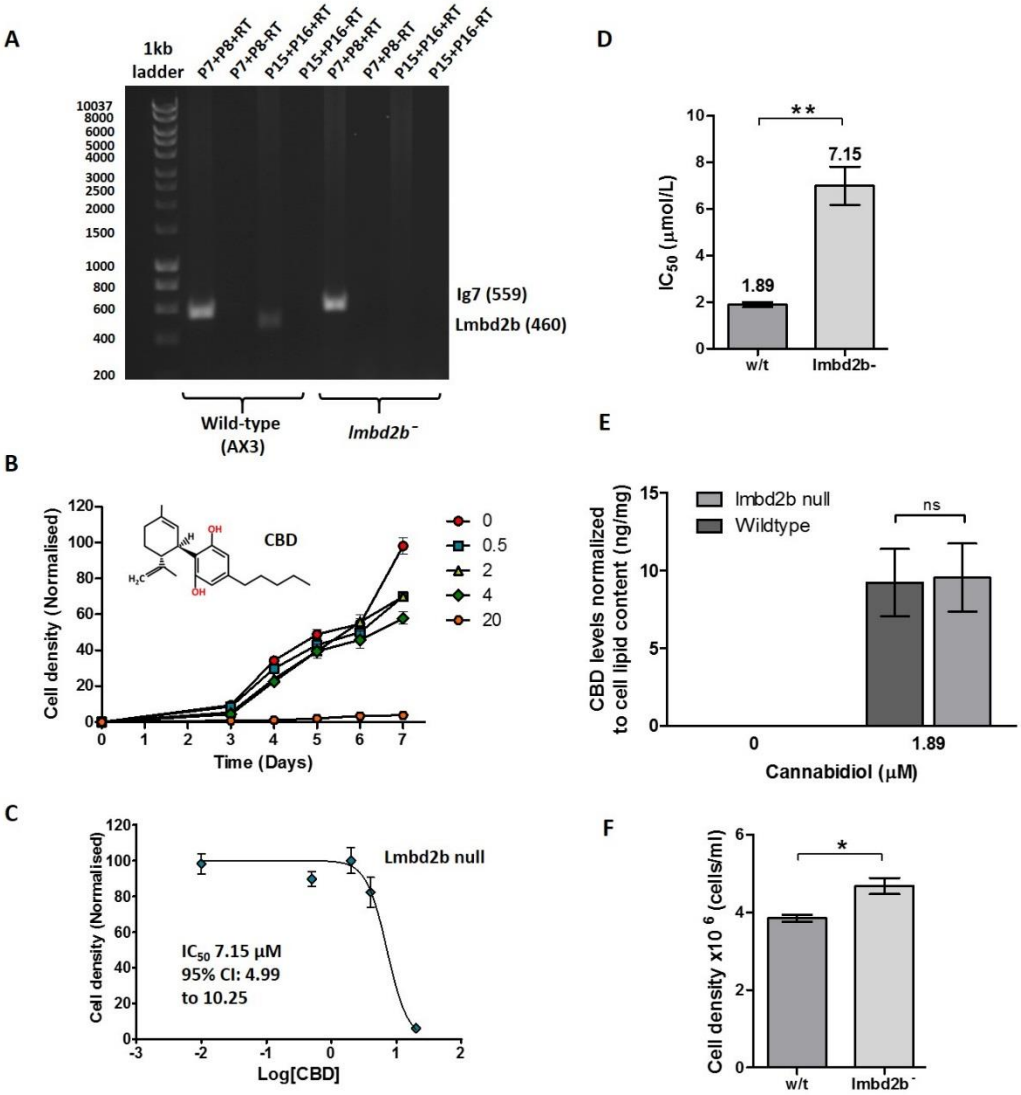

Figure 5.2 Ablation of LMBD2b creates a phenotype with a sensitivity to CBD greater than that found in AX3 wild type cells. (A) The LMBD2b null cell line was confirmed using RT-PCR. The mitochondrial large subunit rRNA gene, *Ig7* was used as a positive control. The negative control lanes contained the same reaction composition less reverse transcriptase (RT) to confirm absence of contaminating DNA. (B) *D. discoideum* LMBD2b null cells were treated with CBD for seven days under a range of concentrations. Cell growth was partially blocked at 20 µM. (C) A dose response curve of normalised *lmbd2b*- cell density against the Log of CBD concentration was used to calculate the IC_{50} value with a 95% confidence interval. (D) IC_{50} values of both AX3 wild-type and *lmbd2b*- cell lines. Data are mean +/- SEM (P<0.01, Students t test, n=6). (E) Cellular CBD levels were quantified within *D. discoideum* wildtype and *lmbd2b*- cell lines using LC-MS following a 12 hour CBD treatment regime. Data are mean +/- SEM (P>0.05, Students t test, n=6). (F) Cell density of AX3 wild-type and *lmbd2b*- cells following 12 hour CBD treatment, prior to CBD quantification using LC-MS analysis. Data are mean +/- SEM (P<0.05, Students t test, n>6).

To investigate whether the resistance to CBD displayed in the *lmbd2b*- cell line was a result of altered uptake or expulsion of CBD we quantified cellular CBD levels. This was done in both the null cell line and wild type (AX3) cells. Both cell lines were treated with 1.89 µM CBD for 12 hours, harvested, and the cellular CBD levels within each were quantified using LC-MS. Using this approach no significant difference in CBD levels ($P>0.05$) was found between wild type (AX3) and *lmbd2b*- cells (Fig 5.2e). Cell density was also measured during the harvesting stage to determine if the *lmbd2b*- cell line exhibited resistance after just 12 hours. Cell density within the *lmbd2b*- cell line was found to be significantly greater ($P<0.05$) than that found for wild type (AX3) cells (Fig 5.2f). Together these data suggest that the resistance observed in the null cell line is not from altered uptake or expulsion of CBD.

5.2.3 Creation of an extra chromosomal vector for the expression of LMBD2b GFP fusion proteins.

In order to be sure that the loss of LMBD2b within the null cell line was responsible for resistance to CBD, we reinstated *lmbd2b* using an extra chromosomal plasmid. If loss of LMBD2b was responsible for resistance then we would expect sensitivity to be reinstated. We therefore investigated this by using the pTX-GFP over-expression plasmid (Levi *et al*, 2000). The open reading frame of *lmbd2b* was amplified from cDNA of wild type (AX3) cells using the Q5® High fidelity DNA polymerase (New England Biolab). Primers used were complementary to both the 5' and 3' extremities of the *lmbd2b* gene. Both the 5' and 3' primers contained extension sequences incorporating restriction sites for the cloning of *lmbd2b* into the pTX-GFP over-expression plasmid. SacI and XbaI restriction sites were used for the 5' and 3' primers respectively. The *lmbd2b*- cell line was then transfected with the over-expression vector and cells selected for using 10 µg/µl G418. Resistant cells were plated upon bacteria and isogenic colonies created.

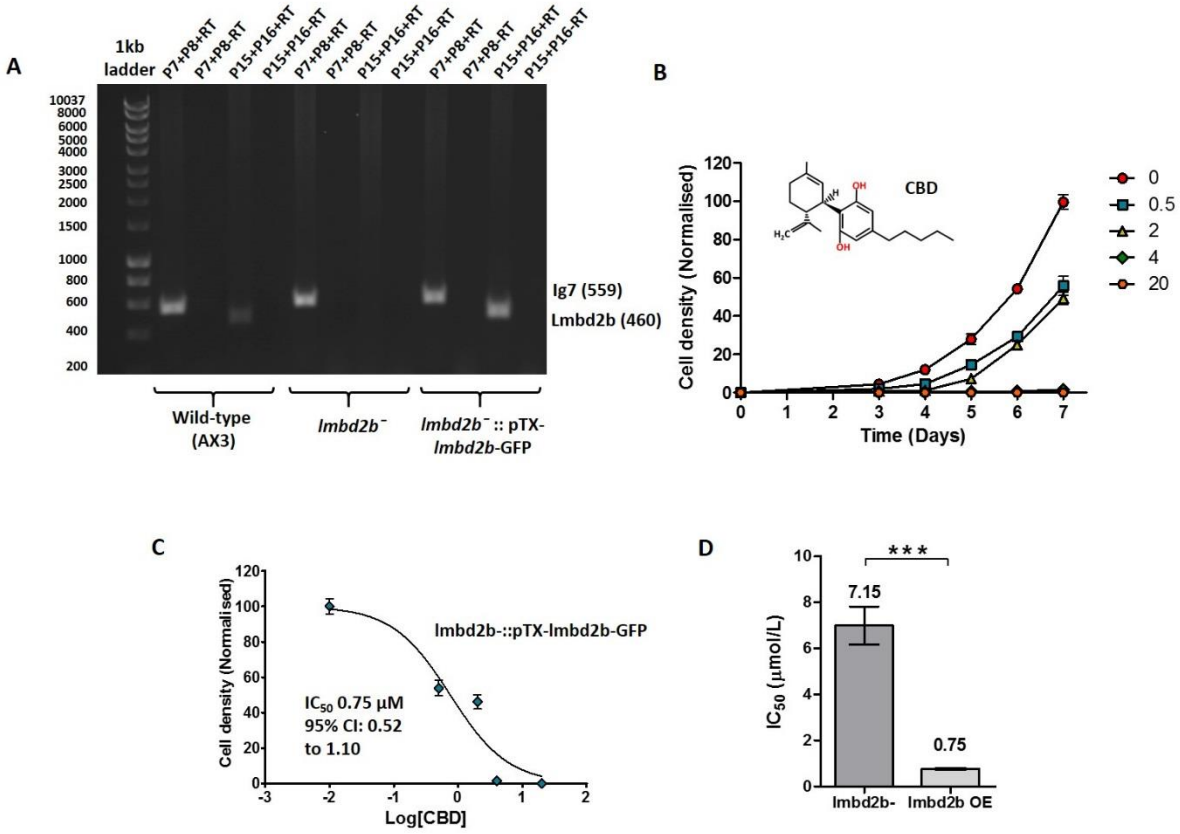

Figure 5.3 Expression of *lmbd2b* within *lmbd2b-* cells using an extra chromosomal vector rescues the CBD sensitive phenotype found in AX3 wildtype cells. (A) Expression of *lmbd2b* within the rescue cell line was confirmed by RT-PCR. The mitochondrial large subunit rRNA gene, *Ig7* was used as a positive control. The negative control lanes contained the same reaction composition less reverse transcriptase (RT) to confirm absence of contaminating DNA. (B) *D. discoideum* rescue cell lines with the *lmbd2b* gene over expressed in *lmbd2b-* cells were treated with CBD for seven days under a range of concentrations. Cell growth was inhibited in a dose dependant manner with a total block at 4 µM. (C) Dose response curves of normalised cell density against the Log (concentration) of CBD was used to calculate the IC_{50} values with a 95% confidence interval. (D) The IC_{50} value of the *lmbd2b* rescue cell line was compared to wild type (AX3) cells. Data are mean +/- SEM (P<0.001, Students t test, n=6).

5.2.4 Rescuing the CBD sensitive phenotype

To confirm that LMBD2b was reinstated in the rescue cell line, cDNA was created from both wild type (AX3) and the rescue cell lines. RT-PCR analysis was then used to confirm the presence of *lmbd2b* expression by the presence of a 460 bp PCR product (Fig 5.3a). The mitochondrial large subunit rRNA gene (*Ig7*) was used as a control producing a 559 bp PCR product in both wild type (AX3) and the rescue cells (Fig 5.3a).

Following confirmation that LMBD2b was reinstated within the null cell line, we carried out growth assays to determine the sensitivity of the rescue cell line to CBD. The rescue cell line was treated with a range of CBD concentrations (0-20 µM) over a one week period and the growth-resistance to CBD assessed. The rescue cell line was found to be sensitive to CBD, with cell growth blocked at 4 µM (Fig 5.3b). Using the rate of cell growth within the exponential phase a dose response curve was plotted of the normalised cell density against the Log of CBD concentration (Fig 5.3c). This secondary plot was used to calculate an IC_{50} value of 0.75 µM with a 95% confidence interval ranging between 0.52 µM and 1.10 µM. When compared to the IC_{50} value of *lmbd2b*- cells, 7.15 µM, the rescue$^-$ cell line showed a significant ($P<0.001$) change in sensitivity to the effects of CBD (Fig 5.3d).

5.2.5 Vitamin B12 (Cobalamin) assay

Because a sub-class of the LIMR family of proteins is known to be involved in the transport of vitamin B12 (cobalamin), we hypothesized that LMBD2b within *D. discoideum* may perform a similar function. We therefore aimed to quantify cellular cobalamin levels within wild type (AX3) cells with the intention of investigating whether these levels changed following CBD treatment. Wild type (AX3) cells were grown within minimal media for 12 hours, then washed and the cellular cobalamin levels quantified using an enzyme-linked immunosorbent assay (ELISA) (see 2.2.5 for method). However, despite using pelleted cells ranging from 2.0×10^6 to 1.0×10^8 cells the ELISA was unable to detect cobalamin within the cell lysates. This included cells treated with CBD or vehicle alone. To ensure the ELISA kit was able to detect cobalamin we tested the kit using an independent source, obtained from Sigma Aldrich. When used on this alternative source the ELISA kit registered a response appropriate to the concentration used. It was therefore concluded that no detectable level of cobalamin is found in *D. discoideum*, at least not by using an ELISA method.

5.3 Discussion

5.3.1 LMBD2b ablation infers a resistance to CBD by a mechanism not involved in cellular CBD uptake

Previous studies have shown that CBD inhibits cellular growth in mammalian cell lines (McAllister *et al*, 2011, Solinas *et al,* 2013), of which we show a similar effect in *D. discoideum*. Using this growth inhibitory effect we screened an insertional mutant library for mutants that

displayed a resistance to CBD. Four independent genes were identified that inferred resistance when disrupted, one of which was the *lmbd2b* gene. In order to confirm that loss of LMBD2b activity results in CBD resistance we recapitulated these findings by showing resistance in an LMBD2b null cell line (kindly donated by Daphne Blumberg, University of Maryland, USA). Sensitivity to CBD was then reinstated by replacing *lmbd2b* back into the null cell line via an over expression vector. These data suggest that LMBD2b is involved in regulating CBD sensitivity within *D. discoideum*. Previous studies have shown that LMBD2b localizes to the cytoplasm of *D. discoideum* and that the protein has a close association with endocytic cups (Kelsey et al, 2012). This would suggest that LMBD2b plays a role in the cellular uptake of CBD, and that LMBD2b ablation would most likely result in a reduced amount of CBD uptake. Similarly, phenotypic analysis showed LMBD2b to belong to the lipocalin-interacting membrane receptor (LIMR) family of proteins. This family of proteins are responsible for the internalization of extracellular lipocalin proteins (Ganfornina et al, 2000). The lipocalin proteins are known to bind to a diverse range of hydrophobic molecules (Asimakopoulou and Weiskirchen, 2015), with certain members being regarded as scavengers for potentially harmful hydrophobic molecules (Redl, 2000). It was therefore likely that LMBD2b facilitates the internalization of CBD into *D. discoideum,* most likely bound to a lipocalin carrier protein, and that the resistance observed was a result of a breakdown in this process. To test whether LMBD2b is involved in the internalization of CBD, LC-MS was used to quantify CBD levels within both wild type (AX3) and LMBD2b null cell lines. Surprisingly, results showed no significant difference in cellular CBD levels between wild type (AX3) and *lmbd2b* null cells. These data would suggest that the ablation of LMBD2b does not infer a resistance by preventing the internalization of CBD into the cell but by some other mechanism.

5.3.2 Involvement of Lipocalin-interacting membrane receptors (LIMR) in cobalamin transport

Interestingly, phenotypic analysis showed that within the LIMR family of proteins a specific subclass exists involved in the cellular uptake of cobalamin. This particular group is of specific clinical interest because of its link to inborn errors of vitamin B12 (cobalamin) metabolism. The human gene of this group '*lmbrd1*' was first identified as having 5 frame shift mutations in 12 cobalamin deficient individuals using homozygosity mapping (Rutsch et al, 2009). These findings have been further supported by later studies that have identified other *lmbrd1* mutations within individuals with a cblF defect in cobalamin metabolism (Gailus et al, 2010). In individuals with this type of defect in cobalamin metabolism, the deficiency results in cobalamin being trapped

in the lysosomes (Gailus et al, 2010). Individuals with a defect in cobalamin metabolism can exhibit a number of symptoms including seizures (Dogan et al, 2012, Kandula et al, 2014 and Lubana et al, 2015). Cobalamin is a water soluble vitamin essential for the correct function and maintenance of the brain and nervous system. Unlike certain bacteria and archaea, humans are unable to synthesis the vitamin *de novo* and acquire the vitamin through dietary uptake (Roth *et al,* 1996). Cobalamin is known to act as a prosthetic group for two enzymes; methylmalonyl-CoA synthase and methionine synthase. Methionine synthase catalyzes the conversion of homocysteine to methionine (Fig 1.3) which takes place within the cytosol of the cell (Ducker and Rabinowitz, 2017). Methionine can then be used for down-stream methylation. In order for this enzymatic reaction to proceed cobalamin is required as a co-factor in the form of methyl-cobalamin. An inefficient conversion of homocysteine to methionine results in increased tissue levels of homocysteine. Previous studies have shown that increased homocysteine levels potentiates seizure onset (Baldelli et al, 2009). A reduction of cellular cobalamin would most likely also result in a reduced conversion of homocysteine to methionine. Numerous case studies have identified and associated a cobalamin deficiency with seizure onset, particularly during childhood (Dogan et al, 2012, Kandula et al, 2014 and Lubana et al, 2015). It may therefore be possible that the anti-convulsant effects of CBD in humans may arise through the cellular uptake and utilization of cobalamin.

We therefore attempted to determine if LMBD2b has a role in transporting cobalamin into the cell. Using an ELISA approach we attempted to determine if cobalamin levels within *D. discoideum* were of a detectable level, and if so does CBD treatment have an effect upon such levels. Unfortunately, using this approach no detectable level of cobalamin was found in *D. discoideum.* The number of cells used in these experiments were increased in an attempt to raise cobalamin levels to within the detectable range of the ELISA. However, cells were raised to the limit of the experimental method with no detection evident. Cobalamin levels within *D. discoideum* are clearly at a level that requires a more sensitive detection means, such as GC-MS or LC-MS. Unfortunately we did not have the facility to quantify cobalamin in this way, or find a collaborator able to quantify levels for us. With the concomitant identification of the *gcvH1* insertional mutant, and the significant data being produced (chapter 6) it was decided that investigation into LMBD2b be stopped and efforts be concentrated upon GCVH1.

In this chapter we recapitulated the resistant phenotype observed in the insertional mutant by ablating the *lmbd2b* gene from wild type (AX3) cells, and showed that LMBD2b null cells have a significant resistance to CBD compared to wild type (AX3) cells. The *lmbd2b* gene was then reinstated back into the null cell line using an extra chromosomal vector and was shown to re-

sensitize cells to CBD once again. This therefore suggests that LMBD2b carries out a role within *D. discoideum* which if disrupted confers a resistance to CBD. This role was initially believed to be through the regulatory uptake of CBD into the cell, however no significant difference in cellular CBD levels was found between wild type (AX3) and the LMBD2b null cell line. This suggests that the resistance in the null cell line is caused by the disruption of a different process in which LMBD2b plays a role. By carrying out phylogenetic analysis on LMBD2b we have shown that LMBD2b is a member of the lipocalin-interacting membrane receptor (LIMR) family of proteins, which are involved in the transport of small hydrophobic molecules. With the possibility that LMBD2b may be involved in the cellular uptake of cobalamin we attempted to quantify cobalamin levels within *D. discoideum*. However, we have shown that no detectable level of cobalamin was found in *D. discoideum* using an ELISA approach. Because a more sensitive process in detecting cobalamin levels was not available and because our research into the other gene *gcvH1* was yielding more significant data we decided not to investigate LMBD2b any further. Our research therefore concentrated more on the *gcvH1* gene identified in the mutant screen (see chapter 6).

Chapter 6

Glycine Cleavage System H-protein

6.1 Introduction

Previous chapters have described the use of a genetic screen to identify mutants showing potential resistance to the cannabinoids cannabidiol (CBD), cannabidiolic acid (CBDA) and cannabidivarin (CBDV). Analysis of these mutants, using either an inverse PCR technique (Kein *et al*, 2004) or whole genome sequencing, has made it possible to identify the genes disrupted within each of these mutants that may infer resistance. Of the 20 insertional mutants that were identified, one mutant displayed partial resistance to CBD. Whole genome sequencing identified the mutant to contain a disruption of *gcvH1* at the 88th base pair within exon 1 with the blasticidin resistance insert.

GCVH1 is a mitochondrial protein, and is a component of the glycine cleavage system (GCS) which is responsible for the metabolic regulation of glycine levels (Kikuchi *et al*, 2008, Okamura-Ikeda *et al*, 1987). The possibility that CBD induces its anti-convulsant effects through the modulation of the glycine cleavage system by targeting the GCVH1 protein is an exciting one, and fits well with what we currently know about seizure onset and progression. By targeting GCVH1, CBD may regulate cellular glycine levels by altering activity of the glycine cleavage system. Glycine is well known to be an inhibitory neurotransmitter in the central nervous system (Dutertre *et al*, 2012) and carries out this function by altering chloride current through its association with the ionotropic glycine receptors (Lynch, 2004). If seizure onset is characterised by an increased activity of excitatory neurotransmission (Scharfman, 2007) then its prevention may be achieved through an increased inhibitory neurotransmission, possibly by increased glycine levels.

Also of interest, is that the glycine cleavage system is linked to the one carbon cycle by its use of tetrahydrofolate. The one carbon cycle is involved in the production of methionine and the methyl donor S-adenosyl methionine (SAM) from homocysteine and 5-methyltetrahydrofolate (Ducker and Rabinowitz, 2017). SAM is responsible for the transfer of a methyl group to a number of acceptor molecules, including neurotransmitters and DNA methyltransferases for DNA methylation (Miller, 2008, Moore et al, 2013). A popular hypothesis at present for understanding epileptogenesis and seizure onset is the DNA methylation hypothesis (Kobow *et al*, 2013). Whereby methylation at key DNA sites has a positive feedback on seizure activity. It is therefore possible that CBD may prevent seizure activity by modulating key components of the one carbon cycle.

In this chapter we undertake a detailed analysis of GCVH1 in *D. discoideum* as a potential target for CBD. We firstly recapitulate the resistant phenotype found within the mutant screen by

ablating *gcvH1* from wildtype (AX3) cells, and then reinstate sensitivity by expressing either the *D. discoideum* or the *H. sapiens* gene extra chromosomally. We look at the bioinformatics of both the *D. discoideum* GCVH1 and the *H. sapiens* GCSH proteins and compare functionality, and show that both proteins localize to the mitochondria when expressed in *D. discoideum* cells. By utilising GC-MS and NMR analysis we look at the cellular levels of key amino acids and metabolites linked to the one carbon cycle, and investigate whether CBD treatment or *gcvH1* ablation affect such levels.

6.2 Results

6.2.1 Bioinformatics analysis

The use of *D. discoideum* as a tractable model organism in biomedical research is possible as it possesses highly conserved genes found within higher organisms that are not found in other simple model organisms. For example it is well documented that *D. discoideum* possesses many genes found in humans that are absent in both *S. cerevisiae* and *S. pombe* (Torija *et al*, 2006). *D. discoideum* is also recognised by the National Institutes of Health (NIH) as one of the few simple model organisms appropriate for biomedical research. To enable the translation of our findings across to humans it was essential to carry out bioinformatics analysis to confirm that both *D. discoideum* and *H sapiens* possess orthologous H-proteins. Comparison of the primary (amino acid) structure of the *D. discoideum* GCVH1 protein with the human GCSH protein indicates some conservation, with an E-value of 3e-34 across 84% of the *D. discoideum* protein sequence. A protein is commonly considered to be a homologue if it has an E-value of approximately 1e-40 or less (Eichinger *et al*, 2005). Despite the E-value being just above this recommended threshold (therefore not considered an orthologue), both proteins are regarded as having the same cellular function within the glycine cleavage system in an accepted genome resource tool (uniprot). Primary sequences for both proteins were also aligned using clustal omega alignment software (Fig 6.1a). This showed that both proteins were highly conserved across most of their length apart from the N-terminus. This region of both proteins is occupied by a mitochondrial localization sequence responsible for ensuring the correct localization to the inner mitochondrial membrane. Within *D. discoideum* (Uniprot ref: Q54JV8) this sequence is made up of the first 30 amino acid residues, while in *H. sapiens* (Uniprot ref: P23434) it is made up of the first 48.

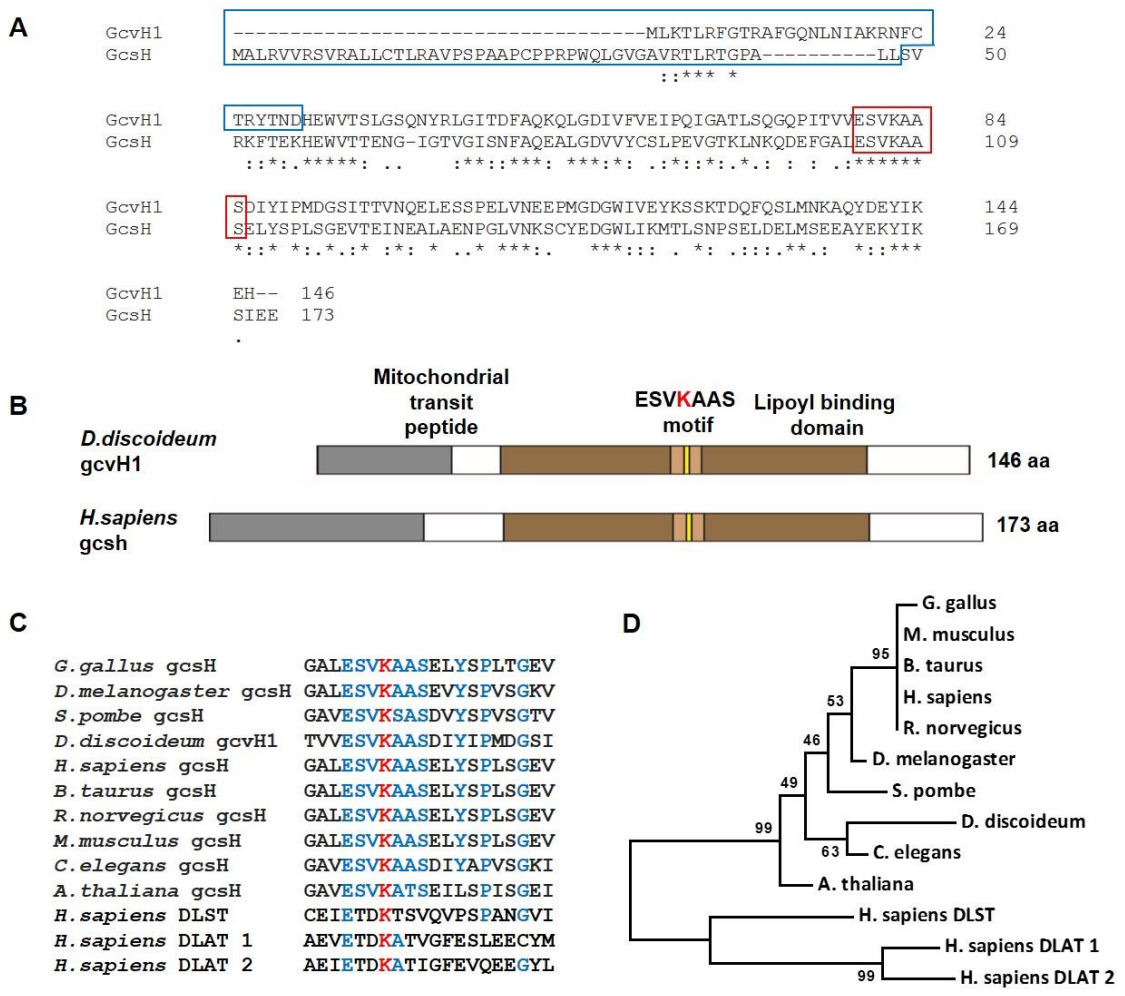

Figure 6.1 Bioinformatics analysis of the *D. discoideum* GCVH1 protein and the *H. sapiens* GCSH protein. (A) Clustal omega sequence alignment software was used to align and compare the *D. discoideum* GCVH1 and the *H. sapiens* GCSH protein. The blue box highlights the mitochondrial localization sequences and the red box highlight the ESVKAAS motif required for lipoic acid binding. (B) Both the *D. discoideum* and the *H. sapiens* proteins are of similar size, and contain highly conserved regions found within each. Such regions include a mitochondrial localisation sequence (grey) and a lipoyl binding domain (brown), containing the ESVKAAS motif for lipoic acid binding (light brown/ yellow). (C) The lipoic acid binding motif is highly conserved across a broad range of biological species. (D) Phylogenetic analysis shows the similarity of the *D. discoideum* H-protein to higher organisms.

Both proteins are approximately the same size, and both possess the same domain structures and motifs. The *D. discoideum* protein contains 146 amino acid residues while the *H. sapiens* protein has 173 (Fig 6.1b). This small difference in size can be mainly attributed to the extra 18 residues found within the *H. sapiens* mitochondrial localization sequence. The other types of domain structures found within both proteins are also consistent, such as the lipoyl binding domain (Fig 6.1b). This domain is found within the centre of both proteins, and consists of 82

amino acid residues within both. Functionally, the lipoyl binding domain is required for the binding of lipoic acid for use as a co-factor, responsible for the shuttling of glycine intermediates around the glycine cleavage system (Kikuchi *et al*, 1982). Both proteins were also found to possess the conserved ESVKAAS motif (Fig 6.1c), which contains the Lysine residue to which the lipoic acid covalently binds. These analyses suggest that both the GCVH1 and human GCSH proteins contain the same domains and motifs, consistent with a conserved cellular role.

The ESVKAAS motif and surrounding residues are found to be highly conserved within the H-protein of a number of organisms (Fig 6.1c), due to the essential function of the lysine residue in binding lipoic acid. We also compared the conservation of the ESVKAAS motif to that of two other lipoyl binding proteins found within humans: Dihydrolipoamide succinyltransferase (DLST), a component of the mitochondrial 2-oxoglutarate dehydrogenase complex; and the two lipoyl binding domains of Dihydrolipoyllysine-residue acetyltransferase (DLAT), a component of the mitochondrial pyruvate dehydrogenase complex. Interestingly, it was found that while the lysine residue was conserved and remained crucial for lipoic acid binding, in both DLST and DLAT the residues immediately surrounding the lysine were not (Fig 6.1c). We further investigated this by comparing the lipoyl binding domains as a whole. Phylogenetic analysis of the lipoyl binding domains show that the *D. discoideum* GCVH1 protein falls within the same clade as higher organisms, while both DLST and DLAT form an outlying group (Fig 6.1d). This further supports the close homology between the *D. discoideum* GCVH1 protein and the *H. sapiens* GCSH protein.

The tertiary structure of *D. discoideum* GCVH1 is very similar to the *H. sapiens* GCSH protein. Using the Protein homology/analogy recognition engine V 2.0 (Kelley et al, 2015) we predicted the tertiary structure of both proteins (Fig 6.2). Protein modelling shows that both the GCVH1 and GCSH proteins possess a predicted structure with alpha helices and beta sheets in similar regions for both proteins. Only at the n-termini of both proteins where the mitochondrial localization sequence is located is there any real difference. Similarly, protein modelling showed that both the GCVH1 and GCSH proteins contain similar hydrophobic and hydrophilic regions. Of particular interest is the hydrophilic pocket adjacent to the ESVKAAS motif (Fig 6.2) found on both proteins

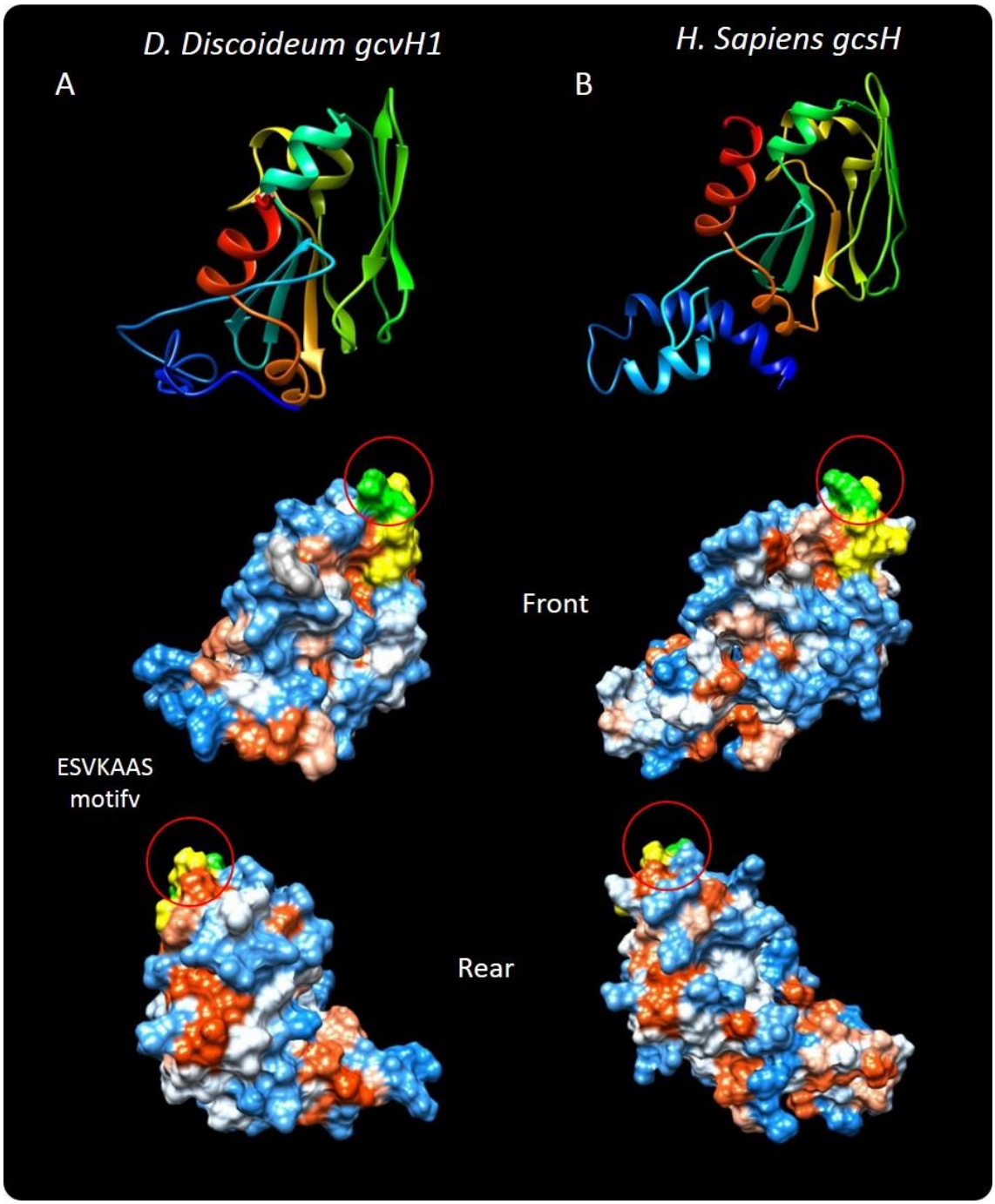

Figure 6.2 Predicted structural analysis of both GCVH1 and GCSH. The tertiary structure of both the (A) *D.discoideum* GCVH1 and (B) the *H. sapiens* GCSH proteins were predicted using protein prediction software Phyre2 (http://www.sbg.bio.ic.ac.uk/phyre2), and displayed as both ribbon and hydrophobicity images. Phyre2 uses homology modelling to predict a proteins tertiary structure based upon the proteins primary sequence and an experimentally gotten three dimensional structure of a homologous protein (Kelley et al, 2015). On the hydrophobicity images blue shows hydrophobic regions of the protein while red shows hydrophilic regions. The yellow region highlights the amino acid residues of the ESVKAAS motif and the green region (circled in red) indicates the position of the essential lysine residue.

Unlike most organisms which have only one copy of the H-protein gene, *D. discoideum* is unusual in that it has 5 copies, *gcvH1- gcvH5,* all of which are located on chromosome 5 (Table 6.1). As to why *D. discoideum* requires five copies of the gene is unclear, especially as only those found on the Watson strand (*gcvH1* and gcvH3) possess the conserved lysine residue (Fig 6.3). All five GCVH proteins in *D. discoideum* are recognised as having lipoyl binding domains (uniprot).

GcvH gene	Dictybase ID	Co-ordinates	E-value	AA number
gcvH1	DDB_G0287773	678742-679484	3e-34	146
gcvH2	DDB_G0290845	4668574-4669371	4e-23	150
gcvH3	DDB_G0287791	709302-709832	1e-17	149
gcvH4	DDB_G0287795	711021-711650	2e-05	209
gcvH5	DDB_G0287861	711961-712452	nss	163

Table 6.1 The *gcvH* gene family within *D. discoideum*. Five genes, denoted *gcvH1-5*, have been identified in the *D. discoideum* genome resource (Dictybase.org) as potential orthologues of the mammalian *gcsH*. These are presented with unique gene identity codes (ID), chromosomal location, genome localisation (co-ordinates), an estimation of overall homology provided through BLAST alignment to give E-values where smaller numbers indicate increased likelihood of similarity (nss = no significant similarity), and their amino acid number.

The lysine residue is crucial for the binding of lipoic acid (Kikuchi *et al*, 1982) and without it the protein would be unable to function correctly. Of the three H-proteins lacking the lysine residue, GCVH2 instead possesses an asparagine residue at position 85, GCVH4 a glutamic acid residue at position 119, and GCVH5 a serine residue at position 94. The lack of the lysine residue in GCVH2, GCVH4 and GCVH5 therefore makes it impossible for the correct binding of lipoic acid. Similarly, only GCVH1 and GCVH5 are known to possess a mitochondrial localization domain, essential for a true orthologue of the human H-protein. From the five potential GCSH encoded proteins, only GCVH1 contains the lipoic acid binding lysine residue, and the mitochondrial targeting sequence, suggesting that GCVH1 is the most likely *D. discoideum* orthologue of the human GCSH protein.

RNA sequence analysis data from the online gene expression depository Bgee (https://bgee.org) was used to check the distribution and levels of *gcsH* expression within both *H. sapiens* and

```
GcvH4      MNKIISNKIINNNIIFRNNFNNLFFIRNFINNKNNNNNNNNNNNNNNNNNNRNKKLKYSP     60
GcvH5      ---------------------------MFLFK--------TTNNLRKSLSNKFFCTRYSK     25
GcvH3      ------------------------MISNFL----------KSNNIKNNSPFRSFCTRYSE     26
GcvH1      ------------------------MLKTLRFGT-------RAFGQNLNIAKRNFCTRYTN     29
GcvH2      ----------------------MNIIKTGIKQS-------LVSGIYSKVGIRAFCTHYSA     31
                                                      .   .   :    :*:

GcvH4      NHQWIKISENKDF------------ATIGITNYVSDIVNNEFNKILKIKLPKINDKIR-L     107
GcvH5      NHLWISINNNNNSNNNNNNNNNIIIGTLGLTENGP---INKFDDVLYIKFPIIKDENQVD     82
GcvH3      SHEWIKFNHRNKT------------CTLGITKYAS----DQLKSIVNINLPDLNSTIT-R     69
GcvH1      DHEWVTSLGS-QN------------YRLGITDFAQ----KQLGDIVFVEIPQIGATLS-Q     71
GcvH2      ELEWVKLSDDNKV------------ATVGLSSFGA----QRLGKINYVELPKEHRKCR-R     74
           .  *:.     .               :*::.       ..: .:  :::*

GcvH4      NQPFLSIWTKEEENIQFKSPL-SGIVSKVNNKFNNQQTTTISTKTTTTTKIKPKLPLKS     166
GcvH5      DEPLTISLDTISDQILLNSPIRNCKLISINQDVLD-----------------------YP     119
GcvH3      KQPFGNIEST-KTVADLFSDV-DGKAVLLNSDVIV-----------------------DP     104
GcvH1      GQPITVVESV-KAASDIYIPM-DGSITTVNQELES-----------------------SP     106
GcvH2      EEKFGVIESSNATAFGLYAPV-SGEVLEVNEKLKK-----------------------SP     110
            : :            :   : .     :*...

GcvH4      NSLFFNNDQDSWTIELKINEPFQTNHLMTEEEYAHYCENTDYK--    209
GcvH5      NYINSSPMSKGWLCKIKFSNINDFNSLMNKNEYDNYCKNKIIKI-    163
GcvH3      TIVSHSPEDKGWLIKMESNDFESFNKMMTKSEYGQFLKDINKSNV    149
GcvH1      ELVNEEPMGDGWIVEYKSSKTDQFQSLMNKAQYDEYIKEH-----    146
GcvH2      SLLNEDPA-NNWMVKFKVSKPDEFKKLMDSNKYKKFVQWYR----    150
             :  .   ..*  : : ..  . : :* . :* .: :
```

Figure 6.3 Sequence alignment of the *D. discoideum* GCVH proteins. Clustal omega sequence alignment software was used to align and compare the five *D. discoideum* GCVH proteins against each other. The red box highlight the ESVKAAS motif required for lipoic acid binding.

M. musculus. Data used by Bgee is based exclusively on normal healthy expression data. It was found that the human *gcsH* gene is expressed within 92 organs throughout the body. Expression levels were found to be greatest within the frontal cortex region of the brain. Both the hypothalamus and prefrontal cortex regions of the brain were also found to be within the top ten expression regions. Data for the *M. musculus gcsH* gene shows the gene to be expressed within 67 organs. Expression levels were found to be greatest in the liver, while expression levels were fourth highest within the brain region as a whole.

6.2.2 Ablation of *gcvH1* from AX3 wildtype cells

To investigate if loss of GCVH1 reduces sensitivity to CBD, an independent *gcvH1*$^-$ mutant was made. The ablation of *gcvH1* from the wild type (AX3) genome was achieved by carrying out homologous recombination using a specially designed knockout construct (Fig 6.4a). The

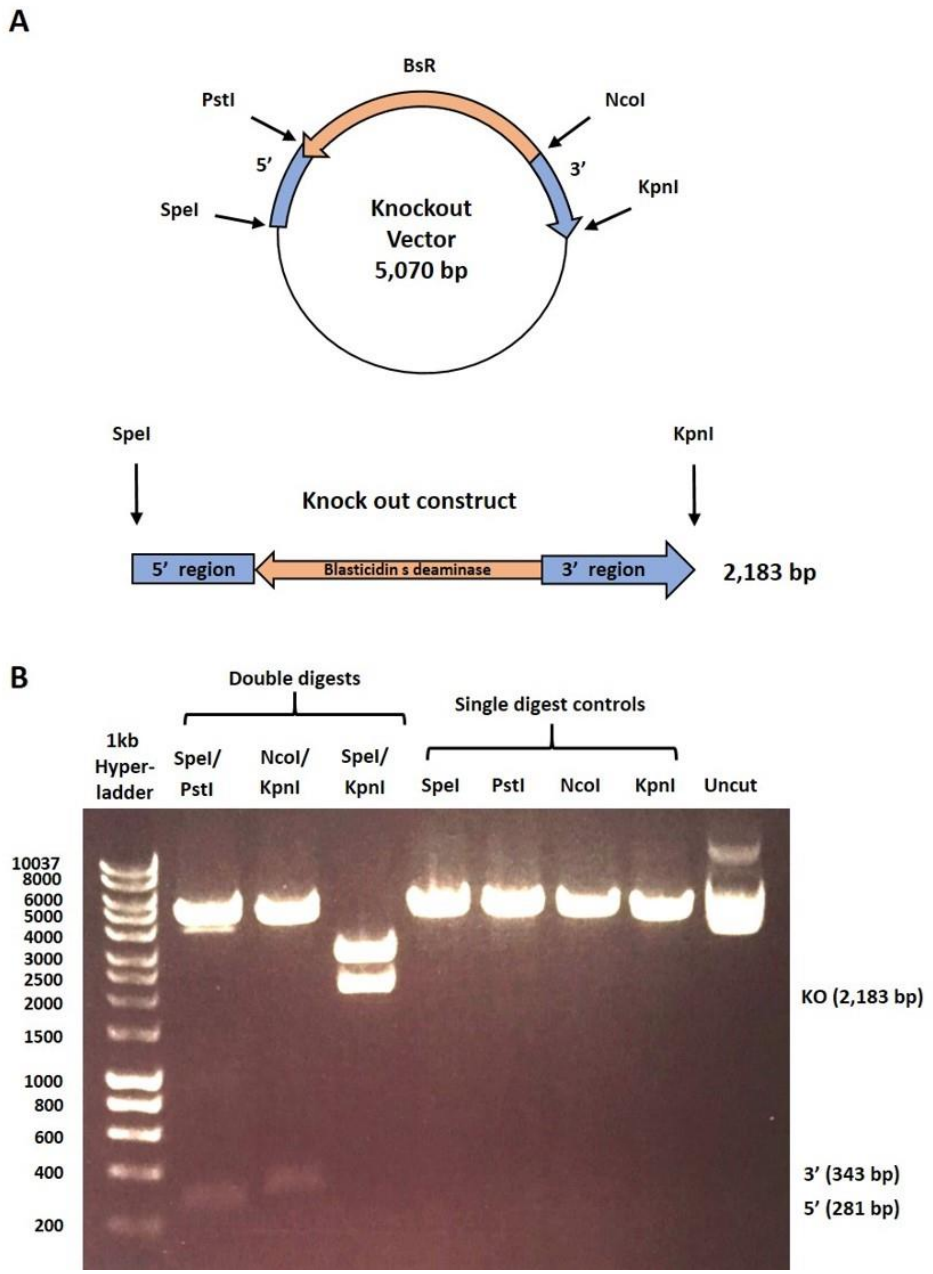

Figure 6.4 Creation of the *gcvH1* knockout vector and confirmation by restriction digest. (A) Schematic showing how fragments from the 5' and 3' regions of the *gcvH1* gene were amplified and ligated into the pLPBLP knock out vector flanking the blasticidin deaminase gene in the opposite orientation. The 5' fragment was ligated into the vector using the restriction enzymes SpeI and PstI, while the 3' fragment was ligated in using NcoI and KpnI. With the 5' and 3' *gcvH1* fragments ligated into pLPBLP the knock-out vector measures 5,070 bp. Prior to transformation the knockout vector was digested with SpeI and KpnI to produce the knockout construct which will undergo homologous recombination with *gcvH1* in the genome. (B) Restriction digest analysis was used to confirm the presence of the fragments within the pLPBLP knockout vector. Double digests included SpeI/ PstI (281 bp) for the 5' fraqgment, NcoI/ KpnI (343 bp) for the 3' fragment, and SpeI/ KpnI (2183 bp) for the knockout construct. Single digests and uncut vector were used as controls.

knockout construct for *gcvH1* was created by cloning the 5' and 3' regions of *gcvH1* into the pLPBLP plasmid at the SpeI/ PstI and NcoI/ KpnI restriction sites respectively (see 2.2.2.11 for method). Construction of the knockout construct was designed so that the ESVKAAS region of GCVH1 would be absent in any truncated protein produced. Thus, the absence of the essential lysine residue required for lipoic acid binding would render any truncated protein functionally redundant.

Both the 5' and 3' fragments were correctly cloned into pLPBLP at the correct location and orientation. The location of each fragment was verified by carrying out a series of double restriction digests upon the knockout vector and visualized with gel electrophoresis (Fig 6.4b). A SpeI/PstI digest was used to confirm the location of the 5' fragment and an NcoI/KpnI digest

the location of the 3' fragment. A further SpeI/KpnI double digest of the knockout vector confirmed the presence of the knockout construct (2183 bp) required for homologous recombination. Single digests of the knockout vector were also carried out as controls to confirm the uniqueness of each restriction site used. In addition to restriction site analysis the knockout construct was also sequenced to confirm its correct construction. Following transfection of wild type (AX3) cells with a purified knock-out construct, cells were selected for blasticidin (20 mg/ml) resistance. Transfected cells resistant to blasticidin were grown to confluency and PCR screened for homologous recombinants (see 2.2.2.12 for method) using six different primer combinations (Fig 6.5a). The screening of 134 potential *gcvH1* null cell lines identified a positive homologous integrant for both the 5' and 3' regions (Fig 6.5b). Isogenic *gcvH1* null cell lines were then created by sub-cloning onto bacterial plates and underwent further PCR screening.

Following the ablation of *gcvH1* and the creation of an isogenic *gcvH1*$^-$ cell line, RT-PCR was used to confirm the loss of *gcvH1* gene expression (Fig 6.5c). Due to the small size of *gcvH1*, primers were designed to amplify the entire open reading frame, with both primers amplifying across the two introns, producing a 422 bp PCR product. This also acted as a secondary control confirming that the amplified product was not derived from contaminating DNA. This approach confirmed that *gcvH1* expression was present within wild type (AX3) cells, but absent in *gcvH1*$^-$ cells. The mitochondrial large subunit rRNA gene, *lg7* was used as a positive control producing a 559 bp band in both wild type (AX3) and *gcvH1*$^-$ cell lines. These data therefore demonstrate both the insertion of the knock out cassette into *gcvH1* and loss of *gcvH1* expression, confirming that this cell line, *gcvH1*$^-$ contains an ablated gene.

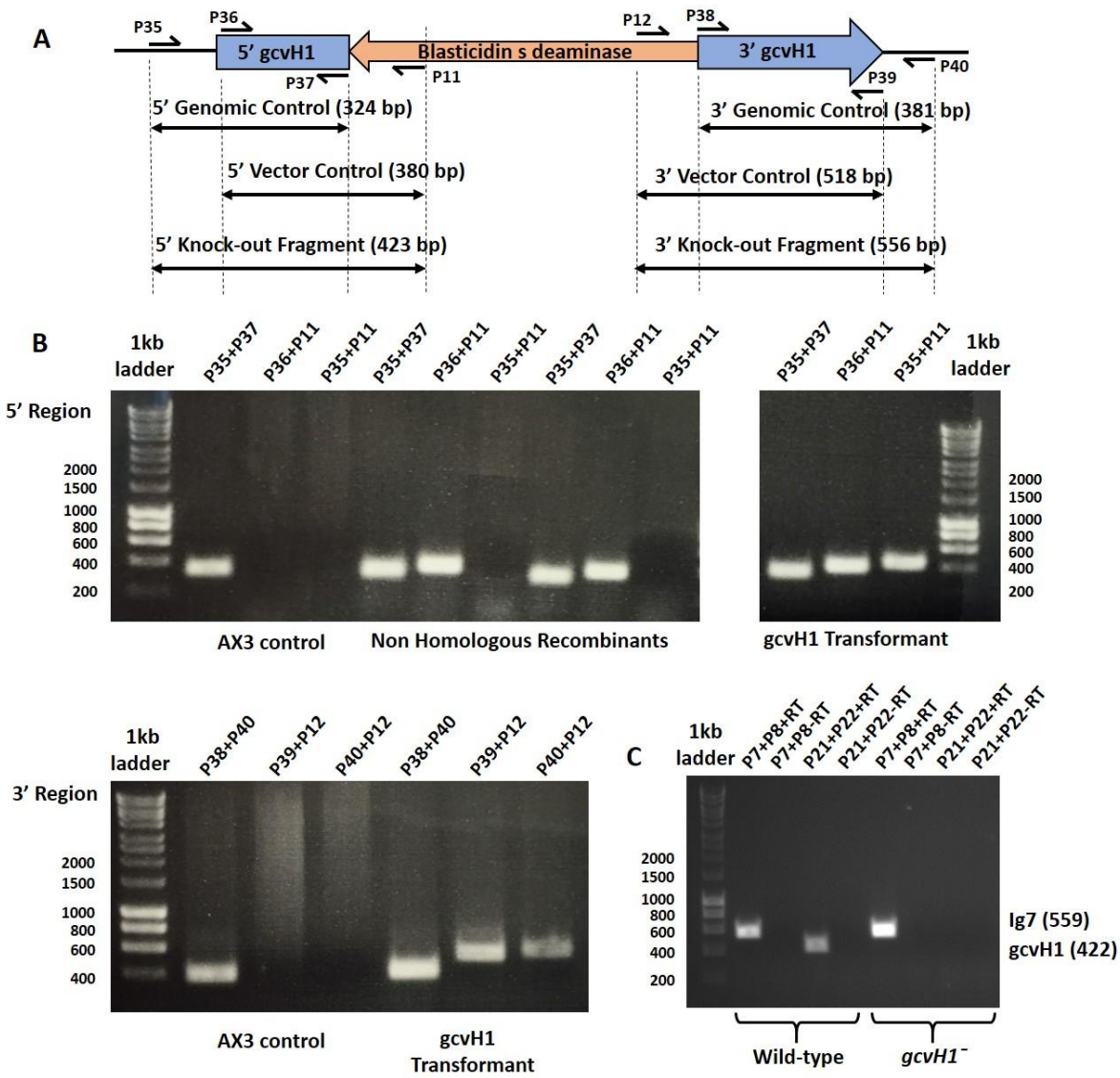

Figure 6.5 PCR screening to identify a *gcvH1* null cell line. (A) A schematic showing the approach used to screen for a *gcvH1* null cell line. Primer combinations (single sided arrows) were designed that would read from outside the *gcvH1* gene (blue) into the blasticidin deaminse gene (orange). Only homologously integrated transformants would possess the unique knock-out fragment for both the 5' and 3' regions of the gene. Further primers labelled 'genomic control' and 'vector control' were designed for both the 5' and 3' regions to act as controls. (B) PCR analysis of all primer combinations were used to identify homologously integrated transformants, which would possess the genomic control band, vector control band and knockout fragment band for both 5' and 3' regions. AX3 wild-type cells were used as a control, producing only genomic control bands. (C) Creation of an isogenic *gcvH1* null cell line was confirmed using RT-PCR. The mitochondrial large subunit rRNA gene, *Ig7* was used as a control.

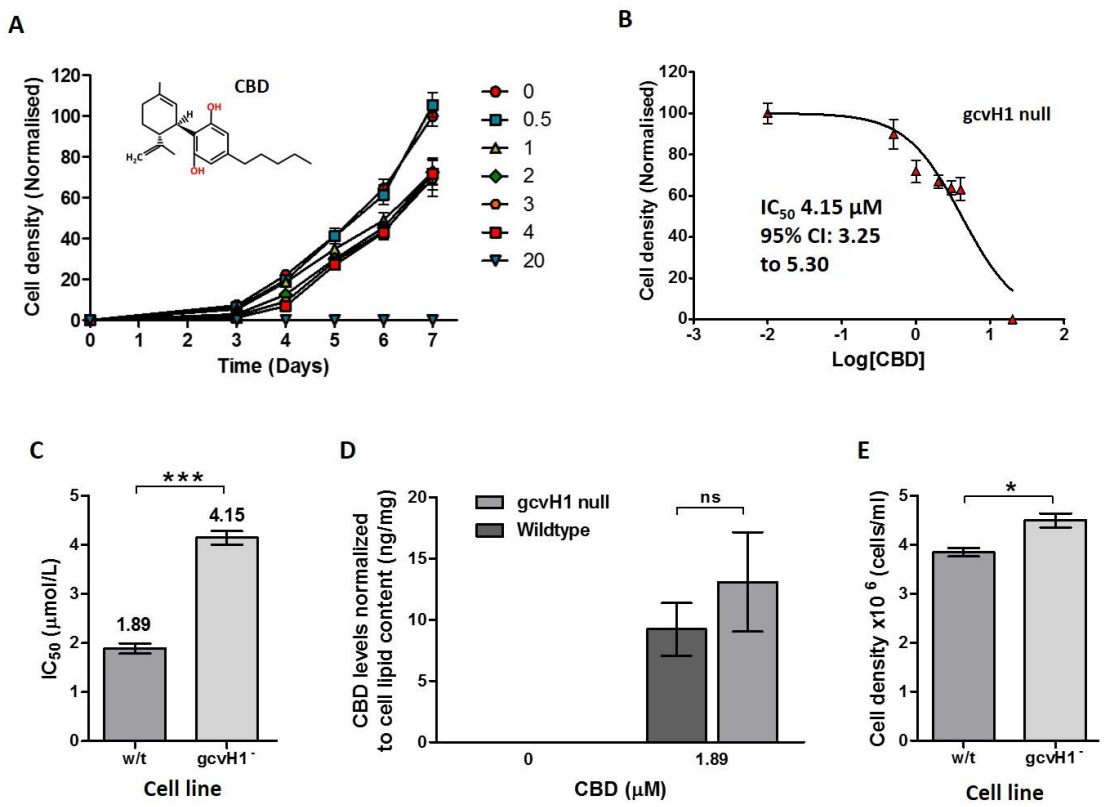

Figure 6.6 Ablation of *gcvH1* creates a CBD-resistant phenotype not explained by reduced CBD uptake or increased removal/degradation. (A) *D. discoideum gcvH1* null cells were treated with CBD for seven days under a range of concentrations. Cell growth was blocked at 20 µM, but displayed partial resistance at all other concentrations (B) A dose response curve of normalised cell density against the Log of CBD concentration was used to calculate the IC_{50} value with a 95% confidence interval. (C) IC_{50} values of both wild-type (AX3) and *gcvH1* null cell lines. Data are mean +/- SEM (P<0.001, Students t test, n=9). (D) Cellular CBD levels were quantified within *D. discoideum* wildtype (AX3) and *gcvH1* null cell lines using LC-MS following a 12 hour CBD treatment regime. Data are mean +/- SEM (P>0.05, Students t test, n>6). (E) Cell density of wild-type (AX3) and *gcvH1* null cells following 12 hour CBD treatment, prior to CBD quantification using LC-MS analysis. Data are mean +/- SEM (P<0.05, Students t test, n>6).

6.2.3 Recapitulation of the *gcvH1* insertional mutant phenotype

Following the ablation of *gcvH1* we repeated the CBD sensitivity growth assay to show a role for GCVH1 in the regulation of CBD sensitivity. In these experiments the *gcvH1*$^-$ cell line was treated with a range of CBD concentrations (0-20 µM) over a one week period and the growth-resistance to CBD assessed. The *gcvH1*$^-$ cell line displayed partial resistance to CBD, with a total block in cell growth at 20 µM (Fig 6.6a). Using the rate of cell growth within the exponential phase a dose response curve was plotted of the normalised cell density against the Log of CBD concentration (Fig 6.6b). This secondary plot was used to calculate an IC_{50} value of 4.15 µM with

a 95% confidence interval ranging between 3.25 µM and 5.30 µM. When compared to the IC_{50} value of wild type (AX3) cells, 1.89 µM, the *gcvH1*$^-$ cell line showed a significant (P<0.001) resistance to the effect of CBD (Fig 6.6c). These data suggest a role for GCVH1 in the regulation of CBD sensitivity, either as a direct target for CBD or through regulating CBD-sensitive signalling.

In addition to overcoming a direct or indirect effect of CBD through loss of GCVH1, other cellular mechanisms may give rise to this phenotype. Loss of *gcvH1* could increase the degradation of CBD, or modulate cellular levels through altered uptake or expulsion. To ensure that the resistance displayed by *gcvH1*$^-$ is not a consequence of increased metabolic degradation or increased/ decreased transport we quantified cellular CBD levels. Both wild type (AX3) and *gcvH1*$^-$ cell lines were treated with CBD at 1.89 µM for 12 hours, then cells were harvested, and cellular CBD content was quantified using liquid-chromatography mass-spectrometry (LC-MS). From this analysis, no significant difference (P>0.05) in cellular CBD content was found between wild type (AX3) and *gcvH1*$^-$ cells (Fig 6.6d). Cell density for each cell line was also quantified prior to LC-MS analysis. Cell density within the *gcvH1*$^-$ cell line was found to be significantly greater (P<0.05) than that of wild type (AX3) cells (Fig 6.6e). This confirmed that *gcvH1*$^-$ cells exhibit resistance to CBD within the same time frame (12 hours) that cellular CBD content was quantified.

6.2.4 GC-MS analysis of glycine, methionine and cysteine levels within AX3 and *gcvH1*$^-$ cell lines.

Due to the possible role that GCVH1 has in glycine metabolism and its close association with the one carbon cycle, we hypothesized that CBD treatment may impact upon the function of both the glycine cleavage system and the one carbon cycle. We therefore determined if CBD treatment or *gcvH1* ablation had an impact upon key metabolites found within the glycine cleavage system and the one carbon cycle, specifically the cellular levels of methionine, glycine and cysteine. It was predicted that following gcvH1 ablation cellular glycine levels would increase as the role of the glycine cleavage system is to primarily degrade glycine. How *gcvH1* ablation would effect methionine and cysteine levels was less clear as no previous studies had looked at this before. To quantify these key metabolites we treated wild type (AX3) and *gcvH1*$^-$ cell lines with 1.89 µM CBD or vehicle over a 12 hour period. Following treatment cells were harvested, washed and the cell lysate extracted. Gas chromatography mass spectrometry (GC-MS) was then used to quantify the methionine, glycine and cysteine levels within treated and untreated cell samples.

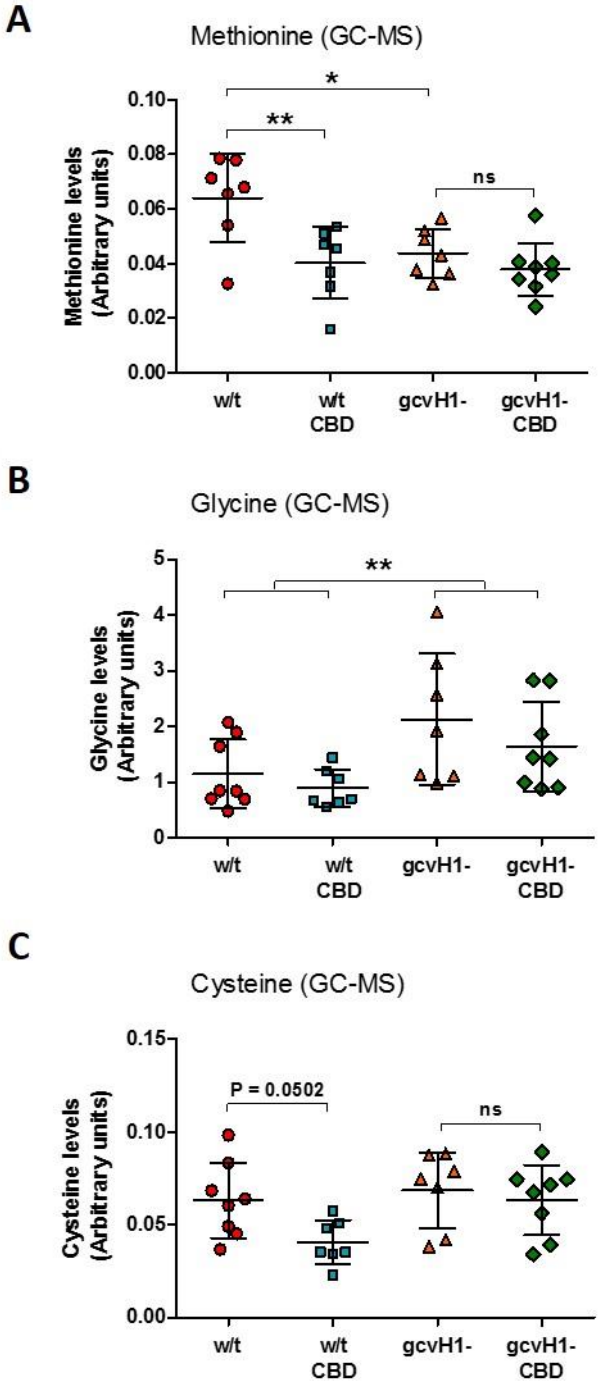

Figure 6.7 GC-MS analysis shows that treatment of AX3 wildtype and *gcvH1*⁻ cell lines with CBD modulates the homeostasis of amino acids found in the one carbon cycle and glycine cleavage system within *D. discoideum*. Both AX3 wildtype and *gcvH1*⁻ cell lines were treated with CBD or vehicle alone, and their amino acid composition analysed by GC-MS. Analysis shows that *gcvH1* ablation and CBD treatment directly alters the cellular composition of (A) methionine (B) glycine and (C) cysteine. Data are mean +/- SEM (*,P<0.05; **,P<0.01; ***,P<0.001, two-way ANOVA, Bonferroni post hoc test, n=6-9).

Methionine levels within the cell are regulated by the one carbon cycle, thus methionine levels were assessed in wild type (AX3) and *gcvH1*$^{-}$ cell lines. GC-MS analysis of the wild type (AX3) cell line showed that CBD treatment significantly lowered ($P<0.01$) cellular methionine levels compared to untreated cells (Fig 6.7a). Similarly, it was also found that methionine levels within untreated *gcvH1*$^{-}$ cells were comparable to that of CBD treated AX3 cells, being significantly lower ($P<0.05$) than untreated AX3 cells. Interestingly, CBD treatment of *gcvH1*$^{-}$ had no effect upon methionine levels when compared to untreated *gcvH1*$^{-}$ cells ($P>0.05$). Together, data is consistent with a GCVH1 dependant reduction in methionine levels following CBD treatment, and that the activity of the glycine cleavage system is necessary for the cellular effect of CBD.

Glycine catabolism is predominantly controlled by the glycine cleavage system, thus glycine levels were assessed in wild type (AX3) and *gcvH1*$^{-}$ cell lines. Analysis of cellular glycine levels by GC-MS showed that *gcvH1*$^{-}$ cells exhibited a significant overall increase ($P<0.01$) in glycine levels compared to wild type (AX3) cells (Fig 6.7b). This supports a role for GCVH1 and the glycine cleavage system in the regulation of glycine levels within the cells. CBD treatment however had no effect upon glycine levels in either wild type (AX3) or *gcvH1*$^{-}$ cells. Glycine analysis within the *gcvH1*$^{-}$ cell line does show levels to be widely variable, indicating that glycine homeostasis maybe disrupted following *gcvH1* ablation.

The main source of cysteine for use in the transsulfuration pathway and the production of glutathione comes from the one carbon cycle, thus cysteine levels were assessed in wild type (AX3) and *gcvH1*$^{-}$ cell lines. GC-MS analysis of the wild type (AX3) cell line shows that CBD treatment caused a trend ($P=0.0502$), whereby cellular cysteine levels are lowered following CBD treatment when compared to vehicle alone treated wild type (AX3) cells (Fig 6.7c). Similar to what was found with methionine levels, analysis showed that CBD treatment of *gcvH1*$^{-}$ cells had no effect upon cysteine levels when compared to untreated *gcvH1*$^{-}$ cells ($P>0.05$). In contrast to methionine however, the cellular cysteine levels within untreated *gcvH1*$^{-}$ cells were more comparable to that of untreated AX3 cells.

6.2.5 Creation of extra chromosomal vectors for the expression of *D. discoideum* GCVH1 and *H. sapiens* GCSH RFP fusion proteins.

Since data presented here suggest that ablation of *gcvH1* infers resistance to the effect of CBD on *D. discoideum* growth, it was important to restore this sensitivity by reintroduction of the protein. To further assess this we re-introduced the *gcvH1* gene back into the null cell line. We

also investigated the possibility that the role of GCVH1 in CBD resistance is conserved within the function of the human orthologue, GCSH. To test these hypotheses, we created extra chromosomal vectors using the pDXA-389-2 mRFPmars over-expression plasmid (Fischer *et al*, 2004). For the *gcvH1* expression vector, primers were designed complementary to the 5' and 3' extremities of *gcvH1* with extension sequences containing either BamHI or EcoRI restriction sites. The 3' primer was also designed to remove the stop codon from *gcvH1* when amplified. The *D. discoideum gcvH1* gene was then amplified from cDNA derived from wild type (AX3) cells and cloned into pDXA-389-2 mRFPmars at the EcoRI and BamHI restriction sites. The resultant expression vector was designed to produce a C-terminal tagged GCVH1-RFP fusion protein when expressed in *D. discoideum*. A C-terminal fusion protein was chosen over an N-terminal fusion protein to avoid interference with the mitochondrial localization sequence. The over expression vector containing the human open reading frame was synthesized using *D. discoideum* codon bias, and cloned into the same vector. Both the *D. discoideum* and the *H. sapiens* over-expression vectors were then transformed into the *gcvH1*$^-$ cell line.

Confirmation of *gcvH1* and *gcsH* expression within the rescue cell lines was confirmed using RT-PCR analysis. cDNA was created from the total RNA of both the *D. discoideum* and *H. sapiens* rescue cell lines and used to check for gene expression. RT-PCR analysis confirmed *gcvH1* expression within the *D. discoideum* rescue cell line through the presence of a 422 bp band (Fig 6.8a). Similarly, the presence of a 537 bp band (Fig 6.8b) produced from the cDNA confirmed expression of the human gene *gcsH* within the human rescue cell line. In both instances the mitochondrial large subunit rRNA gene, *Ig7* was used as an expression control, and produced a 559 bp band in both rescue cell lines.

In addition to gene expression we wished to see if GCVH1-RFP and GCSH-RFP fusion proteins of appropriate sizes were present within both rescue cell lines. This was achieved by carrying out western blot analysis of the cell lysates, using antibodies raised against the RFP component of the fusion proteins. A band of approximately 42 KDa was identified within both the *D. discoideum* and *H. sapiens* rescue cell lines, consistent with both GCVH1 and GCSH tagged to RFP (Fig 6.8c). No such band was found within the cell lysate of wild type (AX3) or *gcvH1*$^-$ cells. A *gcvH1*$^-$ cell line transfected with an empty pDXA-389-2 mRFPmars vector was used as a positive control for RFP, giving a band of approximately 27 KDa, consistent with free RFP protein. Together both RT-PCR and Western analysis of the rescue cell lines confirmed gene expression and protein presence.

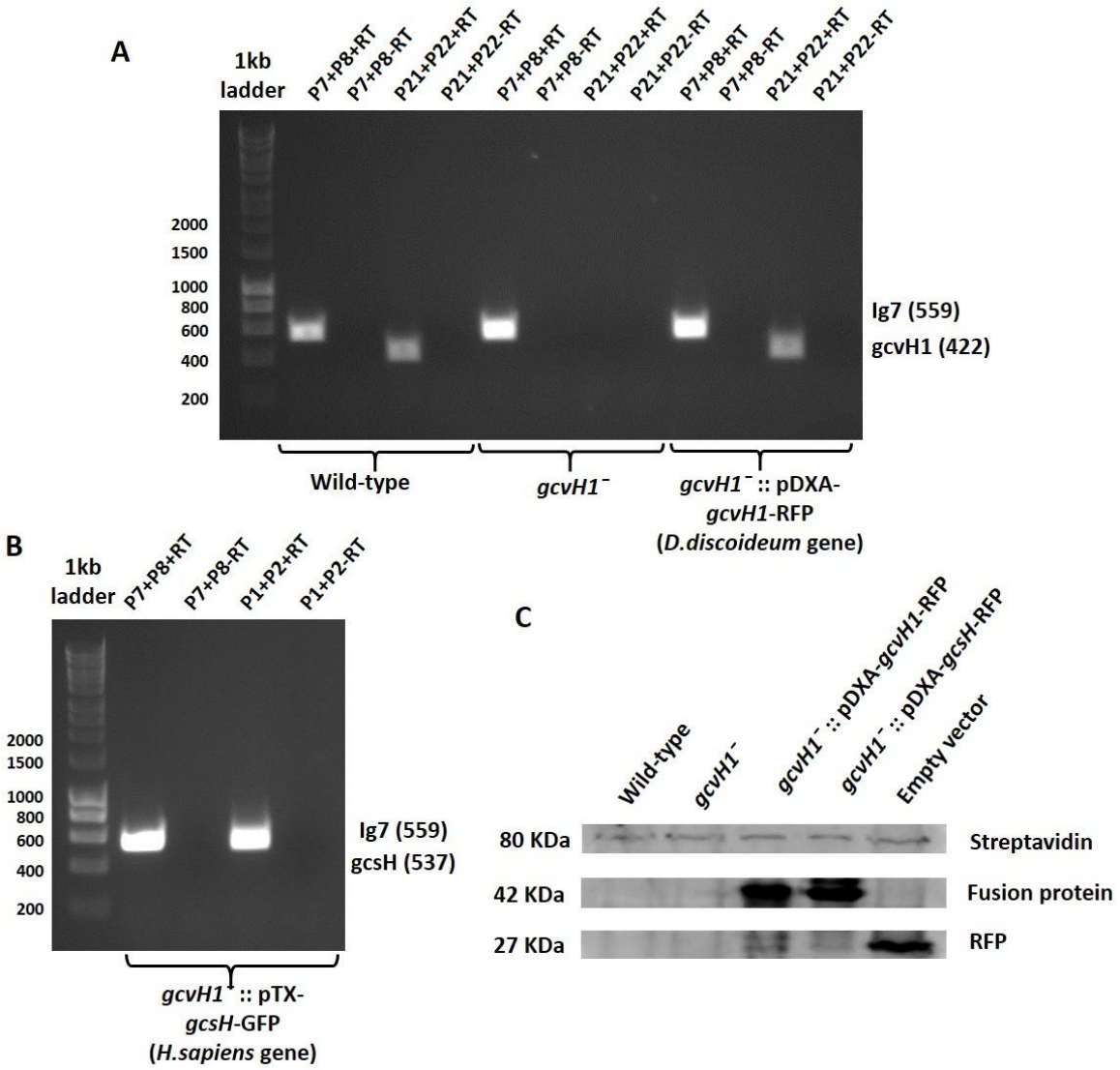

Figure 6.8 GcvH1 gene expression and protein presence was verified in the wild-type, *gcvH1⁻* and rescue cell lines. (A) The absence of *gcvH1* in the null cell line, and the presence of either *gcvH1* or (B) *gcsH* in the rescue cell lines was confirmed by RT-PCR. The mitochondrial large subunit rRNA gene, *Ig7* was used as a positive control. The negative control lanes contained the same reaction composition less reverse transcriptase (RT) to confirm absence of contaminating DNA. (C) The presence of GCVH1-RFP and GCSH-RFP fusion proteins within the rescue cell lines was confirmed by western blot analysis.

6.2.6 Cellular localization of GCVH1 and GCSH.

The introduction of RFP to the c-terminus of GCVH1 and GCSH may have prevented normal localization to the mitochondria. Because both proteins carry out their function within the mitochondria, any re-sensitization to CBD that the null cell line experienced would be questionable if correct localization was not shown. Cells were therefore analyzed using fluorescent microscopy and then validated with immunofluorescence to confirm mitochondrial localization. Fluorescent analysis of cells expressing *gcvH1-RFP* showed localization to small intracellular vesicles resembling mitochondria (Fig 6.9a). Localization was validated by fixing cells and then probing with both RFP and Porin antibodies. Porin is a mitochondrial protein localized to the outer membrane of mitochondria (Troll *et al*, 1992). Fluorescence microscopy of the fixed cells showed co-localization of RFP and Porin (Fig 6.9a), confirming GCVH1-RFP localization to the mitochondria within *D. discoideum* cells. Similarly, fluorescence analysis of the human fusion protein also showed localization to small intracellular vesicles resembling mitochondria (Fig 6.9b). Immunofluorescence was then used to confirm co-localization with Porin, confirming GCSH-RFP localization to the mitochondria also. With both the *D. discoideum* and the *H. sapiens* proteins confirmed to localize to the mitochondria any re-sensitization can be attributed to the reintroduction of the H-proteins.

6.2.7 Rescuing the CBD sensitive phenotype

With both the *D. discoideum* and *H.sapiens* genes confirmed to be expressed in the rescue cell lines, and with the relevant fusion proteins present and correctly localized, we aimed to establish if sensitivity to the effect of CBD upon growth was re-instated. The *gcvH1*$^-$ cells expressing either the *D. discoideum gcvH1* or the *H. sapiens gcsH* genes were assessed for the effect of CBD on growth, as previously described (section 6.2.3). The growth of the *D. discoideum* rescue cell line was inhibited by CBD in a dose dependant manner, with a total block in cell growth at 20 µM (Fig 6.10a). Using the rate of cell growth within the exponential phase a dose response curve was plotted of the normalised cell density against the Log of CBD concentration (Fig 6.10b). This secondary plot was used to calculate an IC_{50} value of 2.17 µM with a 95% confidence interval ranging between 1.64 µM and 2.89 µM. When compared to the IC_{50} value of *gcvH1*$^-$ cells which was calculated to be 4.15 µM, the *D. discoideum* rescue cell line showed a significant increase ($P<0.01$) in sensitivity (Fig 6.10c). Similarly, the growth of the *H. sapiens* rescue cell line was also inhibited by CBD in a dose dependant manner (Fig 6.10d), and an IC_{50} value of 0.82 µM with a 95% confidence interval ranging between 0.67 µM and 1.01 µM

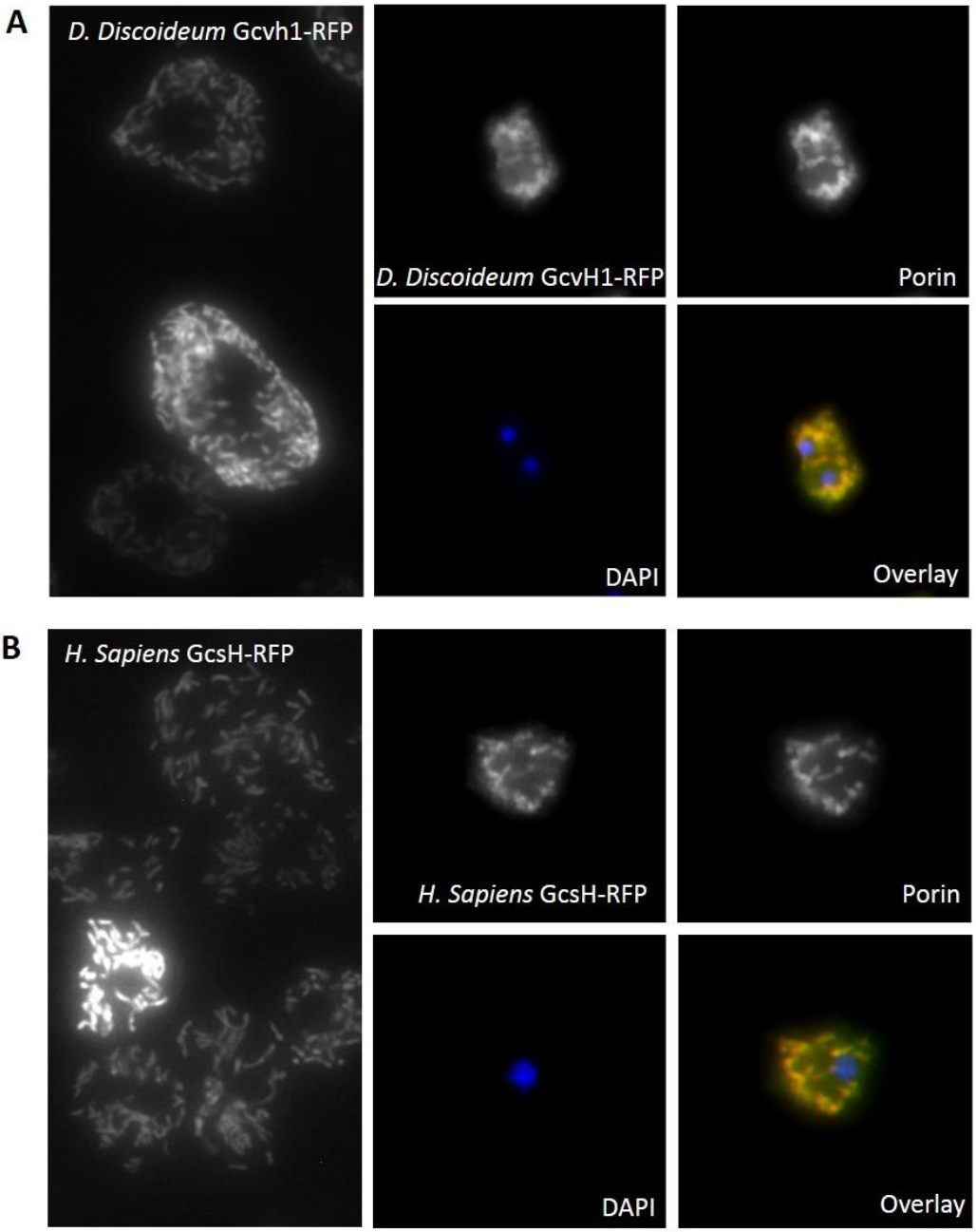

Figure 6.9 Both the *D. discoideum* GCVH1 and the *H. sapiens* GCSH proteins are shown to localize to the mitochondria when expressed as RFP fusion proteins in *D. discoideum*. Fluorescence microscopy was used to show that when expressed in *D. discoideum* (A) the *D. discoideum* GCVH1-RFP and (B) the *H. sapiens* GCSH-RFP fusion proteins localize to cellular compartments that resemble mitochondria. Immuno-fluorescence of *D. discoideum* shows that both GCVH1-RFP and GCSH-RFP co-localizes with Porin, a mitochondrial protein. Fluorescence and immuno-fluorescence images are shown in grey scale for clarity purposes. Nuclear staining is shown using DAPI (blue). Co-localization of both GCVH1-RFP and GCSH-RFP with porin is shown as an overlay of both RFP and GFP.

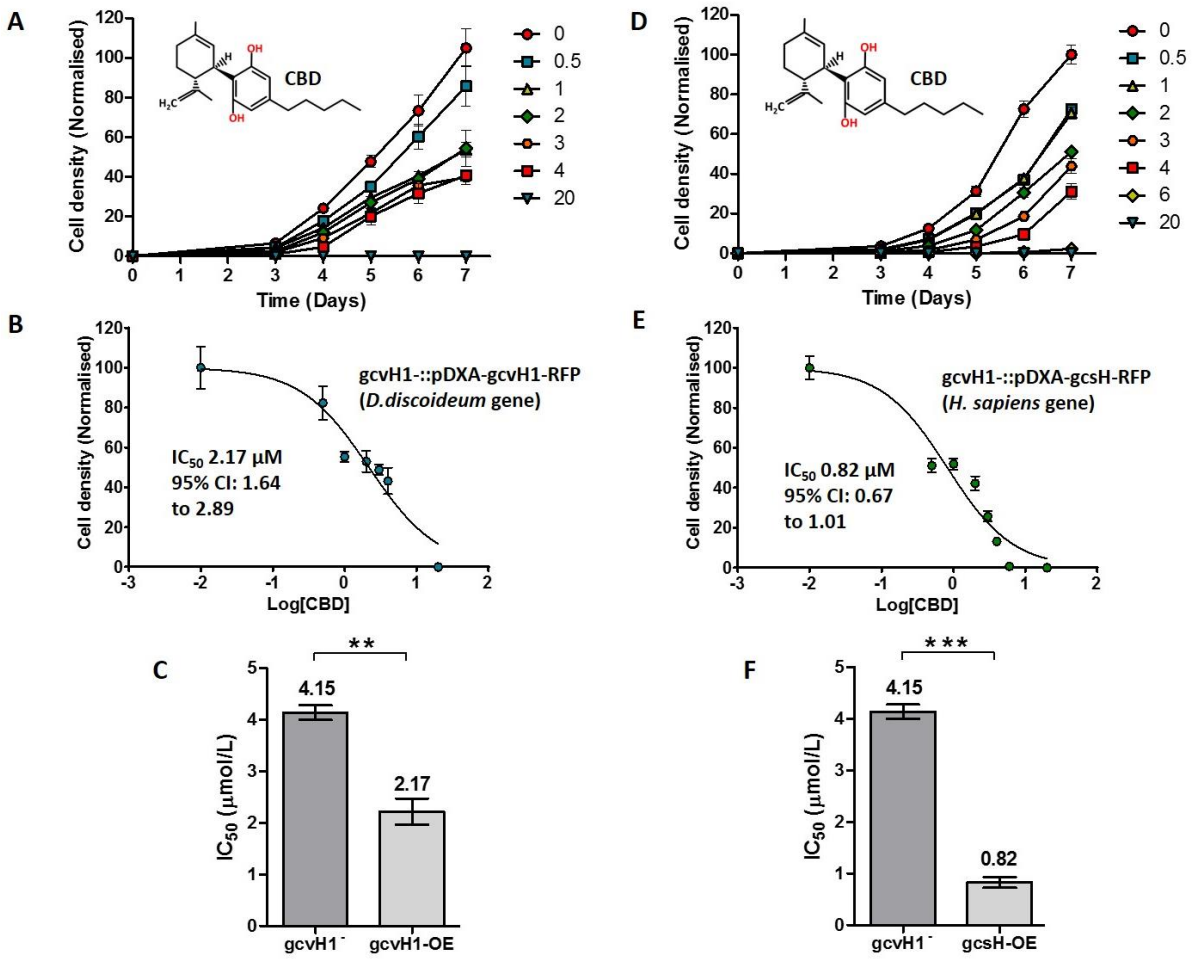

Figure 6.10 Expression of either *gcvH1* or *gcsH* within *gcvH1*⁻ cells using an extra chromosomal vector rescues the CBD sensitive phenotype found in AX3 wildtype cells. *D. discoideum* rescue cell lines with either (A) the *D. discoideum* or (D) the *H. sapiens* gene over expressed in *gcvH1*⁻ cells were treated with CBD for seven days under a range of concentrations. Cell growth was inhibited in both cell lines in a dose dependent manner similar to that found in AX3 wildtype cells. Dose response curves of normalised cell density for (B) *D. discoideum* rescue cells and (E) *H. sapiens* rescue cells against the Log of CBD concentration was used to calculate the IC_{50} values with a 95% confidence interval. The IC_{50} value of the *gcvH1*- cell line compared to (C) the *D. discoideum* rescue cell line and (F) the *H. sapiens* rescue cell line. Data are mean +/- SEM (**,P<0.01; ***,P<0.001, Students t test, n=9).

was calculated from a secondary plot (Fig 6.10e). The *H. sapiens* rescue cell line also showed a significant increase in sensitivity (P<0.001) to CBD when compared to *gcvH1*$^-$ cells (Fig 6.10f). These data clearly shows that reintroducing either the *D. discoideum* or *H. sapiens* gene resensitizes *gcvH1*$^-$ cells to the effect of CBD on growth. Showing that the re-introduction of the *D. discoideum* gene re-sensitizes cells to CBD strengthens the argument that the ablation of *gcvH1* is responsible for the resistant phenotype. Further to this, because the introduction of the human gene also resensitizes cells to CBD, this supports the hypothesis that both proteins possess similar functions. Also, it supports the hypothesis that CBD may have an effect within humans by targeting the GCSH protein.

6.2.8 GC-MS analysis of glycine, methionine and cysteine levels within the GCVH1-RFP and GCSH-RFP rescue cell lines.

Previous GC-MS analysis in this chapter looked at cellular methionine, glycine and cysteine levels within both wild type (AX3) and *gcvH1*$^-$ cells in the absence and presence of CBD. Because *gcvH1*$^-$ cells transfected with the over expression constructs were sensitized to CBD once again, we therefore investigated if rescuing the phenotype affected the cellular levels of the above mentioned amino acids as well. To test this both the *D. discoideum* and the *H. sapiens* rescue cell lines were treated with 1.89 µM CBD for 12 hours and assayed for methionine, glycine and cysteine as previously described (section 6.2.4). Table 6.2 shows an overview of all GC-ms results. Within the *D. discoideum* rescue cell line GC-MS analysis showed that CBD treatment significantly elevated (P<0.001) cellular methionine levels compared to cells treated with vehicle alone (Fig 6.11a). It was also noted that methionine levels were widely variable in the rescue cell line when treated with CBD. GC-MS analysis of cellular glycine levels within the *D. discoideum* rescue cell line showed no significant difference (P>0.05) between the CBD treated and untreated conditions (Fig 6.11b). Neither was there an overall change in glycine levels between the rescue cell line and *gcvH1*$^-$ cells. Analysis within the rescue cell line does show glycine data to be closely grouped again, indicating that glycine homeostasis maybe restored. This is in direct contrast to what was seen in the *gcvH1*$^-$ cell line where glycine data were widely distributed indicating a possible disruption in glycine homeostasis. GC-MS analysis of cellular cysteine levels within the *D. discoideum* rescue cell line showed no significant difference (P>0.05) between CBD treated and untreated conditions. There was however an overall decrease (P<0.001) in cysteine levels within the *D. discoideum* rescue cell line compared to *gcvH1*$^-$ cells (Fig 6.11c).

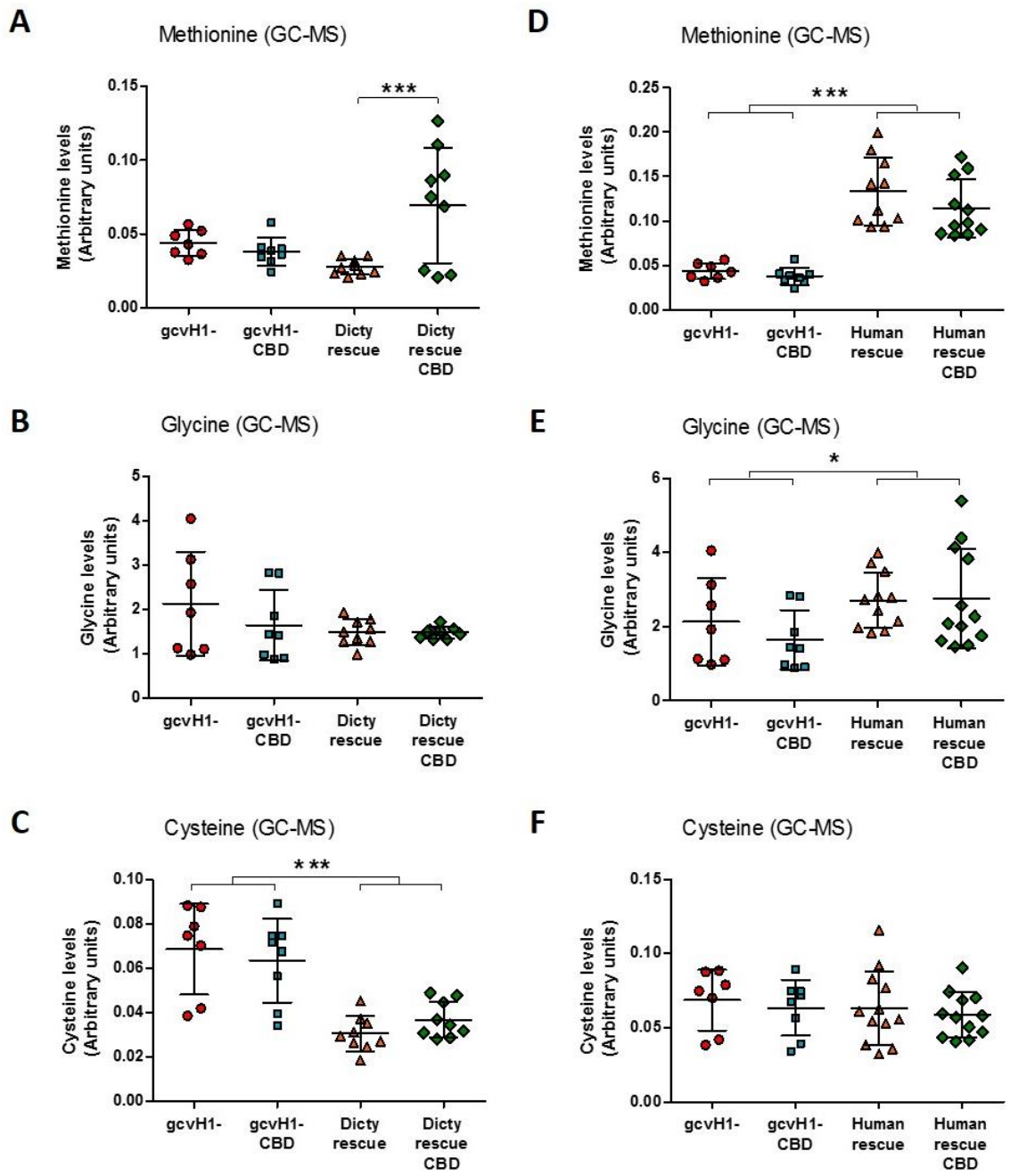

Figure 6.11 GC-MS analysis shows that treatment of both the *D. discoideum* and *H. sapiens* rescue cell lines with CBD alters the cellular levels of key amino acids found in the one carbon cycle and glycine cleavage system. *D. discoideum* rescue cell lines with either (A-C) the *D. discoideum* or (D-F) the *H. sapiens* gene over expressed in *gcvH1-* cells were treated with CBD or vehicle alone. The cellular methionine, glycine and cysteine levels within each cell line was analysed by GC-MS. Data are mean +/- SEM (*,P<0.05; **,P<0.01; ***,P<0.001, two-way ANOVA, Bonferroni post hoc test, n=6-9).

Within the *H. sapiens* rescue cell line GC-MS analysis showed that CBD treatment had no significant (P>0.05) effect upon cellular methionine levels compared to untreated cells (Fig 6.11d). Overall however methionine levels were found to be significantly higher (P<0.001) within the *H. sapiens* rescue cell line compared to *gcvH1*$^{-}$ cells. Earlier in the chapter it was shown that methionine levels within the *gcvH1*$^{-}$ cell line was significantly lower (P<0.05) compared to AX3 cells (Fig 6.7a). The introduction of *gcsH* into the null cell line therefore appears to have reversed this. GC-MS analysis of cellular glycine levels within the *H. sapiens* rescue cell line showed no significant difference (P>0.05) between the CBD treated and untreated conditions (Fig 6.11e). Interestingly, it was found that overall glycine levels within the *H. sapiens* rescue were significantly greater (P<0.05) than the *gcvH1*$^{-}$ cell line. This was unexpected as it was previously shown that the ablation of *gcvH1* elevate glycine levels. It was hypothesised that the introduction of *gcsh* would lower glycine levels. GC-MS analysis of cellular cysteine levels within the *H. sapiens* rescue cell line revealed no significant difference (P>0.05) between CBD treated and untreated conditions. Neither was there any overall change in cysteine levels when compared to *gcvH1*$^{-}$ cells (Fig 6.11f).

Amino Acid	AX3 Wild-type		*gcvH1* null		Dicty rescue		Human rescue	
	-CBD	+ CBD	-CBD	+ CBD	-CBD	+ CBD	-CBD	+ CBD
Methionine	-----	Up	Down	Down	Down	-----	Up	Up
Glycine	-----	-----	Up	Up	Up	Up	Up	Up
Cysteine	-----	Down	-----	-----	Down	Down	-----	-----

Table 6.2 Overview of the GC-MS analysis of methionine, glycine and cysteine within AX3 wild-tpe, *gcvH1*$^{-}$, *D.discoideum* rescue, and *H.sapiens* rescue cell lines. Table shows an overview of whether the cellular amino acid levels increased or decreased within the different cell types, compared to AX3 wild-type (vehicle treated). No change is shown by (-----).

6.2.9 NMR analysis of methionine and glycine

To independently validate changes in amino acid levels following CBD treatment, we employed a nuclear magnetic resonance (NMR) approach. Nuclear magnetic resonance (NMR) was chosen due to its highly sensitive nature and its ability to easily analyse other metabolites of the one carbon cycle not possible with GC-MS. In these experiments cells were treated as previously

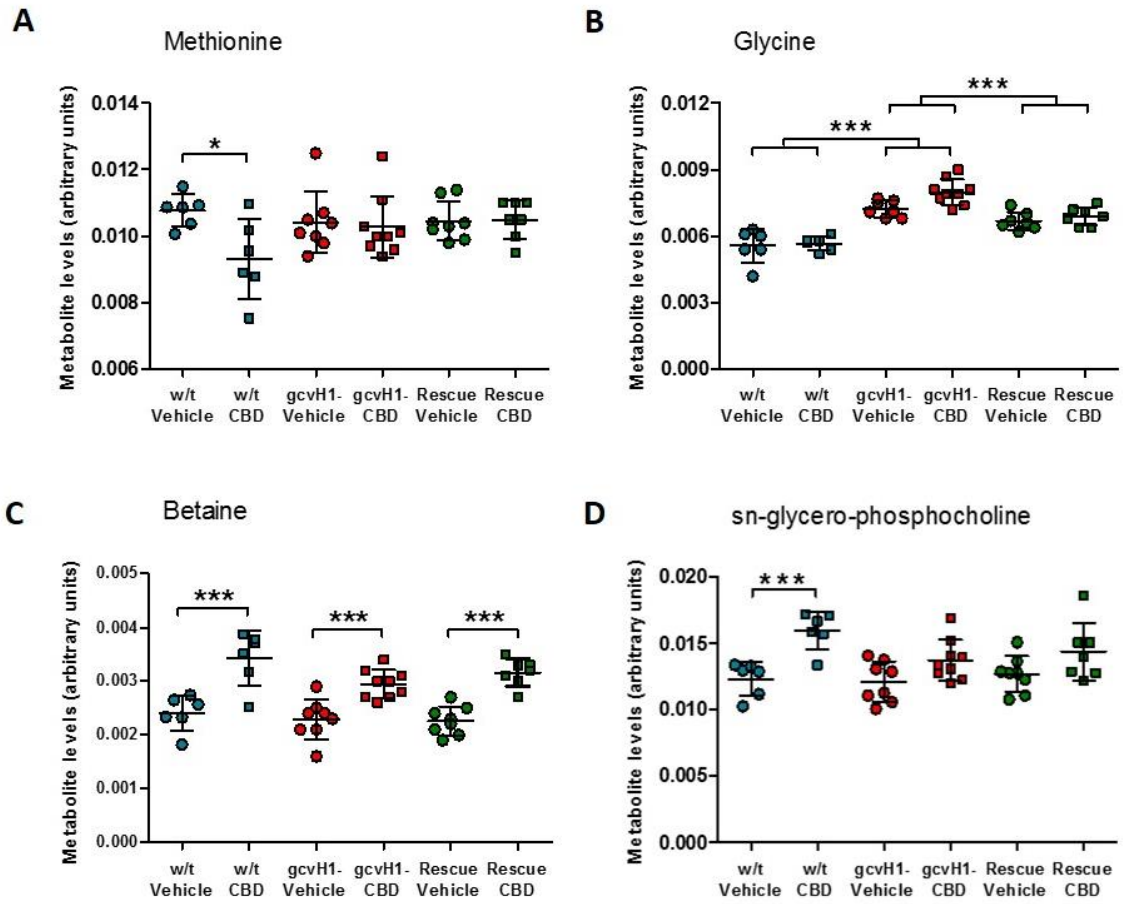

Figure 6.12 NMR analysis shows the effect that CBD treatment has upon cellular amino acid and metabolite levels within AX3 wildtype, *gcvH1*- and *D. discoideum* rescue cell lines. Wildtype (AX3), *gcvH1*$^{-}$ and a rescue cell line with the *D. discoideum* gene reinstated into the null cell line were treated with CBD or vehicle alone. The amino acid and metabolite levels of each were quantified using NMR analysis. Data are mean +/- SEM (*,P<0.05; **,P<0.01; ***,P<0.001, two-way ANOVA, Bonferroni post hoc test, n=6-9).

described for GC-MS analysis (section 6.2.4), and were analysed by collaborators at the University of Reading. NMR analysis showed that methionine levels within CBD-treated wild type (AX3) cells were significantly lower (P<0.05) than untreated wild type cells (Fig 6.12a) and no change was detected between CBD-treated and untreated *gcvH1*$^{-}$ cells (Fig 6.12a). These results corroborate what was found using GC-MS. Analysis of the *D. discoideum* rescue cell line shows no difference between CBD treated and untreated cells when analysed with NMR (Fig 6.12a), neither does the CBD treated rescue cells display a wide distribution of data, in contrast

to that found using GC-MS analysis. The NMR methionine data for wild type (AX3) and *gcvH1*$^-$ corroborates what was found using GC-MS, however the rescue cell line data does not.

Analysis of glycine levels using NMR showed that the *gcvH1*$^-$ cell line overall has significantly elevated ($P<0.001$) glycine levels compared to wild type (AX3) cells (Fig 6.12b). While CBD treatment has no effect upon glycine levels compared to vehicle treated cells in any of the three cell lines tested. This data corroborates with what was found using GC-MS. Using NMR however, we show that overall there is a significant drop ($P<0.001$) in glycine levels within the rescue cell line compared to the *gcvH1*$^-$ cell line (Fig 6.12b), in contrast to that shown by GC-MS analysis where no difference was observed.

6.2.10 NMR analysis of other one carbon cycle metabolites

As well as methionine synthase facilitating methionine production in the one carbon cycle (Okamura-Ikeda *et al*, 1987; Kikuchi *et al*, 1992), methionine can also be produced by the enzyme Betaine-homocysteine methyltransferase (BHMT). This other pathway, also part of the one carbon cycle involves the donation of a methyl group from betaine (trimethylglycine) to homocysteine, concomitantly producing methionine and dimethyl glycine (Obeid, 2013). We therefore investigated whether CBD treatment or *gcvH1* ablation had an effect upon the betaine pathway. As CBD treatment was already shown to reduce methione levels suggesting one carbon metabolism inhibition, it was predicted that CBD would increase betaine levels. To test this we quantified betaine levels within wild type (AX3), *gcvH1*$^-$ and the *D. discoideum* rescue cell lines using NMR. Analysis revealed no difference in cellular betaine levels between all three cell lines when treated with vehicle alone (Fig 6.12c). However, all three cell lines showed a significant increase ($P<0.001$) in betaine levels following treatment with CBD when compared to their respective cell lines treated with vehicle alone (Fig 6.12c).

In addition to betaine we also analysed sn-glycero-phosphocholine. Betaine is produced from the oxidation of choline, of which sn-glycero-phosphocholine is a precursor. To investigate whether betaine level changes were a result of one carbon cycle regulation and not a result of changes in the choline synthesis pathway we analysed levels of sn-glycero-phosphocholine. It was anticipated that CBD would effect sn-glycero-phosphocholine levels as NMR had already shown betaine levels to be effected. NMR showed that sn-glycero-phosphocholine levels within wild type (AX3) cells treated with CBD were significantly greater than that found in untreated

cells (Fig 6.12d). No significant change was found in the other two cell lines, however a trend for increased levels of sn-glycero-phosphocholine following CBD treatment was found.

6.2.11 NMR analysis of metabolites involved in mitochondria energy production

The dysfunction of mitochondria and its energy production has been linked to epilepsy and seizure onset (Rowley and Patel, 2013; Folbergrova and Kunz, 2012; Kang *et al*, 2013). Because the glycine cleavage system is a key component within mitochondria, and thus energy production, we investigated whether CBD also affects the levels of such metabolites. To test this we quantified fumarate, succinate and alpha-keto glutarate levels within treated and untreated wild type (AX3), *gcvH1*$^{-}$ and the *D. discoideum* rescue cell lines using NMR. If CBD was to affect mitochondrial energy production we would expect to see a reduction in these key metabolites, especially with regards to epilepsy. No significant difference was found in fumarate (Fig 6.13a) or succinate (Fig 6.13b) levels between all three cell lines, or between CBD treated and vehicle treated conditions for each cell line. Alpha-keto glutarate levels were however found to be significantly increased ($P<0.05$) in the null cell line following CBD treatment (Fig 6.13c). No significant change was found within the wild type (AX3) and rescue cell lines between CBD treated and untreated conditions. Thus from these analyses CBD has no effect upon energy production within mitochondria, but loss of GCVH1 does cause deregulation of some mitochondrial energy related compounds.

Although not strictly a metabolite involved in mitochondrial energy production, the metabolite oxypurinol has been shown to reduce the amount of ROS produced in the cell by inhibiting xanthine oxidase (Spector, 1988). Excessive levels of ROS have been linked to neuronal damage and seizure onset (Kovac *et al*, 2016). As such, oxypurinol levels were analyzed within the three cell lines. If CBD plays a role in reducing ROS through oxypurinol, we would expect CBD treatment to elevate oxypurinol levels. NMR analysis of oxypurinol found that both wild type (AX3) and the rescue cell lines showed significant increases ($P<0.001$) in oxypurinol levels following CBD treatment (Fig 6.13d). In contrast to this, the *gcvH1*$^{-}$ cell line showed no change in oxypurinol levels following CBD treatment when compared to untreated cells. Interestingly, changes in oxypurinol levels following CBD treatment are lost with the ablation of *gcvH1* but restored with the re-introduction of *gcvH1.*

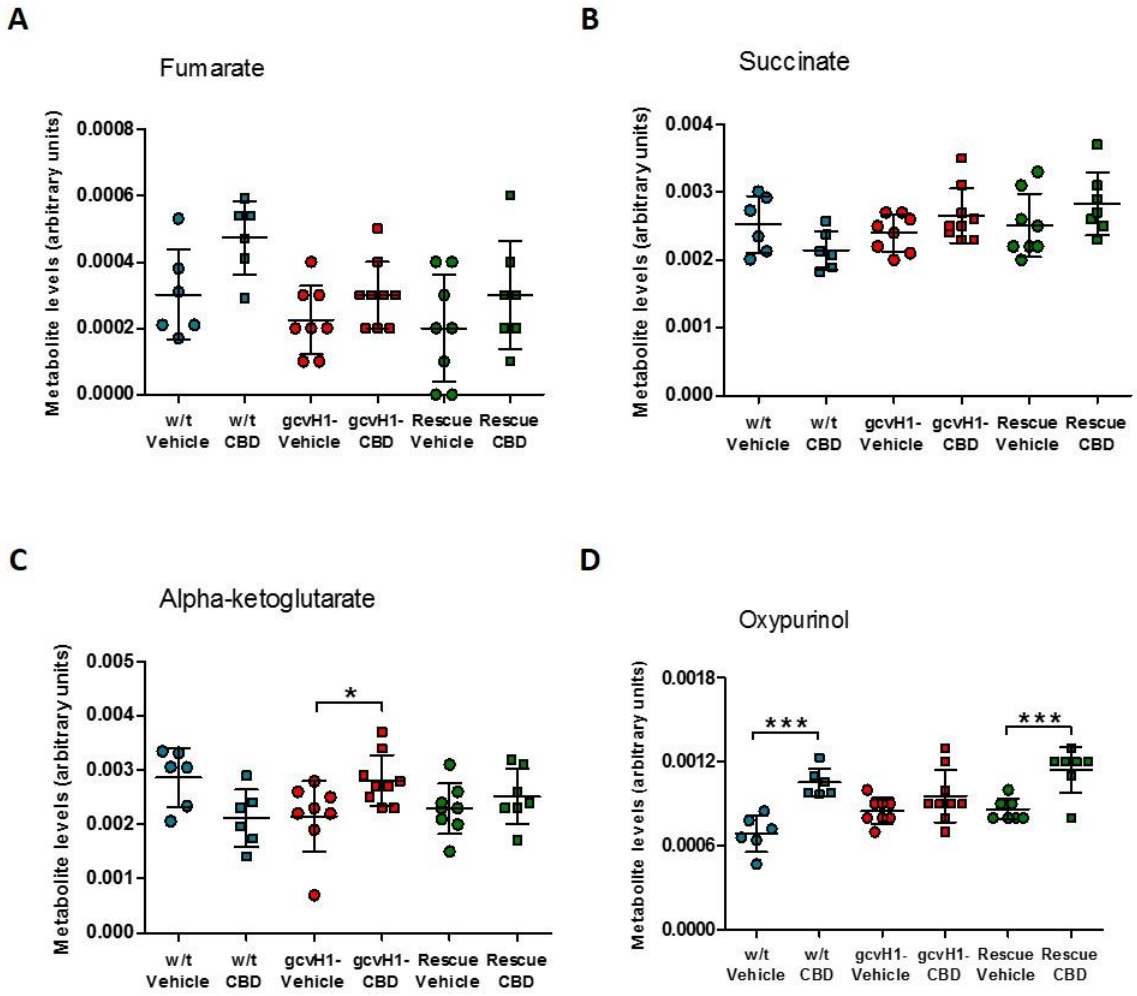

Figure 6.13 NMR analysis shows the effect that CBD treatment has upon cellular amino acid and metabolite levels within Wildtype (AX3), *gcvH1-* and *D. discoideum* rescue cell lines. Wildtype (AX3), *gcvH1-* and a rescue cell line with the *D. discoideum* gene reinstated into the null cell line were treated with CBD or vehicle alone. The amino acid and metabolite levels of each were quantified using NMR analysis. Data are mean +/- SEM (*,P<0.05; **,P<0.01; ***,P<0.001, two-way ANOVA, Bonferroni post hoc test, n=6-9).

6.3 Discussion

6.3.1 The *D. discoideum* GCVH1 protein is likely to be the homologue of the human GCSH protein.

Bioinformatics analysis of both the *D. discoideum* and the *H. sapiens* proteins showed similar size, protein domain structure and key lipoyl binding motifs. These data suggest a conserved cellular role in both systems. This is fundamentally important for the use of *D. discoideum* as a model organism, and allowing translation to humans (Reed *et al*, 2017). Despite the E-value falling just above the threshold recommended for homology (Eichinger *et al*, 2005), both proteins do possess the same highly conserved domains. It appears that the elevated E-value is a direct consequence of the first 30 amino acid residues making up the mitochondria targeting sequence. These sequences usually consist of alternating hydrophilic and positively charged amino acids and can be difficult to predict using bioinformatics approaches (Li et al, 2010). Once correctly localized to the mitochondria, the targeting sequence of these proteins are also cleaved by peptidases and are absent from the functioning protein (Fukasawa *et al*, 2015). We have also shown that any differences in the mitochondrial targeting sequence does not affect correct localization of the human fusion protein expressed within *D. discoideum*. Therefore, any such differences within homology attributed to the first 30 amino acids can be dismissed, as firstly both proteins still correctly localize, and secondly the active protein may not require this region as it is cleaved once inside the mitochondria (Fukasawa *et al*, 2015). Phylogenetic analysis also showed that the *D. discoideum* protein belongs within the H-protein clade alongside higher organisms, while both the human DLST and DLAT proteins formed an outlying group. This further supports the fact that the GCVH1 protein is homologous to the *H. sapiens* GCSH protein.

Unlike other organisms, *D. discoideum* has five copies of the *gcvH* gene, all found upon chromosome five. Of all five copies only *gcvH1* and *gcvH3* possess the essential lysine residue required for lipoic acid binding. Similarly, only *gcvH1* and *gcvH5* possess the mitochondrial targeting sequence region for mitochondrial localization. Therefore, only the GCVH1 protein is likely to localise to the mitochondria with a functioning ESVKAAS region. It therefore stands to reason that the ablation of *gcvH1* may prevent glycine cleavage system activity as none of the other four gene copies appear to have the ability to carry out the same role. The extra copies of *gcvH1* likely arose from retrotransposition duplication and replication slippage. The lack of introns within *gcvH4* and the higher density of adenines at its 3' end suggest a product of retrotransposition duplication (Finnegan, 2012). In comparison *gcvH5* also has no introns and is immediately upstream of *gcvH4*, suggesting that *gcvH5* could be a duplication product through

replication slippage of *gcvH4* (Viguera *et al,* 2001). Taken in its entirety however, *gcvH1* appears to be the only functioning copy able to contribute to the glycine cleavage system, with the protein showing strong homology to the human counterpart.

6.3.2 The glycine cleavage system is likely to control sensitivity to CBD

CBD has been shown to inhibit cellular growth in mammalian cell lines (McAllister *et al*, 2011, Solinas *et al,* 2013), and we show a similar effect in *D. discoideum*. Using this effect, we carried out a genetic screen and identified GCVH1 to partially regulate this growth inhibitory effect. To confirm if this resistance was a direct result of *gcvH1* disruption we ablated *gcvH1* from wild type (AX3) cells and found *gcvH1*$^-$ to also be partially resistant to CBD. By recapitulating these findings we have shown that GCVH1 and most likely glycine cleavage system function is responsible for regulating sensitivity to CBD.

The resistant phenotype that we observed in the *gcvH1*$^-$ cell line could have been attributed to other factors resulting in reduced cellular levels of CBD. Cellular levels of xenobiotics such as CBD can be reduced by lowering the rate by which they are taken up into the cell, as already shown with the anti-convulsant VPA (Terbach *et al*, 2011). Similarly, such levels can be reduced through increased cellular removal of xenobiotics via drug transporters (Miranda *et al*, 2013, Liang *et al,* 2015). However, it has not been suggested that GCVH1 function is related to drug metabolism, but is most likely involved in glycine metabolism within the glycine cleavage system (Kikuchi *et al,* 1982). Furthermore, the tertiary structure of GCVH1 is not consistent with that of a protein involved in drug transport. GCVH1 does not have transmembrane regions necessary for moving xenobiotics across membranes, making it unlikely that GCVH1 is involved in cellular uptake or removal directly.

GCVH1 activity may however facilitate CBD removal indirectly. One possible mechanism by which this could occur is through xenobiotic degradation. Briefly, certain lipophilic xenobiotics will undergo a multi-step process to facilitate their removal from the cell (Xu *et al*, 2005). This drug metabolism process involves a two-step mechanism. In phase I of drug metabolism, either reactive or polar groups are introduced to the xenobiotic substrate making them more hydrophilic (Zanger and Schwab, 2013). Phase II of drug metabolism then involves the conjugation of a charged species to the xenobiotic in order to facilitate its removal (Prescott, 1984). A number of charged species are known to be involved in this conjugation step, of which glycine is one of them (Badenhorst *et al*, 2013). To investigate whether resistance in *gcvH1*$^-$ was

a result of increased drug metabolism, LC-MS was used to quantify CBD levels within both wild type (AX3) and *gcvH1*$^{-}$ cells. Results showed no significant difference between the wild type (AX3) and *gcvH1*$^{-}$ cell lines, while *gcvH1*$^{-}$ cells did still show a significant resistance. These findings clearly show that the ablation of *gcvH1* does not infer a resistance by increasing drug metabolism. Interestingly, there appeared to be a trend, whereby CBD levels were slightly elevated in the *gcvH1*$^{-}$ cell line. This may suggest that CBD treatment actually had the opposite effect and lowered drug metabolism levels. A number of studies have shown that CBD inhibits drug metabolizing enzymes, specifically those of the cytochrome P450 isoforms (Yamaori *et al*, 2011; Jiang *et al*, 2013). This inhibition of key metabolizing enzymes has been shown to prevent the degradation of other medications concomitantly administered with CBD (Jaeger *et al*, 1995). In essence CBD appears to prevent drug metabolism, not facilitate it, as supported by numerous studies (Yamaori *et al*, 2011; Jiang *et al*, 2013). It is therefore clear that the resistant phenotype of *gcvH1*$^{-}$ is not a result of increased CBD clearance from the cell, and that GCVH1 must regulate this sensitivity in some other manner.

6.3.3 CBD and GCVH1 regulate methionine and cysteine levels

If CBD regulates the activity of the glycine cleavage system and the one carbon cycle through GCVH1, we would expect to find changes in their amino acids and metabolites following CBD treatment or *gcvH1* ablation. The investigation into these metabolites is especially relevant as a number of them play key roles in a number of cellular functions, and are linked to epilepsy onset and its progression. For example, the amino acids glycine, homocysteine and dimethylglycine are known to be either agonists or antagonists of the neuronal NMDA receptor (Ranjana and Surojit, 2009; Cummings and Popescu, 2015; Lee *et al*, 2017). The NMDA receptor is an ion channel protein found at synaptic junctions that activates when both glycine and glutamate bind to it (Vyklicky *et al,* 2014). While the synaptic plasticity function of NMDA receptors and their role in learning and memory is well researched (Baez *et al*, 2018), studies have also linked genetic variants of NMDA receptors to epilepsy (Sibarov *et al*, 2017). A recent study has shown that genetic defects of certain genes encoding the NMDA receptor subunits result in the onset of certain childhood epilepsies (Addis et al, 2017). Further studies have also shown that the NMDA receptor is instrumental in seizure induced neuronal death, both *in vitro* (Desphand *et al*, 2008, Kovac *et al*, 2012) and *in vivo* (Ormandy *et al*, 1989, Fujikawa *et al*, 1994). As well as being involved in the production of potential neurotransmitters, the one carbon cycle and glycine cleavage system are also involved in the production of other species essential for

key cellular roles. These include the production of s-adenosyl methionine (SAM), adenosine and glutathione, all of which have been linked to epileptogenesis and seizure progression (Dhediya *et al*, 2016; Boison, 2005; Mueller *et al*, 2001). The regulation of the one carbon cycle could therefore affect the onset of seizures and epilepsy progression.

To determine whether CBD treatment or *gcvH1* ablation affects the glycine cleavage system and the one carbon cycle, we quantified these key amino acids and metabolites, especially those potentially linked to epilepsy. Analysis showed that methionine levels were only reduced in wild type (AX3) cells and not *gcvH1*$^-$(Fig 6.7a). This contrast between cell lines suggest that CBD induces a reduction in methionine levels within wild type (AX3) cells because the proposed target (GCVH1) of CBD is present. Whereas, we see no change in the null cell line because the molecular target of CBD is now absent. It also suggests that CBD inhibits GCVH1 function as methionine levels in the treated wild type (AX3) cells are similar to those found in both treated and untreated *gcvH1*$^-$ cells (Fig 6.7a).

Analysis showed that CBD treatment had no effect upon glycine levels in both the wild type (AX3) and *gcvH1*$^-$ cell lines (Fig 6.7b). Overall however glycine levels were significantly higher in the null cell line compared to wild type (AX3) cells. This increase in glycine levels within *gcvH1*$^-$ is most likely a result of *gcvH1* being ablated. It also suggests that within *D. discoideum* cells the glycine cleavage system operates in the forward reaction, primarily catabolizing glycine to CO_2. Similarly, the variability of data for both the treated and untreated *gcvH1*$^-$ suggests a disruption of glycine homeostasis within the cell.

Similar to that found with methionine, cysteine levels were only affected following CBD treatment in those cell lines possessing the *gcvH1* gene (Fig 6.7c). Cysteine levels within the treated and untreated *gcvH1*$^-$ cells however, were of a level comparable to untreated wild type (AX3) cells. This suggests that while CBD treatment had no effect upon the null cell line, it was still able to maintain normal cellular cysteine levels. It is possible that cysteine homeostasis within the cell is more tightly regulated compared to methionine, or the one carbon cycle plays only a minor role in cysteine homeostasis. Unlike methionine, treatment of wild type (AX3) cells with CBD only resulted in a negative trend, whereby cysteine levels were lowered in the treated group. This difference in significance, could be a result of cysteine being positioned within the one carbon cycle further away from the glycine cleavage system than is methionine (Fig 1.3). If CBD does indeed target GCVH1 then any changes seen in metabolite levels may be reduced the further down the pathway we travel from the glycine cleavage system.

6.3.4 Rescuing the CBD sensitive phenotype.

Immunofluorescence showed that both proteins correctly localized to the mitochondria, confirming that localization was not affected by the RFP tag at their n-terminus. It also confirms that the exact sequence of the mitochondrial targeting sequence region was not important for correct localization, as the human protein correctly localized within *D. discoideum*. Studies have shown that the correct localization of mitochondrial proteins could instead rely on a localization sequence found within the protein and not at the n-terminus (Li *et al*, 2009). Whether this is the case here we are unsure, as there are other highly conserved regions within both proteins such as the conserved HEWVT motif immediately next to the mitochondrial targeting sequence of both proteins. Our data does suggest that correct localization depends upon the type of amino acids found with the targeting sequence.

Although both tagged proteins localize to mitochondria, our data does not demonstrate enzymatic activity of the proteins; the RFP tag may have interfered with the proteins ability to bind lipoic acid. To validate this we tested sensitivity to CBD in both the *D. discoideum* and *H. sapiens* rescue cell lines and found that reinstating either gene re-sensitized cells to CBD. Interestingly, it was found that the rescue cell line with the human protein was more sensitive. A number of reasons may explain this difference in sensitivity such as differential inhibition of activity of the fluorescent tag or differential protein degradation. Another reason could be down to the genes expression levels within the cells. Because genes were expressed in extra chromosomal vectors with constitutively active promoters we had no way of regulating expression levels. A more accurate method would have been to knock each gene independently back into the genome of the *gcvH1*$^{-}$ cells. This will have reinstated expression of the gene back to basal levels. However, this is a time consuming process and was still not guaranteed due to the presence of the RFP tag. Also, we were initially only interested in whether the proteins presence re-instated sensitivity or not. As such, the over expression vector approach was used.

6.3.5 GC-MS analysis of glycine, methionine and cysteine levels within the GCVH1-RFP (*D.discoideum*) and GCSH-RFP (*H.sapiens*) over expression cell lines.

Because *gcvH1*$^{-}$ cells transfected with the over expression constructs were re-sensitized to CBD, we investigated whether rescuing the phenotype would also reverse the changes seen in methionine, glycine and cysteine levels. Unlike the sensitivity to CBD however, it was found that transfecting *gcvH1*$^{-}$ cells with the over expression vectors did not reverse cellular levels of these

amino acids. The only amino acid which did show reversal was methionine. As to why we don't see a complete reversal in conditions for all three amino acids is unclear, however it is possible that this is an effect of gene expression levels. A number of studies within other organisms has shown that over expression of the glycine cleavage system H-protein can have a significant impact upon the phenotype. The over expression of the H-proteins within *A. thaliana* and *N. tabacum* have been shown to significantly affect plant growth (Simkin *et al,* 2017), electron transport rate and CO_2 uptake (Timm *et al*, 2012), plus an increase in plant biomass (Lopez-Calcagno *et al,* 2018). These studies show that significant changes are exhibited following over-expression. As such, it is highly likely that the over-expression of the H-protein within *D. discoideum* could also induce significant changes that could affect amino acid levels within the cells. This would also explain why the over expression data for GC-MS differs to that found using NMR. As such the complex interplay of one carbon cycle components is thus difficult to interpret.

6.3.6 NMR analysis

NMR enabled both validation and quantification for methionine and glycine, and additional analysis of other metabolites, including betaine, sn-glycero-phosphocholine, oxypurinol, fumarate, succinate and alpha ketoglutarate. While the results observed for methionine and glycine corroborated those observed using GC-MS, the over-expression data did not. These differences can be explained as outlined above in 6.3.5. Within the one carbon cycle there are two routes responsible for the methylation of homocysteine; the Betaine-homocysteine methyltransferase (BHMT) route and the Methionine Synthase (MS) route. The BHMT route catalyses up to 50% of homocysteine metabolism within humans (Feng *et al,* 2011). However, unlike the Methionine Synthase route, it does not have a direct link with the glycine cleavage system, as it uses betaine as the methyl donor instead of 5'-methyl-tetrahydrofolate (Ducker and Rabinowitz, 2017). If CBD was to regulate methionine production by acting upon the one carbon cycle through the glycine cleavage system, it is possible that both the methionine synthase and BHMT routes are effected. If CBD blocks the Methionine synthase pathway as suggested by methionine levels within wild type (AX3) cells (Fig 6.7a), then it is possible that the Betaine-homocysteine methyltransferase route is up regulated. NMR analysis of betaine across all three cell lines however showed that betaine levels remained consistent. However, CBD treatment significantly elevated betaine levels within all three cell lines compared to vehicle alone (Fig 6.12c). Firstly, this suggests that the BHMT route of methionine production is

unaffected by the absence of *gcvH1*. Secondly, it clearly shows that CBD treatment inhibits the Betaine-homocysteine methyltransferase pathway, as shown by elevated levels of betaine. So far our data has shown that CBD affects the one carbon cycle, however we are unsure how this then manifests across to seizure prevention. If CBD elevates cellular betaine levels as our data shows then this may be another example by which CBD attenuates seizures. Studies have linked homocysteine to epilepsy, with one study finding that homocysteine potentiates seizures and cell loss in the pilocarpine model of status epilepticus (Baldelli *et al*, 2010). Because betaine is responsible for the direct methylation of homocysteine, elevated betaine levels may therefore reduce seizure susceptibility by lowering homocysteine levels. To support this, a study has shown that betaine attenuates neurotoxicity in embryonic brain cells and rat cortical slices induced by glutamate (Park *et al*, 1994). A previous study also demonstrated that betaine has a direct inhibitory effect in blocking neuronal excitations induced by either homocysteine or glutamate (Wuerthele *et al*, 1982). Therefore, the increased levels of cellular betaine induced by CBD treatment may help to combat seizure onset.

The changes observed in sn-glycero-phosphocholine appear to be caused by changes in cellular betaine levels (Fig 6.12d). Sn-glycero-phosphocholine is a precursor to choline, and betaine is the principal metabolite of choline (Lee *et al*, 1993). The trend of increased sn-glycero-phosphocholine levels following CBD treatment mirrors what we see with betaine, however a significant increase in sn-glycero-phosphocholine was only seen in wild type (AX3) cells. We would expect the intensity of any effect caused by CBD treatment to diminish the further we go from the original source of disruption. As such, the changes we see in sn- glycero-phosphocholine are likely to be an effect caused from elevated betaine levels, and are not themselves the cause of betaine level changes.

Although not specifically looked for with NMR analysis, the data for oxypurinol levels were found to be interesting. NMR analysis showed that oxypurinol levels were consistent within all three cell lines when untreated (Fig 6.13d). However, oxypurinol levels significantly increased in only those cell lines possessing the *gcvH1* gene. This again suggests that GCVH1 may be a target for CBD. This data is also interesting as oxypurinol is known to be the active metabolite of allopurinol, shown to have positive effects as a treatment for intractable epilepsies (Tada *et al*, 1991). This anti-convulsant effect is induced through its use as an adjunctive therapy, by acting as an adenosine agonist (Togha *et al*, 2007). Oxypurinol has also been shown to directly inhibit the activity of Xanthine Oxidase, an enzyme involved in the production of cellular ROS (Spector, 1988). While oxypurinol is not linked to the glycine cleavage system or the one carbon cycle, this data does show that CBD is able to increase cellular levels of this endogenous anti-

convulsant. However, this is only achieved in the presence of GCVH1, and through what mechanism remains uncertain.

Mitochondrial disease and dysfunction, especially in energy production has been widely attributed to seizure onset in a number of different epilepsies (Folbergrova and Kunz, 2012; Kang *et al*, 2013; Rowley and Patel, 2013). Because of the location of GCVH1 within the mitochondria we were interested in whether CBD treatment altered any of the key metabolites involved in energy production. We therefore analyzed intermediate metabolites of the citric acid cycle, specifically fumarate, succinate and alpha ketoglutarate. NMR analysis showed that CBD treatment had no effect upon fumarate (Fig 6.13a) and succinate (Fig 6.13b) levels, but did significantly increase alpha ketoglutarate levels in the null cell line (Fig 6.13c). However, this significance appears to be the result of an outlier in the untreated *gcvH1*$^{-}$ group. This data therefore suggests that CBD plays no role in combating dysfunctional seizure activity by regulating intermediate metabolites of the citric acid cycle.

Summary

In this chapter we have shown that the *D. discoideum* and *H. sapiens* H-proteins are homologous to one another and are involved in glycine homeostasis. It was shown that both proteins correctly localize to the mitochondria in *D. discoideum*. The ablation of *gcvH1* from wild type (AX3) cells provided a resistant phenotype to the effects of CBD on growth. Introducing the *D. discoideum* or the *H. sapiens* gene back into the *gcvh1*$^{-}$ cells reinstated the sensitive phenotype. Both GC-MS and NMR analysis then verified that CBD directly regulates the cellular levels of the amino acids and metabolites found within the one carbon cycle, which has been shown to directly affect key cellular functions that have been linked to epileptogenesis and seizure progression in animal models. We also show using a preliminary computational approach that CBD has the potential to bind to the H-protein, and may interfere with the binding of the lipoic acid co-factor.

Chapter 7

Translational Studies

7.1 Introduction

Previous chapters have shown that within *D. discoideum* CBD directly regulates the cellular levels of the amino acids and metabolites found within the one carbon cycle. Of specific interest were the amino acids methionine, glycine and cysteine, the regulation of which can directly affect key cellular functions that have been linked to epilepsy (Kobow et al, 2013), neurotransmission (Betz *et al*, 2006) and neuroprotection (Mosharov *et al*, 2000). Thus, to investigate a similar role for CBD in preventing seizure onset via the regulation of the one carbon cycle, we translated our findings to both *in vitro* and *in vivo* mammalian seizure models, focusing on methionine, glycine and cysteine levels.

Research into the mechanisms of epileptogenesis and seizure onset, as well as the development of novel anticonvulsants has been facilitated by the use of animal seizure models (Kandratavicius *et al*, 2014). Such models vary in their design and allow the study of both acute and chronic seizure mechanisms. The mode of action in which epileptic stimuli is induced in these models is diverse, ranging from a pharmacological approach using stimulants such as pilocarpine (Cifelli and Grace, 2012) or pentylenetetrazole (Sugaya *et al*, 1989), to genetic approaches employing animals with genetic mutations causing epileptic phenotypes (Zabinyakov *et al*, 2017). The variability of these models allow studies to be carried out both *in vitro* and *in vivo*. The use of i*n vitro* approaches has several advantages over *in vivo* models, such as the relative ease of producing the cell culture, the reduced number of animals required for experimentation, the low expense involved, and the ability to screen quickly for novel anticonvulsants. Rat primary hippocampal neurons in particular have been used to great effect in studying the acute effects of seizures and the molecular mechanisms involved with anticonvulsants (Chang *et al*, 2014). However, *in vivo* studies are more clinically relevant to what is found in human epilepsy, allowing a whole organism approach to studying epilepsy. Similarly, *in vivo* studies allow the interaction and protection mechanisms associated with the donor organ to take place, which are unavailable within *in vitro* studies. Historically, seizure induction within *in vivo* models relied upon pharmacological and electrical methods such as pilocarpine treatment (Cifelli and Grace, 2012) and electrical kindling (Goddard, 1967). However, the applicability of such models has been questioned, and some models remain controversial as to their relevance to human epilepsies (Bertram, 2007). With advances in genome editing, *in vivo* models can now be created that are directly related to human etiologies (Hwang et al, 2013, Sander and Joung, 2014). For example, the *Scn1a*$^{+/-}$ mouse model displays the characteristics of Dravet syndrome, a severe

form of childhood epilepsy, where Dravet patients often have mutations in one copy of the *Scn1a gene* (Kalume *et al*, 2013). The *Scn1A* gene is responsible for the production of the alpha subunit for the sodium channel protein $Na_V1.1$ (Bender *et al*, 2012). As such it is now possible to use animal epilepsy models that directly mimic the clinical features of distinct human epilepsies.

In this chapter we investigate a role for the one carbon cycle and as a target for CBD, in seizure control and epilepsy using *in vitro* and *in vivo* animal models. We induce seizure activity in the presence or absence of CBD using *in vitro* and *in vivo* epilepsy models, and examine methionine, glycine and cysteine levels using GC-MS analysis. Previous studies have shown that individuals with epilepsy can have altered levels of plasma homocysteine (Baldelli *et al*, 2010), although there is contention as to whether these changes result from the epileptic condition itself or the anticonvulsants being taken. Studies have shown that increased levels of homocysteine within the plasma decreases the threshold at which seizure onset occurs (Baldelli *et al*, 2010). Initially we set out to quantify homocysteine, methionine, cysteine and glycine levels within the *in vitro* and *in vivo* models. Unfortunately, due to the detection levels of the GC-MS equipment used it was impossible for us to analze homocysteine. However, because methionine production is directly linked to homocysteine in the one carbon cycle it was hypothesised that methionine levels may also change within the plamsa. It was hypothesized that methionine levels within epileptic animals would be less than those in normal animals, while CBD would elevate methionine levels. If methionine levels were found to change within the plasma this may suggest that the changes in homocysteine of epileptic individuals may arise from regulation of the one carbon cycle. Glycine and cysteine levels were also investigated due to their close relationship with the one carbon cyle also. Similarly, it was also hypothesized that glycine and cysteine levels would decrease under conditions, but be elevated following CBD treatmenmt. Firstly we translated our findings across to an acute seizure model using rat primary hippocampal neurons. We then moved into *in vivo* studies where we looked at the effects seizure inducement and CBD treatment has upon amino acid levels within the plasma of an epilepsy model using lithium-pilocarpine (Li-Pilo) treated rats. Finally, we also investigate the effects of seizure inducement and CBD treatment upon amino acid levels within the plasma and brain of two different *Scn1a* mutant epilepsy models. In these experiments we hypothesized similar changes in methionine, glycine and cysteine levels to that of the plasma.

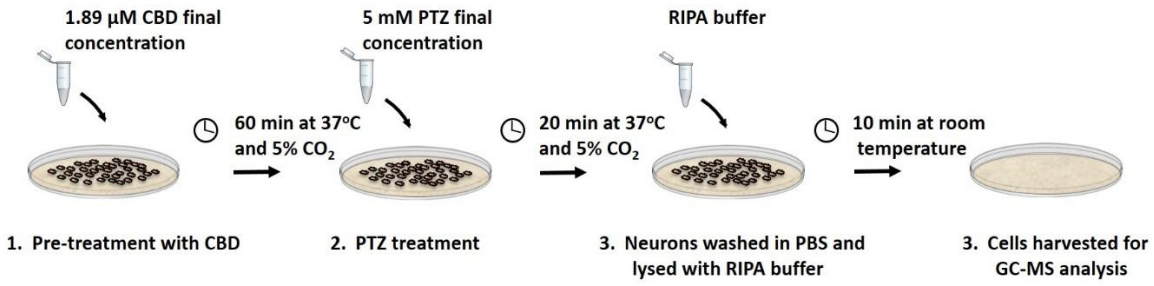

Figure 7.1 Schematic showing an overview of rat primary hippocampal neurons treated with CBD and Pentylenetetrazole. Primary hippocampal neurons were seeded onto 6 well plates in neurobasal media and matured for 21 days. Intervention groups were treated with CBD to a final concentration of 1.89 µM, then incubated for 1 hour. Following CBD treatment neurons were treated with PTZ (5 mM final concentration) for 20 minutes, and cells harvested for GC-MS analysis.

7.2 Results

7.2.1 Amino acid analysis of Primary hippocampal neurons

Because CBD treatment was shown to effect cellular levels of methionine, glycine and cysteine within *D. discoideum* (chapter 6), we hypothesized that CBD treatment may also affect levels of these amino acids in mammalian neuronal cells. We also hypothesized that because CBD is used as an anticonvulsant, the cellular levels of methionine, glycine and cysteine may also be altered in neurons. We therefore set out to investigate if methionine, glycine and cysteine levels were changed in rat primary hippocampal neurons, in the absence and presence of CBD. Previous studies have shown that treatment of primary cultured neurons with 5 mM pentylenetetrazole (PTZ) induces bursting activity in a manner similar to seizure-like activity in hippocampal slices or *in vivo* (Sugaya et al., 1989). Intervention groups were treated with 1.89 µM CBD for one hour, and then treated with pentylenetetrazole for 20 minutes (Fig 7.1) (see 2.2.11.2 for method). GC-MS analysis of the cell lysates showed no significant difference ($P>0.05$) in methionine levels between untreated and CBD treated primary hippocampal neurons (Fig 7.2a). However, when neurons were treated with PTZ methionine levels were found to be significantly elevated ($P<0.001$) compared to both untreated and CBD treated neurons. Interestingly, methionine levels in the intervention group were found to be significantly lower ($P<0.05$) than the PTZ treated group. Analysis of glycine and cysteine by GC-MS found no significant differences ($P>0.05$) across all conditions (fig 7.2 b and c). These data therefore show that PTZ treatment elevates cellular methionine levels in primary hippocampal neurons, and that this increase is attenuated by CBD treatment.

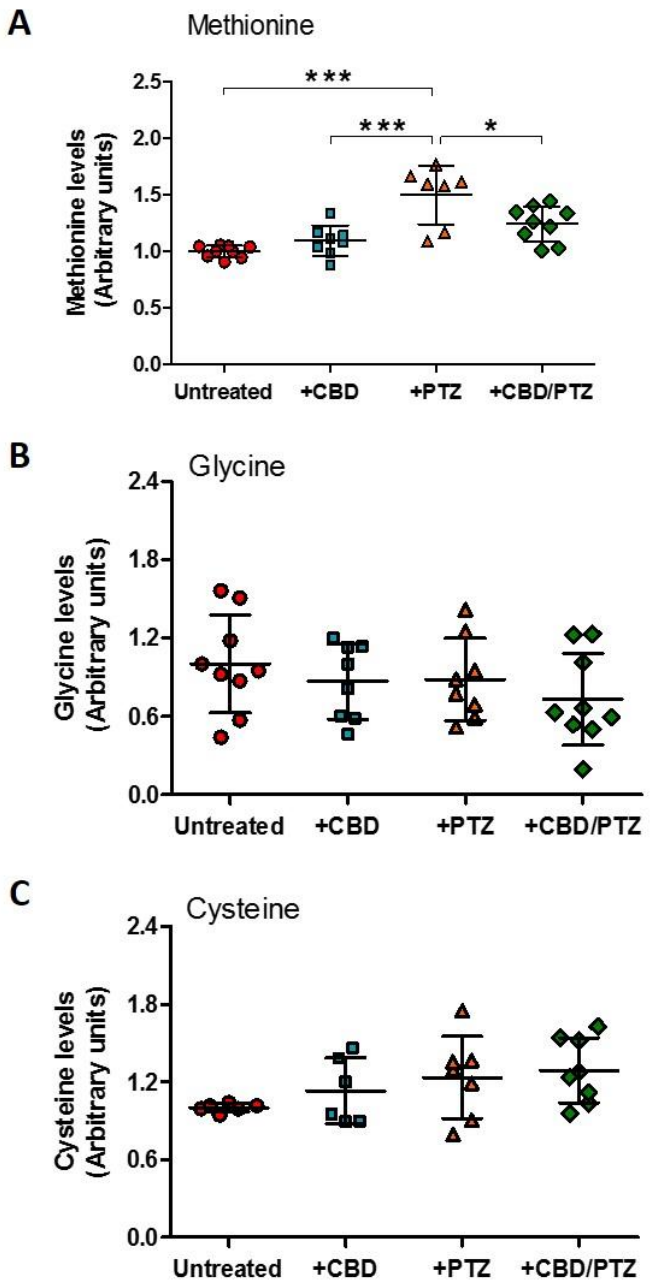

Figure 7.2 GC-MS analysis of the rat acute seizure model using primary hippocampal neurons treated with CBD and pentylenetetrazole. Rat primary hippocampal neurons treated with CBD and/or pentylenetetrazole were analysed for (A) methionine, (B) glycine and (C) cysteine levels using GC-MS. Data are mean +/- SEM (*,P<0.05; **,P<0.01; ***,P<0.001, one-way ANOVA, Tukey post hoc test, n=6-9).

7.2.2 Amino acid analysis of plasma samples from a Rat lithium-pilocarpine (Li-Pilo) seizure model

We further investigated if status epilepticus within an *in vivo* epileptic seizure model affected methionine, glycine and cysteine plasma levels, and whether CBD treatment also attenuated any changes. The first line of investigation taken was to analyze the amino acid levels from the plasma of a rat lithium-pilocarpine (Li-Pilo) seizure model. Male Wistar rats (3-4 weeks old) were treated with lithium chloride (127 mg/kg) and pilocarpine (25 mg/kg) via subcutaneous injection as per Modebadze et al, (2016). Intervention groups were also treated with CBD (200 mg/kg) orally. Plasma was extracted from animals prior to culling and the amino acid levels quantified by ourselves using GC-MS. All animal handling was carried out by our collaborators in Reading. GC-MS analysis of the plasma samples showed no significant difference ($P>0.05$) in methionine levels between untreated healthy and epileptic animals (Fig 7.3a). However, when the epileptic animals were treated with CBD, methionine levels were found to be significantly ($P<0.05$) elevated compared to the untreated epileptic animals. No significant difference ($P>0.05$) was found in both glycine (Fig 7.3b) and cysteine (Fig 7.3c) levels between both healthy and epileptic animals, or between untreated and CBD treated epileptic animals. These data therefore show that plasma methionine levels are unchanged in this seizure model, however when treated with CBD plasma methionine levels are significantly elevated ($P>0.05$). No data is available for healthy animals treated with CBD, as these experiments were not carried out by our collaborators in Reading to reduce the number of animals used.

7.2.3 Amino acid analysis of blood samples from a homozygous SCN1A mouse model of Dravet syndrome, treated with CBD

As well as the lithium-pilocarpine seizure model (7.2.2) we also hypothesized that CBD may affect methionine levels in the plasma of seizure models with specific etiologies. In particular we wished to study a Dravet syndrome epilepsy model, since phase 3 clinical trials have shown efficacy of CBD in patients with these syndromes. To date more than 800 different mutations

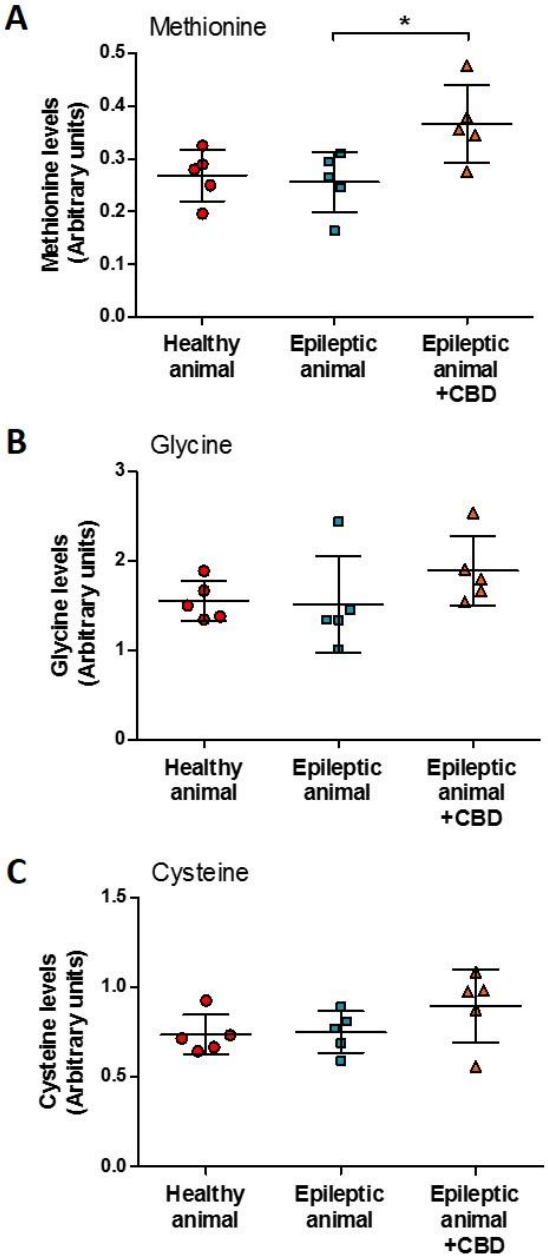

Figure 7.3 GC-MS analysis of plasma from a rat lithium and pilocarpine induced seizure model treated with CBD. Plasma samples obtained from a rat pilocarpine seizure model, treated with CBD or vehicle alone were compared to that of healthy non-epileptic animals. GC-MS analysis was used to compare (A) methionine, (B) glycine and (C) cysteine levels between groups. Data are mean +/- SEM (*,P<0.05, one-way ANOVA, Tukey post hoc test, n=5).

have been reported within SCN1A, a voltage-gated sodium channel, linked to Dravet syndrome (Miller *et al*, 2014). We therefore investigated whether seizure induction or CBD treatment affected methionine, glycine and cysteine levels within the plasma of a Dravet syndrome mouse model, lacking both copies of the *Scn1a* gene. Mice were injected twice daily with either CBD (100 mg/kg) or the vehicle alone (ethanol: kolliphor®: 0.9% saline at a 2:1:17 ratio) from day 8 postnatal to day 25, or the animals death if sooner. All animal handling was carried out by our collaborators in Reading. GC-MS analysis of the plasma samples showed no significant difference ($P>0.05$) in both methionine (Fig 7.4a) and glycine (Fig 7.4b) levels between healthy and epileptic animals, or between untreated and CBD treated animals. Analysis of cysteine however, showed a significant drop ($P<0.05$) in plasma levels within the epileptic animals compared to the healthy animals (Fig 7.4c). Treatment with CBD had no effect ($P>0.05$) upon plasma cysteine levels in both the healthy and epileptic animals. These data suggest that a mouse SCN1A$^{-/-}$ seizure model with a predisposition to seizure, has increased plasma cysteine levels, while CBD has no effect upon all three amino acid levels within the plasma. The relatively low n-number obtained for the epileptic group was a result of the animals dying from seizures before blood could be collected. Unfortunately, due to the small number of samples available for analysis in the epileptic group it was not possible to interpret CBD and epilepsy-related changes in these amino acids.

7.2.4 Amino acid analysis of blood samples from a heterozygous SCN1A mouse model of Dravet syndrome, treated with CBD

Because of the lethality observed in the homozygous SCN1A mouse model due to seizure activity, our collaborators at Reading University created a heterozygous SCN1A mouse model. This was achieved by cross breeding male 129S-Scn1a$^{tm1Kea/Mmjax}$ heterozygote mice (Jackson Laboratory, USA) with female C57BL/6 mice (Charles River, UK) to obtain the hybrid *Scn1a*$^{+/-}$. These hybrid animals displayed the characteristic seizures associated with Dravet syndrome, while being less susceptible to seizure-induced death. The mice were treated with CBD (100 mg/kg) twice daily via subcutaneous injections or with vehicle alone (ethanol: kolliphor®: 0.9% saline at a 2:1:17 ratio), for 6 weeks from day 8 postnatal (see 2.2.14). Blood was removed and analyzed by GC-MS at a later date. GC-MS analysis of the plasma samples showed no significant

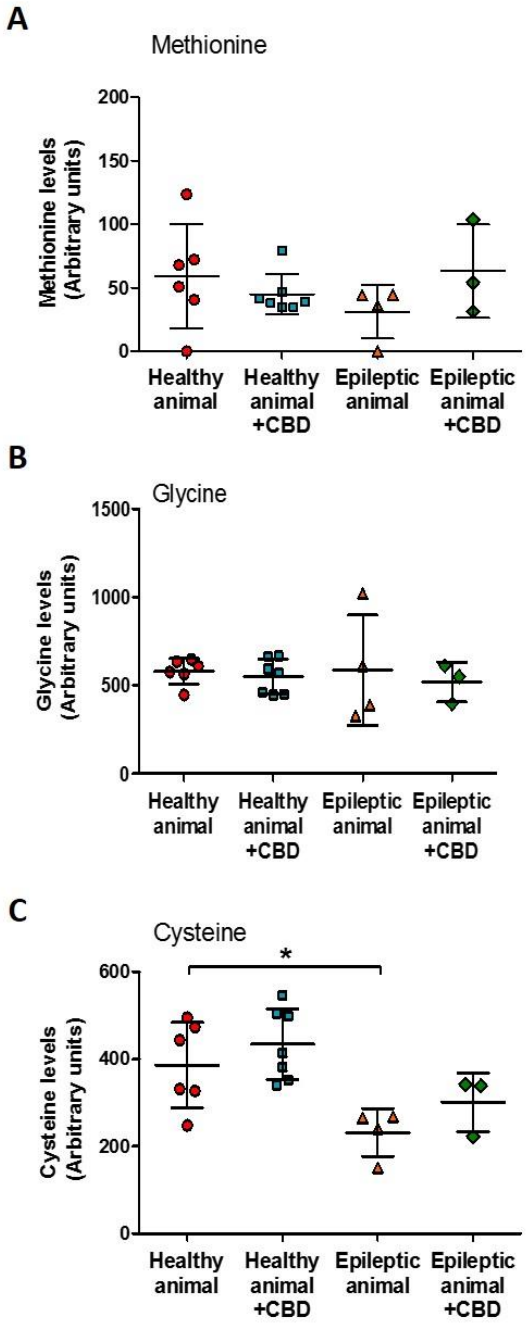

Figure 7.4 GC-MS analysis of plasma from a mouse Scn1a$^{-/-}$ (severe Dravet syndrome) seizure model treated with CBD. Plasma samples obtained from a mouse Dravet syndrome seizure model treated with CBD or vehicle alone were compared to that of healthy non-epileptic animals. GC-MS analysis was used to compare (A) methionine, (B) glycine and (C) cysteine levels between groups. Data are mean +/- SEM (*,P<0.05, two-way ANOVA, Bonferroni post hoc test, n=3-7).

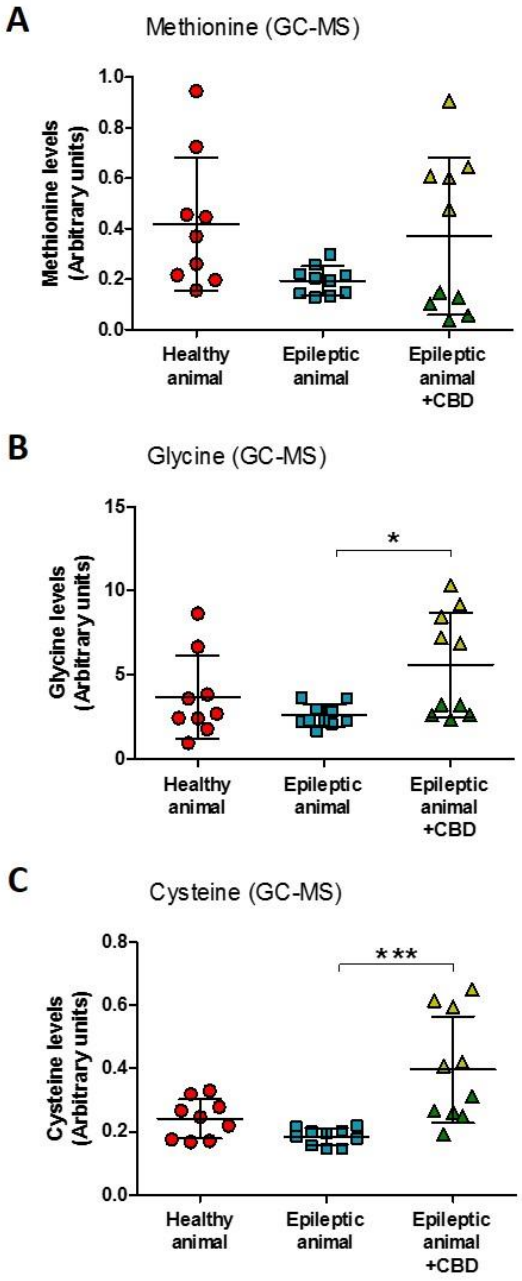

Figure 7.5 GC-MS analysis of plasma from a SCN1A$^{+/-}$ (mild Dravet syndrome) mouse seizure model treated with CBD. Plasma samples obtained from *Scn1A*$^{+/-}$ epileptic mice were treated with CBD or vehicle alone, and compared to that of healthy homozygous animals. GC-MS analysis was used to compare (A) methionine, (B) glycine and (C) cysteine levels between groups. Data are shown as mean ± SEM (*,P<0.05; **,P<0.01; ***,P<0.001, Welchs ANOVA, Games-Howell post hoc test, n=9+).

difference (P>0.05) in methionine, glycine and cysteine levels between healthy and epileptic animals (Fig 7.5). There was also no significant difference (P>0.05) in methionine levels between CBD treated epileptic animals and vehicle treated epileptic animals (Fig 7.5a). However, significant increases in glycine (P<0.05) (Fig 7.5b) and cysteine levels (P<0.001) (Fig 7.5c) were found in the epileptic animals following CBD treatment. Unusually, data for the CBD treated epileptic animals diverged into two distinct and separate groups for all three amino acids (Fig 7.5).

7.2.5 Amino acid analysis of brain samples from a heterozygous SCN1A mouse model of Dravet syndrome, treated with CBD

The site of seizure induction is the brain, thus brain tissue was analyzed for methionine, glycine and cysteine levels from the heterozygous *scn1a* animal. Brain extracts were prepared by homogenisation and lysates were analysed by GC-MS (see 2.2.14). GC-MS analysis showed that methionine levels within the epileptic animals were significantly elevated (P<0.05) compared to the healthy animals (Fig 7.6a). Treatment of the epileptic animals with CBD further elevated methionine levels significantly when compared to the vehicle treated epileptic animals (P<0.01) or the vehicle treated healthy animals (P<0.001). Glycine levels were found to follow a similar trend to that observed with methionine, significantly increasing in the brains of epileptic animals (P<0.001) compared to the healthy animals (Fig 7.6b). When treated with CBD however, the epileptic animals showed no significant change (P>0.05) in glycine levels compared to the vehicle treated epileptic animals, although a trend was observed. CBD treated epileptic animals still showed significantly raised (P<0.001) glycine levels when compared to the vehicle treated healthy animals however. In contrast to methionine and glycine, cysteine levels were found to significantly decrease (P<0.001) in the epileptic animals when compared to the healthy animals (Fig 7.6c). No significant change (P>0.05) was found in cysteine levels within the epileptic animals following CBD treatment, although a trend was evident whereby cysteine levels were reduced with CBD treatment. Cysteine levels within the CBD treated epileptic animals were still found to be significantly lower (P<0.001) than the healthy animals. These data suggest that a predisposition to seizures in heterozygote SCN1A animals correlates with elevated methionine and glycine in the brain, but reduces cysteine levels. These data also suggest that CBD treatment within *Scn1a*$^{+/-}$ mice further elevates methionine levels, with a trend for increasing glycine and reducing cysteine levels.

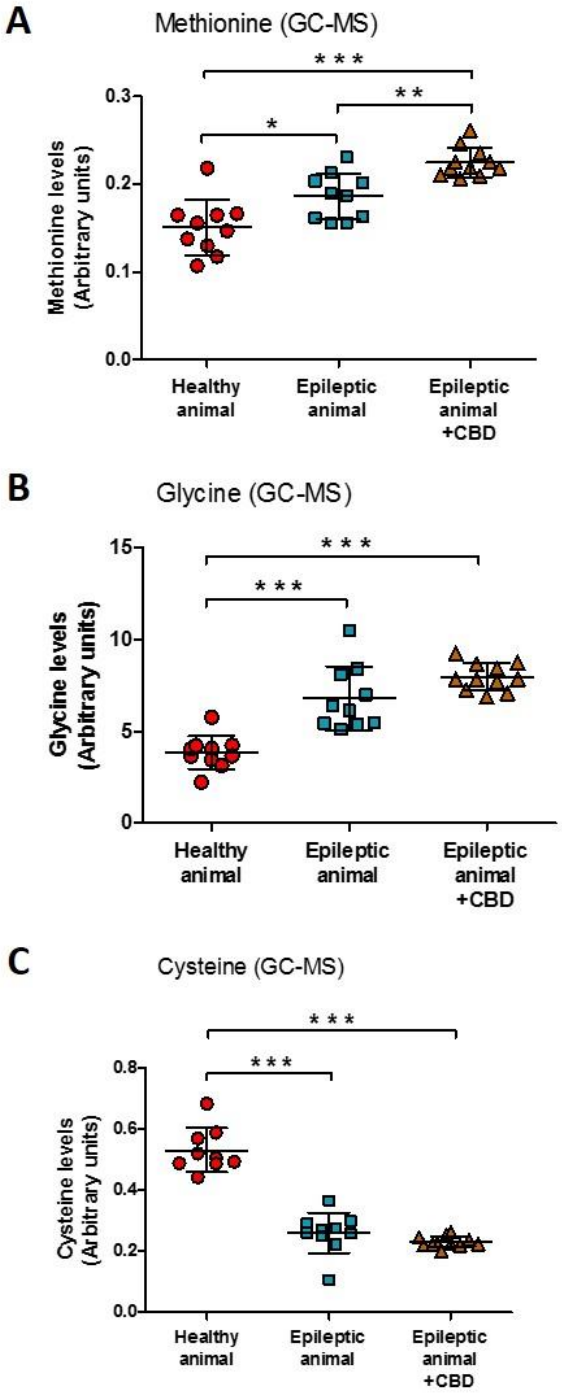

Figure 7.6 GC-MS analysis of brain (cortex) samples from a SCN1A$^{+/-}$ (mild Dravet syndrome) mouse seizure model treated with CBD. Brain (cortex) samples obtained from heterozygous SCN1A$^{+/-}$ mice that had been treated with CBD or vehicle alone were compared to that of healthy homozygous animals. GC-MS analysis was used to compare (A) methionine, (B) glycine and (C) cysteine levels between groups. Data are mean +/- SEM (*,P<0.05; **,P<0.01; ***,P<0.001, one-way ANOVA, Tukey post hoc test, n=9-10).

7.3 Discussion

7.3.1 CBD attenuates an increase in methionine levels attributed to PTZ treatment in rat primary hippocampal neurons

In order to investigate a role for CBD and the one carbon cycle in seizure control and epilepsy we firstly translated our findings across into an *in vitro* model using rat primary hippocampal neurons. Cells were exposed to pentylenetetrazole, while intervention groups were also pre-treated with CBD. PTZ treatment had no effect upon glycine and cysteine levels, although PTZ treatment did significantly elevate methionine levels, and this increase was attenuated with CBD treatment. Interestingly, this decrease in cellular methionine levels found in the intervention group was also observed in wild type (AX3) *D. discoideum* cells following CBD treatment (Fig 6.7a). However, the primary neurons do not exhibit a drop in methionine levels following CBD treatment alone, but only after the neurons have been subjected to PTZ and CBD treatment. These data suggest that CBD prevents changes in methionine levels caused by pentylenetetrazole treatment.

The possibility that CBD treatment may prevent seizure onset through regulating methionine levels is interesting, and is supported by a range of previous studies. The key role of the one carbon cycle is the production of s-adenosyl methionine (SAM), via the utilization of methionine (Fig 1.3), and is known to be the primary methyl group donor within cells (Ulrey, 2005). In turn SAM is responsible for the methylation of a number of proteins and neurotransmitters, and DNA through DNA methyltransferases (Ulrey, 2005). DNA methylation may also play a role in the onset of epileptogenesis and seizure progression, termed the methylation hypothesis (Kobow *et al*, 2013). Similarly, recent studies have shown that CBD directly increases global DNA methylation, although this has been attributed to enhancing DNMT1 expression (Pucci *et al*, 2013). Other studies have also investigated how cannabinoids affect the expression levels of specific genes. For example CBDA, the precursor to CBD, was initially thought to inhibit Cyclooxygenase 2 (COX2) activity by directly interacting with the protein, however it has now been shown that CBDA also inhibits COX2 expression (Takeda *et al*, 2014). This reduced expression, for both *cox2* and other genes could be attributed to an increase in methylation as a result of CBD treatment. In turn, this increase in methylation maybe regulated through the activity of the one carbon cycle as shown by our previous data (chapter 6). As such, the reduced levels of methionine seen in CBD treated primary neurons (Fig 7.2a) and *D. discoideum* wild type (AX3) cells (Fig 6.7a) may be the result of an increase in SAM production.

The anti-convulsant effects of CBD may also arise from increased cellular levels of free adenosine. Following the transfer of a methyl group from SAM, the resultant s-adenosylhomocysteine (SAH) molecule breaks down to produce both adenosine and homocysteine (Ducker and Rabinowitz, 2017). Adenosine is well known as an endogenous anti-convulsant within the brain (Young and Dragunow, 1994), which terminates brief seizures. Therefore, any mechanism that may increase endogenous levels of adenosine may enhance its anticonvulsant effect. This elevated level of adenosine may occur through the concomitant breakdown of SAM during DNA methylation, which in turn is instigated by CBD treatment. Unfortunately, we were unable to quantify adenosine levels within the cell lines, but future work in this area may shed new light upon CBD function if adenosine levels were investigated.

7.3.2 CBD regulates methionine levels within the plasma of Lithium-pilocarpine treated rats

Using *in vivo* models we initially investigated methionine, glycine and cysteine levels within the plasma of healthy and epileptic (Li-Pilo) rats, with intervention groups treated orally with CBD. No significant change in amino acid levels was detected between healthy and epileptic animals (Fig 7.3). This is in contrast to what was observed in the primary neurons experiment, whereby seizure activity significantly elevated methionine levels (Fig 7.2a). This difference in response to seizure activity could be attributed to a number of factors. Firstly, the primary neuron experiment was an acute seizure model (Chang *et al*, 2014), while the li-Pilo treated rats were a chronic seizure model (Curia *et al,* 2008). Secondly, it is possible that amino acid changes are not observed in animals with a predisposition to seizure, but rather only manifest as a direct response to seizure onset. This is supported by a study that looked at amino acid levels within the hippocampus of pilocarpine treated rats. In this study an increase in these amino acid concentrations was reported during the recurrent seizure period (Cavalheiro *et al*, 1994).

Analysis of the amino acids within epileptic animals treated with CBD showed no changes in either glycine or cysteine, however a significant increase in methionine was detected in the plasma of CBD treated epileptic animals. This is comparable to the acute seizure model in that only methionine underwent a response. However in the acute model treated with PTZ, methionine levels decreased following CBD treatment, while in the Li-pilo rat seizure model methionine levels increased. This could also be attributed to the reasons already mentioned above. It is also possible that during seizure activity CBD elicits its anticonvulsant properties by lowering cellular methionine levels while concomitantly increasing plasma levels.

7.3.3 CBD treatment affects amino acid levels within the plasma of SCN1A$^{+/-}$ mice.

The first *in vivo* model analyzed by our collaborators was a homozygous SCN1A mouse model, replicating the Dravet syndrome etiology. While *Scn1a*$^{-/-}$ animals displayed the characteristics of Dravet syndrome, the survival rate of these animals was very low. As such the data obtained from the epileptic groups for both treated and untreated animals is limited, with both groups having a very low sample number. Unfortunately, this low sample number does not allow us to interpret the data.

To overcome the issue of survival within the *Scn1a*$^{-/-}$ epileptic group, our collaborators created a heterozygous SCN1A mouse model. The model was found to be less susceptible to seizure-induced deaths, while the animals retained the characteristic behavior commonly observed with Dravet syndrome (Harkin et al, 2007., Marini et al, 2011). The *Scn1a*$^{+/-}$ mouse model has now been widely accepted as a suitable system for the analysis of Dravet syndrome, with a number of genetic variations now covering the diverse range of *Scn1a* mutations associated with the syndrome (Griffin et al, 2018). Recent studies have also used this model to screen for anticonvulsants specific to the treatment of Dravet syndrome (Hawkins *et al*, 2007). The data obtained by our collaborators investigating the effects that CBD has on the *Scn1a* models have not yet been published. Similarly, this data is not available through contractual agreement with the industry sponsor of the project. Using the *Scn1a*$^{+/-}$ model we show that blood levels of glycine, methionine and cysteine do not provide a trait marker for epilepsy in this model, since levels do not significantly change between the healthy and *Scn1a*$^{+/-}$ mice. However, treatment of *Scn1a*$^{+/-}$ animals with CBD significantly elevated blood glycine and cysteine levels, suggesting a role of CBD in chronic regulation of one carbon cycle components during treatment. Unusually, treated *Scn1a*$^{+/-}$ animals also showed two distinct groups of animals with elevated or unchanged glycine and cysteine levels, or elevated and reduced methionine levels. Although the basis of this divergent response remains unclear, several mechanisms may be proposed. The two groups could reflect the heterogeneous response of patient populations to CBD treatment (and other anti-epileptic treatments). For example, the recent clinical trial for CBD treatment of Lennox-Gastaut sufferers showed that only 44% of individuals treated with CBD experienced a >50% reduction in drop seizures, compared to 24% for vehicle alone treatment (Thiele et al, 2018). Alternatively, the two groups could represent animals that are likely to develop recurrent seizures or have recently experienced micro-seizures that are not lethal nor evident through

behavioral analysis. Further detailed *in vivo* studies, and clinical patient sampling are necessary to investigate these options in greater detail.

7.3.4 Both Seizures and CBD treatment affect amino acid levels within the brain of SCN1A$^{+/-}$ mice.

As well as analysing plasma samples from the *Scn1a*$^{+/-}$ animals, we also analysed methionine, glycine and cysteine levels within whole brains samples. In contrast to the *in vitro* study using primary neurons (7.2.1), CBD treatment further elevates methionine and possibly glycine levels. While the difference between acute and chronic seizure models could explain these differences, it is possible that the effects of CBD vary depending upon the region of brain analyzed. In the acute seizure model, the primary neurons were isolated from the hippocampus, while in the *Scn1a*$^{+/-}$ chronic seizure model samples were derived from the entire brain, including the cortex, thalamus and cerebellum regions. Because mutation of SCN1A has been linked to other epilepsy syndromes such as Lennox-Gastaut syndrome (Selmer *et al,* 2009), it is hard to establish which of these regions is critical for the therapeutic effect of CBD. Others have shown the involvement of SCN1A within the hippocampus (Isom, 2014) and in the temporal lobe (Rossi, 2014). These data suggest however that CBD is able to alter methionine levels within the brain, supporting a role for CBD in regulating the one carbon cycle.

Interestingly, cysteine levels within the brain were found to drop during seizure activity (Fig 7.6c), consistent with a disruption of the one carbon cycle. While CBD is not shown here to significantly affect cysteine levels, it remains likely that potential changes in cysteine may be masked through variable effects in distinct brain regions. CBD treatment was previously shown to increase cysteine levels within the plasma of these animals (Fig 7.5c). The possibility that CBD regulates cysteine levels is interesting.

As well as having an anti-convulsant effect, CBD has anti-oxidant properties (Hampson *et al*, 1998). It is possible that this anti-oxidant role may stem from the regulation of cysteine levels through the glycine cleavage system and the one carbon cycle. Any changes within the one carbon cycle will directly affect the transsulfuration pathway, which leads to the production of glutathione (Mosharov *et al*, 2000). Glutathione is the cells primary endogenous anti-oxidant and is made up of the amino acids cysteine, glycine and glutamate (Mosharov *et al*, 2000). The cysteine used in glutathione production feeds directly from the one carbon cycle (Vitvitsky et al, 2006), therefore if CBD regulates the one carbon cycle it could also regulate glutathione

production. During seizure episodes ROS production is elevated (Patsoukis *et al,* 2004), while CBD has been shown to reduce ROS levels (Mecha et al, 2012., Sun *et al*, 2017). Whether this antioxidant effect of CBD is caused by increasing glutathione levels, via the one carbon cycle remains to be determined. Thus, a mechanism of CBD through regulating the one carbon cycle may impact on both seizure control and antioxidant effects.

7.4 Summary

In this chapter we have used a number of *in vitro* and *in vivo* seizure models, and have shown that seizure occurrence directly regulates methionine, glycine and cysteine levels. Within an acute seizure model using rat primary hippocampal neurons we showed that seizure activity elevates cellular methionine levels, while intervention with CBD attenuates these changes. We also show that plasma methionine levels within a lithium-pilocarpine seizure model are elevated when treated with CBD. We further analyzed methionine, glycine and cysteine levels within the plasma and brain tissue of a mouse $SCN1A^{+/-}$ seizure model, shown to have the clinical characteristics associated with Dravet syndrome. We show that both seizures and CBD treatment affect methionine, glycine and cysteine levels within the brain, while CBD treatment affects such levels within the plasma of $SCN1A^{+/-}$ mice.

Conclusion

Conclusion

The aims of this research was to identify and investigate potential molecular targets for the cannabinoids CBD, CBDA and CBDV. Previous research has shown cannabinoids to have a negative effect upon cell proliferation in mammalian cell lines (McAllister *et al*, 2011, Solinas *et al,* 2013). We therefore investigated if cannabinoids have a similar effect upon *D. discoideum*, and if so could we use this effect as a basis to screen a mutant library. It was found that all three cannabinoids inhibit cell proliferation in a dose dependant manner, and at concentrations that are physiologically relevant. It was also shown that cannabinoids have no effect upon multi-cellular development at concentrations which inhibit cell proliferation. This suggests that the cannabinoids induce their effects through a distinct molecular mechanism rather than a general toxic effect. Using this growth inhibition effect a mutant library was screened for insertional mutants that displayed a resistance to the effects of the cannabinoids. A number of mutants were identified and four genes of interest were independently identified that inferred a resistance when disrupted. It was initially thought that three of these genes may be linked to the one carbon cycle; these being *reductase A*, *lmbd2b* and *gcvH1*. Both *reductase A* and *lmbd2b* were initially investigated but subsequently set aside due to lack of convincing data. Subsequent investigations focused primarily upon *gcvH1* due its role in the metabolism of the neurotransmitter glycine, and its close association with the one carbon cycle. In order to validate the results found in the mutant screen an independent *gcvH1* null cell line was created and was shown to have a significant resistance to CBD when compared to wild type (AX3) cells. To be sure that the resistance observed in the *gcvH1* null cell line was not a result of changes in cellular uptake and expulsion, or degradation of CBD, we quantified cellular CBD levels following treatment. It was shown that no significant difference existed in cellular CBD levels between the *gcvH1* null and wild type (AX3) cells, suggesting that resistance is a result of some other mechanism. Investigation into the effects of both CBDA and CBDV upon the *gcvH1* null cell line showed that both cannabinoids inhibited cell proliferation in a manner comparable to wild type (AX3) cells. This further suggests that cellular transport or degradation is not involved, while also confirming GCVH1 only has a role in regulating CBD sensitivity. The role of GCVH1 in regulating CBD sensitivity was further validated by reinstating *gcvH1* back into the null cell line by use of an extra chromosomal vector. It was shown that when reinstated, the rescue cell line was re-sensitized to the effects of CBD. In order to determine whether the human homologue GCSH has a similar function to GCVH1 we independently expressed the human gene within the null cell line. It was shown that when the human *gcsH* gene was expressed in the *gcvH1* null cell line, sensitivity to CBD was also re-instated. This suggests that both the *D. discoideum* GCVH1

and the *H. sapiens* GCSH proteins have similar function in regulating CBD sensitivity. We also investigated whether both proteins correctly localized to the mitochondria within the *gcvH1* null cell line. By using immunofluorescence we were able to confirm this. Because GCVH1 and GCSH were identified as being potential molecular targets for CBD, predicted docking analysis was carried out on both for potential CBD-protein interactions. It was found that both proteins have regions in which CBD may interact. Of particular interest was a region located adjacent to the lysine residue essential for lipoic acid binding. It may be possible that CBD could inhibit GCVH1 function by targeting this region and preventing lipoic acid binding. Because of the close association between the glycine cleavage system and the one carbon cycle it was questioned whether CBD treatment had an effect upon metabolite levels within the one carbon cycle. GC-MS and NMR analysis was used to show that methionine levels were significantly lower in wild type (AX3) cells following CBD treatment compared to untreated wild type (AX3) cells. Interestingly no change in methionine levels was detected in the *gcvH1* null cell line when treated with CBD and compared to the untreated *gcvH1* null group. This supports the possibility that GCVH1 is a molecular target for CBD.

The possibility that CBD may regulate metabolites of the one carbon cycle is interesting, especially as many of these metabolites are recognised as having either positive or negative roles in seizure onset. Elevated levels of homocysteine have been linked to seizure onset (Baldelli *et al*, 2010), while a deficiency in cobalamin which is required for the successful conversion of homocysteine to methionine has also been linked to seizure onset (Dogan et al, 2012, Kandula et al, 2014 and Lubana et al, 2015). Similarly, homocysteine, glycine and dimethyl glycine are known neuronal NMDA receptor agonists or antagonists (Ranjana and Surojit, 2009; Cummings and Popescu, 2015; Lee *et al*, 2017), while glycine itself is an important inhibitory neurotransmitter in the central nervous system (Dutertre *et al*, 2012). The primary role of the one carbon cycle is the production of s-adenosyl methionine (SAM), the cells principal methyl donor (Ulrey, 2005). Studies have linked CBD to changes in global DNA methylation (Pucci *et al*, 2013), while it has also been proposed that DNA methylation may be a key process in epileptogenesis (Kobow *et al*, 2013). Again, adenosine is regarded as an endogenous anti-convulsant within the brain (Young and Dragunow, 1994), which terminates brief seizures. Similarly, the cysteine produced in the one carbon cycle is fed into the transsulfuration pathway for the production of glutathione, the cells primary anti-oxidant (Mosharov *et al*, 2000). This is relevant as ROS production is elevated during seizures (Patsoukis *et al,* 2004), while CBD has been shown to reduce ROS levels (Mecha et al, 2012., Sun *et al*, 2017). With so many possible

mechanisms within the one carbon cycle in which seizure onset can be regulated, it was deemed essential to translate these findings across into mammalian seizure models.

Initially our research concentrated upon the effects of CBD treatment within an acute seizure model using primary hippocampal neurons, particularly with regards to methionine levels. Within this *in vivo* model it was shown that during seizure activity induced by pentylenetetrazole, methionine levels were significantly elevated, however if cells were pre-treated with CBD this effect was attenuated. We further investigated the effects of CBD treatment upon methionine levels within *in vivo* seizure models. Initially we looked at methionine levels within the plasma of a rat lithium-pilocarpine seizure model and showed that methionine levels were significantly elevated when treated with CBD. We then investigated the effects of CBD upon methionine levels within the plasma and brain tissue of a mouse Dravet syndrome model. This particular model was heterozygous for the *Scn1A* gene, a voltage-gated sodium channel, and displayed the clinical characteristics associated with Dravet syndrome. It was shown that CBD treatment affected glycine and cysteine levels within the plasma, while both seizures and CBD treatment affected methionine, glycine and cysteine levels within the brain tissue.

While the data presented in this study clearly shows that seizure activity and CBD treatment effects certain metabolites within the one carbon cycle, the most prominent limitation of our study is that the key mechanism by which CBD infers its anticonvulsant effect is not determined. Similarly, are the changes we observe in methionine levels the direct cause of the anti-convulsant effects seen in CBD treatment, or are they an effect resulting from a change in one of the other metabolites? Also, if changes in methionine are responsible for the anti-convulsant effects of CBD, how do these changes facilitate this? It is also possible that the anti-convulsant effects of CBD result from the regulation of the one carbon cycle in its entirety, including all its metabolites. For example CBD may regulate the cycle whereby key metabolites such as glutathione, adenosine and glycine all increase, thereby having a positive effect in preventing seizures. While other metabolites such as homocysteine and cysteine decrease, thereby increasing the threshold required for seizure inducement. In order to identify the exact cause, further research will need to be undertaken.

As already mentioned above, future avenues of investigation should include the role that methionine may have in preventing epileptogenesis. It has already been shown that CBD induces DNA methylation (Pucci *et al*, 2013) and that its precursor CBDA is able to inhibit the expression of certain key enzymes (Takeda *et al*, 2014). It would therefore be desirable to

explore the effects that CBD has upon the expression of key enzymes such as the cytochrome P450 family of enzymes. Studies have already shown that CBD inhibits the function of this family of enzymes. It would be beneficial to determine whether this inhibition arises from reduced expression levels due to increased DNA methylation.

Future studies should also investigate how CBD treatment effects the levels of homocysteine, glutathione, adenosine and s-adenosyl methionine within seizure models. As already mentioned above, some of these are endogenous anti-convulsants or prevent seizure onset in some way, while others such as homocysteine have been shown to be pro-convulsants. Quantifying the levels of each of these would help identify the exact therapeutic mechanism in which CBD prevents seizures.

In this study we propose the glycine cleavage system H-proteins as being the molecular target for CBD. While the confirmation of this was not within the scope of this study, it would be advantagous to investigate this further. Identifying the molecular target for CBD would have positive repercussions by allowing the development of more specific pharmaceuticals with more tolerable side effect profiles. Future studies could firstly look at the potential binding sites of CBD within GCVH1, and determine which key amino acid residues are essential for its binding. This could be achieved using site directed mutagenesis. Similarly, an x-ray crystallography approach could be adopted to confirm an interaction between both protein and CBD, and therefore identify precise binding regions.

In summary, our data suggests that the anticonvulsant effects of CBD may originate from the regulation of one carbon cycle components. It also suggests that this regulation is achieved through an interaction between the glycine cleavage system H-protein and CBD. This study has therefore identified a new and exciting area of cannabinoid research, specifically with regards to the role that CBD has in preventing seizure onset. One implication of this is that it may increase the focus of future research into one carbon cycle components and their link to epilepsy. This will hopefully lead to the development of new anti-convulsant drugs, and help to decrease the number of individuals with refractory epilepsy.

References

Alexander, S. and Alexander, H. 2011. Lead genetic studies in *Dictyostelium discoideum* and translational studies in human cells demonstrate that sphingolipids are key regulators of sensitivity to cisplatin and other anticancer drugs. *Seminars in Cell and Developmental Biology.* **22**: 97-104.

Adley, K, M., Keim, M. and Williams, R, S. 2006. Pharmacogenetics: defining the genetic basis of drug action and inositol trisphosphate analysis. *Methods of Molecular Biology*. **346:** 517-534

Anzenbacher, P. and Anzenbacherová, E. 2001. Cytochromes P450 and metabolism of xenobiotics. *Cellular and Molecular Life Sciences*. **58:** 737–747

Asimakopoulou, A. and Weiskirchen, R. 2015. Lipocalin 2 in the pathogenesis of fatty liver disease and non-alcoholic steatohepatitis. *Clinical Lipidology*. **10(1):** 47-67

Badenhorst, C, P., Van der Sluis, R., Erasmus, E. and Van Dijk, A, A. 2013. Glycine conjugation: importance in metabolism, the role of glycine N-acyltransferase, and factors that influence interindividual variation. *Expert Opinion on Drug Metabolism and Toxicology*. **9(9):** 1139-53

Baez, M, V., Cercato, M, C. and Jerusalinsky, D, A. 2018. NMDA receptor subunits change after synaptic plasticity induction and learning and memory acquisition. *Neural Plasticity.* Article ID: 5093048

Baldelli, E., Leo, G., Andreoli, N., Fuxe, K., Biagini, G. and Agnati, L, F. 2010. Homocysteine potentiates seizures and cell loss induced by pilocarpine treatment. *Neuromolecular Medicine*. **12(3):** 248-259

Bender, A, A., Morse, R, P., Scott, R, C., Holmes, G, L. and Lenck-Santini, P. 2012. SCN1A mutations in Dravet syndrome: Impact of interneuron dysfunction on neural networks and cognitive outcome. *Epilepsy and Behaviour.* **23(3):** 177-186

Bertram, E. 2007. The Relevance of Kindling for Human Epilepsy. *Epilepsia.* **48:** 65-74

Betz, H., Gomeza, J., Armsen, W., Scholze, P. and Eulenberg, V. 2006. Glycine transporters: essential regulators of synaptic transmission. *Biochemical Society Transactions*. **34:** part 1

Bih, C, I., Chen, T., Nunn, A, V, W., Bazelot, M., Dallas, M. and Whalley, B, J. 2015. Molecular Targets of Cannabidiol in Neurological Disorders. *Neurotherapeutics.* **12(4):** 699-730

Boeckeler, K., Adley, K., Xu, X., Jenkins, A., Jin, T. and Williams, R. S. 2006. The neuroprotective agent, valproic acid, regulates the mitogen-activated protein kinase pathway through

modulation of protein kinase A signalling in Dictyostelium discoideum. *European Journal of Cell Biology*. **85:** 1047-1057.

Boison, D. Adenosine and epilepsy: from therapeutic rationale to new therapeutic strategies. *Neuroscientist.* **11(1):** 25-36

Bozzaro, S. 2013. The model organism Dictyostelium discoideum. *Methods in Molecular Biology.* **983:** 17-37

Breen, G., Harwood, A. J., Gregory, K., Sinclair, M., Collier, D., ST Clair, D. and Williams, R. S. 2004. Two peptidase activities decrease in treated bipolar disorder not schizophrenic patients. *International Journal of Bipolar Disorders*. **6:** 156-161.

Brzostowski, J. A., Sawai, S., Rozov, O., Liao, X. H., Imoto, D., Parent, C. A., Kimmel, A. R. 2013. Phosphorylation of chemoattractant receptors regulates chemotaxis, actin reorganization and signal relay. *Journal of Cell Science.* **126**: 4614-4626.

Buers, I., Pennekamp, P., Nitschke, Y., Lowe, C., Skryabin, B, V. and Rutsch, F. 2016. Lmbrd1 expression is essential for the initiation of gastrulation. *Journal of Cellular and Molecular Medicine.* **20(8):** 1523-1533

Bushra, R., Shoaib, M, H., Naeem, M, I. and Aslam, N. 2013. Aceclofenac: a new effective and safe NSAID. *International Journal of Drug Delivery Technology*. **4(1):** 34-42

Calderwood, D, A. 2004. Talin controls integrin activation. *Biochemical Society Transactions*. **32(3):** 434-7

Carrier, E, J., Auchampach, J, A. and Hillard, C, J. 2006. Inhibition of an equilibrative nucleoside transporter by cannabidiol: A mechanism of cannabinoid immunosuppression. *PNAS*. **103(20):** 7895-7900

Cavalheiro, E, A., Fernandes, M, J., Turski, L. and Naffah-Mazzacoratti, M, G. 1994. MG. Spontaneous recurrent seizures in rats: amino acid and monoamine determination in the hippocampus. *Epilepsia.* **35(1):** 1-11

Chang, P., Orabi, B., Deranieh, R. M., Dham, M., Hoeller, O., Shimshoni, J. A., Yagen, B., Bialer, M., Greenberg, M. L., Walker, M. C. and Williams, R. S. 2012. The antiepileptic drug valproic acid and other medium-chain fatty acids acutely reduce phosphoinositide levels independently of inositol in Dictyostelium. *Disease Models and Mechanisms*. **5:** 115-124.

Chang, P., Terbach, N., Plant, N., Chen, P. E., Walker, M. C. and Williams, R. S. 2013. Seizure control by ketogenic diet-associated medium chain fatty acids. *Neuropharmacology*. **69:** 105-114.

Chang, P., Walker, M. C. and Williams, R. S. 2014. Seizure-induced reduction in PIP3 levels contributes to seizure-activity and is rescued by valproic acid. *Neurobiology of Disease*. **62:** 296-306.

Chang, P., Zuckermann, A. M., Williams, S., Close, A. J., Cano-Jaimez, M., McEvoy, J. P., Spencer, J., Walker, M. C. and Williams, R. S. 2015. Seizure control by derivatives of medium chain fatty acids associated with the ketogenic diet show novel branching-point structure for enhanced potency. *Journal of Pharmacolgy and Experimental Therapeutics*. **352:** 43-52.

Cifelli, P. and Grace, A, A. 2012. Pilocarpine Induced Temporal Lobe Epilepsy in the Rat is Associated with Increased Dopamine Neuron Activity. *International Journal of Neuropsychopharmacology*. **15(7):** 957-964

Cocorocchio, M., Ives, R., Clapham, D., Andrews, P. L. and Williams, R. S. 2015. Bitter tastant responses in the amoeba Dictyostelium correlate with rat and human taste assays. *ALTEX*. **33(3):** 225-36

Cocorocchio, M., Baldwin, A. J., Stewart, B., Kim, L., Harwood, A. J., Thompson, C. R. L., Andrews, P. L. R. and Williams, R. S. B. 2018. Curcumin and derivatives function through protein phosphatase 2A and presenilin orthologues in Dictyostelium discoideum. *Disease Models and Mechanisms.* **11(1)**

Coffman, B, L., Rios, G, R., King, C, D. and Tephly, T, R. 1997. Human UGT2B7 Catalyzes Morphine Glucuronidation. *Drug Metabolism and Disposition*. **25:** No 1

Cornillon, S., Gebbie, L., Benghezal, M., Nair, P., Keller, S., Wehrle-Haller, B., Charette, S, J., Brückert, F., Letourneur, F. and Cosson, P. 2006. An adhesion molecule in free-living Dictyostelium amoebae with integrin β features. *EMBO Reports*. **7(6):** 617-621

Cummings, K, A. and Popescu, G, K. 2015. Glycine dependant activation of NMDA receptors. *The Journal of General Physiology*. **145(6):** 513-527

Cunliffe, V. T., Baines, R. A., Giachello, C. N., Lin, W. H., Morgan, A., Reuber, M., Russell, C., Walker, M. C. and Williams, R. S. 2015. Epilepsy research methods update: Understanding the causes of epileptic seizures and identifying new treatments using non-mammalian model organisms. *Seizure*. **24:** 44-51.

Curia, G., Longo, D., Biagini, G., Jones, R, S, G. and Avolia, M. 2008. The pilocarpine model of temporal lobe epilepsy. *Journal of Neuroscience Methods*. **172:** 143-157

De Petrocellis, L., Ligresti, A., Moriello, A. S., et al. (2011). Effects of cannabinoids and cannabinoid-enriched cannabis extracts on TRP channels and endocannabinoid metabolic enzymes. *British Journal of Pharmacology*. **163**: 1479-1494.

De Petrocellis, L., Vellani, V., Schiano-Moriello, A., Marini, P., Magherini, P, C., Orlando, P. and Di Marzo, V. 2008. Plant-derived cannabinoids modulate the activity of transient receptor potential channels of ankyrin type-1 and melastatin type-8. *Journal of Pharmacology and Experimental Therapeutics.* **325(3):** 1007-1015

Desphande, L, S., Lou, J, K., Mian, A., Blair, R, E., Sombati, S., Attkisson, E. and DeLorenzo, R, J. 2008. Time course and mechanism of hippocampal neuronal death in an in vitro model of status epilepticus: Role of NMDA receptor activation and NMDA dependent calcium entry. *European Journal of Pharmacology*. **583:** 73–83

Devinsky, O., Cilio, M., R., Cros, H., et al. (2014) Cannabidiol: Pharmacology and potential therapeutic role in epilepsy and other neuropsychiatric disorders. *Epilepsia*. **55**: 791-802.

Devinsky, O., Cross, J, H., Laux, L., Marsh, E., Miller, I., Nabbout, R., Scheffer, I, E., Thiele, E, A. and Wright, S. 2017. Trial of Cannabidiol for Drug-Resistant Seizures in the Dravet Syndrome. *The New England Journal of Medicine*. **376(21):** 2011-2020

Devinsky, O., Patel, A, D., Cross, J, H., Villanueva, V., Wirrell, E, C., Privitera, M., Greenwood, S, M., Roberts, C., Checketts, D., VanLandingham, K, E. and Zuberi, S, M. 2018. Effect of Cannabidiol on Drop Seizures in the Lennox–Gastaut Syndrome. The New England Journal of Medicine. **378:** 1888-1897

Dhediya, R, M., Joshi, S, S., Gaibhiye, S, V., Jalgaonkar, S, V. and Biswas, M. 2016. Evaluation of antiepileptic effect of S-adenosyl methionine and its role in memory impairment in pentylenetetrazole-induced kindling model in rats. *Epilepsy and Behaviour*. 61: 153-157

Dogan, M., Arivuca, S., Peker, E., Akbavram, S., Dogan, S, Z., Ozdemir, O. and Cesur, Y. 2012. Psychotic disorder, hypertension and seizures associated with vitamin B12 deficiency: a case report. *Human and Experimental Toxicology.* **31(4):** 410-413.

Ducker, G. S. & Rabinowitz, J. D. 2017. One-Carbon Metabolism in Health and Disease. *Cell Metabolism.* **25:** 27-42

Dutertre, S., Becker, C. and Betz, H. 2012. Inhibitory glycine receptors: An update. *Journal of Biological Chemistry.* **287:** 40216-40223.

Eichenger, L., Pachebat, J. A., Glockner, G., et al. (2005). The genome of the social amoeba *Dictyostelium discoideum. Nature* **435**: 43-57.

Eickholt, B. J., Williams, R. S. B. and HARWOOD, A. J. 2005. Mood stabilizers and the cell biology of neuronal growth cones. *Clinical Neuroscience Research*. **4:** 189-199

Elikottil, J., Gupta, P. and Gupta, K. 2009. The Analgesic Potential of Cannabinoids. *Journal of Opioid Management.* **5(6):** 341-357

Elphick, L. M., Pawolleck, N., Guschina, I. A., Chaieb, L., Eikel, D., Nau, H., Harwood, J. L., Plant, N. J. and Williams, R. S. 2012. Conserved valproic-acid-induced lipid droplet formation in Dictyostelium and human hepatocytes identifies structurally active compounds. *Disease Models and Mechanisms***. 5:** 231-240.

Englander, J., Cifu, D, X. and Diaz-Arrastia, R. 2014. Seizures after Traumatic Brain Injury. *Archive of Physical Medicine and Rehabilitation*. **96(6):** 1223-1224

Eustáquio, A, S., Härle, J., Noel, J, P. and Moore, B, S. 2008. S-Adenosyl-L-Methionine Hydrolase (Adenosine-Forming), a Conserved Bacterial and Archeal Protein Related to SAM-Dependent Halogenases. *ChemBioChe*. **9(14):** 2215-2219

Feng, Q., Kalari, K., Fridley, B, L., Jenkins, G., Ji, Y., Abo, R., Hebbring, S., Zhang, J., Nye, M, D., Leeder, J, S. and Weinshilboum, R, M. 2011. Betaine-homocysteine methyltransferase: human liver genotype phenotype correlation. *Molecular Genetics and Metabolism*. **102(2):** 126–133

Fey, P., Kowal, A. S., Gaudet, P., Pilcher, K. E., Chisholm, R. L. 2007. 'Protocols for growth and development of Dictyostelium discoideum.' *Nature Protocols*. **2:** 1307-16

Finnegan, D, J. 2012. Retrotransposons. *Current Biology*. **22(11**): R432-R437

Finsterer, J., Mahjoub, S. Z. 2012. Epilepsy in mitochondrial disorders. *Seizure*. **21**: 316-321.

Fischer, M., Haase, I., Simmeth, E., Gerisch, G. and Muller-Taubenberger, A. 2004. A brilliant monomeric red fluorescent protein to visualize cytoskeleton dynamics in Dictyostelium. *FEBS Letters*. **577:** 227-232

Folbergrova, J. and Kunz, W, S. 2012. Mitochondrial dysfunction in epilepsy. *Mitochondrion*. **12:** 35-40.

Friedrich, M., Meier, D., Schuster, I. and Nellen, W. 2014. A Simple Retro-element Based Knock-Down System in Dictyostelium: Further Insights into RNA Interference Mechanisms. *PLOS one*. 10(6): e0131271

Fujikawa, D, G., Daniels, A, H. and Kim, J, S. 1994. The competitive NMDA receptor antagonist CGP 40116 protects against status epilepticus-induced neuronal damage. *Epilepsy Research*. **17:** 207–219

Fukasawa, Y., Tsuji, J., Fu, S., Tomii, K., Horton, P. and Imai, K. 2015. MitoFates: Improved Prediction of Mitochondrial Targeting Sequences and Their Cleavage Sites. *Molecular and Cellular Proteomics*. **14(4):** 1113-1126

Gailus, S., Suormala, T., Malerczyk-Aktas, A.G,, Toliat, M,R., Wittkampf, T., Stucki, M., Nürnberg, P., Fowler, B., Hennermann, J,B. and Rutsch, F. 2010. A novel mutation in LMBRD1 causes the cblF defect of vitamin B12 metabolism in a Turkish patient. *Journal of Inheritable Metabolic Disorders*. **33:** 17-24

Ganfornina, M, D., and Gutiérrez, G., Bastiani, M. and Sánchez, D. 2000. A phylogenetic analysis of the lipocalin protein family. *Molecular Biology and Evolution*. **17(1):** 114-26

Gilsbach, B, K., Ho, F, Y., Vetter, I, R., Haastert, P, J, M., Wittinghofer, A. and Kortholt, A. 2012. Roco kinase structures give insights into the mechanism of Parkinson disease-related leucine-rich-repeat kinase 2 mutations. *PNAS*. 109(26): 10322-10327

Goddard, G, V. 1967. Development of Epileptic Seizures through Brain Stimulation at Low Intensity. *Nature.* **214:** 1020-1021

Gonzalez-Kristeller, D, C., Farage, L., Fiorini, L, C., Loomis, W, F. and Silva, A, M. 2008. The P450 oxidoreductase, RedA, controls development beyond the mound stage in Dictyostelium discoideum. *BMC Developmental Biology*. **8(8):** doi:10.1186/1471-213X-8-8

Hagedorn, M., Neuhaus, E, M. and Soldati, T. 2006. Optimized fixation and immunofluorescence staining methods for Dictyostelium cells. *Methods in Molecular Biology*. **346:** 327-338

Hampson, A, J., Grimaldi, M., Axelrod, J. and Wink, D. 1998. Cannabidiol and Delta 9-tetrahydrocannabinol are neuroprotective antioxidants. *Proceedings of the National Academy of Sciences.* **95:** 8268–8273

Harkin, L. A., MCmahon, J. M., Iona, X., Dibbens, L., Pelekanos, J. T., Zuberi, S. M., Sadleir, L. G., Andermann, E., Gill, D., Farrell, K., Connolly, M., Stanley, T., Harbord, M., Andermann, F.,

Wang, J., Batish, S. D., Jones, J. G., Seltzer, W. K., Gardner, A., C., Sutherland, G., Berkovic, S. F., Mulley, J. C. and Scheffer, I. E. 2007. The spectrum of SCN1A-related infantile epileptic encephalopathies. *Brain*. **130:** 843-52.

Hawkins, N, A., Abderson, L, L., Gertler, T, S., Laux, L., George, A, L. and Kearney, J, A. 2007. Screening of conventional anticonvulsants in a genetic mouse model of epilepsy. *Annals of Clinical and Translational Neurolgy*. **4(5):** 326-339

Henzler-Wildman, K. and Kern, D. 2007. Dynamic personalities of proteins. *Nature.* **450:** 964-72

Hikuchi, H., Oshima, Y., Ichimura, A., Gokan, N., Hasegawa, A., Hosaka, K., Kubohara, Y. (2006). Anti-leukemic activities of *Dictyostelium* secondary metabolites: A novel aromatic metabolite, 4-methyl-5-n-pentylbenzene-1,3-diol, isolated from *Dictyostelium* mucoroides suppresses cell growth in human leukemia K562 and HL-60 cells. *Life Sciences.* **80**: 160-165.

Hill, A. J., Mercier, M. S., Hill, T. D. M., et al. (2012). Cannabidivarin is anticonvulsant in mouse and rat. *British Journal of Pharmacology*. **167**: 1629-1642.

Hwang, W, Y., Fu, Y., Reyon, D., Maeder, M, L., Tsai, S, Q., Sander, J, D., Peterson, R, T., Yeh, J, R. and Joung, J, K. 2013. Efficient genome editing in zebrafish using a CRISPR-Cas system. *Nature Biotechnology*. **31(3):** 227-229

Isom, L, L. 2014. "It Was the Interneuron With the Parvalbumin in the Hippocampus!" "No, It Was the Pyramidal Cell With the Glutamate in the Cortex!" Searching for Clues to the Mechanism of Dravet Syndrome – The Plot Thickens. *Epilepsy Currents*. **14(6):** 350-352

Ivens, S. Kaufer, D. Flores, L, P. Benchmann, I. Zumsteg, D. Tomkins, O. Seiffert, E. Heinemann, U. Friedman, A. 2007. TGF-b receptor-mediated albumin uptake into astrocytes is involved in neocortical epileptogenesis. *Brain*. **130**: 535-47

Jaeger, W., Benet, L, Z. and Bornheim, L, M. 2008. Inhibition of cyclosporine metabolism by cannabidiol in mouse and human microsomes. *Xenobiotica.* **26(3):** 275-284

Jiang, R., Yamaori, S., Okamaoto, Y., Yamamoto, I. and Waanabe, K. 2013. Cannabidiol Is a Potent Inhibitor of the Catalytic Activity of Cytochrome P450 2C19. *Drug Metabolism and Pharmacokinetics***. 28(4):** 332–338

Jobst, B, C. and Cascino, G, D. 2015. Resective epilepsy surgery for drug-resistant focal epilepsy: a review. *The Journal of the American Medical; Association.* **313(3):** 285-93

Jones, N. A., Hill, A. J., smith, I., Bevan, S. A., Williams, C. M., Whalley, B. J. and Stephens, G. J. 2010. Cannabidiol displays antiepileptiform and antiseizure properties in vitro and in vivo. Journal *of Pharmacolgy and Experimental Therapeutics*. **332:** 569-77.

Jones, N. A., Glyn, S. E., Akiyama, S., Hill, T. D., Hill, A. J., Weston, S. E., Burnett, M. D., Yamasaki, Y., Stephens, G. J., Whalley, B. J. and Williams, C. M. 2012. Cannabidiol exerts anti-convulsant effects in animal models of temporal lobe and partial seizures. *Seizure*. **21:** 344-52.

Kalume, F., Westenbroek, R, E., Cheah, C, S., Yu, F, H., Oakley, J, C., Scheuer, T. and Catterall, W, A. 2013. Sudden unexpected death in a mouse model of Dravet syndrome. *Journal of Clinical Investigation.* **123(4):** 1798-1808

Kandratavicius, L., Balista, P, A., Lopes-Aguiar, C., Ruggiero,R, N., Umeoka, E, H., Garcia-Cairasco, N., Bueno-Junior, L, S. and Leite, J, P. 2014. Animal models of epilepsy: use and limitations. *Neuropsychiatric Disease and Treatment*. **10:** 1693-1705

Kandula, T., Peters, H., and Fahey, M. 2014. Cobalamin E defect, a rare inborn error of vitamin B12 metabolism: value of early diagnosis and treatment. *Journal of Clinical Neuroscience*. **21:** 1815-1817.

Kang, H, Lee, Y. and Kim, H, D. 2013. Mitochondrial disease and epilepsy. *Brain and Development.* **35:** 757-761

Keim, M., Williams, R, S. and Harwood, A, J. 2004. An inverse PCR technique to rapidly isolate the flanking DNA of dictyostelium insertion mutants. *Molecular Biotechnology*. **26(3):** 221-224

Kelley, L. A., Mezulis, S., Yates, C. M., Wass, M.N. and Sternberg, M. J. E. 2015. The Phyre2 web portal for protein modelling, prediction and analysis. *Nature Protocols*. **10**: 845-858

Kelsey, J. S., Fastman, N. M. and Blumberg, D. (2012). Evidence of an evolutionary conserved LMBR1 domain-containing protein that associates with endocytic cups and plays a role in cell migration in Dictyostelium discoideum. *Eukaryotic Cell*. **11(4):** 401-416

Kikuchi, G. & Hiraga, K. 1982. The mitochondrial glycine cleavage system. Unique features of the glycine decarboxylation. *Mol Cell Biochem*, **45:** 137-49.

Klein, B. D., Jacobson, C. A., Metcalf, C. S., Smith, M. D., Wilcox, K. S., Hampson, A. J. and Kehne, J. H. 2017. Evaluation of Cannabidiol in Animal Seizure Models by the Epilepsy Therapy Screening Program (ETSP). *Neurochemical Research*. **42:** 1939-1948.

Kobow, K., El-Osta, A. and Blumcke, I. 2013. The methylation hypothesis of pharmacoresistance in epilepsy. *Epilepsia.* **54:** 41-47

Kovac, S., Domijan, A, M., Walker, M, C. and Abramov, A, Y. 2012. Prolonged seizure activity impairs mitochondrial bioenergetics and induces cell death. *Journal of Cell Science*. **125:** 1796–1806

Kovac, S., Domijan, A, M., Walker, M, C. and Abramov, A, Y. 2014. Seizure activity results in calcium- and mitochondria independent ROS production via NADPH and xanthine oxidase activation. *Cell Death and Disease*. **5:** e1442

Kovac, S., Dinkova-Kostova, A., and Abramov, A. 2016. The Role of Reactive Oxygen Species in Epilepsy. *Reactive Oxygen Species*. **1(1):** 38–52.

Kuspa, A. and Loomis, W. F. 1992. Tagging developmental genes in Dictyostelium by restriction enzyme-mediated integration of plasmid DNA. *PNAS*. **89:** 8803-8807.

Kuspa, A. 2006. Restriction Enzyme-Mediated Integration (REMI) mutagenesis. Dictyostelium discoideum protocols. Methods in molecular biology™, vol. Human Press.

Kwan, P., and Brodie, M. J. (2000). Early identification of refractory epilepsy. *The New England Journal of Medicine*. **342**: 314-319.

Lafolie, P., Beck, O., Lin, Z., Albertioni, F. and Boreus, L. 1996. Urine and Plasma Pharmacokinetics of Codeine in Healthy Volunteers: Implications for Drugs-of-Abuse Testing. *Journal of Analytical Toxicology***. 20:** 541-546

Leach, J, P., Mohanraj, R. and Borland, W. 2012. Alcohol and drugs in epilepsy: **Pathophysiology, presentation, possibilities, and prevention. *Epilepsia*. 53(Suppl.4): 48-57**

Lee, H, C., Fellenez-Maloney, M., Liscovitch, M. and Blusztajn. 1993. Phospholipase D-catalyzed hydrolysis of phosphatidylcholine provides the choline precursor for acetylcholine synthesis in a human neuronal cell line. *PNAS*. **90:** 10086-10090

Lee, M., Lin, Y., Tu, Y., Tseng, Y, J., Chan, M. and Chen, H. 2017. Effects of sarcosine and N, N-dimethylglycine on NMDA receptor mediated excitatory field potentials. *Journal of Biomedical Science*. **24:**18

Levi, S., Polyakov, M. and Egelhoff, T, T. 2000. Green fluorescent protein and epitope tag fusion vectors for Dictyostelium discoideum. *Plasmid.* **44(3):** 231-238

Li, M., Zhong, Z., Zhu, J. et al. 2009. Identification and Characterization of Mitochondrial Targeting Sequence of Human Apurinic/Apyrimidinic Endonuclease 1. *The Journal of Biological*

Liang, Y., Li, S. and Chen, L. 2015. The physiological role of drug transporters. *Protein and Cell*. **6(5):** 334–350

Linden, I, J, M., Heijer, M., Afman, L, A., Gellekink, H., Vermeulen, S, H, H, M., Kluijtmans, K, A, J. and Blom, H, J. 2006. The methionine synthase reductase 66A>G polymorphism is a maternal risk factor for spina bifida. *Journal of Molecular Medicine*. **84(12):** 1047-1054

Lopez-Calcagno, P, E., Fisk, S., Brown, K, L., Bull, S, E., South, P, F. and Raines, C, A. 2018. Overexpressing the H-protein of the glycine cleavage system increases biomass yield in glasshouse and field-grown transgenic tobacco plants. *Plant Biotechnology Journal*. **2018:** 1-11

Lubana, S, S., Alfishawy, M., Singh, N. and Atkinson, S. 2015. Vitamin B12 deficiency and elevated folate levels: an unusual cause of generalized tonic-clonic seizure. *American Journal of Case Reports*. **16:** 386-389.

Lucido, M, J., Orlando, B, J., Vecchio, A, J. and Malkowski, M, G. 2016. The crystal structure of aspirin acetylated human cyclooxygenase-2: insight into the formation of products with reversed stereochemistry. *Biochemistry.* **55(8):** 1226–1238

Lynch, J, W. 2004. Molecular Structure and Function of the Glycine Receptor Chloride Channel. *Physiological Review*. **84:** 1051-1095.

Marini, C., Scheffer, I. E., Nabbout, R., Suls, A., De Jonghe, P., Zara, F. and Guerrini, R. 2011. The genetics of Dravet syndrome. *Epilepsia.* **52** Suppl 2, 24-9.

Maschio, M. 2012. Brain Tumor-Related Epilepsy. *Current Neuropharmacology*. **10(2):** 124-133

Mattson, R, H., Cramer, J, A., Williamson, P, D. and Novelly, R, A. 1978. Valproic acid in epilepsy: Clinical and pharmacological effects. *Annals of Neurology*. **3(1):** 20-25

May, S, W. and Padgett, S, R. 1983. Oxidoreductase Enzymes in Biotechnology: Current Status and Future Potential. *Nature Biotechnology*. **1:** 677–686

McAllister, S, D., Murase, R., Christian, R, T., Lau, D., Zielinski, A, J., Allison, J., Almanza, C., Pakdel, A., Lee, J. Limbad, C., Liu, Y., Debs, R, J., Moore, D, H. and Desprez, P. 2011. Pathways mediating the effects of cannabidiol on the reduction of breast cancer cell proliferation, invasion, and metastasis. *Breast Cancer Research and Treatment*. **129(1):** 37-47.

McKinney, J, D., Richard, A., Waller, C., Newman, M, C. and Gerberick, F. 2000. The Practice of Structure Activity Relationships (SAR) in Toxicology. *Toxicological Sciences*. **56:** 8-17

McPartland, J. M., Matias, I., Di Marzo, V., Glass, M. (2006). Evolutionary origins of the endocannabinoid system. *Gene*. **370**: 64-74.

Mecha, M., Torrao, A, S., Mestre, L., Carrillo-Salinas, F, J., Mechoulam, R. and Guaza, C. 2012. Cannabidiol protects oligodendrocyte progenitor cells from inflammation-induced apoptosis by attenuating endoplasmic reticulum stress. *Cell Death and Disease*. **3:** e331

Meisler, M, H and Kearney, J, A. 2005. Sodium Channel Mutations in Epilepsy and other Neurological Disorders. *The Journal of Clinical Investigation*. **115**: 2010-17

Menon, K, V, N., Angulo, P. and Lindor, K, D. 2001. Severe cholestatic hepatitis from troglitazone in a patient with nonalcoholic steatohepatitis and diabetes mellitus. *American Journal of Gastroenterology*. **96:** 1631-1634

Miller, A, L. 2008. The Methylation, Neurotransmitter, and Antioxidant Connections between Folate and Depression. *Alternative Medicine Review*. **13:** 216-226

Miller, A, R., Hawkins, N, A., McCollom, C, E. and Kearney, J, A. 2014. Mapping genetic modifiers of survival in a mouse model of Dravet syndrome. *Genes, Brain and Behaviour*. **13(2):** 326-339

Miranda, E, R., Zhuchenko, O., Toplak, M., Santhanam, B., Zupan, B., Kuspa, A. and Shaulsky, G. 2013. ABC Transporters in Dictyostelium discoideum Development. *PLOS one*. **8(8):** 1-11

Mittermaier, A. and Kay, L, E. 2006. New tools provide new insights in NMR studies of protein dynamics. *Science*. **312:** 224-8

Modebadze, T., Morgan, N, H., Pérès, I, A, A., Hadid, R, D., Amada, N., Hill, C., Williams, C., Stanford, I, M., Morris, C, M., Jones, R, S, G., Whalley, B, J. and Woodhall, G, L. 2016. A Low Mortality, High Morbidity Reduced Intensity Status Epilepticus (RISE) Model of Epilepsy and Epileptogenesis in the Rat. *PLOS one.* **11(2):** e0147265

Moore, L, D., Thuc, L. and Guoping, F. 2013. DNA Methylation and Its Basic Function. *Neuropsychopharmacology REVIEWS.* **38:** 23-38.

Moreno-Layseca, P. and Streuli, C, H. 2014. Signalling pathways linking integrins with cell cycle progression. *Matrix Biology*. **34:** 144-153

Morgan, C. J. A. and Curran, H. V. (2008). Effects of cannabidiol on schizophrenia-like symptoms in people who use cannabis. *The British Journal of Psychiatry*. **192**: 306-307

Mosharov, E., Cranford, M, R. and Banerjee, R. 2000. The quantitatively important relationship between homocysteine metabolism and glutathione synthesis by the transsulfuration pathway and its regulation by redox changes. *Biochemistry*. **39(42):** 13005-11

Mueller, S, G., Trabesinger, A, H., Boesiger, P. and Wieser, H, G. 2001. Brain glutathione levels in patients with epilepsy measured by in vivo (1)H-MRS. *Neurology.* **57(8):** 1422-7

Muller-Taubenberger, A., Kortholt, A. and Eichinger, L. 2013. Simple system--substantial share: the use of Dictyostelium in cell biology and molecular medicine. *European Journal of Cell Biology*. **92:** 45-53.

Myint, P, K., Staufenberg, E, F, A. and Sabanathan, K. 2005. Post-stroke seizure and post-stroke epilepsy. *Postgraduate Medical Journal*. **82(971):** 568-572

Myre, M, A. (2012). Clues to gamma-secretase, Huntington and Hirano body normal function using the model organism Dictyostelium discoideum. *Journal of Biomedical Science.* **19**: Article Number 41.

Nabissi, M., Morelli, M, B., Offidani, M., Amantini, C., Gentili, S., Soriani, A., Cardinali, C., Leoni, P. and Santoni, G. 2016. Cannabinoids synergize with carfilzomib, reducing multiple myeloma cells viability and migration. *Oncotarget*. **7(47):** 77543-77557

Nelson, S. A., Li, Z., Newton, I. P., Fraser, D., Milne, R. E., Martin, D. M. A., Schiffmann, D., Yang, X., Dormann, D., Weijer, C. J., Appleton, P. L., Nathke, I. S. (2012). Tumorigenic fragments of APC cause dominant defects in directional cell migration in multiple model systems. *Disease, Models and Mechanisms.* **5**: 940-947

Nissen, S, E. and Wolski, K. 2007. Effect of rosiglitazone on the risk of myocardial infarction and death from cardiovascular causes. *The New England Journal of Medicine.* **356(24):** 2457-2471

Obeid, R. 2013. The Metabolic Burden of Methyl Donor Deficiency with Focus on the Betaine Homocysteine Methyltransferase Pathway. *Nutrients*. **5:** 3481-3495.

Okamura-Ikeda, K., Fujiwara, K. and Motokawa, Y. 1987. Mechanism of the glycine cleavage reaction PROPERTIES OF THE REVERSE REACTION CATALYZED BY T-PROTEIN. *The Journal of Biological Chemistry.* **262:** 6746-6749.

Ormandy, G, C., Jope, R, S. and Snead, O, C. 1989. Anticonvulsant actions of MK-801 on the lithium-pilocarpine model of status epilepticus in rats. *Experimental Neurology*. **106:** 172–180

Osborne, P, B., Chieng, B. abd Christie, M, J. 2000. Morphine-6b-glucuronide has a higher effcacy than morphine as a mu-opioid receptor agonist in the rat locus coeruleus. *British Journal of Pharmacology*. **131:** 1422-1428

Otto, G. P., Cocorocchio, M., Munoz, L., Tyson, R. A., Bretschneider, T. and Williams, R. S. 2016. Employing Dictyostelium as an Advantageous 3Rs Model for Pharmacogenetic Research. *Methods in Molecular Biology.* **1407:** 123-30.

Pandey, A, V. and Flück, C, E. 2013. NADPH P450 oxidoreductase: Structure, function, and pathology of diseases. *Pharmacology and Therapeutics*. **138(2):** 229-254

Park, M, J., Kim, S, R., Huh, H., Jung, J, H. and Kim, Y, C. 1994. Betaine attenuates glutamate induced neurotoxicity in primary cultured brain cells. *Archives of Pharmacal Research*. **17(5):** 343-347

Patsoukis, N., Zervoudokis, G., Panagopoulos, N, T., Georgiou, C, D. Angelatou, F. and Matsokis, N, A. 2004. Thiol redox state (TRS) and oxidative stress in the mouse hippocampus after pentylenetetrazol-induced epileptic seizure. *Neuroscience Letters*. **357(2):** 83-86

Pertwee, R, G. 2008. The diverse CB1 and CB2 receptor pharmacology of three plant cannabinoids: Δ9-tetrahydrocannabinol, cannabidiol and Δ9-tetrahydrocannabivarin*. British Journal of Pharmacology.* **153(2):** 199-215

Poduri, A. 2017. When Should Genetic Testing Be Performed in Epilepsy Patients? *Epilepsy Currents.* **17(1):** 16-22

Porter, T, D. 2012. New insights into the role of cytochrome P450 reductase (POR) in microsomal redox biology. *Acta Pharmaceutica*. **2(2):** 102-106

Prescott, L, F. 1984. Drug conjugation in clinical toxicology. *Biochemical Society Transactions*. **123(1):** 96-99.

Ranjana, P. and Surojit, P. 2009. Homocysteine-NMDA receptor mediated activation of extracellular-signal regulated kinase leads to neuronal cell death. *Journal of Neurochemistry*. **110(3):** 1095-1106

Rapaccini, V., Esposito, S., Strinati, F., Allegretti, M., Manfroi, E., Miconi, F., Pitzianti, M., Prontera, P., Principi, N. and Pasini, A. 2018. A Child with a c.6923_6928dup

(p.Arg2308_Met2309dup) SPTAN1 Mutation Associated with a Severe Early Infantile Epileptic Encephalopathy. *International Journal of Molecular Science.* **19(7):** doi:10.3390

Raunio, R., Kuusisto, M., Juvonen, R, O. and Pentikäinen, O, T. 2015**.** Modeling of interactions between xenobiotics and cytochrome P450 (CYP) enzymes. *Frontiers in Pharmacology*. **6:** article 123

Reddy, D, S. 2014. Clinical pharmacology of current antiepileptic drugs. *International Journal of Pharmaceutical Sciences and Nanotechnology*. **7(1):** 2305-2319

Redl, B. 2000. Human tear lipocalin. *Biochimica et Biophysica Acta.* **1482:** 241-248

Reed, L, K., Baer, C, F. and Edison, A. 2017. Considerations when choosing a genetic model organism for metabolomics studies. *Current Opinion in Chemical Biology*. **36**: 7-14

Robery, S., Mukanowa, J., Percie Du, S. N., Andrews, P. L. and Williams, R. S. 2011. Investigating the effect of emetic compounds on chemotaxis in Dictyostelium identifies a non-sentient model for bitter and hot tastant research. *PLoS. One*: **6:** e24439.

Robery, S., Tyson, R., Dinh, C., Kuspa, A., Noegel, A. A., Bretschneider, T., Andrews, P. L. and Williams, R. S. 2013. A novel human receptor involved in bitter tastant detection identified using Dictyostelium discoideum. *Journal of Cell Science*. **126:** 5465-5476.

Rossi, M, A. 2014. SCN1A and Febrile Seizures in Mesial Temporal Epilepsy: An Early Signal to Guide Prognosis and Treatment? *Epilepsy Currents*. **14(4):** 189-190

Roth, J, R., Lawrence, J, G. and Bobik, T, A. 1996. Cobalamin (coenzyme B12): synthesis and biological significance. *Annual Review of Microbiology*. **50:** 137-181

Rowley, S. and Patel, M. 2013. Mitochondrial involvement and oxidative stress in temporal lobe epilepsy. *Free Radical Biology and Medicine*. **62:** 121-131

Rutsch, F., Gailus, S., Miousse, I, R., Suormala, T., Sagné, C., Toliat, M, R., Nürnberg, G., Wittkampf, T., Buers, I., Sharifi, A., Stucki, M., Becker, C., Baumgartner, M., Robenek, H., Marquardt, T., Höhne, W., Gasnier, B., Rosenblatt, D, S., Fowler, B. and Nürnberg, P. 2009. Identification of a putative lysosomal cobalamin exporter altered in the cblF defect of vitamin B12 metabolism. *Nature Genetics*. **41(2):** 234-9

Ryan, D., Drysdale, A. J., Lafourcade, C., et al. (2009). Cannabidiol targets mitochondria to regulate intracellular Ca^{2+} levels. *The Journal of Neuroscience*. **18**: 2053-2063.

Sander, J, D. and Joung, J, K. 2014. CRISPR-Cas systems for editing, regulating and targeting genomes. *Nature Biotechnology*. **32(4):** 347-355

Scharfman, H, E. 2007. The Neurobiology of Epilepsy. Current Neurology and Neuroscience Reports. **7(4)**: 348–354

Schwartz, M, A. and Assoian, R, K. 2001. Integrins and cell proliferation. *Journal of Cell Science*. **114:** 2553-2560

Segota, I., Mong, S., Neidich, E., Rachakonda, A., Lussenhop, C. J., Franck, C. (2013). High fidelity information processing in folic acid chemotaxis of *Dictyostelium* amoebae. *Journal of the Royal Society Interface.* **10**: Article no. 20130606.

Selmer, K. K., Lund, C., Brandal, K., Undlien, D. E. and Brodtkorb, E. 2009. SCN1A mutation screening in adult patients with Lennox-Gastaut syndrome features. *Epilepsy Behaviours*. **16:** 555-7.

Shimshoni, J. A., Dalton, E. C., Jenkins, A., Eyal, S., Kwan, K., Williams, R. S., Pessah, N., Yagen, B., Harwood, A. J. and Bialer, M. 2007. The effects of CNS-active Valproic acid constitutional isomers, cyclopropyl analogues and amide derivatives on neuronal growth cone behaviour. *Molecular Pharmacology*. **71:** 884-892.

Sibarov, D, A., Bruneau, N., Antonov, S, M., Szepetowski, P., Burnashev, N. and Giniatullin, R. 2017. Functional Properties of Human NMDA Receptors Associated with Epilepsy-Related Mutations of GluN2A Subunit. *Frontiers in Cellular Neuroscience*. **11:** Article 155

Simkin, A, J., Lopez-Calcagno, P, E., Davey, P, A., Headland, L, R., Lawson, T., Timm, S., Bauwe, H. and Raines, C, A. 2017. Simultaneous stimulation of sedoheptulose 1,7-bisphosphatase, fructose 1,6-bisphophate aldolase and the photorespiratory glycine decarboxylase-H protein increases CO2 assimilation, vegetative biomass and seed yield in Arabidopsis. *Plant Biotechnmology Journal*. **15:** 805–816

Singhi, P. 2011. Infectious causes of seizures and epilepsy in the developing world. *Developmental Medicine and Child Neurolgy*. **53(7):** 600-609

Solinas, M., Massi, P., Cinquina, V., Valentil, M., Bolognini, D., Gariboldi, M., Monti, E., Rubino, T. and Paraolaro, D. 2013. Cannabidiol, a Non-Psychoactive Cannabinoid Compound, Inhibits Proliferation and Invasion in U87- MG and T98G Glioma Cells through a Multitarget Effect. *PLOS one*. **8(10):** e76918.

Sousa, S, F., Ribeiro, A, J., Coimbra, J, T., Neves, R, P., Martins S, A., Moorthy, N, S., Fernandes, P, A. and Ramos, M, J. 2013. Protein-ligand docking in the new millennium--a retrospective of 10 years in the field. *Current Medicinal Chemistry*. 20(18): 2296-314.

Spector, T. 1988. Oxypurinol as an inhibitor of xanthine oxidase-catalyzed production of superoxide radical. *Biochemical Pharmacology*. **37(2):** 349-52

Stoker, M., O'Neill, C., Berryman, S. and Waxman, V. 1968. Anchorage and growth regulation in normal and virus-transformed cells. *International Journal of Cancer*. **3:** 683-693.

Sucgang, R., Chen, G., Liu, W., et al. (2003). Sequence and structure of the extrachromosomal palindrome encoding the ribosomal RNA genes in *Dictyostelium. Nucleic Acids Research*. **31**: 2361-2368.

Sugaya, E., Sugaya, A., Takagi, T., Tsuda, T., Kajiwara, K., Yasuda, K. and Komatsubara, J. 1989. Pentylenetetrazole-induced changes of the single potassium channel in primary cultured cerebral cortical neurons. *Brain Research.* **497(2):** 239-44

Sun, S., Hu, F., Wu, J. and Zhang, S. 2017. Cannabidiol attenuates OGD/R-induced damage by enhancing mitochondrial bioenergetics and modulating glucose metabolism via pentose-phosphate pathway in hippocampal neurons. *Redox Biology*. **11:** 577-585

Tada, H., Morooka, K., Arimoto, K. and Matsuo, T. 1991. Clinical effects of allopurinol on intractable epilepsy. *Epilepsia.* **32:** 279-283

Takeda, S., Misawa, K., Yamamoto, I., Watanabe, K., et al. (2008). Cannbidiolic acid as a selective cyclooxygenase-2 inhibitory component in cannabis. *Drug Metabolism and Disposition*. **36**: 1917-1921.

Takeda, S., Okazaki, H., Ikeda, E., Abe, S., Yoshioka, Y., Watanabe, K. and Aramaki, H. 2014. Down-regulation of cyclooxygenase-2 (COX-2) by cannabidiolic acid in human breast cancer cells. *The Journal of Toxiciological Science*. **39(5):** 711-716

Tellex-Zentenoa, J. F., Ronquillob, L. H., Wiebe, S. (2005). Sudden unexpected death in epilepsy: Evidence based analysis of incidence and risk factors. *Epilepsy Research*. **65**: 101-115.

Terbach, N., Shah, R., Kelemen, R., Klein, P, S., Gordienko, D., Brown, N, A., Wilkinson, C, J. and Williams, R, S, B. 2011. Identifying an uptake mechanism for the antiepileptic and bipolar disorder treatment valproic acid using the simple biomedical model Dictyostelium. *Journal of Cell Science.* **124(13):** 2267-2276

Thiele, E. A., Marsh, E. D., French, J. A., Mazurkiewicz-Beldzinska, M., Benbadis, S. R., Joshi, C., Lyons, P. D., Taylor, A., Roberts, C., Sommerville, K. and Group, G. S. 2018. Cannabidiol in patients with seizures associated with Lennox-Gastaut syndrome (GWPCARE4): a randomised, double-blind, placebo-controlled phase 3 trial. *Lancet.* **391:** 1085-1096.

Timm, S., Florian, A., Arrivault, S., Stitt, M., Fernie, A, R. and Bauwe, H. 2012. Glycine decarboxylase controls photosynthesis and plant growth. *Federation of European Biochemical Societies Letters*. **586:** 3692-3697.

Togha, M., Akhondzadeh, S., Motamedi, M., Ahmadi, B. and Razeghi, S. 2007. Allopurinol as adjunctive therapy in intractable epilepsy: A double-blind and placebo-controlled trial. *Archives of Medical Research*. **38(3):** 313-316

Torija, P., Robles, A. and Escalante, R. 2006. Optimization of a large-scale gene disruption protocol in Dictyostelium and analysis of conserved genes of unknown function. *BMC Microbiology.* doi:10.1186/1471-2180-6-75

Troll, H., Malchow, D., Muller-Taubenbergerg, A., Humbelg, B., Lottspeicht, F., Eckeg, M., Gerischg, G., Schmidl, A. and Benzl, R. 1992. Purification, Functional Characterization, and cDNA Sequencing of Mitochondrial Porin from Dictyostelium discoideum. *The Journal of Biological Chemistry.* **267(15):** 21072-21079

Uchinomiya, K. and Iwasa, Y. (2013). Evolution of stalk/spore ratio in a social amoeba: Cell-to-cell interaction via a signaling chemical shaped by cheating risk. *Journal of Theoretical Biology.* **336**: 110-118

Ujváry, I. and Hanuš, L. 2016. Human Metabolites of Cannabidiol: A Review on Their Formation, Biological Activity, and Relevance in Therapy. *Cannabis and Cannabinoid Research.* **1(1):** 90-101

Ulrey, C, L., Liu, L., Andrews, L, G. and Tollefsbol, T, O. 2005. The impact of metabolism on DNA methylation. *Human Molecular Genetics***. 14:** 139–147

Vasiev, B. and Weijer, C. J. (2003). Modelling of *Dictyostelium discoideum* slug migration. *Journal of Theoretical Biology.* **223**: 347-359.

Viguera, E., Canceil, D. and Ehrlich, S, D. 2001. Replication slippage involves DNA polymerase pausing and dissociation. *EMBO Journal*. **20(10):** 2587-95.

Vining, E, P, G., Freeman, J, M., Ballaban-Gil, K., Camfield, C, S., Camfield, P, R., Holmes, G, L., Shinnar, S., Shuman, R., Trevathan, E., Wheless, J, W. and The Ketogenic Diet Multi-Center

Study Group. 1998. A Multicenter Study of the Efficacy of the Ketogenic Diet. *JAMA Neurology*. **55(11):** 1433-1437

Vitvitsky, V., Thomas, M., Ghorpade, A., Gendelman, H, E. and Banerjee, R. 2006. A functional transsulfuration pathway in the brain links to glutathione homeostasis. *The Journal of Biological Chemistry*. **281(47):** 35785-93

Vyklicky, V., Korinek, M., Smejkalova, T., Baliki, A., Krausova, B., Kaniakova, M., Lichnerova, K., Cerny, J., Krusek, J., Dittert, I., Horak, M. and Vyklicky, L. 2014. Structure, Function, and Pharmacology of NMDA Receptor Channels. *Physiological Research Journal*. **63:** S191-S203

Waheed, A., Ludtmann, M. H., Pakes, N., Robery, S., Kuspa, A., Dinh, C., Baines, D., Williams, R. S. and Carew, M. A. 2014. Naringenin inhibits the growth of Dictyostelium and MDCK-derived cysts in a TRPP2 (polycystin-2)-dependent manner. *British Journal of Pharmacology*. **171:** 2659-2670.

Walker, J, L. and Assoian, R, K. 2005. Integrin-dependent signal transduction regulating cyclin D1 expression and G1 phase cell cycle progression. *Cancer Metastasis Reviews*. **24(3):** 383-93

Wallace, J, L. 2008. Prostaglandins, NSAIDs, and Gastric Mucosal Protection: Why Doesn't the Stomach Digest Itself? *Physiologicial Reviews-American Journal of Physiology*. **88:** 1547–1565

Williams, R. S. B., Eames, M., Ryves, W. J., Viggars, J. and Harwood, A. J. 1999. Loss of a prolyl oligopeptidase confers resistance to lithium by elevation of inositol (1,4,5) trisphosphate. *The EMBO Journal.* **18:** 2734-2745.

Williams, R. S. B., Cheng, L., Mudge, A. W. and Harwood, A. J. 2002. A common mechanism of action for three mood-stabilizing drugs. *Nature.* **417:** 292-295.

Williams, R. S., Boeckeler, K., Graf, R., Muller-Taubenberger, A., Li, Z., Isberg, R. R., Wessels, D., Soll, D. R., Alexander, H. and Alexander, S. 2006. Towards a molecular understanding of human diseases using Dictyostelium discoideum. *Trends in Molecular Medicine*. **12:** 415-424.

Williamson, I., Hill, R, E. and Bickmore, W, A. 2011. Enhancers: From Developmental Genetics to the Genetics of Common Human Disease. *Developmental Cell.* **21(1):** 17-19

Wojnar, P., Lechnar, M., Merschak, P. and Redl, B. 2001. Molecular cloning of a novel lipocalin-1 interacting human cell membrane receptor using phage display. *The Journal of Biological Chemistry*. **276(23):** 20206–20212.

Wuerthele, S, E., Yasuda, R, P., Freed, W, J. and Hoffer, B, J. 1982. The effect of local application of homocysteine on neuronal activity in the central nervous system of the rat. *Life Sciences*. **31(24):** 2683-2691

Xing Du., Yi Li., Yuan-Ling Xia., Shi-Meng Ai., Jing Liang., Peng Sang., Xing-Lai Ji. and Shu-Qun Liu. 2016. Insights into Protein–Ligand Interactions: Mechanisms, Models, and Methods. *International Journal of Molecular Sciences.* **17:** 144

Xu, C., Li, C, Y. and Kong, A, T. 2005. Induction of Phase I, II and III Drug Metabolism/Transport by Xenobiotics. *Archives of Pharmacal Research*. **28(3):** 249-268.

Xu, X., Muller-Taubenberger, A., Adley, K. E., Pawolleck, N., Lee, V. W., Wiedemann, C., Sihra, T. S., Maniak, M., Jin, T. and Williams, R. S. 2007. Attenuation of phospholipid signaling provides a novel mechanism for the action of valproic acid. *Eukaryotic Cell***. 6:** 899-906.

Yamaori, S., Ebisawa, J., Okushima, Y., Yamamoto, I. and Watanabe, K. 2011. Potent inhibition of human cytochrome P450 3A isoforms by cannabidiol: Role of phenolic hydroxyl groups in the resorcinol moiety. *Life Sciences*. **88:** 730-736

Young, D. and Dragunow, M. 1994. Status epilepticus may be caused by loss of adenosine anticonvulsant mechanisms. *Neuroscience*. **58(2):** 245-261

Zabinyakov, N., Bullivant, G., Cao, F., Fernandez Ojeda, M., Jia, Z, P., Wen, X, Y., Dowling, J, J., Salomons, G, S. and Mercimek-Andrews, S. 2017. Characterization of the first knock-out aldh7a1 zebrafish model for pyridoxine-dependent epilepsy using CRISPR-Cas9 technology. *PLoS One*. **12(10):** e0186645

Zanger, U, M. and Schwab, S. 2013. Cytochrome P450 enzymes in drug metabolism: Regulation of gene expression, enzyme activities, and impact of genetic variation. *Pharmacology & Therapeutics.* **138:** 103-141

Zhao, S, Z., Reynolds, M, W., Lejkowith, J., Whelton, A. and Arellano, F, M. 2001. A comparison of renal-related adverse drug reactions between rofecoxib and celecoxib, based on the World Health Organization/Uppsala Monitoring Centre safety database. *Clinical therapeutics*. **23(9):** 1478-91